

# Design Considerations for the Glenohumeral Endoprosthesis

About the cover

Design: A.J. van der Pijl and R. Oosterom.

The blue image on the front cover contains a computer drawing of the new prosthesis described in Chapter 10 (top) and the superior part of the humerus and scapula (below). The watermark is the famous '*Vitruvian*' (about 1490) of Leonardo da Vinci (1452 - 1519). The List of Symbols can be found at the inside of the unfoldable back cover, which also includes a short summary.

# Design Considerations for the Glenohumeral Endoprosthesis

**Proefschrift**

ter verkrijging van de graad van doctor

aan de Technische Universiteit Delft,

op gezag van de Rector Magnificus prof.dr.ir. J.T. Fokkema,

voorzitter van het College voor Promoties,

in het openbaar te verdedigen op dinsdag 1 februari 2005 om 10:30 uur

door Rogier OOSTEROM

ingenieur in de luchtvaart en ruimtevaart

geboren te Alkmaar

Dit proefschrift is goedgekeurd door de promotoren:

Prof. ir. A. Beukers

Prof. dr. P.M. Rozing

Toegevoegd promotor:

Dr. ir. H.E.N. Bersee

Samenstelling promotiecommissie:

Rector Magnificus	voorzitter
Prof. ir. A. Beukers	Technische Universiteit Delft, promotor
Prof. dr. P.M. Rozing	Universiteit Leiden, promotor
Dr. ir. H.E.N. Bersee	Technische Universiteit Delft, toegevoegd promotor
Prof. dr. ir. H.G. Stassen	Technische Universiteit Delft
Prof. dr. C.N. van Dijk	Universiteit van Amsterdam
Prof. dr. O. Gagey	Bicêtre University Hospital
Dr. ir. N.J.J. Verdonchot	Katholieke Universiteit Nijmegen
Prof. dr. M.J.L. van Tooren	Technische Universiteit Delft, reservelid

*Published and distributed by:* DUP Science

DUP Science is an imprint of  
Delft University Press  
P.O. Box 98  
2600 GM Delft  
The Netherlands  
Telephone: +31152785678  
Telefax: +31152785706  
E-mail: DUP@Library.TUdelft.NL

ISBN 90-407-2572-1

Keywords: shoulder prosthesis, design, stability

Copyright © 2004 by R. Oosterom

All rights reserved. No part of the material protected by this copyright notice may be reproduced or utilised in any form or by any means, electronic or mechanical, including photocopying, recording or by any information storage and retrieval system, without written permission from the publisher: Delft University Press. If any questions arise about the figures used in the thesis please contact R. Oosterom, email: R.Oosterom@LR.TUdelft.NL

# Table of Contents

Table of Contents	v
List of Abbreviations	xi
Preface	xiii
Reader's guide	xv
<b>1 Introduction</b>	<b>1</b>
1.1 The clinical problem . . . . .	3
1.2 DIPEX . . . . .	3
1.3 Goal of the study . . . . .	4
1.4 Strategy of the study . . . . .	4
1.5 Structure of the thesis . . . . .	6
<b>2 The shoulder joint and its replacement</b>	<b>9</b>
2.1 Introduction . . . . .	11
2.2 Shoulder Anatomy . . . . .	11
2.2.1 The Humerus . . . . .	12
2.2.2 The scapula . . . . .	12
2.2.3 Glenohumeral relationships . . . . .	14
2.2.4 Shoulder joint pathology and indications for a shoulder replacement . . . . .	14
2.3 Shoulder joint biomechanics . . . . .	18
2.3.1 Glenohumeral articulation . . . . .	18
2.3.2 Range of motion . . . . .	19
2.3.3 Joint forces and contact area . . . . .	19
2.3.4 Shoulder joint stability . . . . .	20
2.4 Shoulder joint replacements . . . . .	21

2.4.1	History . . . . .	21
2.4.2	Present used shoulder replacement systems . . . . .	23
2.4.3	The surgical process . . . . .	27
2.4.4	Facts on shoulder replacements . . . . .	28
2.4.5	Complications after shoulder replacements . . . . .	29
2.4.6	Design of the shoulder prosthesis . . . . .	31
2.5	Conclusions . . . . .	33
<b>3</b>	<b>The hip, knee, ankle joint and their replacement</b>	<b>35</b>
3.1	Introduction . . . . .	37
3.2	The hip joint . . . . .	37
3.2.1	Anatomy . . . . .	37
3.2.2	Biomechanics . . . . .	38
3.2.3	History of hip replacements . . . . .	39
3.2.4	Facts . . . . .	40
3.2.5	Complications . . . . .	42
3.3	The knee joint . . . . .	43
3.3.1	Anatomy . . . . .	43
3.3.2	Biomechanics . . . . .	45
3.3.3	History of knee replacements . . . . .	46
3.3.4	Facts . . . . .	48
3.3.5	Complications . . . . .	49
3.4	The ankle joint . . . . .	50
3.4.1	Anatomy . . . . .	50
3.4.2	Biomechanics . . . . .	51
3.4.3	History of ankle replacements . . . . .	53
3.4.4	Facts . . . . .	54
3.4.5	Complications . . . . .	56
3.5	Design . . . . .	57
3.5.1	Wear . . . . .	60
3.5.2	Biological bone deposition . . . . .	62
3.5.3	Stress shielding . . . . .	62
3.5.4	Loosening . . . . .	63
3.6	Conclusions . . . . .	64
<b>4</b>	<b>Translational stiffness of the replaced shoulder joint</b>	<b>67</b>
4.1	Introduction . . . . .	69
4.2	Definitions . . . . .	70
4.2.1	Joint positions and articulation regions . . . . .	70
4.2.2	Joint translational stiffness . . . . .	71

---

4.2.3	Stability . . . . .	72
4.2.4	Subluxation . . . . .	73
4.2.5	Dislocation . . . . .	73
4.3	Methods . . . . .	73
4.3.1	Assumptions . . . . .	73
4.3.2	Calculation of joint displacements, subluxation force and joint translation stiffness . . . . .	74
4.4	Results . . . . .	77
4.5	Discussion . . . . .	81
4.6	Conclusions . . . . .	83
<b>5</b>	<b>Force-controlled testing of shoulder prostheses</b>	<b>85</b>
5.1	Introduction . . . . .	87
5.2	Methods and Materials . . . . .	88
5.2.1	Specimen structure . . . . .	88
5.2.2	Force-controlled fatigue testing . . . . .	89
5.2.3	Method of measurement and evaluation . . . . .	91
5.3	Results . . . . .	94
5.4	Discussion . . . . .	95
5.5	Conclusions . . . . .	97
<b>6</b>	<b>Effect of joint conformity on glenoid component fixation</b>	<b>99</b>
6.1	Introduction . . . . .	101
6.2	Materials and Methods . . . . .	103
6.2.1	Specimen structure . . . . .	103
6.2.2	Force-controlled fatigue testing . . . . .	104
6.2.3	Method of measurement and evaluation . . . . .	104
6.3	Results . . . . .	105
6.4	Discussion . . . . .	106
6.5	Conclusions . . . . .	109
<b>7</b>	<b>Effect of glenoid component inclination on its fixation and humerus subluxation</b>	<b>111</b>
7.1	Introduction . . . . .	113
7.2	Methods . . . . .	114
7.2.1	Specimen structure . . . . .	114
7.2.2	Force-controlled fatigue testing . . . . .	115
7.2.3	Method of measurement and evaluation . . . . .	115
7.3	Results . . . . .	118
7.4	Discussion . . . . .	120

7.5	Conclusions . . . . .	123
<b>8</b>	<b>Investigation of the adhesion performance of UHMWPE</b>	<b>125</b>
8.1	Introduction . . . . .	127
8.2	Materials . . . . .	128
8.3	Surface treatments . . . . .	128
8.4	Analyses . . . . .	131
8.5	Results . . . . .	132
8.6	Discussion . . . . .	137
8.7	Conclusions . . . . .	140
<b>9</b>	<b>Effect of the cement-prosthesis interface on FE Modelling</b>	<b>141</b>
9.1	Introduction . . . . .	143
9.2	Experimental investigation of the coefficient of friction between PMMA and UHMWPE . . . . .	144
9.2.1	Methods and materials . . . . .	144
9.2.2	Results . . . . .	146
9.2.3	Discussion . . . . .	147
9.3	The effect of interface conditions on Finite Element Modelling of the artificial shoulder . . . . .	150
9.3.1	Methods and materials . . . . .	150
9.3.2	Results . . . . .	152
9.3.3	Discussion . . . . .	153
9.4	Conclusions . . . . .	155
<b>10</b>	<b>A self-stabilizing shoulder endo-prosthesis</b>	<b>161</b>
10.1	Introduction . . . . .	163
10.2	Design requirements . . . . .	164
10.3	The design . . . . .	167
10.3.1	Restoring joint stability . . . . .	167
10.4	The design in detail . . . . .	173
10.4.1	Orientation of the ligaments . . . . .	173
10.4.2	Ligament forces . . . . .	175
10.4.3	Bone anchor and ligament stresses . . . . .	175
10.5	Summary of the design description and reflection to the requirements	177
10.6	Challenges . . . . .	179
10.7	Spin-off applications . . . . .	179
10.8	Conclusions . . . . .	180

---

<b>11 Conclusions</b>	<b>183</b>
11.1 Accomplishments . . . . .	185
11.2 Future research . . . . .	188
<b>A Medical terminology</b>	<b>191</b>
A.1 Terminology . . . . .	193
A.2 Ligaments, muscles and the glenoid labrum . . . . .	193
<b>B Biomaterials</b>	<b>197</b>
B.1 Introduction . . . . .	199
B.2 Bone and cartilage . . . . .	199
B.3 Materials for joint replacements . . . . .	201
<b>C Color Figures</b>	<b>209</b>
<b>References</b>	<b>220</b>
<b>List of Publications</b>	<b>247</b>
<b>List of Figures</b>	<b>249</b>
<b>List of Tables</b>	<b>251</b>
<b>Summary</b>	<b>255</b>
<b>Samenvatting</b>	<b>259</b>
<b>Acknowledgements</b>	<b>263</b>
<b>Curriculum Vitae</b>	<b>265</b>



# List of Abbreviations

<i>ACL</i>	Anterior Cruciate Ligament
<i>ADL</i>	Activities of Daily Living
<i>AN</i>	Avascular Necrosis
<i>AP</i>	Anterior-Posterior
<i>BW</i>	Body Weight
<i>CoF</i>	Coefficient of friction
<i>CoR</i>	Center of rotation
<i>DIPEX</i>	Development of Improved endo-Prostheses for the upper EXtremities
<i>DoF</i>	Degree of freedom
<i>FU</i>	Follow-up
<i>HA</i>	Hemi-Arthroplasty
<i>HR</i>	Humeral Resurfacing
<i>ML</i>	Medial-Lateral
<i>OA</i>	Osteo-Arthritis
<i>PCL</i>	Posterior Cruciate Ligament
<i>PMMA</i>	Polymethyl-Methacrylate
<i>RA</i>	Rheumatoid-Arthritis
<i>RC</i>	Rotator Cuff
<i>RoM</i>	Range of Motion
<i>SI</i>	Superior-Inferior
<i>TJR</i>	Total Joint Replacement
<i>TSR</i>	Total Shoulder Replacement
<i>UHMWPE</i>	Ultra-High-Molecular-Weight-Poly-Ethylene



# Preface

Some people can be very enthusiastic about a subject, spending a lot of their time on it. Others are passionate and the subject becomes part of them. Without a doubt, Prof. dr. ir. H.G. Stassen can be regarded as part of the second group. Somewhere in 1998 he started up yet another project, aiming at the improvement of the shoulder replacement. This project focuses on the patient, design and surgical factors and is entitled 'DIPEX', which stands for Development of Improved endo-Prostheses for the upper EXtremities.

The present PhD thesis is part of this project, with a focus on the design of the prosthesis and takes place at the Faculty of Aerospace Engineering, Section of Production Technology. At first sight, this location may not seem to be the most logical choice, but, during time, links with the medical oriented subject and the engineering group became clear. Many engineers within the group can be seen as non-conformists, having an open mind for new solutions and always come up with unexpected design ideas. This is beneficial in a project in which new solutions for complex problems must be found.

The result is a thesis, which describes both improvements of the presently used anatomical prostheses as well as the exploration of conceptually new designs. Many approaches have been used, with the help of many people from different disciplines. Modelling (Chapters 4 and 9), experimental techniques (Chapters 5, 6, 7 and 9, surface modification techniques (Chapter 8) as well as three-dimensional Computer-Aided-Design (Chapter 10) have been used to come to the final result. Therefore, the research in the thesis can rather be seen as a broad exploration of the possibilities of the applied methods on the research aim, which is the improvement of the glenohumeral prosthesis, then as fundamental research focusing on the improvement of the method itself.



## Reader's guide

Writing up the research of the present PhD study into a thesis is made challenging as it is meant for readers from both the technical workspace as well as from the medical field, for whom it may be troublesome to understand the medical and technical terminology, respectively. Hopefully I succeeded in this, by adding explanations where necessary and a List of Symbols at the inside of the back cover. Additionally, two appendices describe detailed anatomical aspects of the shoulder and biological materials as well as biomaterials, respectively. The List of Symbols is attached to better understand those parts of the thesis, in which symbols are frequently used.

Chapters 1, 2 and 3 can be regarded as introductory chapters, describing the background of the thesis, the shoulder and the lower extremities, respectively. Especially for those readers, who are not familiar with the aspects of these body parts, it may be of assistance to first read these chapters, to better understand the relevancy of the studies in the following chapters.

Chapters 4 through 10 are written so that it is made possible to read them independently, without knowledge of the preceding chapters. The conclusions and future challenges of the presented work are given in Chapter 11, which also reflects on the work done and it brings the results in a clinical perspective.

At the end of the thesis, subsequently the List of Publications, List of Figures and List of Tables, as well as a Dutch and English Summary are presented. The Acknowledgements and Curriculum Vitae bring the thesis to the end.



# Chapter 1

## Introduction



*Opening Ceremony of the Olympic Games, Athens, 2004*



## 1.1 The clinical problem

Joint pathology due to diseases as osteo-arthritis (OA), rheumatoid-arthritis (RA) or Rotator Cuff (RC) arthropathy can result in eroded and distorted articular surfaces, decreased bone properties and weakened surrounding soft-tissues, such as ligaments and muscles. A Total Shoulder Replacement (TSR) can be a helpful treatment with long-term pain relief and functional improvement (e.g. increased abduction and external rotation) as main objectives. Although post-operative pain relief is achieved in most cases, functional improvement is not enough to perform all 'Activities of Daily Living' (ADL), needed to live an independent life, and also long-term component fixation is still an unsolved problem and results of the TSR must be improved, to increase patient satisfaction.

## 1.2 DIPEX

In 1999, a multidisciplinary, interfacultair program at the Delft University of Technology has been launched, to improve the shoulder replacement, focusing on the above mentioned influencing factors. The program is entitled 'DIPEX' (Development of Improved endo-Prostheses for the upper EXtremities) and is divided in six sub-projects, focusing on patient factors, the surgeon and design factors.

The first project aims at improving the efficiency and quality of the surgical procedure, by a rigorous evaluation of the surgical process. The second project deals with visualization techniques for improved pre-operative planning, to improve the predictability of this surgical procedure. Project three investigates shoulder functionality of healthy subjects to develop requirements for joint functionality to perform ADL. Additionally, this project compares the pre- and post-operative joint functionality with the developed requirements. Component fixation is the subject of project four, using improved computer models to investigate the effect of design parameters and bone ingrowth fixation. Project five aims at improving the prosthesis design, using modelling and experimental techniques, such as a wear and fixation simulator. Finally, project six aims at improving alignment tools for the surgeon, which must lead to more accurate insertion of the prosthetic components. Both mechanical alignment and computer navigation, as well as camera assisted shoulder surgery have been investigated.

The goal of the DIPEX program is to improve the involving aspects of the complete shoulder replacement, with respect to long-term patient satisfaction and independency in all day live and time as well as quality of the surgery. The present study, as a part of project five, aims at improvement of the shoulder replacement by focusing on the design of the prosthesis.

### 1.3 Goal of the study

Design of the shoulder prosthesis influences, among others, the surgical procedure, shoulder joint biomechanics, pain relief, tissue reactions, survival and ease of a revision, if necessary. As a result, an optimal design is difficult to achieve, also because different diseases result in different joint pathologies, which ask for specific solutions. The design of the prosthesis involves the design concept as well as prosthesis geometry, materials and method of fixation. The conceptual prosthesis design can either be an anatomical design or a non-anatomical design. The anatomical design aims at restoring the natural geometry of the bone tissues and makes use of the surrounding soft-tissues to obtain post-operative joint compression and functionality. The anatomical design shows good results in the case both the soft and hard tissues are of proper quality and the articular shape still provides enough bone volume for insertion and fixation of the components. The non-anatomical design more neglects the anatomical geometry and articulation of the natural joint, but focuses on the functional requirements of the shoulder joint, its pathology and total tissue state. Beforehand, the design concept and geometry of a new non-anatomical prosthesis are not known. However, certain requirements, such as articular geometry, biomechanics and surgical limitations, must be kept in mind.

The ultimate goal of this study is to improve post-operative shoulder joint functionality, with improved long-term glenoid component fixation focusing on shoulder prosthesis design, without demanding additional surgical effort.

In the case joint anatomy and mechanical properties are close to normal and only articular surfaces are affected, for example due to osteo-arthritis the anatomical design seems to be the answer for a TSR. Improvements with respect to prosthesis design for this patient group can be achieved in terms of component fixation, wear, joint stability and the surgical process.

A more destroyed joint, in which both hard and soft-tissues are affected, common status in the case of late stage rheumatoid-arthritis and RC-arthropathy, asks for a different approach, which might lead to both new anatomical and new non-anatomical design concepts. This is due to weakened or even cancelled-out joint functions, which must be taken over by the new design. One example is the deteriorated stabilization function of the pathologic RC muscles, which has to be taken over by the new prosthesis. These two different joint conditions asks for a specific research strategy.

### 1.4 Strategy of the study

Three different research directions to improve the TSR are investigated in this PhD study (see Figure 1.1):

1. Geometrical improvement of the Ultra-High-Molecular-Weight-Polyethylene (UHMWPE) anatomical cemented glenoid component design,
2. Investigation of adhered fixation of the UHMWPE anatomical cemented glenoid component,
3. Development of a new self-stabilizing non-anatomical shoulder prosthesis.

The conventional, anatomical glenohumeral replacement will be looked at, investigating the effect of glenoid component geometry and orientation on glenoid component fixation and glenohumeral functionality. The glenohumeral conformity, by adapting the glenoid radius of curvature  $R_g$ , and the glenoid inclination angle  $\gamma$  have been investigated. Glenohumeral conformity determines contact stresses, humeral head translations and glenoid component tilting. Glenoid component inclination, a combined surgical and patient factor, determines glenoid component tilting, as well as humeral head subluxation and dislocation.

The second research direction focuses on direct improvement of glenoid component fixation, leaving component geometry intact. The common fixation method for glenoid components is cementing them into overreamed bone, using Polymethyl-Methacrylate (PMMA) bone-cement. The advantage over bone-ingrowth fixation is the direct post-operative fixation, whereas the large amount of bone to be removed, dangerous thermal effects of cement polymerization and cement particles due to abrasion are drawbacks of this method of fixation. However, bone ingrowth fixation also shows difficulties, such as increased component thickness, due to the metal backing, increased wear and special attention for initial component fixation in the 6 to 8 weeks post-operative, necessary for stable bone ingrowth. In this project cemented glenoid components are investigated.

UHMWPE glenoid components have poor adhesion properties, especially in combination with PMMA bone cement, which is more a filler than an adhesive. This implies that cemented UHMWPE components are rather fixed by mechanical locking, using design details such as grooves and holes, which also requires deep bone removal. Improving the adhesion performance of UHMWPE, by means of surface modification methods, might lead to improved fixation of presently used components and to new designs, more or completely relying on adhesion instead of mechanical locking with the additional benefit of less bone removal.

The third research direction is the development of a conceptually new shoulder prosthesis for patients with lost stability function, for example for patients suffering from rheumatoid-arthritis or isolated RC arthropathy. At present, there is no long-lasting prosthesis for these patient groups, providing sufficient functionality and strength to perform ADL.

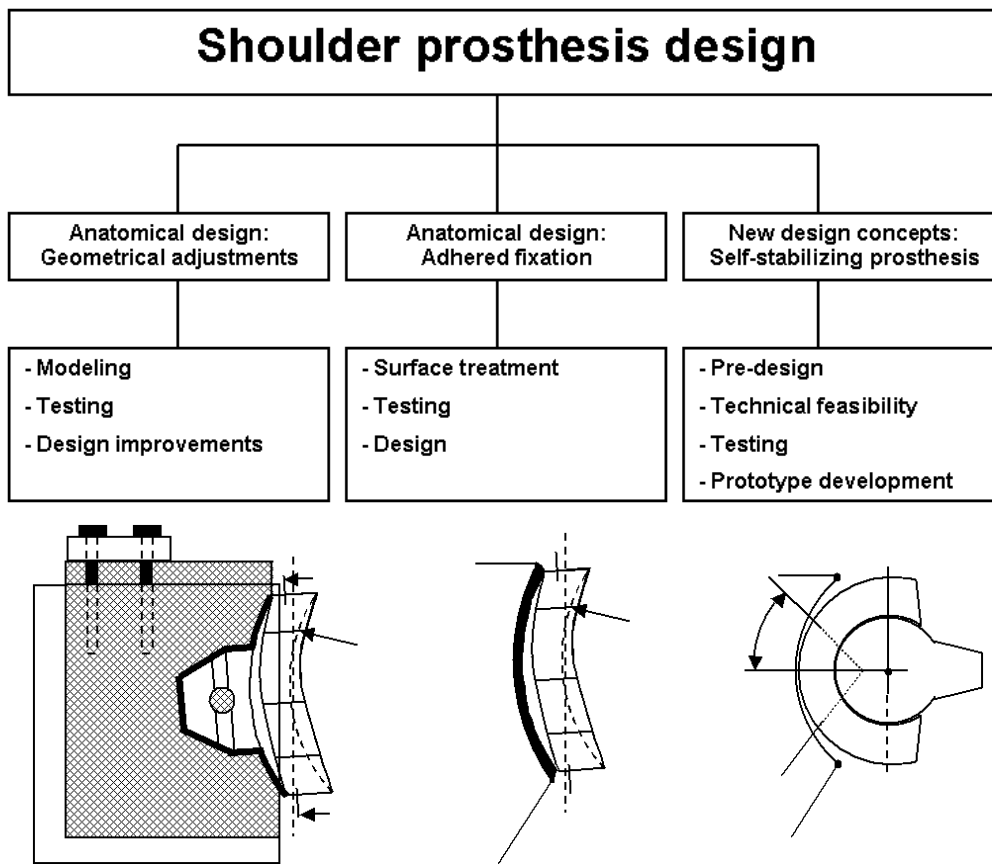


Figure 1.1: *The proposed research strategy of the PhD study as part of the design project within the DIPEX program*

## 1.5 Structure of the thesis

This PhD thesis begins with the background of the shoulder joint, in terms of shoulder anatomy, biomechanics and orthopedics (Chapter 2). Following is a comparable overview about the hip, knee and ankle joint (Chapter 3). A rigid-body model of the artificial shoulder is presented and used to investigate the effect of prosthesis geometry on joint translations and stability (Chapter 4). Subsequently, a force-controlled experimental test set-up is described (Chapter 5), whereafter the results will be presented of the studies into the effect of joint conformity and glenoid component inclination on its fixation as well as on humeral head subluxation (Chapters 6 and 7), using this test set-up. The study to investigate adhesion performance of UHMWPE by applying different surface modification methods is described in Chapter 8. The coefficient of friction between PMMA and UHMWPE and its effect on stresses in a Finite Element Model of a cemented glenoid component have been investigated, which is described in Chapter 9. Chapter 10 presents the development of a concep-

tually new self-stabilizing prosthesis design. Chapter 11 gives the conclusions and future recommendations.

Three appendices are included to provide additional background of this PhD study. Appendix A gives additional information about the anatomy of the shoulder joint and medical terminology. An overview of biomaterials, both host-tissues and artificial materials, is given in Appendix B. Appendix C provides color representations of those figures by which this may lead to improved understanding.



## Chapter 2

# The shoulder joint and its replacement



*Some shoulder strength during a rings session*



## 2.1 Introduction

The healthy shoulder joint, or glenohumeral joint, provides us a large range of motion. Together with the cooperation of the other bone elements and articular joints of the shoulder girdle, it gives us even a larger range of motion, enabling us to easily perform all 'Activities of Daily Living' (ADL). Unfortunately, shoulder pathology, due to both traumatic and atraumatic events, can cause disability already in young persons. At present, good treatment methods, such as the Total Shoulder Replacement (TSR), are available for many patients. However, after a TSR it is difficult to obtain enough joint functionality to perform main ADL and also long-term component fixation is still an unsolved problem.

To investigate possible design improvements of the shoulder prosthesis, proper understanding of the background of the shoulder is a requisite. This involves shoulder anatomy (such as articular geometry, dimensions and surrounding structures, including their location and function), biomechanics (for example joint forces and range of motion) and orthopedics (such as the surgical procedure, implant design, failure scenarios). Subsequently, this chapter describes the anatomy, biomechanics and orthopedics of the shoulder joint.

## 2.2 Shoulder Anatomy

Designing (conceptually) new prosthesis components for the shoulder joint, requires knowledge of the dimensions of the glenoid and humerus and their static as well as dynamic relationships. Not taking into account these relationships, might lead to difficulties, especially with the surgical procedure, post-operative joint functionality and long-term component fixation.

The shoulder girdle consists of three bones, namely the humerus, the scapula and the clavicle (see Figures 2.1 and 2.2). The thorax is not seen as part of the shoulder girdle, although it plays an important role in shoulder dynamics and the maximal range of motion of the shoulder [264]. The shoulder girdle has three synovial joints. The articulation between the humerus and the glenoid cavity of the scapula forms the glenohumeral joint, often referred to as the shoulder joint. The clavicle articulates with the sternum and the acromion, forming the sterno-clavicular and acromio-clavicular joint, respectively. Additionally, during many upper arm tasks, the scapula moves with respect to the thorax, forming the scapulo-thoracic gliding plane (which is not an articulation in the true sense).

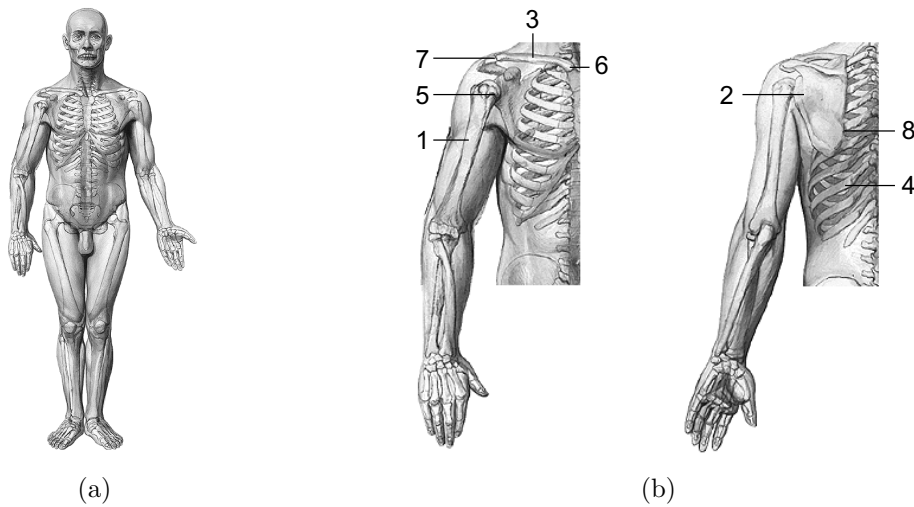


Figure 2.1: *The Body and the Shoulder. (a) The skeletal system of the human body. (b) Anterior (Left) and Posterior view of the upper extremities. 1. humerus 2. scapula 3. clavícula 4. thorax 5. glenohumeral joint 6. sterno-clavicular joint 7. acromio-clavicular joint 8. scapulo-thoracic gliding plane. Adapted from Sobotta*

### 2.2.1 The Humerus

The upper arm, or humerus, is a long bone, with a rather large geometrical variation [238]. The articular surface makes up a sphere of about  $120^\circ$  and is tilted upward approximately  $45^\circ$ , with respect to its long axis [128]. The bicipital groove, through which the long head of the m. biceps passes from its origin on the superior rim of the glenoid cavity, lies between the two tuberculi, approximately 1 cm lateral from the central axis of the humerus. The muscle (m.) tuberculum minus is the insertion for the m. subscapularis and the tuberculum major for the m. supraspinatus, m. infraspinatus and m. teres minor, from superior to inferior [128] (see Figures 2.2 and 2.3a, as well as Table 2.1 and Appendix A for more detailed dimensions).

### 2.2.2 The scapula

The scapula forms a connection between the humerus and the thorax and together with the clavícula it forms a closed chain mechanism [264]. The scapula plays an important role in the range of motion of the shoulder girdle [251]. The scapula is a thin, triangular shaped bone, with high in-plane stiffness as it can be seen as a rigid framework [216], made out of a thin sheet becoming thicker at the outer margins (see Figure 2.3b). It also functions as a main attachment structure for almost all shoulder muscles.

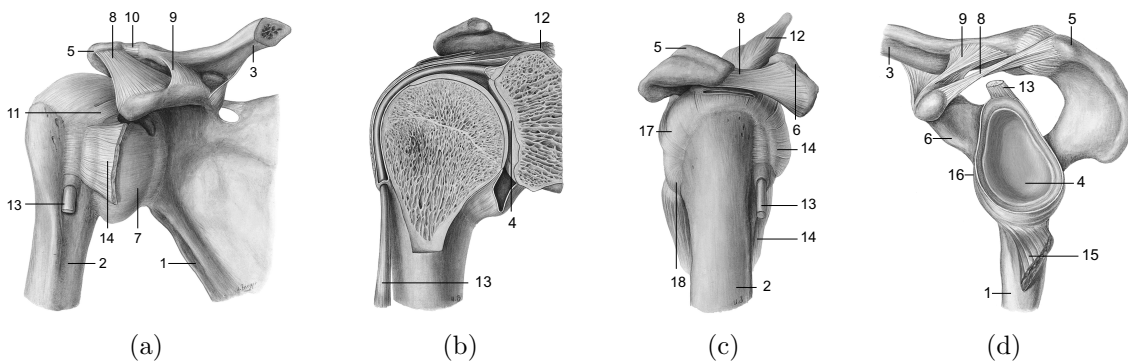


Figure 2.2: *The glenohumeral joint. (a) Anterior view of the shoulder, including the humerus, scapula and lateral clavicle. (b) Frontal section of the right glenohumeral articulation. (c) Lateral view on the right glenohumeral articulation with the proximal humerus and Rotator Cuff (RC). (d) Lateral view on the left glenohumeral articulation. 1. scapula 2. humerus 3. clavicle 4. glenoid cavity 5. acromion 6. processus coracoideus 7. ligament.(lig.) glenohumerale (inferior, medium, superior) 8. lig. coraco-acromiale 9. lig. trapezoideum 10. lig. acromioclaviculare 11. lig. coracohumerale 12. muscle (m.) supraspinatus\* 13. m. biceps brachii, caput longum 14. m. subscapularis\* 15. m. triceps brachii, caput longum 16. labrum glenoidale 17. m. infraspinatus\* 18. m. teres minor\* \*Rotator Cuff muscles. See Figure C.1 in Appendix C for color representations. Adapted from Sobotta*

In the anatomical position, the scapula has a slight superior directed tilt of  $3^\circ$  to  $5^\circ$  and is rotated  $30^\circ$  forward relative to the frontal plane [265]. The glenoid cavity, a concavity at the lateral scapula, together with the coracoid process, the acromion and the coracoacromial ligament can be seen as a resilient socket surrounding the humeral head. It also gives the glenohumeral joint extra stability and prevents subluxation of the humeral head in upward direction during the normal range of motion [271] (see Figure 2.2d).

### The Glenoid cavity

The glenoid is part of the lateral scapula and is a shallow, pear shaped socket [176], tilted upward about  $5^\circ$ , retroverted approximately  $7^\circ$ . The height (SI-direction) and width (AP-direction) are 3.5 to 4 cm and 2.5 to 3 cm, respectively [125]. The arc of enclosure in an anterior-posterior (AP) and superior-inferior (SI) view is  $66 \pm 12^\circ$  and  $45.5 \pm 15^\circ$ , respectively, according to McPherson et al. (1997). The depth of the glenoid cavity in an AP view and SI view is  $5 \pm 1$  mm and  $2.9 \pm 1$  mm, respectively [203] (see Table 2.1).

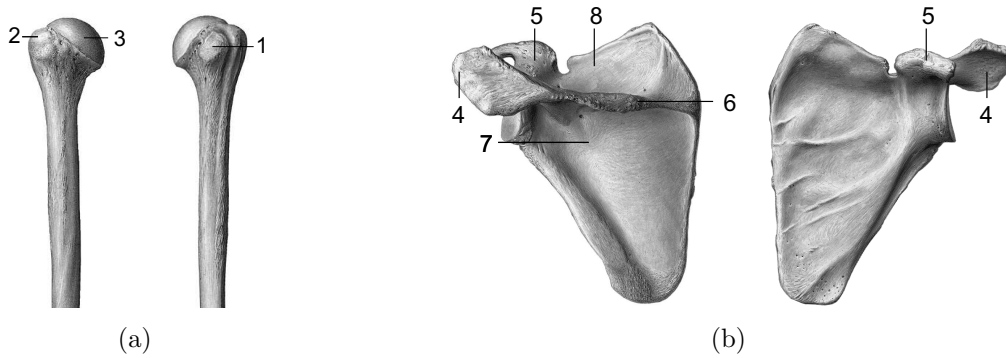


Figure 2.3: *The humerus and scapula. (a) Posterior (left) and anterior view of the proximal humerus. (b) Posterior (left) and anterior view of the scapula. 1. tuberculum minus 2. tuberculum major 3. caput humeri 4. acromion 5. proc. coracoideus 6. spina scapulae 7. fossa infraspinata 8. fossa subscapularis. Adapted from Sobotta*

### 2.2.3 Glenohumeral relationships

Many dimensions of the glenoid and humerus are measured by Ianotti et al. (1992) and McPherson et al. (1997) [121, 203], which are given in Table 2.1. Additionally, using stereophotogrammetry, Soslowsky et al. (1992) mapped articular dimensions of the glenohumeral joint [293]. The cartilage surface of the humeral head for male and female measure  $1734 \pm 204$  and  $1336 \pm 220 \text{ mm}^2$ , respectively, and of the glenoid cavity  $579 \pm 169$  and  $468 \pm 93 \text{ mm}^2$ , respectively. Surface area ratio of the glenoid and humeral head average 3.12 and 2.90 for male and female subjects, respectively. The radius of curvature of the glenoid cavity and humeral head depends on the presence of cartilage (see Table 2.2). Cartilage decreases and increases the radius of curvature of the glenoid cavity and humeral head, respectively, being thicker at the center of the humeral head and at the rim of the glenoid cavity. As a result, cartilage increases joint conformity ( $\kappa$ ), defined as  $\frac{R_h}{R_g}$  (see the List of Symbols), up to almost 1.

### 2.2.4 Shoulder joint pathology and indications for a shoulder replacement

Shoulder joint pathology can be the result of a trauma (such as due to a traffic accident) or due to progressing diseases (such as osteo-arthritis (OA), rheumatoid-arthritis (RA)), avascular necrosis (AN) and Rotator Cuff (RC) arthropathy. This section only discusses joint pathology due to these four diseases, as they are the main indications for a TSR [141]. X-ray representations of the diseased joints are given in Figure 2.5.

Table 2.1: *Dimensions of the glenoid cavity and humeral head, AP and SI stand for anterior-posterior and superior-inferior, respectively [121, 203] (see Figure 2.4 and the List of Symbols)*

Geometrical parameter	Figure 2.4	Ianotti (1992)		McPherson (1997)
		Mean (SD)	Range	Mean (SD)
$R_h$ (mm)	(AC)	24 (2.1)	19-28	23.1 (2.3)
Humeral head height (mm)	(BC)	20 (2.0)	15-24	-
Humeral neck-shaft angle (°)		45 (5.0)	30-55	141 (8.6)
Lateral off-set (mm)	(FH)	56 (5.7)	43-67	-
$R_g$ (mm)		-	-	32.2 (7.6)
Glenoid height (mm)	(MN)	39 (3.7)	30-48	33.9 (3.9)
Glenoid width (lower) (mm)	(LK)	29 (3.1)	21-35	-
Glenoid width (upper) (mm)	(OP)	23 (2.7)	18-30	-
Glenoid arc of enclosure (AP) (°)		-	-	66 (12)
Glenoid arc of enclosure (SI) (°)		-	-	45.5 (15)
Glenoid trabecular				
Bone depth (AP) (mm)		-	-	20.9 (6.7)
Glenoid depth cavity (mm)		-	-	5 (1.1)

Table 2.2: *Radius of curvature (mean±SD) (mm) of the glenoid cavity and humeral head for male and female subjects, measured with and without the cartilage layer [293]*

Radius of curvature (mm)	Including cartilage		Excluding cartilage	
	Male	Female	Male	Female
Humeral head ( $R_h$ )	26.85±1.40	23.27±1.69	26.10±1.41	23.15±2.09
Glenoid cavity ( $R_g$ )	26.37±2.42	23.62±1.56	34.56±1.74	30.28±3.16

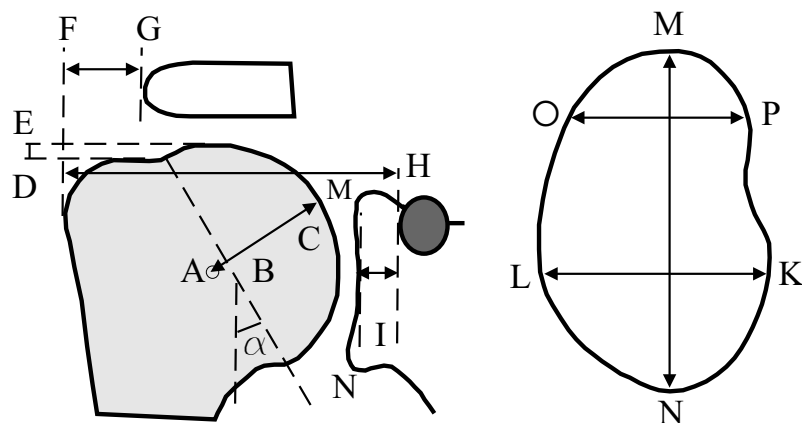


Figure 2.4: Geometrical parameters of the humerus, glenoid and their relation. Adapted from Ianotti et al. (1992) [121]. (see Table 2.1)

*Osteoarthritis* is a bone and cartilage disease, characterized by loss of joint space between the articular surfaces, which can be demonstrated radiographically, humeral head enlargement due to osteophytes and posterior glenoid erosion with accompanying humeral head subluxation, resulting in limited glenohumeral articulation and pain. However, the soft-tissues, such as the RC, are unaffected [335]. The flattened articular surfaces harden proper articulation [207].

*Rheumatoid-arthritis* (RA) is a joint disease, affecting both bone and surrounding soft-tissues, in the glenohumeral joint especially the glenoid cavity, humeral head and the RC muscles [256, 207]. Over time, the disease progresses, thereby weakening the surrounding joint muscles, causing increased humeral head migration towards superior and medial [167]. Different stages of RA (1 through 5) are defined by Larsen et al. (1977) [162], indicating the progress of degradation of the glenohumeral joint. Grade 1 shows minimal deformed bone structures and some muscle weakness, grade 3 shows medium deformed destructive bone abnormalities and radiographic joint space narrowing and stage 5 includes mutilating abnormality where not much is left over from the original articular surfaces [170, 291]. Medialization of the glenohumeral joint is due to erosion of the glenoid bone stock, a result of RC damage with accompanying increased humeral translations [167]. As a result, joint functionality decreases, shoulder pain dramatically increases and the patient is more and more unable to perform 'Activities of Daily Living' (ADL), becomes disabled and becomes dependent on his environment. Unfortunately, most patients are indicated for a shoulder replacement in the end stage of RA [291].

*RC arthropathy* occurs after a RC defect, when the uncovered humeral head cartilage surface is being abraded against the coracoacromial arch (see Figure 2.5c). Over time, the coracoacromial arch becomes excavated and the humeral head erodes to

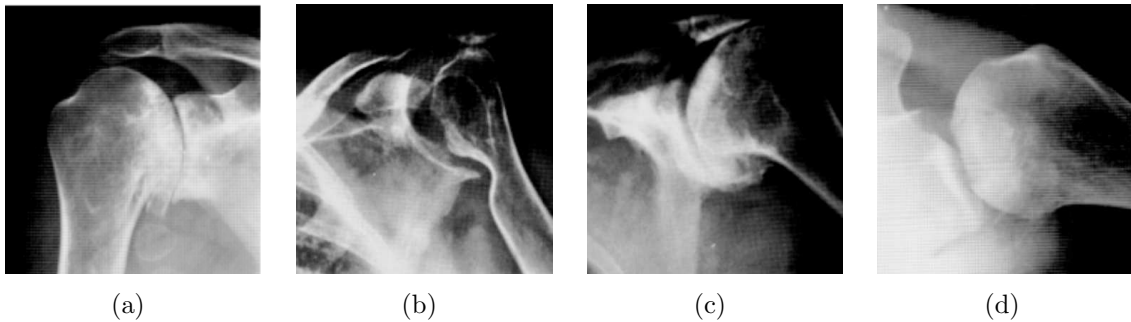


Figure 2.5: *X-ray examples of shoulder pathology. (a) Osteo-arthritis of the shoulder, with a somewhat enlarged and flattened humeral head and peripheral osteophytes. (b) Severely affected shoulder due to rheumatoid-arthritis, with erosion of the subchondral and adjacent bone structures, both of the humeral head and the lateral scapula. (c) Example of RC arthropathy, especially expressed by the severe upward subluxation of the humerus, even against the acromion, which also shows erosion. (d) Osteonecrosis of the shoulder. A collapse of subchondral bone, with humeral head distortion and early glenohumeral arthritis. Adapted from Matsen et al. (1998) [207]*

superior. Furthermore, it is characterized by massive RC tears and by both glenoid and humeral cartilage as well as bone loss. According to Neer et al. (1983), mechanical causes play a predominant role in RC arthropathy [225]. This is also demonstrated by increased glenohumeral instability, as the joint compression force has disappeared [207].

*Avascular Necrosis* is a disease resulting from the temporary or permanent loss of blood supply to the bone cells. Without this blood supply, bone necrosis, or osteonecrosis, occurs. It can, amongst others, be caused by systematic use of corticosteroids, trauma or illnesses with vasculitis. Early stage of this disease is difficult to recognize, as there is no pain or decrease of joint functionality. In a later stage, AN, or osteonecrosis, can be seen on radiographs, as bone density decreases. Next, a fracture of the superocentral subchondral bone may occur with an accompanying later full collapse of the subchondral bone. After that, the irregular humeral head destroys the glenoid cartilage surface, resulting in secondary degenerative joint disease [207, 141] (see Figure 2.5d).

In general, the main indication for a shoulder replacement is pain, followed by excessive decrease of joint functionality and radiographic evidence, when repeated non-surgical methods, such as medication and physiotherapy, were not successful. However, a shoulder replacement can only be successful on the condition that the anatomy allows for a proper reconstruction, meaning that enough bone stock and muscle strength are available. Standardized diagnostic tools can be useful to compare the pre-operative condition of a specific patient with healthy subjects and based

on the results, a decision can be made to perform a TSR or hemi-arthroplasty (HA), in which only the humeral head is replaced [59, 207]. As mentioned above, the main causes for excessive pain and functional decrease as indicated for a TSR or HA are late stage RA, OA, AN and RC arthropathy. These different indications ask for different approaches with respect to surgical treatment and prosthetic components. These will be described in more detail in Section 2.4.2.

## 2.3 Shoulder joint biomechanics

### 2.3.1 Glenohumeral articulation

Motion of the shoulder girdle is a complex ensemble of multiple bone elements and muscles in contrast to the more singular ball-in-socket behaviour of the hip joint. However, the type of articulation of the glenohumeral joint is rather similar, although it receives active assistance of the scapula.

The center of rotation (CoR) of the glenohumeral joint is still a subject of discussion, mainly focusing on its position during articulation [73, 139, 293, 244]. Doorenbosch et al. (2001), Kelkar et al. (2001) and Soslowsky et al. (1992) conclude that the CoR is fixed [73, 139, 293], although Poppen and Walker (1976) state that the humeral head shows small translations, mainly as a result of cartilage deformation [244]. The almost constant CoR in natural glenohumeral joints during humeral movements implies that, if humeral head translations occur, these are the result of external subluxation forces, for example when carrying a bag.

The scapulohumeral rhythm, so called by Codman (1934) [56], explains the combined motion of the humerus and scapula during shoulder motions, especially glenohumeral and scapular rotation during arm abduction. Three phases can be distinguished [251] (see Appendix A for the medical terminology):

- The first phase (about the first 50° of abduction):  
During this phase there is a large variability in the rhythm, although the contribution of the scapula is rather small. This phase is also called the setting phase [122], as during this period the scapula orients itself to the plane of elevation,
- The second phase (from about 50° to 140° of abduction):  
Although this is the most consistent part with respect to the scapulohumeral rhythm, ratios of 1:1.25 [19, 244] to 1:2 [122] are found. It might be that this is more the result of the projection during measurements than true differences in subjects,

- The third phase (from about  $140^\circ$  of abduction to maximal elevation ( $\sim 180^\circ$  [125])):

There is discussion about the contribution of the scapular rotation during this phase. It is found that during this third part of abduction mainly scapular rotation occurs, such as by Bagg and Forrest (1988) [19], although others state that the contribution of the glenohumeral joint is increasing [337].

### 2.3.2 Range of motion

Shoulder functionality is a complex ensemble of bone structures, muscles and ligaments, controlled by neuromuscular input. It must provide enough Range of Motion (RoM) to perform 'Activities of Daily Living' (ADL), pick up forces which can be as high as several times body weight (BW) and still it must be stable to prevent a joint dislocation. The shoulder allows for a large range of motion, approximately  $180^\circ$  abduction,  $50^\circ$  adduction,  $75^\circ$  internal and external rotation and  $120^\circ$  flexion and  $13^\circ$  extension [125] (see Appendix A).

Not much is known about the range of motion necessary to perform ADL. An example is the study of Magermans et al. (2004), investigating the required joint angles to perform 6 common ADL tasks for 24 female subjects, using a six degree of freedom (DoF) electromagnetic tracking device (Flock of Birds) [186]. These tasks required forward- and retroflexion, abduction and adduction as well as internal and external rotation. Maximal humeral elevation, scapula latero and axial rotation angles were measured as well as the plane of elevation. Results are given in Table 2.3.

### 2.3.3 Joint forces and contact area

Not much research has been performed on loading conditions of the shoulder joint and only by using computer models or experimental testing with cadaver material, such as described by [11, 108] and [245], respectively. In the case of a shoulder replacement it would be very interesting to investigate the joint loading similar to studies of the hip joint, in which a telemeterized prosthesis has been used [27].

Although the shoulder is not a weight bearing joint, joint contact forces can reach several times body weight (BW). In literature it is found that arm abduction to  $90^\circ$  results in joint contact forces ranging between  $370\text{ N}$  ( $\sim 0.5$  times BW) [108] up to  $\sim 650\text{ N}$  (0.89 times BW) [245]. Adding weights during abduction, increases the joint contact force up to  $2070\text{ N}$  ( $\sim 3$  times BW) ( $90^\circ$  abduction, straight arm with an additional weight of  $110\text{ N}$ ) [40].

The contact area between glenoid cavity and humeral head during articulation depends on elevation angle and ranges between  $87$  (at  $0^\circ$  abduction) and  $507\text{ mm}^2$  (at  $120^\circ$  abduction), respectively [293].

Table 2.3: *Maximal angles ( $^{\circ}$ ) (Mean (SD), (5<sup>th</sup> percentile, 95<sup>th</sup> percentile)) of the bone elements of the shoulder as found during performing 6 common ADL tasks. The 5th percentile is considered to be the minimal required joint angle [186]. \*Lifting a 40 N bag at 90° elevation*

<b>ADL task</b>	<b>Typical movement</b>	<b>Scapula laterorotation</b>	<b>Plane of elevation</b>	<b>Elevation angle</b>	<b>External rotation</b>
Combing hair	Forward flexion	34.4 (9.4), (19.3, 50.1)	58.5(14.3), (35.7, 80.1)	89.8 (9.3), (73.1, 102.0)	70.2 (18.9), (37.7, 93.4)
Perineal care	Retroflexion	3.8 (7.6), (-7.5, 15.2)	-67.2 (24.3), (-27.5, -87.4)	35.0 (10.3), (20.5, 48.5)	-105.4 (25.2), (-71.1, -131.6)
Eat with spoon	Abduction	25.9 (8.8), (13.3, 39.7)	60.0 (14.4), (36.3, 84.5)	73.5 (12.6), (56.3, 95.0)	49.3 (14.0), (30.6, 74.4)
Reaching	Elbow flexion	33.3 (4.8), (25.8, 37.9)	72.6 (11.7), (57.5, 86.3)	121.4 (6.5), (111.4, 126.4)	60.6 (36.4), (4.7, 91.8)
	Abduction				
Washing axilla	Adduction	29.0 (8.5), (16.2, 40.5)	99.6(8.9), (83.0, 116.8)	53.0 (10.8), (36.6, 124.0)	15.2 (6.8), (0.3, 23.7)
Lifting*	Internal rotation	22.6 (13.2), (3.3, 40.4)	79.2 (18.8), (41.4, 101.2)	63.6(22.8), (33.5, 99.0)	-47.7(25.3), (-76.4, 7.7)

### 2.3.4 Shoulder joint stability

In clinical studies, instability is often referred to as large translations of the humeral head in the glenoid cavity or even as a joint dislocation [31, 193, 350, 353]. In this chapter the same definition is used, whereas in Chapter 4 a more technical definition is given.

For a shoulder to be stable, this implies that any eccentric force should be counteracted by a compensatory force, re-centering the total joint force. Shoulder instability is a problem due to the relatively small and shallow glenoid cavity, which allows for a large range of motion, but only provides small intrinsic stability. The shoulder joint contributes to 45% of all joint dislocations within the human body [138]. In healthy shoulders, stability is guaranteed by passive and active stabilizers as can be seen in Table 2.4. The neural system provides the control of the force balance at different positions and its response depends on the type of movement [104, 342]. This sensory modality, or proprioception, is provided by receptors in articular, muscular and cutaneous structures. A defect in this system, which can be the result of a joint replacement, leads to a deficit in proprioception [342], thereby decreasing shoulder stability.

To a large extent, the RC-muscles will compress the humeral head into the glenoid cavity, thereby centralizing the joint contact force (see Figure 2.2c for the orientation

Table 2.4: *Static, passive and dynamic, active stabilizers of the shoulder [125]*

Static, passive stability		Dynamic, active stability
Soft-tissues	Articular surface	Muscles
coracohumeral and glenohumeral ligaments, labrum, capsule	joint concavity, scapular inclination, intra-articular pressure	Rotator Cuff muscles, m. biceps, m. deltoid

of the RC muscles). In the extreme shoulder positions, the relative stiff ligaments form a more rigid constraint, preventing the humeral head to dislocate out of the glenoid cavity.

## 2.4 Shoulder joint replacements

### 2.4.1 History

A definition of a joint replacement can be derived from the definition of Quinet and Winters (1992):

*'A joint replacement is an orthopaedic surgical procedure, including resection of the convex surface and preparation of the concave surface, after which both can be replaced by a synthetic structure, fixed by bone ingrowth, press-fit or by bone cement [254].'*

The first total shoulder replacement was designed by the French dentist J.P. Micheals and was performed already in 1893 by the French surgeon Péan, 26 years before the first hip replacement. The artificial joint was constructed out of platinum with a rubber ball and allowed for abduction and flexion. Although increased strength and function was obtained, it had to be removed within two years due to an infection [179, 141].

At present, a series of four different anatomical humeral prosthesis designs are developed (see Figure 2.6). In 1955, Neer reported his first results of glenohumeral replacements with the humeral head prosthesis, that he designed in 1951 [223]. The hemi-arthroplasty was indicated to treat a severely comminuted fracture of the humeral head. This design showed its effectiveness and indications increased towards more general joint diseases, such as OA and RA. Since then, the basics of shoulder replacements has not been changed, focusing on reconstruction of the natural

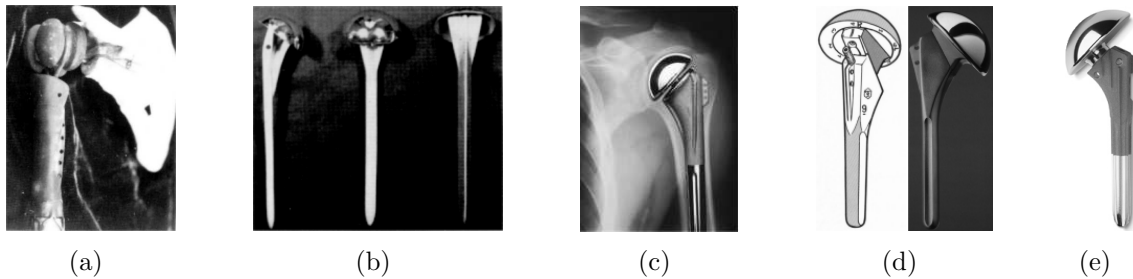


Figure 2.6: Overview of historic shoulder replacements. (a) First shoulder prosthesis, implanted by Péan in 1893. Adapted from Lugli (1978) [179]. (b) First generation modern shoulder prosthesis. Adapted from Neer (1955) [223]. (c) Second generation, example of DePuy. (d) Third generation Aequalis (Tornier) prosthesis. Adapted from Walch and Boileau (1999) [334]. (e) Fourth generation shoulder prosthesis from Centerpulse with a modularity about 3 axes

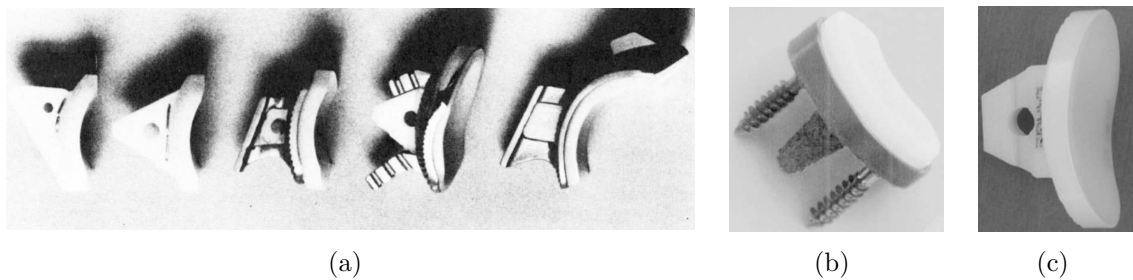


Figure 2.7: Conceptually different glenoid components. (a) From left to right: the original and standard All-Polyethylene component, and the standard sized, 200% and 600% enlarged metal backed components. Adapted from Neer et al. (1982) [224]. (b) and (c) Modern metal backed and All-Polyethylene glenoid components from Biomet and Tornier, respectively

anatomy of the glenohumeral joint [98]. During the following decades research aimed at improving the humeral component with respect to infection, long-term fixation and joint functionality. Neer adjusted his design into the first generation in 1974, with two different head sizes and the use of glenoid components (see Figure 2.7). He reported his outstanding results in 1982 [224]. Second generation humeral head components allowed for better modularity, with separated head and stems. Later, this design was modified and a neck-part was added to allow for better off-set adjustability. With this third generation it was possible to position the head eccentrically on the neck [334]. The fourth generation allows for even more adjustability, with modularity about 3 axes. This concept allows for optimal reconstruction of the anatomy and for correction after misalignment during positioning of the humeral stem [98]. Around 1974 the first glenoid component was drawn and the concept of the 'Total Shoulder Replacement' (TSR) was born [224, 207]. The main design criteria of the

glenoid component was long-standing component fixation and good shoulder functionality, consisting of shoulder stability and a proper range of motion. As will be discussed later in this thesis, there are contradictory design criteria for this component, which may be the background of the post-operative complications. As a result, much research has been done on design improvements, resulting in many designs, all with their own advantages and disadvantages.

To prevent joint instability, constrained or hooded glenoid components were used [76] (see the second right and right component in Figure 2.7a). These components compensate for the eccentric forces, which is in healthy shoulders done by natural stabilizers, such as the ligaments and RC muscles. It may be that pathologic shoulders more and more rely on the constrained glenoid component for shoulder stability, at the expense of the surrounding muscles and ligaments. However, the eccentric (subluxation) force finally has to be transmitted by the fixation of the constrained component to the underlying bone structure. Early loosening led to the discussion to abandon this type of glenoid component (see Section 2.4.6).

Several materials have been used for glenoid components, such as Teflon (Tetra-Fluor-Ethylene), High-Density-Poly-Ethylene and Ultra-High-Molecular-Weight-PE (UHMWPE). Present research is focused on improving mechanical properties of Polyethylene, such as Hylamer, by DePuy Dupont Orthopaedics, Warsaw, IN, to minimize wear rates of, amongst others, glenoid components.

In general, two types of glenoid components are used, the metal backed and the all poly-ethylene component (see Figure 2.7b and c). The metal backed glenoid components consists of a metal shell with a rim, in which the poly-ethylene part is positioned, after it is screwed in the glenoid bone stock to obtain primary fixation. During time, this primary fixation is taken over by bone ingrowth fixation, which is normally achieved within 6 to 8 weeks. The all poly-ethylene component is fixed by Polymethyl-Methacrylate (PMMA) bone cement and is mechanically locked by pegs or a keel. Bone ingrowth fixation is commonly used in young, more active patients, whereas cemented fixation is the standard procedure for older patients, who might have insufficient metabolism, necessary for bone ingrowth fixation.

### **2.4.2 Present used shoulder replacement systems**

At present, several types of shoulder replacements are available. The choice depends on indication and specific joint conditions. Common used prosthesis types are of the anatomical design, mainly indicated for humeral fractures, OA and RA, with the last indication showing most complications when inserting an anatomical prosthesis. Non-anatomical designs are used to improve results of shoulder replacements, especially for the RA patient group, namely the constrained glenoid component [246, 207], the bipolar prosthesis [357, 98] and the reversed prosthesis [98, 82, 356]. If non of the described systems are an option or if a primary

shoulder replacement failed, a shoulder arthrodesis can be performed, in which the humerus and scapula are fused [93, 207] (see Figure 2.8a for an example). This section describes the anatomical Hemi- and Total Shoulder Replacement (TSR) as well as commonly used non-anatomical shoulder prostheses.

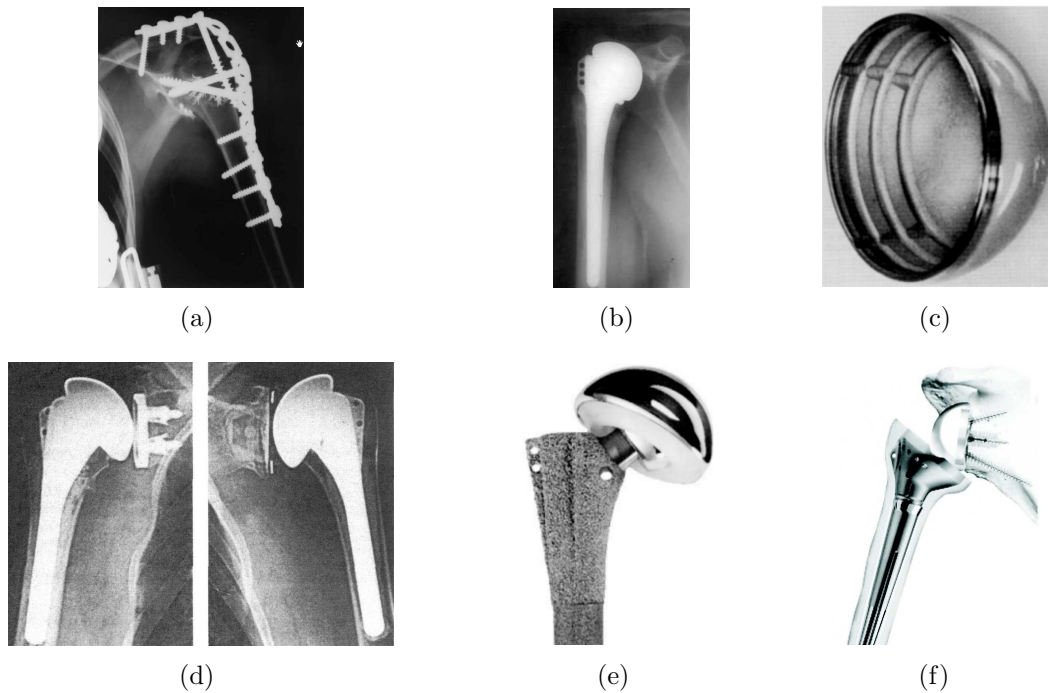


Figure 2.8: *The shoulder arthrodesis and overview of conceptually different shoulder replacement systems. (a) Shoulder arthrodesis. Adapted from Diaz et al. (2003) [68]. (b) Hemi-arthroplasty. Adapted from Kelly and Norris (2003) [141]. (c) Humeral resurfacing implant. Adapted from Levy et al. (2004) [171]. (d) TSR with a press fit humeral component in combination with an uncemented (left) and cemented glenoid component (right). Adapted from Boileau et al. (2002) [34]. (e) Bipolar prosthesis from Biomet Inc. (f) Delta reversed total shoulder prosthesis from DePuy*

### Hemi-Arthroplasty (HA)

When decided to perform a shoulder replacement, using the anatomical prosthesis, the surgeon must choose between a Hemi-Arthroplasty (HA) and a Total Shoulder Replacement (TSR). In some conditions, the TSR shows better results than a HA, with respect to joint functionality, pain relief and stability. However, this must be weighed against the additional complications after inserting a glenoid component, such as glenoid component loosening [141].

A Hemi-Arthroplasty (see Figure 2.8b) is indicated if the radiographic joint space between the articular surfaces is sufficient in an AP view, with the humerus in internal, neutral and external rotation. This space indicates that the anatomical glenoid surface still allows for natural articulation. In healthy glenohumeral joints, this space is approximately 5 mm, but in late stage RA patients, this can decrease to less than 2 mm. Also, in the case of posterior glenoid erosion, a glenoid component should be inserted. Although in many cases it might be better to perform a HA, it must be noted that glenoid resurfacing after a HA is more common than a glenoid revision after a TSR [98, 141]. Additionally, some studies demonstrate that inserting a glenoid component in concentric eroded glenoid surfaces were beneficial with respect to pain relief and post-operative joint functionality [141].

### **Humeral Resurfacing (HR)**

An alternative for a conventional humeral replacement is humeral resurfacing (HR), or surface replacement, using a humeral shell component (see Figure 2.8c). The indications for this surface replacement are the same as for the conventional stemmed prostheses. If not implanted in severely weakened and soft humeral bone, results are comparable with conventional stemmed humeral components [171]. The surface replacement has the advantage of bone stock preservation as well as avoidance of difficulties with inserting a humeral component in the elbow joint, if necessary. However, glenoid component insertion is made more difficult, as less bone is removed from the humeral head, compared to a conventional humeral head replacement.

### **Total Shoulder Replacement (TSR)**

Main indications to also replace the glenoid cavity, which is a TSR (see Figure 2.8d), is osteo-arthritis with posterior glenoid wear. In the case of rheumatoid-arthritis, a glenoid component should not be inserted when irreparable Rotator Cuff (RC) tears are present or if the RC is excessively weakened. Inserting a glenoid component without proper RC function, will lead to early loosening and failure [59, 98, 141] and another replacement must be considered.

In the case of OA, a TSR provides better results than a HA, as found in a multi-center study including 601 patients [74]. In a study of Torchia et al. (1997) 100 patients with 113 shoulder replacements were followed over 15 years. Overall implant survival was 93% and 87% after 10 and 15 years, respectively. 14 complications requiring re-operations were found [320]. A long-term follow-up study in relatively young patients, demonstrated that a hemi-arthroplasty showed slightly worse results compared to a TSR, with a survival rate of 73 and 84% after 15 years, respectively. There is a relation between the chance of a glenoid component revision and the presence of a RC tear [297].

### **Bipolar shoulder replacement**

The bipolar shoulder replacement was first invented by A. Swanson in 1975 [311], where after it was further developed by Biomet Inc. in 1990. The design hypotheses of the bipolar prosthesis are easy surgery, joint stability and minimizing glenoid bone erosion. The bipolar prosthesis consists of a metal shell with a UHMWPE inlay, in which a small metal head is positioned, covered by a constraining ring, leading to an inner and outer bearing (see Figure 2.8e). Depending on the friction and radius of curvature of both articulations, either the inner (Metal-on-UHMWPE) or the outer (metal against the glenoid bone) bearing is articulating during shoulder motions. Ideally, it is the inner bearing, minimizing glenoid and possibly acromion wear. A follow-up study of averagely 2,9 years with 108 bipolar replacements, only showed 8 re-operations, including a revision to a TSR, reinsertion of the humeral stem with cement, a RC repair and reinsertion of a humeral component with larger shell and longer neck length [357].

### **Reversed shoulder replacement**

As stated by Habermeyer and Ebert (1999) [98]:

*'In the case of a weakened or disappeared Rotator Cuff, abduction is still made possible by the Deltoid muscle, if an opposite directed force leads to a fixed center of rotation.'*

This is the basis of the development of the reversed prosthesis (see Figure 2.8f). The reversed shoulder prosthesis is made out of a humeral and glenoid component, but, in contrast to the conventional design, the concave and convex components are reversely positioned on the humerus and glenoid, respectively. An example is the 'Delta' shoulder prosthesis design, developed in 1986 by Grammont (see Figure 2.8f). The Center of Rotation (CoR) is medialized towards the center of the glenoid sphere and positioned to distal, leading to an increased moment arm of the deltoid muscle. Additionally, deltoid muscle pre-stress is improved as the humerus is resected below the insertion of RC muscles, leading to a more superior positioned humerus. Although in a study by Grammont and Baulot (1993) including 14 patients, who are followed for two years after a shoulder replacement by the 'Delta' prosthesis, joint functionality and pain relief clearly improved, complications were multiple. However, taking into account the pathologic condition of the indicated patients in this study, the design shows reasonable results, compared to conventional prosthetic systems [94]. In a more recent study by Woodruff et al. (2003), 17 patients were followed for 5 years after inserting an improved Delta prosthesis. A variable improvement of pain relief and functionality was found, but also radiolucent lines around all humeral components and 5 glenoid components, which is of great concern [356]. Although joint stability clearly improved directly post-operative, this

improvement decreases during time leading to decreased joint functionality. In the case no other surgical options are available and after careful patient selection, the reversed shoulder prosthesis is one of the options to treat excessive deteriorated glenohumeral joints [82]. However, conceptually new prosthesis designs are necessary for patients with lost anatomical stability.

### **2.4.3 The surgical process**

Compared to hip replacements, the shoulder replacement is found more difficult to perform. This is due to the large amount of surrounding delicate soft-tissues, the inferior exposure of the joint, especially of the glenoid cavity, and the limited amount of bone material for proper component fixation, which requires accurate surgery and proper alignment tools. Only the lateral glenoid of the scapula is visible and approachable from lateral, which complicates the application of conceptually new fixation methods.

A common procedure is the so called 'Deltopectoral approach', but also the 'Transacromial' and 'Posterior approach' are used [207]. For the Transacromial approach, an incision near the acromioclavicular joint and an osteotomy of the acromion allows for a view on the glenohumeral joint, whereas for the Posterior approach an incision near the acromion, towards posterior and medial to the spine of the scapula and a resection of the deltoid tendon on the scapula is necessary. For the Deltopectoral approach, after a skin incision, the deltoid is divided without detachment and the glenohumeral joint is exposed after opening the joint capsule.

Gentle external rotation and slight extension shows the humeral articular surface. Humeral head osteotomy must allow for an anatomical reconstruction using available humeral components, without cutting near or even below the cuff insertions (see Section 2.2), which describes the insertion locations of the RC muscles in the two tuberosities of the proximal humerus). Using trial humeral components, the exact patient specific humeral head diameter, height and, if the component allows for this, off-set and eccentricity can be determined, as well as detailed preparation of the humerus. It must be validated that the lateral and superior position of the humeral head is equal to its original anatomy, using the trial component. Additionally, it must be ensured that enough post-operative range of motion can be achieved, without joint impingement.

The aim of the glenoid replacement is reconstruction of the glenoid cavity, which requires complete and accurate bone support for good fixation of the glenoid component. By using unaffected landmarks, the surgeon must orientate the affected glenoid articular surface so, that an eventual correction can be made. This reconstruction can normally be achieved by using a spherical reamer, which creates an optimal support for the glenoid component. Further preparation of the glenoid surface might be necessary, depending on component design. The selected glenoid component must

cover the maximal amount of the prepared bone, without overhanging. This should be rigorously checked by the surgeon, by applying an eccentric force on the glenoid, which may not show any tilting  $\lambda$  (see the List of Symbols). After cleaning, a small amount of cement can be inserted, so that there is direct glenoid to bone contact at the glenoid surface. The component must be kept in position by the surgeon until the cement has hardened.

After non-absorbable sutures are placed in secure bone and the range of motion is validated again, the humeral stem and head component can be inserted. After checking the joint rigorously for debris and foreign material, the joint and wound are closed. In the case of RA, the same procedure as above is used, but special care should be taken because of the fragile tissues. The surgeon must be aware of sufficient tissue laxity and enough bone volume for long-term glenoid component fixation. If there is any doubt, a glenoid component should not be inserted [207] and the surgeon should switch to a HA or a non-anatomical prosthesis (see Section 2.4.2 and Figure 2.8).

#### **2.4.4 Facts on shoulder replacements**

The results in terms of long-term survival rates are quite good, with 84% survival after 15 years [297, 353]. This number is similar to survival rates of hip and knee replacements, which are often remarked as excellent, with survival rates of 85% after 15 years for hip replacements [174] and 90% after 10-15 years for knee replacements [178], respectively. However, comparison of survival rates of shoulder replacements with hip and knee replacements fails, due to the large difference in post-operative functionality. The post-operative functionality after a TSR is unsatisfactory as 'activities of daily living' can not always be performed [105], leading to a relatively low number of annual loading cycles with accompanying relatively low forces [185]. In contrast to this, hip and knee joints allow for a sufficiently large post-operative range of motion [131] and undergo a high number of load cycles with higher forces due to the need of walking. Within the same 15 years, these joints have undergone a much more intensive load spectrum compared to artificial shoulder joints and therefore these joints performed much better in terms of component fixation. Additionally, the number of complications after a TSR is large, with 14% complications within 12 years, although these complications do not always have to lead to surgical interventions [353]. Shoulder replacements in RA patients, in general, show lower survival rates than in OA patients [254].

The number of annual shoulder replacements in 1997 in the USA (11.000), is far less compared to hip and knee replacements (280.000 and 338.000, respectively). Also, it is found that in the case of the shoulder joint, the 2 replacements per surgeon per year is much smaller than for hip and knee replacements, with 13 and 15 annual replacements per surgeon, respectively [1]. This has a direct effect on surgical expe-

rience and quality and, therefore, on the results of the replacements, as investigated by Kredel et al. [153]. The worse results of shoulder replacements, compared to hip and knee replacements might be a result of the lower number of replacements per surgeon.

### 2.4.5 Complications after shoulder replacements

Unfortunately, complications after a TSR are multiple and involve both the survival rates as well as post-operative functionality (see Figure 2.9). Loosening of the humeral component is very uncommon and clinical findings are rare, but present [353]. However, stress shielding, frequently found after a hip replacement, can be demonstrated after a shoulder replacement. A relation was found between the diameter of the humerus, the humeral stem size and the occurrence of stress shielding. In the group showing stress shielding, a relative large stem size was used [221] (see also Figure B.2 in Appendix B).

Glenoid component loosening is one of the main complications after a TSR [353, 105]. In a study of Hasan et al. (2002), who investigated unsatisfactory total shoulder replacements, 59% showed glenoid component loosening [105]. Clear difference must be made between a loosened glenoid component and radiographic loosening, indicated by radiolucent lines around the glenoid component. Radiolucent lines are small gap openings at the interface of the fixation of the component and, although this is difficult, they can be detected at radiographs [220]. These radiolucent lines can already be present soon after the surgery, but can be stable or progressive and therefore long-term radiographic control is necessary [291].

Several studies demonstrate glenoid component wear [110, 353]. One of the reasons behind the high rates of glenoid component loosening might be the small UHMWPE particles, as they cause osteolysis, which is a disease, affecting the bone formation cells [149]. As a result, the bone-implant interface weakens and implant loosening might occur rapidly. By using FE simulations, it is found that contact stresses exceed the UHMWPE yield strength during abduction and is more pronounced in metal backed components [309], which might be due to UHMWPE deformation and wear. Additionally, due to rim deformation and worn glenoid components, the stabilizing function of the component is disturbed.

In general, joint functionality increases after a shoulder replacement, although not always sufficiently to perform all ADL. Especially tasks requiring high abduction angles, such as combing hair and reaching, can not be performed. It is possible to apply compensatory mechanisms using clavicle retraction, providing additional humeral external rotation, needed for higher elevation angles. However, these compensatory mechanisms might cause problems in other joints, which will finally affect the total motion of the shoulder girdle. The problem behind bad post-operative joint functionality is probably the lack of RC function [186].

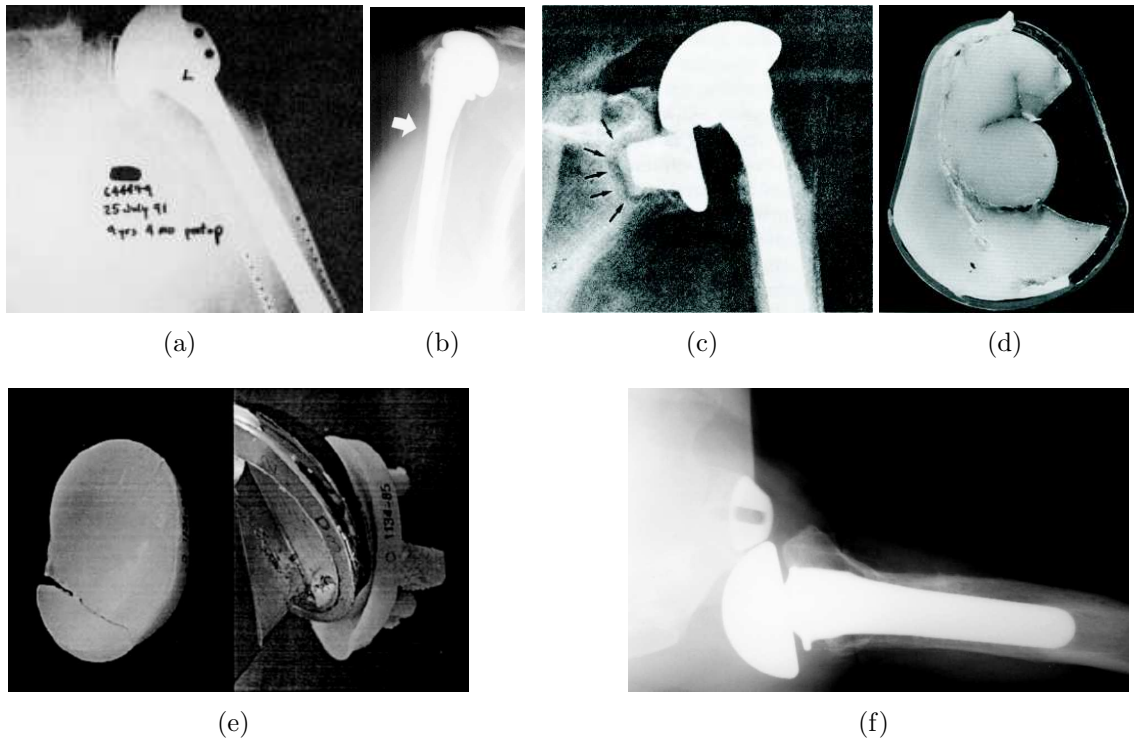


Figure 2.9: Overview of common complications after a shoulder replacement. (a) Humeral component loosening. Adapted from Wirth and Rockwood (1994) [352]. (b) Image, taken 7 years after a hemi-arthroplasty, clearly demonstrates bone resorption in the proximal-lateral region. Adapted from Nagels et al. (2003) [221]. (c) A loosened cemented glenoid component, with an unstable humeral head, in superior direction. Adapted from Wirth and Rockwood (1996) [353]. (d) An excessive worn glenoid component showing secondary, metal-on-metal wear. Adapted from Wirth and Rockwood (1996) [353]. (e) A failed glenoid component, with a secondary facet matching the humeral radius of curvature  $R_h$  (left), with a deformed inferior rim, maybe caused by abutment of the humeral stem (right). Adapted from Hertel and Ballmer (2003) [110]. (f) SI view, demonstrating posterior instability after glenoid component revision. Adapted from Sanchez et al. (2003) [273]

## 2.4.6 Design of the shoulder prosthesis

Design of shoulder joint implants is, next to the patient factor, the surgery and post-operative care, one of the four factors, influencing the results of shoulder replacements. Shoulder prosthesis design involves the design concept, geometry, design details, materials, production technique and method of fixation. Meanwhile, the surgery and the shoulder anatomy are part of the design process, as they form boundary conditions with respect to implantation, dimensions and functionality.

### The humeral component

In this thesis, the humeral component is not discussed in detail as the focus in this study is on the glenoid component; at present still the main site of complications [353]. As mentioned before, anatomical reconstruction is the main design goal of the humeral replacement, which can be achieved by adjusting prosthesis geometry and dimensions.

An example is the lateralization of the humerus, that is the distance FH in Figure 2.4. Excessive lateralization hardens insertion of the prosthetic components, as the joint is difficult to close by the surrounding capsule and also muscle attachment might become difficult. Both difficulties lead to a tight joint, which might also result in decreased post-operative joint functionality. Additionally, the moment arms of surrounding muscles might decrease, leading to higher muscle and joint forces [166], which is not beneficial, certainly not for the weaker patient group. Unfortunately, in a study by Pearl and Kurutz (1999), investigating four commercially available prosthetic systems, none of the systems was able to identically replace the anatomical head and an averaged total displacement of the CoR of  $14.8 \pm 6.5$  mm was found [238]. However, the new fourth generation humeral components show a big improvement, as the head can be adjusted around three axes and positioned eccentric on the humeral stem [98]. Thereby, the humeral head can be adjusted to the patients specific anatomy and for corrections during surgery, if necessary.

Humeral fixation can either be cemented, fixed by bone-ingrowth or by press-fit. All methods are used and long-term fixation easily outperforms that of glenoid components.

Stress shielding decreases bone thickness or density at specific locations (see Chapter 3 and Appendix B) and is recognized as a late complication after shoulder replacement [221]. Both humeral stem design and material selection influence this phenomenon. It is either made out of CoCr or Titanium, of which the latter has the advantage of better matching the flexural properties of the underlying bone material (see Appendix B). Stem length can also be adjusted to decrease stress shielding, as a shorter stem leads to a more proximal load distribution into the anatomical humerus. Another option is the use of a so-called 'isoelastic' humeral component, made out of composites, which allows for better matching the flexural properties of

the humerus [270]. In the 90's, much research was focused on these composite materials to be used for orthopedic applications and, although even at the time of writing composites for in-vivo applications in orthopedics are still under investigation, no follow-up study is available.

### **The glenoid component**

The main goal of the glenoid replacement is to provide a good, long-standing articular surface, with better orientation than the natural, pathologic surface and good pain relief. Only cemented glenoid components are discussed as the uncemented components are not being investigated in this thesis.

Glenoid components consist of a concave proximal and commonly a convex distal surface, with a radial thickness ranging between 4 and 7 *mm*. Component thickness influences the contact stresses, affecting the wear rate [309] and ease of insertion of the prosthetic components (in general, a thicker component is more difficult to implant, as it tightens the joint). Main geometrical design parameters are the radius of curvature  $R_g$ , constraint angle  $\theta_0$  and thickness (see the List of Symbols).

At the distal side, design details such as a keel, pegs and grooves must improve cemented fixation of the component (see Figure 2.10). There is still a continuing discussion whether keels or pegs should be used. In an extensive comparison study by Lazarus et al. (2002), including 39 keeled and 289 pegged glenoid prostheses, it was concluded that pegged glenoid components showed better cementing, indicated by better cement filling and better surface matching between bone and the glenoid component, although the surgeon might play an important role in the procedure [164]. In an experimental study by Anglin et al. (2000) it was found that a curved backing outperforms a flat backing, which might be due to the fact that the joint contact forces are transmitted into the underlying bone more by compression than by shear [13].

The discussion about using cemented or uncemented glenoid components (see Figure 2.8) is still continuing. The advantage of uncemented glenoid implants is the self-regenerating fixation, whereas the increased total component thickness hardens surgery and tightens surrounding soft-tissues. Additionally, dissociation of the UHMWPE inlay is sometimes found [339]. Although there are groups who abandoned uncemented glenoid components [34], others couldn't find a difference [338]. The constrained glenoid component is developed to create stability in the glenohumeral joint in the case of RC pathology [246] (see Figure 2.7a). This constrained glenoid component prevents the humerus to translate in superior direction during abduction. The occurring eccentric forces will now be transmitted by the component into the underlying bone, harming glenoid component fixation. However, there is probably not sufficient bone stock behind the constrained glenoid component to completely cover the backside, as required for a TSR [207]. During time, the shoulder more and more relies on this constraint angle for joint stability, at the expense

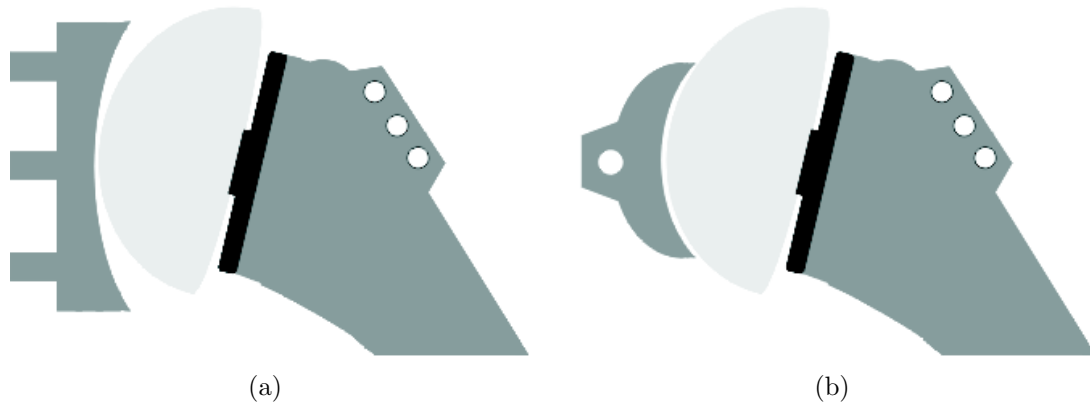


Figure 2.10: *Schematic representations of two conceptually different glenoid components. (a) A large, non-conform, unconstrained, pegged glenoid component with a flat backside. (b) A small, keeled, conform, constrained glenoid component, with a curved backside*

of glenoid component fixation. Even in case of accurate patient selection, complications are multiple [246, 247] and recent follow-up studies of the constrained glenoid replacement were not found. Wirth and Rockwood question the efficacy of the design, even as a salvage procedure. Although the constraint design prevents shoulder instability, not all design criteria are taken into account. It may be that during time eccentric forces are more and more carried by this component and early loosening is the result. From a biomechanical point of view, they state that there is a design error and that glenohumeral forces are underestimated [353]. The design dilemma, between improved joint stability and component interface loading still is unsolved and is a problem especially in patients with a weakened or disappeared RC, such as in the case of RA and RC-arthropathy.

Glenoid component wear is the result of the joint compression force, translations of the humeral head relative to the glenoid surface and is furthermore influenced by material properties, surface geometry and roughness. The most frequent used material for glenoid components is UHMWPE, extensively investigated in the past (see Chapter 8). Although not recognized as very important, wear is an occurring problem and the optimal geometry is still not found, although conform articulations may be beneficial [110, 309].

## 2.5 Conclusions

Due to the many commercial prostheses available on the market, it is clear that the optimal prosthesis design is still to be found. However, as a result of the many influencing factors, such as joint anatomy and pathology, patient characteristics,

surgical difficulties, experience and approach, post-operative care etc., it is a challenge to clinically evaluate the effectiveness of a (conceptually) new design. This also applies for comparing clinical studies to find out how the four factors influence the results after a shoulder replacement and how to find a better design, to improve the post-operative results.

However, some conclusions can be drawn. Although survival rates are comparable to hip and knee replacements, often referred to as excellent, post-operative joint functionality is inferior, especially for the patient groups with severe rheumatoid-arthritis and Rotator Cuff-arthropathy. Additionally, the main complication in all patient groups is glenoid component loosening. In future, these two shortcomings after a TSR should receive most attention, especially focusing on the surgery and the design of the prosthesis components, keeping in mind the still available and lost anatomical structures of the patient. A future design is necessary, providing enough joint functionality and solving the problem of shoulder instability, with a long-lasting fixation technique.

For the designer of prosthesis' components, the patient characteristics and many surgical aspects are a given. However, component design still allows for many adjustments and improvements, including component fixation and surgical alignment tools.

Component geometry, such as conformity and constraint, with respect to the glenohumeral relationships and fixation, is one of the design aspects to improve the TSR. Component material is another design aspect to improve results of the TSR, although it takes more effort to implement, as it has to fulfill standardization requirements which ask for an extensive test and validation program. Next to this, the design concept should not be fixed early in the design process. In the case of severely destructive glenohumeral joints, it may be worthwhile to let go the anatomical design and to search for conceptually new designs.

## Chapter 3

# The hip, knee, ankle joint and their replacement



*Stretching of some joints of Patricia Moreno during her routine in the floor exercise finals, Olympic Games, Athens, 2004*



## 3.1 Introduction

The number of shoulder replacements (11.000 in 1997 in the U.S.A) is much smaller compared to hip and knee replacement (280.000 and 338.000 in 1997 in the U.S.A, respectively), which is also reflected in the research on these two joint replacements. On the other hand, the ankle joint replacement is still far from successful and is not a common procedure. This chapter describes the anatomy, biomechanics and orthopedics of the hip, knee and ankle joint to learn a lesson to be used for shoulder prosthesis design. Although joint replacements in these three joints have to deal with different requirements as compared to joint replacements in the upper extremities, many design issues are similar. The lower extremities are different in that they are weight carrying joints, with many repetitive high loading cycles due to walking activities. However, joint replacement aspects such as diagnoses, joint biomechanics and post-operative complications show similarities. Subsequently, the hip, knee and ankle joint will be discussed.

## 3.2 The hip joint

### 3.2.1 Anatomy

The hip, or *articulatio coxae*, is a relatively constrained and thereby stable joint, where the proximal femoral head articulates against the deep acetabulum in the pelvis (see Figure 3.1). The acetabular labrum covers the femoral head beyond its maximal diameter. The femoral head and acetabulum slightly deviate from the pure spherical shape, best fitting in maximal retroflexion, that is in the position for comfortable standing [265].

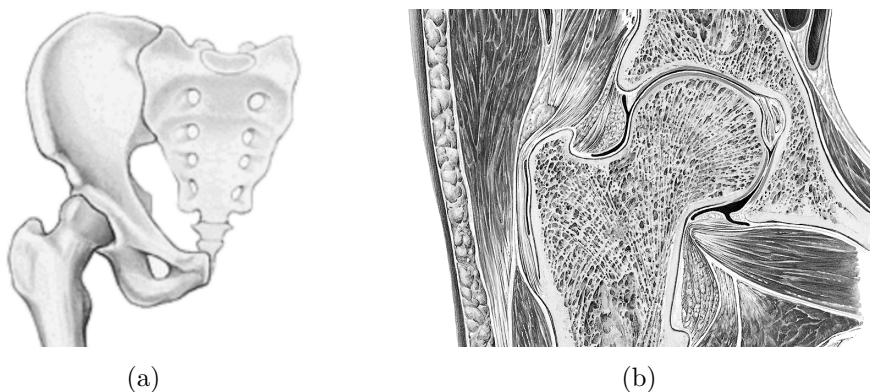


Figure 3.1: *The hip joint (articulatio coxae). (a) Frontal view on the hip joint. (b) Anterior section of the hip joint. See Figure C.2a in Appendix C for a color representation. Adapted from Sobotta*

### 3.2.2 Biomechanics

#### Joint articulation

The hip joint is seen as a 'ball-in-socket' joint, with a fixed center of rotation (CoR) during articulation, thereby it has three rotational degrees of freedom. However, the position of the CoR influences the muscle moment arms and forces and thereby also the hip joint contact forces. A more superior, lateral and posterior located CoR will increase the hip joint contact forces [298].

#### Joint Range of Motion

Ante- and retroflexion, which are articular rotation about the medial-lateral axis are maximal  $120^\circ$  and  $13^\circ$ , respectively, abduction and adduction, that is rotation about the anterior-posterior axis, is maximal  $40^\circ$  and  $20^\circ$ , respectively, and exo- and endorotation are  $13^\circ$  and  $36^\circ$ , respectively. Maximal angles of the femur may be slightly larger, due to cooperation of the pelvis [265], similar to the scapulohumeral rhythm in the shoulder girdle (see Section 2.3).

#### Joint forces and articular area

First in-vivo force measurements are done by Rydell (1966), resulting in contact forces between 2.3 and 3.3 times body weight (BW) during walking [269]. Static joint forces were measured by Davy et al. (1988), in which was found that double limb stance resulted in a contact force of 1 times BW, single limb stance in 2 times BW and during the stance phase of gait 2.8 times BW [66]. The joint reaction forces during slow walking and stumbling were 3 times BW and 8.7 times BW, respectively, which was measured by a telemeterized prosthesis [27]. A later, much more extensive study by Bergmann et al. (2001) resulted in a complete load spectrum of the hip joint, although the number of patients was limited to four [28]. In that study, maximal joint reaction forces occurred during walking and stair climbing, with magnitudes of 2.4 times BW and 2.5 times BW, respectively. Except for stumbling, no higher forces are found during ADL. Implant torques, which is the moment about the stem axis, were found to be 19 Nm during stair climbing. In pathological joints, forces and moments can be substantial higher, as less optimal muscles are activated with probably smaller moment arms [28]. Using a mathematical model, Komistek et al. (1998) calculated hip, knee and ankle forces during walking, by data obtained from a human cadaver. The results show somewhat lower values compared to the measurements, ranging between 1.9 and 2.6 times BW, depending on gait speed [152]. A comparison between patients with a hip implant and control subjects showed a lower walking speed in patients, due to a lower cadence and stride length, resulting in lower joint contact forces [298]. The surface area of the acetabulum without and including the acetabulum labrum is  $2880\text{ cm}^2$  and  $3680\text{ mm}^2$ , respectively [313].

## Joint stability

The hip is one of the most stable joints of the body, a result of the deep acetabulum and surrounding ligaments. As a result, not much is mentioned in literature about anatomical hip joint instability.

### 3.2.3 History of hip replacements

It wasn't before 1850 that good surgical procedures were available to perform a joint replacement, as that was the time of the introduction of anesthesia methods and antiseptic techniques (sterilization methods). Many ideas were tried out, starting in the late nineteenth century, all focusing on removing the articulating surfaces, simply by resection and replacing, interposition of other materials and the first trials of the present endo-prosthesis [305]. First trials of treating patients with joint diseases in hip and knee existed in the form of interposition of materials between the articular surfaces. Subsequently, muscle and fascia tissues have been used in 1902 [217, 218], pig's bladder in 1918 [18] and fascia lata in 1920 [45, 181]. Next, arthritic treatment was also done by resection of osteophytes<sup>1</sup> and reshaping of the articulating structures [282], although results were not very encouraging [287].

Parallel and as a continuation of the interposition concept, the replacement of the articular surface with other (mostly synthetic) materials have been investigated. Subsequently, ivory in 1890 by Gluck [92] and rubber by Delbet in 1919 [304] have been used to replace materials. Glass, a brittle, inert material, also has been used, although it was not able to withstand the high hip forces and fractures were found frequently [288]. From the late 1930's, stainless steel was applied in joint prostheses [206, 317, 349]. Smith-Petersen was advised by Venable et al. (1937) [327] to use Vitallium (a Cobalt-Chromium-Alloy) as replacement material and he used this in 500 replacements between 1938 and 1948. This was continued by other surgeons, who performed 1000 hip cup-replacements until 1957 with 85% good results [17]. McKee developed a metal-on-metal prosthesis, which was supposed to be fixed by Methyl-Methacrylate, but not before the collaboration with Watson-Farrar and their bone cement [239, 304] (see Figure 3.2). Unfortunately, a good RoM without impingement could not be obtained with this design and little was done to improve it and as a result the metal-on-metal designs were abandoned for a long period [9]. In 1952, Haboush used two cups to replace both the femoral head and acetabular articular surface, which were fixed by (probably the first time in history) acrylic cement [99]. Townley (1964) continued this concept by subsequently better reshaping the femoral head and fitting the femoral cup onto an intramedullary stem in 1952. This prosthesis was later used in combination with an acetabular component, first made of polyurethane (1960), later of polyethylene (1977) [321]. Tronzo,

---

<sup>1</sup>little, though painful, deformed or grown bone spots, e.g. due to a changed stress distribution

in the late 1960's, used a polyethylene ball articulating against a metal acetabular component. It was first press-fitted into the acetabulum, as there was no acrylic cement available at that time in the USA, later they were all cemented [282, 304]. In the period between 1960 and 1970 this concept has been used more extensively. Although results of this concept showed high failure rates, research was and is still going on [22, 302, 303]. In 1969, the first sintered stainless steel stem was implanted, which actually is the first bone ingrowth prosthesis [282]. Finally, Sir John Charnley must be credited for the development for what we now call 'modern joint replacement' (between 1958 and 1963). He started with Teflon (Tetra-Fluor-Ethylene) for application in the acetabular component, but this material showed high wear rates. The introduction of High-Density-Polyethylene (HDPE) improved the results of the joint replacements dramatically [47] and presently used designs are still based on this material [239, 282, 305] (see Figure 3.2). In a more recent study it was found that Teflon showed 1.600 times higher wear rates than the presently used Ultra-High-Molecular-Weight-Polyethylene (UHMWPE) [201].

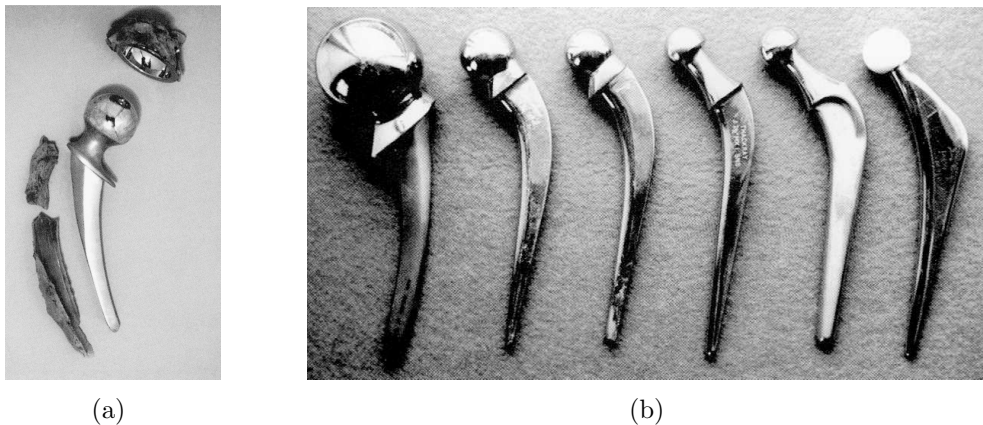


Figure 3.2: *Example of historical hip prostheses. (a) The McKee hip prosthesis (1951). (b) Development of the Charnley hip prostheses including the modern hip prosthesis with a ceramic head (most right) [148]*

### 3.2.4 Facts

In the USA, 280.000 hip replacements were performed in 1997 on a population of 285 million [174], whereas at present worldwide 1 million hip replacements are being performed annually [148]. In The Netherlands 30.000 hip and knee replacements are performed annually on a population of almost 16 million. This implies that approximately 2% of the Dutch population have a replaced hip or knee, assuming a rather conservative survival rate of 10 years [118].

Indications for hip replacements include osteo- and rheumatoid-arthritis, avascular necrosis, traumatic arthritis, certain hip fractures, bone tumors, bone deformities or Paget's disease<sup>2</sup> and ankylosis spondylitis<sup>3</sup> [229]. Radiographic evidence and persistent pain are a requisite for a hip replacement. Contra-indications include active infections, poor medical conditions (which can decrease the results of the hip replacements), obesity [229, 254], neuropathy and significant peripheral vascular diseases [254].

Post-operative improved patient satisfaction is significant, especially with respect to pain relief, improved quality of sleep, and improved walking ability [131] and many other important social aspects [348]. However, although walking velocity might increase and motion characteristics become more natural, post-operative functionality never returned to natural level [174]. Hip replacements show survival rates (when symptomatic aseptic loosening was clear or revision replacement had to be carried out [254]) of about 97% after 8 years [102], 93% after 10 years and 85% after 15 years [174].

As survival rates of hip replacements are good, the different available designs are limited to anatomical designs. At present, the femoral resurfacing, the conventional total hip and the bipolar prostheses are used (see Figure 3.3).

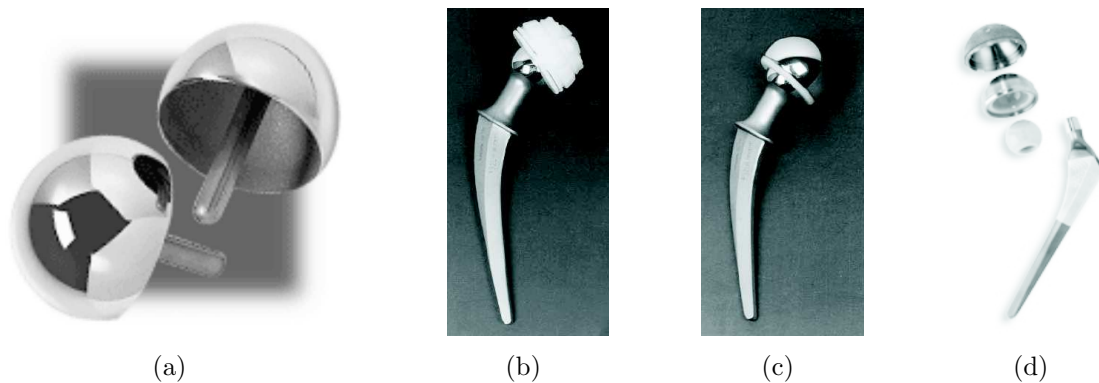


Figure 3.3: Overview of presently used hip prostheses. (a) The ReCap<sup>™</sup> Femoral Resurfacing System from Biomet Inc. (b) Lubinus total hip endoprosthesis (Link, Hamburg, Germany) [290]. (c) The Vario-Cup bipolar hip endoprosthesis (Link, Hamburg, Germany) [290]. (d) The Trident<sup>®</sup> Ceramic Hip System (Stryker, Kalamazoo, Michigan, USA)

<sup>2</sup>excessive breakdown of bone tissue, followed by abnormal formation of low quality bone, resulting in pain and joint stiffening

<sup>3</sup>stiffening of the joint due to inflammation

### 3.2.5 Complications

As hip replacements are very routine surgeries, intra-operative complications (such as bone fracture, misalignment) as well as short-term post-operative complications (such as infection, dislocations) are very rare nowadays and mainly only long-term complications occur [118].

Focused on design aspects, the following complications, which may finally lead to revision surgery, are of importance: joint instability (dislocation), acetabular wear, stress shielding, component loosening and component failure, such as dissociation or fracture of both components and wear through of the acetabular component (see Figure 3.4).

According to Morrey (1997) and Scifert et al. (1999) joint instability occurs in 2-3% and 2-11% after primary hip replacements, respectively [211, 276]. It is more pronounced in the case of females and elderly and is furthermore influenced by acetabular and femoral component design [211] (see Figure 3.4a). After revision surgery, instability rates increase significantly to 5-25% [276].

Acetabular wear, the result of relative movements between the compressed soft concave and hard convex surfaces, is a slow but clearly progressing process in load carrying joint replacements and is a major complication after hip replacements (see Figures 3.4b and c). Linear wear rates in the order of magnitude of 0.05 and 0.1 *mm/year* for molded and machined UHMWPE, cemented acetabular components, respectively, were found by Bankston et al. (1995) [21]. In general, metal backed acetabular components show higher wear rates, as also demonstrated by Perez et al. (1998). A linear wear rate of 0.25 *mm/year* was found, which is rather high compared to other studies [240]. It is generally known that wear particles cause bone osteolysis, which accelerates component loosening [118, 198, 258, 260] (see Figure 3.4d). As prosthesis design has been improved and last longer, this is becoming a more important issue. Not only because of component failure, but also due to bone loss which finally will result in component loosening [198].

Stress shielding (see Figure 3.4d), is the result of taking over the load carrying function of the natural femoral head by the femoral component (see section 3.5 and Appendix B). It is a long-term complication after primary hip replacements and can be a serious problem in the case of revision surgery. All available prosthetic hip systems show stress shielding [266].

Component loosening of both the femoral and acetabular component is still an issue after hip replacements. A distinction must be made between radiographic and clinical loosening, which can be twice as high for radiographic loosening [254, 213]. There is a large spread in the number of complications related to component loosening, as it is influenced by many aspects and many different definitions of loosening are being used. Using component displacement and reorientation, such as subsidence, as a criterion for component loosening, then the loosening rates are between 7.5% after 5-12 years and 11% after 12-15 years [213], although a revision surgery was

not always necessary. Radiographic evidence of loosening was high in cemented hip replacements, with 20% and 30-40% reported femoral loosening after 5 and 10 years, respectively, whereas the acetabular component showed much lower loosening rates, although progressively increasing after more than 10 years FU [65].

Using revision surgery due component loosening as a criterion, not more than 2% of the acetabular component loosened after more than 10 year [232]. After 20 years, 16% femoral revisions due to loosening were found by Soyer et al. (1997) [294], whereas another study showed 11% acetabular component loosening after a mean of 6 years, which is a high number compared to other studies. The authors relate this to the design of the component [132]. If subsidence is used to define loosening, then 11% cemented cups loosened within 12-15 years and 10% loosened within 10-14 years FU, whereas only 7.5% of the non-cemented cups loosened within 5-12 years FU, as reported by [213]. Cemented femoral prostheses show better results than non-cemented ones, in terms of patient score, pain relieve and component subsidence [71]. One main problem of non-cemented femoral stems is the need for good bone ingrowth during the first 6 to 8 post-operative weeks. If good bone ingrowth fails, a fibrous tissue network will grow between implant and bone and during the first months stem migration will occur. This migration seems to be a good predictor for late loosening [118, 144].

Dissociation of the acetabular or femoral components, that is the undesirable disassembly of the modular components, is rare nowadays, although it might still happen (see Figures 3.4e and f). In a large study of Heck et al. (1995) including over 60.000 hip replacements, 0.15% of the acetabular components dissociated and 0.26% of the femoral heads dissociated from the femoral stem after a median of 5 years FU [107]. Component fracture also is rare (see Figures 3.4g and h), as metal alloys and component design have been improved in the last decennia. In the study of Heck et al. (1995), an incidence of femoral stem fracture of 0.27% was found [107].

The above mentioned complications must not be seen as the result of single acting failure mechanisms. Many mechanisms are involved in the damaging process, triggering or activating each other in a chain of failure mechanisms, where the increasing damage is an evolving process [118].

## **3.3 The knee joint**

### **3.3.1 Anatomy**

At the knee, or articulatio genus, four bones come together, namely the femur, tibia, fibula and the patella, forming the largest joint of the body, consisting of three ar-

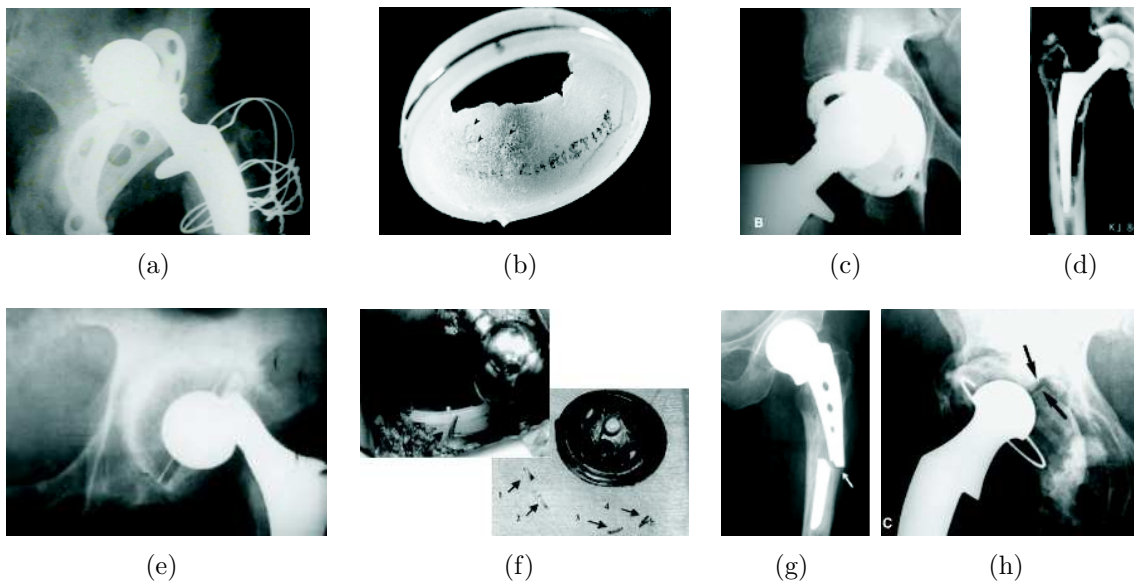


Figure 3.4: *Complications after Total Hip Replacements. (a) Femoral head component dislocation [347]. (b) Severe wear through acetabular component, probably due to the presence of cement particles [198]. (c) Femoral head off-set change due to acetabular component wear [190]. (d) Femoral and acetabular component loosening after severe stress shielding and osteolysis [6]. (e) Femoral component dissociation after rising from a chair. (f) Acetabular component failure due to dissociation. (g) Stem fracture in non-cemented hemi-arthroplasty. (h) Acetabular component failure due to fracture [190]*

tifications (see Figure 3.5). The main articulation is between the medial and lateral condyles of the femur and tibia, that is the tibiofemoral joint. The patellofemoral joint, which is the gliding articulation between the patella and the patellar groove of the femur, results in an increased moment arm of the quadriceps muscle and protects the tibiofemoral articulation. The fibula is actually not a part of the knee, as it is connected at the *facies articularis fibularis* at the inferior part of the proximal tibia, although it contributes in weight bearing. The tibiofemoral articulation is separated by the medial and lateral menisci. These menisci deepen and enlarge the articular surfaces (thereby they are load carrying to a large extend and probably assisting the ligaments in knee joint stability [2]) and improve lubrication and cushioning [86, 127]. The knee joint contains four ligaments, of which the main function is to control knee stability. The anterior and posterior cruciate ligaments of the knee (ACL and PCL, respectively), named after their location of fixation at the tibia (see Figure 3.5), prevent the tibia from extensive sliding forward and backward on the femur, respectively [277]. At full extension, the ACL is taut, tends to rotate the tibia and limits overextension.

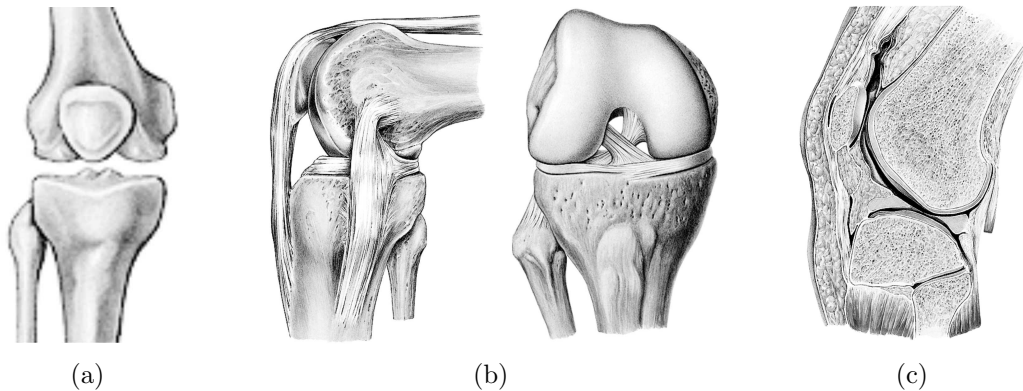


Figure 3.5: *The knee (articulatio genus). (a) Frontal view on the knee joint. (b) Medial (left) and anterior view on the knee joint. See Figures C.2b and c in Appendix C for color representations. Adapted from Sobotta*

### 3.3.2 Biomechanics

#### Joint articulation

Knee joint articulation is more than rotation about a fixed hinge with a non-constant medial-lateral (sagittal) axis. It involves a complex kinematic system of rotations and translations during knee flexion. Until recently, it was assumed that during knee flexion the femur moves from front to back on the tibia, known as 'roll-back' [32]. However, at present it seems that the knee, behaves like a ball-in-socket joint about its medial condyle, while the lateral side moves from front to back, rotating around the center of the medial side [32, 188]. This is also confirmed by Freeman and Pinskerova (2004), although from  $120^\circ$  to full flexion they state that both femoral condyles roll back on the tibia [83].

#### Joint RoM

Maximal knee flexion, that is articular rotation about the non-constant sagittal axis, is  $160^\circ$  according to Rozendal [265], although others found a slightly smaller maximal flexion angle of  $150^\circ$  [180]. Maximal knee stretching leads to a small enforced axial 'end-rotation', consisting of exo-rotation of the tibia or endo-rotation of the femur. In the flexed knee, axial rotation of the femur and tibia is made possible. Endo-rotation is very limited, but exo-rotation can vary between  $0^\circ$  and  $60^\circ$  [265].

#### Joint forces and articular area

Tibiofemoral joint contact forces can be very high, during level and downhill walking up to 6 times BW and 8 times BW, respectively [160]. Iso-kinetic (constant angular

velocity) prescribed motions were measured in healthy subjects by Baltzopoulos [20] and Kellis [140]. The maximal joint compression and subluxation forces were 7.53 times BW at  $30^\circ/s$  ( $80^\circ$  knee flexion) and 3.89 times BW at  $90^\circ/s$ , in posterior direction, respectively [140]. Maximal patellofemoral joint compression forces can be much larger. Level and downhill walking can result in 1.8 times BW [230] and 5 times BW to 7 times BW [159], respectively. During high demanding tasks, e.g. during jumping and weightlifting, patellofemoral joint forces can be as high as 12 times BW and 20 times BW, respectively [160].

The articular surface area of the tibial plateau and femur are 2250 and 2950  $mm^2$ , respectively [293]. The articular contact area of the tibiofemoral joint with intact and damaged menisci can reach 1150  $mm^2$  and 520  $mm^2$ , respectively, indicating their importance [86]. The contact area in the patellofemoral joint depends on articular angle, but can be as high as 5.800  $mm^2$  [115].

### **Joint stability**

Knee joint stability is achieved by the anterior and posterior cruciate ligaments (ACL and PCL, respectively). Without limiting normal knee articulation, certain fiber bundles of the ligaments are always tensioned, pulling the convex femoral condyles into the concave tibia condyles. In the extremes of knee articulation they prevent the femoral condyles from excessive translations or from a dislocation [265].

### **3.3.3 History of knee replacements**

Knee replacements started with simply resection of the whole knee in 1861, which resulted in a good Range of Motion (RoM), but also in a lack of joint stability [79]. Meanwhile, also soft-tissue interposition was tried out (see the history of hip replacements). Verneuil in 1860 and later Murphy in 1913 used fascia lata with subcutaneous fat interposition, of who especially Murphy obtained good results [218, 331]. In 23 knees, chromicized pig bladder was positioned between the two articulating surfaces of the knee. In the 1920's this concept was continued by the use of prepatellar bursa [44] and fascia lata by Albee [4] and Osgood and Wilson [248]. Speed and Trout (1949) reported 44.6% good results in 65 treated knee joints [296] and Miller and Friedman (1952) had 30% good results in 37 treated knee joints [205]. Nylon also has been used as interposition material, which showed good early results, although the material deteriorated in a later stage [154, 248]. In general, the concept to interposition material between the articular layers was not satisfactory [305]. Also in knee joints debridement has been used, although somewhat later than in hip joints, which is a more conservative treatment in which osteophytes were resected. Although in 1940 Haggart used this method as one of the first [100], Magnuson was credited for popularising this method of treatment [182]. Results were encouraging,

in the case of correct indications and good post-operative care [305]. Thereafter, the focus was more on resurfacing of articular surfaces, beginning with the distal femur in 1940 by Campbell. He used Vitallium plates, screwed to the femur, which showed poor results [46]. Smith-Petersen used another design, which evolved by other surgeons into a stemmed femoral component, which was used frequently but never obtained good results [127, 323]. Replacements of the tibia had their origin in the 1950's, adjusted to fit with the two condyles and showed satisfactory results [182, 200, 257, 321]. Already in 1960 a hinged knee prosthesis has been used, a design in which the tibia and femoral components are connected by a hinge, only allowing for rotation about the sagittal axis (flexion and extension) [340] (see Figure 3.6a). This design was especially indicated in the case of patients with an unstable knee [261]. Another popular hinged prosthesis, the St. George hinged prosthesis, was implanted in a relatively large number of patients in Europe and the United States [305]. The modified hinged prosthesis design of Shiers [283] was used on a large scale in England [305]. Relatively bad results of eight hinged prosthesis after five years follow-up were reported by Young of the Mayo clinic [363]. Later designs did not show better results and especially loosening was frequent. The main issue of this hinged design is that rigidly fixed components experience high stresses, as the hinge is a constraint for translations and rotations between femur and tibia, as occurring in the natural knee joint. However, hinged knee prostheses are still being used, especially in patients suffering from knee instability [261]. The basis for the presently used Total Knee Arthroplasty also has its origin in the 1960's when Gunston together with Sir Charnley implanted two metal runners on the femoral side, articulating against two grooved polyethylene inserts [96] (see Figure 3.6b). Although the four cemented components were difficult to align and didn't lead to natural knee joint kinematics, the results were satisfactory compared to earlier used components. Improved instruments led to more accurate insertion, but didn't give the desired results and better designs were needed [39, 41]. At the Hospital for Special Surgery (HSS) (New York) unicondylar prostheses were developed and implanted, but they showed poor results. Therefore, the duocondylar prostheses were developed, which actually consisted out of two connected unicondylar prostheses, fixed by bone cement. These designs only allowed for simple kinematics, actually only flexion and extension, which led to high loosening rates as they had to act as a constraint for the other motions. During this period, the patella-femoral joint was not taken into account, which could have improved the results dramatically [305]. The poor results, difficulties with component alignment and soft-tissue treatment were the motivation to improve the designs. Coventry implanted two femoral components linked by a bar and two tibial trays joined by an anterior bar, to preserve the cruciate ligaments (see Figure 3.6c). Although early results were promising, so that it was even considered to be the first true total knee prosthesis, on the long-term component failure occurred and the patellar-femoral joint gave problems. In these designs, natural knee kinematics could still not be obtained and future designs

had to be better. A big step forward was done by Walker, Ranawat and Insall at the HSS, with the total condylar knee replacement (see Figure 3.6d). They used one-piece, cemented components together with new instrumentation, resulting in reproducible insertion [123, 124]. The design concept has not been changed since then and shows excellent functionality and good component survival [305, 333].

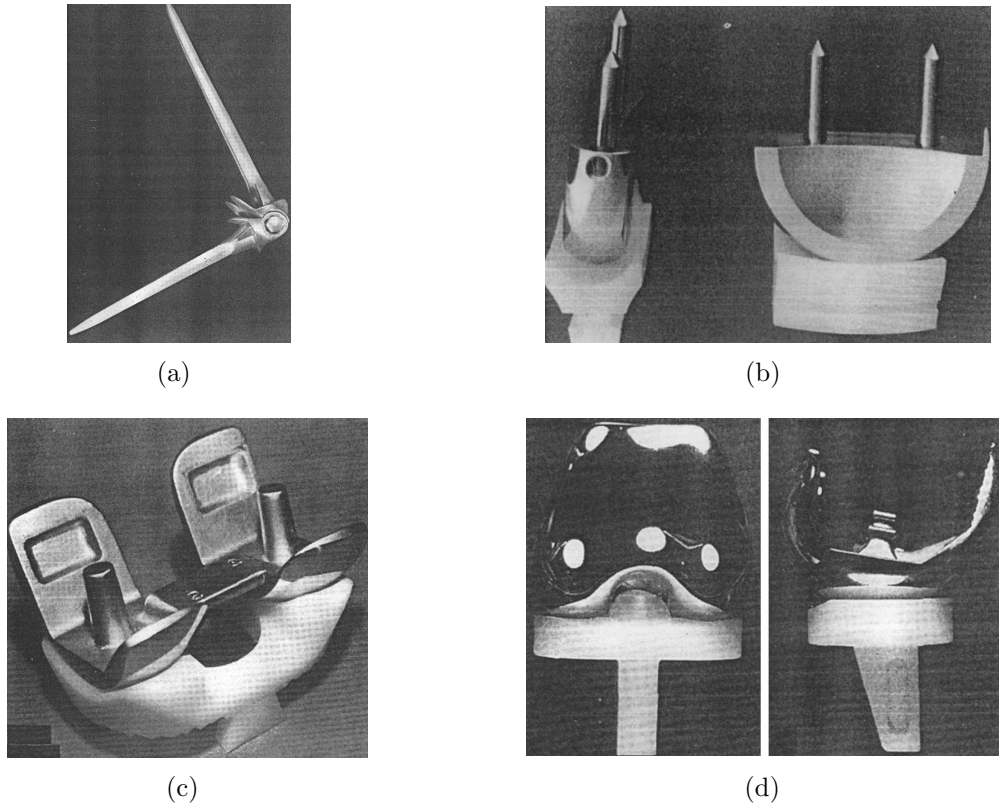


Figure 3.6: *Examples of historical knee prostheses. (a) The Young hinged prosthesis (1960), fixed with cortical screws through the femoral and tibial components. (b) The polycentric knee (1960), consisting out of four cemented components, which preserved the cruciate ligaments. (c) The Geometric total knee replacement (1970) (d) The total condylar prosthesis (1974). All Figures are from [302]*

### 3.3.4 Facts

Knee replacements lagged behind hip replacements until the 1990's, when results start to improve and nowadays in the USA even more knees than hips are being replaced, which will become a global trend. 338,000 knee replacements were carried out in 1997 [1] and this number still increases every year [3]. Indications for knee replacements are very similar to hip replacements, such as osteo- and rheumatoid-arthritis

(OA and RA), avascular necrosis (AN), traumatic arthritis and correction of significant deformities. Radiographic evidence and persistent pain are determinative for a knee replacement, as patients, who do not have significant loss of joint space, tend to be less satisfied with their clinical result after total knee replacements [229, 254]. Contra-indications include active infections (knee sepsis), poor medical conditions (affecting anesthesia and post-operative results), obesity [229, 254], neuropathy and significant peripheral vascular diseases [254].

In general, 90% of the knee replacements last for about 10-15 years [178], although this number depends on the specific indication. Patients suffering from RA, in general, show lower survival rates than OA patients. An example is a 6 year follow-up (FU) study, showing 83% and 95% good results in RA and OA patients, respectively [254]. A large study, including 9200 arthroplasties followed for 15 years showed 97% survival at 10 and 15 years. This high number is due to some favorable parameters, as it were primary replacements, patients were older than 60 years and metal backed condylar tibial components were used [254].

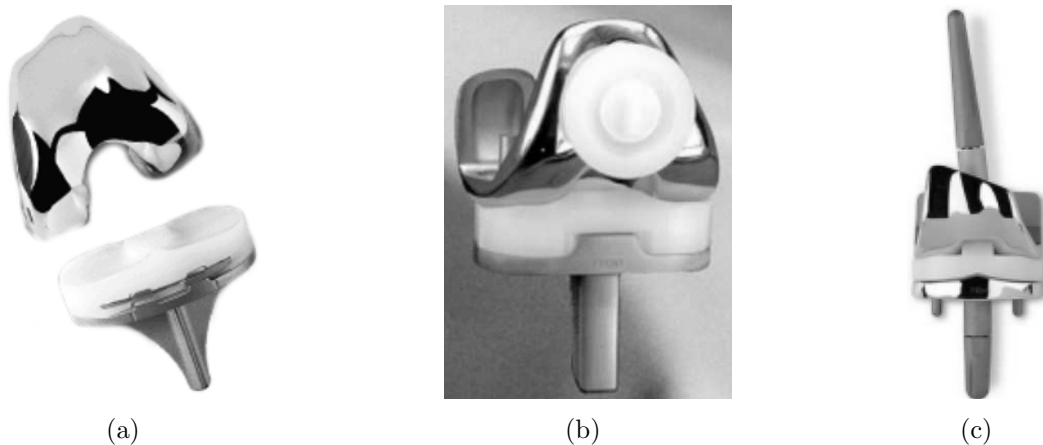


Figure 3.7: *Examples of presently used knee prostheses. From left to right: Biomet posterior constraint, Sulzer kinematic total knee, Biomet anatomic graduated component*

### 3.3.5 Complications

Complications after knee replacements related to prosthesis design include wear, fracture and loosening of the femoral, tibial and patellofemoral component as well as knee instability.

Most frequent are patellofemoral joint complications, in the form of tendon rupture, instability, component dissociation or loosening, resulting in anterior knee pain [178, 254]. The main cause for patellofemoral joint complications is bad functionality of the knee extensor mechanism.

Wear is a failure mechanism in knee replacements, which is the result of improved longevity of knee implants (see Figure 3.8a and b). It is studied extensively in retrieval [88, 199] and by wear simulation studies [332]. After a successful replacement, revision due to completely worn components is still very uncommon, although revisions of tibial components due to osteolysis of the underlying bone is seen more often [42].

Not as frequent as in hip replacements, also in femur components after knee replacements stress shielding occurs [118, 169], which finally may lead to fracture, component failure and loosening [118, 241]. In one study, 44% bone loss after 1 year was found above the femur component, which can lead to periprosthetic fracture and failure of the femoral component [241].

Component loosening still is a problem in knee replacements [198, 254, 316], especially in stabilizing prostheses. For example, within 2 years post-operatively, 6 out of 107 (5.6%) revisions due to acetabular component loosening in RA patients were found [316].

Component fracture in TKA is frequently described and is mainly a result of material shortcomings [54, 312] (see Figures 3.8c and d, which demonstrate fractured femoral and acetabular components, respectively). Tibial component fracture in primary and revision TKA occurred in 0.26 and 0.72% of the replacements, respectively. Furthermore, component fracture is design depended, for example by introducing stress concentrations, as found in an extensive study including 7683 TKA's [54]. Knee instability (see Figure 3.8e), is the result of several factors, including surgical factors (soft-tissue treatment, component selection and positioning), patient factors (joint pathology) and design factors (conceptual design, wear of especially the tibia component) [263].

## **3.4 The ankle joint**

### **3.4.1 Anatomy**

The ankle joint, or *articulatio talocruralis*, is a complex kinematical system of the tibia, fibula and the talus (see Figures 3.9 and 3.10). The talus fits into the 'mortise and tenon' type of joint, formed by the distal tibia and the medial and lateral malleoli, resulting in a very stable joint. The ankle joint is normally referred to as the joint between the distal end of the tibia and the superior talus, the tibiotalar joint [160]. Contrary to other mammals the ankle joint of the human is guided by a rim on the talus, which separates the tibia and the fibula sliding tracks. Together with the subtalar joint (the articulation between the talus and the calcaneus) these joints act as a two axis articular joint. The talus is a passive bone element, no muscles are attached to it and it only undergoes compulsive movements.

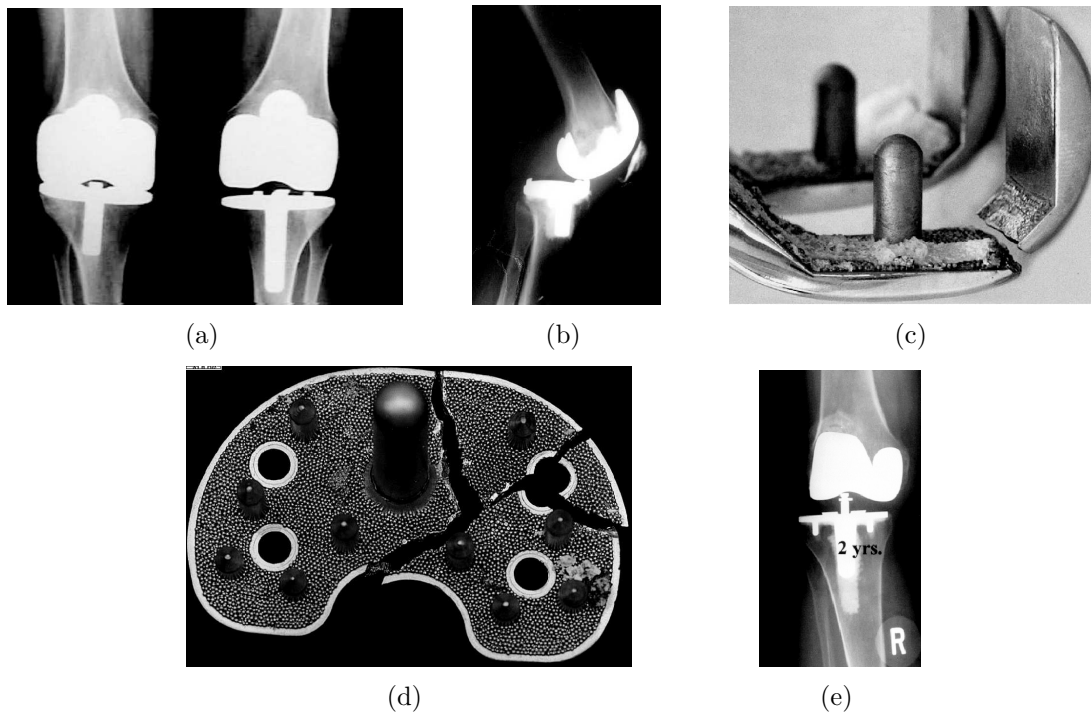


Figure 3.8: *Complications after Total Knee Replacements. (a) Excessive wear of a tibial component (left) vs. direct post-operative situation. (b) Unstable TKA due to polyethylene wear, implanted with posterior stabilizing knee components [263]. (c) Fracture of a femoral component [312]. (d) Fracture of the medial part of a tibia metal backing [312]. (e) Dislocated TKA, implanted with a posterior stabilizing knee component [89]*

### 3.4.2 Biomechanics

#### Ankle joint articulation

Although the ankle joint is often referred to as a single axis, dorsiflexion and plantarflexion hinge, multiple joint motions are possible and the axis orientation may slightly vary [103, 150, 228]. This is due to the anatomical shape and the surrounding soft-tissues. The non-constant axis of rotation is due to the glide-slide character of the tibiotalar joint and the difference in radius of curvature of the distal tibia and talus [24, 228, 341].

#### Joint RoM

The ankle joint allows for dorsi- and plantarflexion, that is articular rotation about the non-constant saggital axis. In standing position, maximal dorsiflexion is  $30^\circ$  [180] and maximal plantarflexion is  $60^\circ$ , although both joint angles might show a large

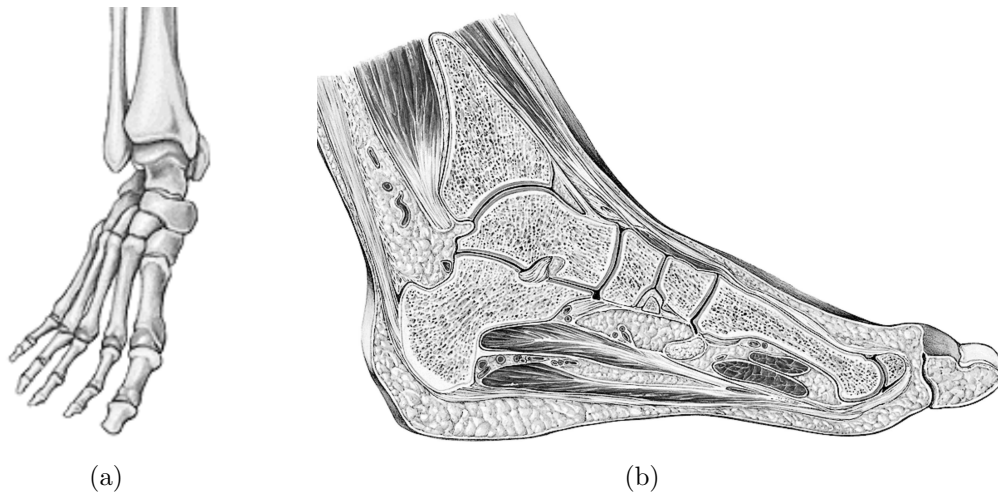


Figure 3.9: *The ankle joint (articulatio talocruralis). (a) Frontal view on the foot, including the ankle. (b) Medial-lateral section of the ankle joint. See Figure C.2d in Appendix C for a color representation. Adapted from Sobotta*



Figure 3.10: *X-ray of the ankle joint. (a) Medial-lateral (b) Anterior-posterior. Adapted from Sobotta*

variation [265]. Two other main joints of the foot are the subtalar joint, allowing for eversion and inversion, that is articular rotation about the superior-inferior axis, and the tarsal joint, allowing for supination, that is the articular combination of plantar flexion, tarsal inversion, and forefoot adduction and is the opposite of pronation (see Figure A.1, in Appendix A).

### Ankle joint forces and articular area

Forces at the ankle joint were measured using force plates by Stauffer et al. (1977), including 5 healthy subjects, 9 diseased subjects, pre-operatively and 6 of them also post-operatively. During level walking the subluxation force reached 0.36 times BW for all subject groups, whereas the maximal joint compression force was 5.5 times BW and 3 times BW for both the healthy and pre- and post-operative patients [300]. In a 3D joint model of the lower extremities (including 4 bone segments, 47 muscles, 3 joints, an inverse dynamic solution procedure and optimization for muscle redundancy) ankle joint forces exceeded 4 and 10 times BW during walking at 1.5 *m/s* and running at 5 *m/s*, respectively [91].

The large contact area of the ankle joint is due to the fact that it is the most conform joint in the body [284] and in cadaver measurements it is found to be 1408 *mm*<sup>2</sup> (by summing the medial, center and lateral area) [156].

### Joint stability

The anatomical ankle joint is very stable, as a result of the cooperation of three articular surfaces (tibiotalar, the medial malleolus and talus and the lateral malleolus and talus) with the ligamentous and muscular structure [228].

### 3.4.3 History of ankle replacements

The history of ankle joint replacements is not that extensive as for the hip and knee joint. In general, more conservative treatments were applied, such as adjusted shoes, orthoses and, if surgery was really needed, than it wasn't an replacement. Debridement has been used, such as removal of osteophytes from the tibia and talus. And mostly, patients with a pathologic ankle joint were treated by an arthrodesis, in which the ankle joint is fused [24, 100] (see Figure 3.11). If performed well, the patient is pain free and has a stable ankle joint [305], which can occur in 59% to 75% of the treated patients [35, 191, 196]. Already in 1878, the first ankle arthrodesis was described [60] and thereafter more than 30 techniques have been presented, indicating the difficulty of this surgery. Complications included infection, skin wrinkling, nerve injury and non-union of the bone elements [100, 191]. However, after an arthrodesis, patients need a long period of immobilization, ankle joint stability is not always achieved and natural gait pattern is disturbed [227]. This leads to excessive stressing of other joints of the ankle as well as the knee joint [305] and also high pseudo-arthritis, infection rates and pain were found, leading to multiple joint problems [24, 114].

The disadvantages of ankle arthrodeses in combination with good results of hip and knee replacements increased the motivation for the development of ankle prosthe-

ses [114, 305]. The first described ankle prosthesis was the St. George Bucholz [146], followed by many others. In general, they consisted out of a metallic, convex and high-density polyethylene concave component, fixed by Polymethyl-Methacrylate (PMMA) bone cement in the talus and distal tibia, respectively. Reversed and 'ball-in-socket' implants also existed.

As also seen in knee prosthesis design, there was (and still is) a design conflict. On the one hand, a constrained/conform device provides good joint stability but on the other hand it shows high loosening rates as it acts as a constraint for the joint translations and multiple rotations. The unconstrained device has better long-term component fixation and mobility, but is also more painful and could lead to joint impingement. Ankle replacements are difficult as demonstrated by the type and number of complications, such as wound healing problems and deep infections. Furthermore, post-operative motion was limited, pain was still present and fracture of both malleoli occurred. Despite these complications, early post-operative successes (less than 5 years FU) showed a survival rate of 80-85%, which unfortunately rapidly decreased thereafter to 35-75% at more than 5 years FU [97]. Especially young (and thus more active) patients, who have undergone previous foot surgery, showed bad results. 62 Imperial College London Hospital (ICLH) implants were followed for an average period of 5.5 years and 21% failed and required attempted arthrodesis and not more than 21% had a satisfactory outcome [35, 292]. Very poor results were reported by Wynn and Wilde (1992), discussing 36 constrained Conaxial ankle replacements, of which 27% loosened at 2 year, 60% at 5 year and 90% at 10 year. As a result, it is recommended not to use this prosthesis anymore [292, 359]. These results were not very encouraging and ankle joint replacements dropped, although they have been taken up again not long ago, based on semi-constraintness, but unfortunately follow-up doesn't exceed 5 years and quality judgment of presently used prosthesis will take more time [3, 60, 97].

#### **3.4.4 Facts**

In 1995, 5.000 Total Ankle Replacements (TAR) have been carried out in the USA, which is negligible compared to the number of hip and knee replacements in that year (246.000 and 312.000, respectively) [1].

Indications for a TAR were expanded in the 1970's to RA and severe pathologic ankle joints and also for traumatic arthritis [228]. Unfortunately, not so long ago, FU with longer durations have shown extensive fall in results of the TAR and some groups even advised to not implant ankle prostheses [35, 325, 359]. Recently, interest increased and early results seem more promising [228, 305], although follow-ups of more than 5 years are scarce. However, some ankle prosthesis designs are commercially available (see Figure 3.12).

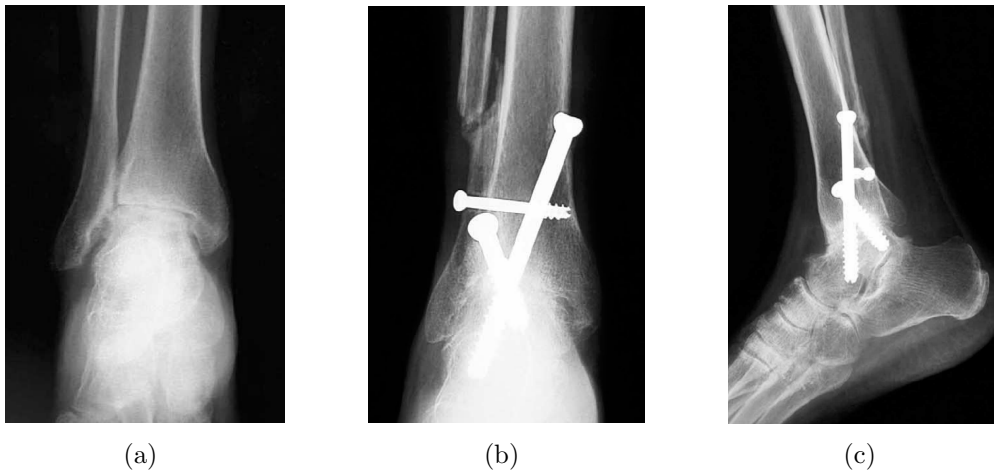


Figure 3.11: *Examples of a successful ankle arthrodesis [38]. (a) Pre-operative anteroposterior radiograph showing ankle arthrosis. (b,c) Post-operative anteroposterior and medial-lateral radiographs*

Contra-indications for an ankle replacement are talus necrose, deep infections in or around the ankle joint, severe osteoporosis and arteriosclerosis, a charcot joint, difficulties after malleo-resections, inevitable risks of high post-operative joint loads (e.g. due to psychiatric or neurological disorders) [151].

Ankle replacement is behind hip and knee replacement with respect to development, which can be seen clearly from the results. Two remarks should be made when describing the results of the ankle replacement, namely the more pronounced distinction between results in terms of direct post-operative improvement of the ankle joint and long-term survival of the replacement and the large spread in results. Direct post-operative improvement, in terms of pain relief and RoM can be considerable, as described in the study of 40 patients by Rudigier et al. [267]. The direct post-operative Kofoed ankle score, which is determined by the level of pain, mobility and joint functionality with a maximum up to 100, increased from 34.75 to 91.25 and persistent pain relief disappeared in every patient. Post-operative RoM of only five patients was less than  $25^\circ$  and even 14 patients had normal ankle flexion of  $40$  to  $60^\circ$  for 4 years. Whereas pre-operative 23 patients were able to walk not more than 1 km, post-operative this number of patients decreased to only 2. But unfortunately, post-operative complications occurred relatively short after implantation, including wound edge necrosis, infections which required component removal and a continuing bone ossification for which an arthrodeses was necessary [267]. In the kinematical study by Stauffer et al. (1977), ankle motions during walking were compared between healthy, pathologic and treated ankle joints, showing  $24.4^\circ$ ,  $19.5^\circ$  and  $23.1^\circ$  flexion, respectively. The general walking pattern was maintained for diseased and operated ankles, as were the ankle joint subluxation forces (0.36 times BW), but

the joint compression forces decreased from 4.5-5.5 to 3 times BW [300]. Results of the study about the Mayo constrained ankle prosthesis are investigated, including 160 replacements, indicated for rheumatoid-arthritis, post-traumatic osteo-arthritis and osteo-arthritis for 60, 35 and 5%, respectively [150]. The mean post-operative RoM was  $5^\circ$  and  $19^\circ$  dorsi- and plantarflexion, respectively, with a large scatter. Complications were found in 19 replacements, including superficial and deep infections, malleolar fracture, migration of the wire from the tibia, dislocation of the tibia, component ulceration of the medial aspect of the ankle, and additionally 94 re-operations had to be performed, because of serious complications. After 17 years, 57 replacements failed at an average of 4.4 years and they recommended to stop using this specific ankle prosthesis design [150].

Recent studies show promising more results. In a study from Doets et al. (2005), in which 76 patients underwent 93 ankle replacements with a mobile-bearing total ankle prosthesis showed a survival of 90% and 48%, in the case of neutral ankles and ankles with a varus-valgus deformity, respectively [72].

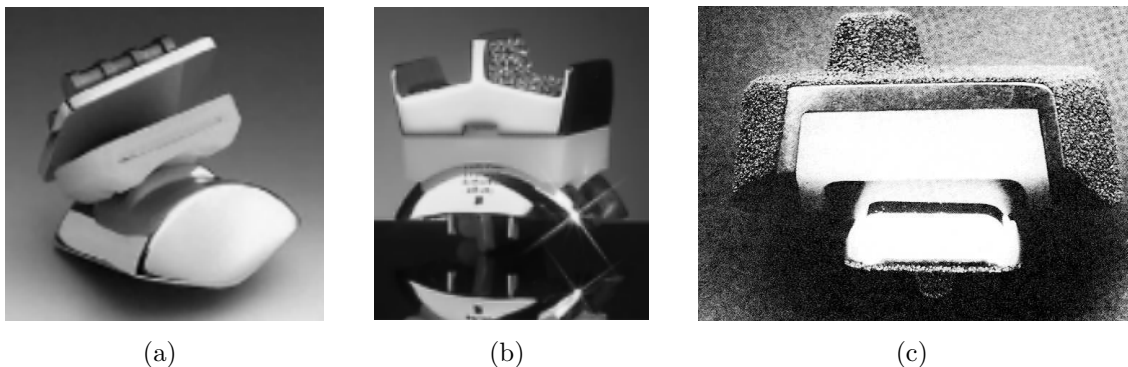


Figure 3.12: *Examples of presently used ankle prostheses. (a) The mobile bearing, semi-constrained STAR ankle (Scandinavian total ankle replacement). (b) The ESKA total ankle replacement. (c) The constrained agility ankle implant (dePuy)*

### 3.4.5 Complications

Compared to hip and knee replacements, less information is found in literature about complications of ankle joint replacements, although the percentage of complications is far more. It is recommended to not use the ankle Mayo constrained ankle prosthesis, as not less than 36% of 204 ankle replacements failed, defined by component removal [147]. Post-operative complications include superficial or deep infections, wound healing difficulties, malleolar fractures, dislocation of the talar component,

ulceration of the medial aspect of the ankle joint [147, 269], wound edge necrosis, infections leading to component removal, a continuing ossification resulting in an arthrodesis, component damage [267] and aseptic loosening of the components, mainly in constrained and cemented components [172, 269] (see Figure 3.13). Ankle instability is also mentioned as a complication, especially in the unconstrained designs [172]. According to Michelson et al. (2000), all ankle replacements concepts show good results in the first 2 to 3 years, whereafter a rapid decline of survival rates is demonstrated, including implant loosening, pain and component failure, leading to recommendations against the general use of ankle replacements [204].

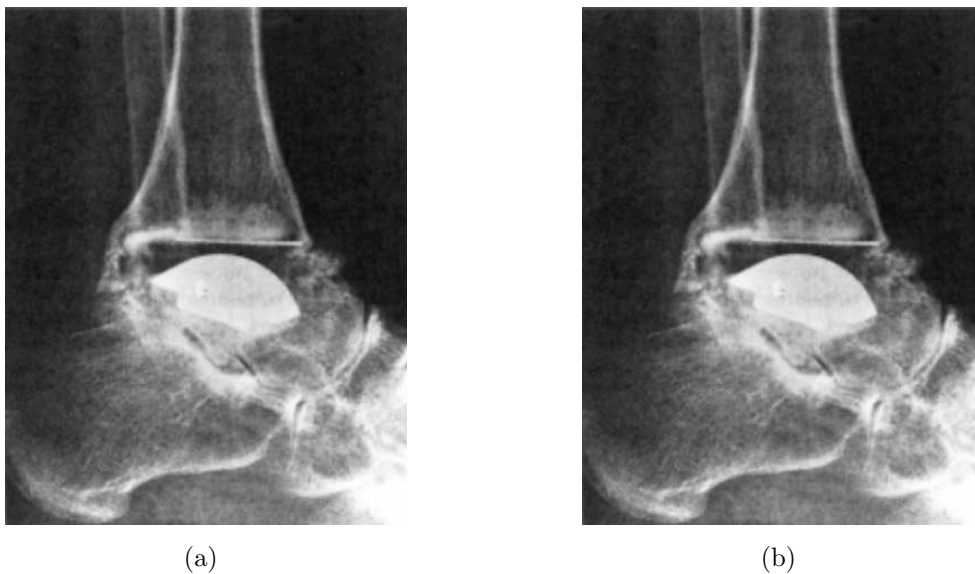


Figure 3.13: *Complications after Total Ankle Replacements. (a) Direct post-operative X-ray. (b) X-ray, twelve years post-operative, demonstrating marked subsidence of the talar component, indicating a loosened component [147]*

### 3.5 Design

The main goal of a joint replacement is long-term pain relief and restoring joint functionality to live an independent life. Results have been improved in the last decennia, especially for hip and knee replacements, but long-term complications still occur in hip, knee and especially ankle replacements [107, 178], as described above. Thus, conceptually new or adjusted prosthesis designs are under investigation to improve the results. Design criteria and research on design improvements focuses on the mentioned complications, in general and more specific for the hip, knee and ankle joint, will be discussed in this section.

Joint endo-prostheses in load bearing joints, which must allow for a certain range of motion, all have some main design criteria in common, which are relieving the patient from excessive pain, restoring natural functionality (the combination of a natural Range of Motion and joint strength), ease of surgery and that it should fulfill these tasks for a reasonable period without complications. To what extent these main objectives are achieved depends mainly on four factors, namely the patient, surgical, design and post-operative care factors [43].

The level of pain, a very subjective parameter, is, among others, caused by joint impingement and component loosening. Impingement, that is jamming of the joint against a hard constraint at certain joint positions, is directly depended on the geometrical design and kinematical behaviour of the replaced joint. Early loosening results in relative motion between the prosthesis-bone or cement-bone interfaces and can cause joint pain, e.g. pain in the proximal femur [118]. The design must allow for enough range of motion (RoM), while keeping in mind joint stability and fixation strength.

Examples of geometrical design parameters are the constraint angle  $\theta_0$  of the concave component (a large constraint angle results in a decreased RoM and increased stability) and also the CoR of the joint, which determines muscle moment arms. Ease of implantation of prosthetic components is mainly determined by surgical approach, patient position during surgery, type of alignment guides (mechanical tools or by camera assisted surgery) and component design [70, 315]. Although many research is focused on this subject, clear understanding of the influence of the design on post-operative alignment is difficult due to the amount of involving parameters [315]. From a design point of view, long-term survival, a difficult objective, is determined by implant failure (wear, implant fracture, dissociation of modular components, etc.), implant loosening (determined by radiographic evidence, excessive subsidence, migration, component micromotions or even complete displacement from the natural position) and the biological and biomechanical reaction of the host body to the implant (e.g. a tissue reaction such as osteolysis due to wear debris and bone adaptation due to bone remodelling, respectively).

The number of daily activities has been investigated by Morlock et al. (2001) [214]. The number of walking and stair climbing steps per day were found to be an average of 2337, leading to over 850.000 steps per year. A higher number was measured by Schmalzried et al. (1998), exceeding 900.000 steps per year, although there was large scatter in the data [281]. As 85% of the hip and 97% of the knee replacements function properly after 15 years, respectively, the total number of load cycles can by far exceed 10 million. This is an important design input, with respect to wear of the UHMWPE component and fatigue of the fixation.

The general design issues, such as wear, stress shielding and biological bone deposition, will be discussed on the basis of the hip joint, although they can also be applied on the knee and ankle joint.

One of the main goals of joint replacements is to restore joint functionality, which is done by careful component selection and accurate positioning. Reconstruction of the original joint can furthermore be improved by good adjustment of modular components, which is allowed for by many present used prosthetic systems. This is particularly helpful in developmental dysplasia of the hip and posttraumatic arthritis [197], to achieve the best fit for the individual patient. However, although component modularity can be beneficial for prosthesis adjustment, it introduces new problems, such as increasing risk of fretting, wear debris (a source for increasing component wear [103]), as well as dissociation and mismatching of components [23, 134]. Modular component design should focus on minimizing the mentioned problems, while keeping in mind the ease of surgery.

### **The hip joint**

Most design issues of the hip prosthesis are related to long-term aspects. The host tissues, the artificial material as well as the interfaces. Due to the many repetitive load cycles in combination with the high forces, the main focus of the hip replacement is on acetabulum component wear, stress shielding of the proximal femur and subsidence of the femoral stem. During time, the ensemble of surface wear, subsidence and stress shielding will lead to increasing deterioration of the materials and fixation. These design issues will be discussed extensively.

### **The knee joint**

Next to the more general design issues as discussed for the hip replacement, the main design issue of the knee replacement is the design conflict between knee stability, wear and component loosening. To solve knee instability, a posterior stabilized or constrained prosthesis can be inserted, but the enforced limited degrees of freedom will increase the interface stresses at the fixation of the implant [263]. Several studies compared the posterior cruciate ligament (PCL)-retaining and PCL-substituting total knee replacement (TKA), with respect to knee stability. It was found that the PCL-retaining TKA didn't improve knee stability while PCL-substituting TKA did improve knee stability compared to the pre-operative condition, respectively [219]. To improve knee stability during flexion, a posterior stabilizing prosthesis should be used [178].

Wear rates decrease in the case of increasing joint conformity, but this may lead to high loosening rates in the case of not using a mobile bearing. This is due to the fact that the knee joint shows small translations of the articular center of rotation. A mobile bearing knee consists of a metal, convex femoral component and flat, metal

tibial component with a UHMWPE, perfectly fitting disc in between. A design taking into account the knee rotation about the medial pivot point, leads to both a more normal motion pattern and improved joint stability [32].

### **The ankle joint**

The design issues of the ankle replacement, are very similar to the hip and knee joint, in that fixation, low wear rates, joint stability and pain relief must be guaranteed for a long period.

Ankle prostheses can be constrained (such as the Mayo, Imperial College London Hospital and Conaxial ankle replacements), semi-constrained (such as the STAR ankle replacement) and unconstrained (such as the Newton and Irvine ankle replacement). The prosthesis consists out of 3 or 2 components, which are fixed by pegs, different shaped stems and cylindrical or rectangular bars (see Figure 3.12). As so many fixation concepts are available, it can be stated that component fixation in ankle replacements is difficult, which is the result of the few bone material to fixate and the multiple joint rotations and translations during joint articulation. Recently, the number of metal backed components fixed by bone ingrowth is increasing.

The design conflict is very similar to the knee prosthesis, in that both joint stability and fixation must be guaranteed. Although constrained prostheses provide joint stability, they might show high loosening rates, as discussed previously. However, although unconstrained ankle prostheses demonstrate lower loosening rates, they might lead to soft-tissue and malleolar impingement [228].

The ankle replacement requires high surgical accuracy, as even an error of 1 to 2 *mm* of soft-tissue tensioning can affect joint laxity. Therefore, the three part ankle prosthesis, including a UHMWPE meniscal disc available in a range of thickness in between the metal parts, is often used to adjust ligament tension [228].

#### **3.5.1 Wear**

Wear occurs mainly in the UHMWPE cup components and is a continuing process, even more pronounced in the lower extremities due to the high number of annual walking steps with accompanying high joint forces. Design of the convex, metal head component is important in preventing wear of itself and the counteracting UHMWPE cup component. The head radius of curvature shows a design conflict with respect to wear. A smaller head leads to smaller relative motions between the two contact surfaces and a thicker polyethylene liner can be used, leading to slightly decreased contact stresses [309], with accompanying decreased wear. On the other hand, a bigger head can reduce wear due to a larger contact surface and thus lower contact stresses, although concave component thickness must be decreased due to limited joint space. The discussion is still continuing, but femoral heads with a

radius of curvature larger than 32 mm seem to be unfavorable compared to smaller ones, as they show higher wear rates [65].

Although femoral head surface properties influence glenoid component wear, clear statements are difficult, as an unambiguous relation between surface roughness and wear in component retrieval studies is not found [75, 78, 103]. It may be that not only the surface roughness  $R_a$  but also the roughness skewness  $R_{sk}$  is of importance.  $R_{sk}$  is a measure for the distribution of the peaks and valleys of the surface, positive and negative if more peaks or more valleys are present, respectively (see Figure 3.14). A negative skewness indicates small craters at the surface, which can be filled with fluid, leading to improved lubrication [78]. As a result, a high surface roughness in combination with a negative skewness can show very low wear rates.

To minimize the occurrence of completely worn components, component thickness should be at least 6 mm [65], a more pronounced issue in the case of small joints and metal backed components. A common component thickness of 7-8 mm in combination with a high wear rate of 300  $\mu\text{m}$  per year [278], leads to a wear through period of more than 20 years and direct implant failure due to wear is not likely to happen. Increasing age, level of activity, femoral head size, decreasing polyethylene thickness, and insertion of total hip prostheses without cement all increase polyethylene wear [69].

The method of UHMWPE component manufacturing has some influence on the wear. Molded components show lower wear rates compared to machined ones, especially directly post-operatively, with values of 50 and 110  $\mu\text{m}/\text{year}$  for molded and machined components, as found in a patient follow-up study [21].

Furthermore, wear is influenced by the method of sterilization. Using gas sterilization, such as ethylene oxide or gas plasma, decreases immediate oxidative degradation but does not improve wear resistance. Using gamma-irradiation, avoids oxidation and results in cross-linking, leading to decreased wear rates. However, long-term oxidation will occur, thereby decreasing wear resistance [202].

Wear of UHMWPE components decreases in the case of using a ceramic counteracting head component, made of zirconium or aluminum oxide, as compared to metal heads made of CoCr [78, 103, 278]. Zirconium oxide heads show a more negative skewness with better fracture resistance than aluminium oxide heads, resulting in an even more decreased wear rate [78]. Annual wear rates of CoCr against UHMWPE are 100-300  $\mu\text{m}$ , aluminum oxide (femoral head radius of 32-28 mm) or zirconium oxide (femoral head radius of 22 mm) against UHMWPE show 50-150  $\mu\text{m}$  and CoCr-CoCr and aluminum-oxide pairings show an annual wear rate of only 2-20  $\mu\text{m}$  [278]. Third body wear, the result of mainly the hard cement particles containing barium sulfate or zirconium, can cause damage to both the acetabular and femoral components [274]. The femoral head component must be hard and strong enough to prevent scratching of the smooth head and, due to their hardness, ceramics are superior to metal heads.

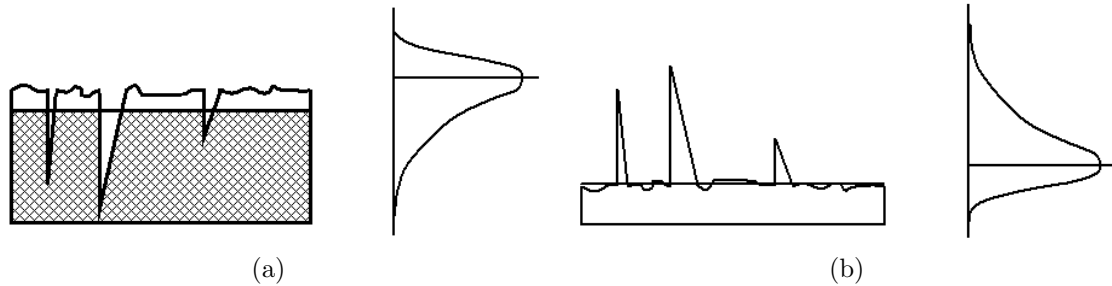


Figure 3.14: Representation of surface skewness  $R_{sk}$  of the femoral head. (a) Negative skewness, (b) positive skewness. A negative skewness can have a positive effect on wear rates of UHMWPE components [78]

### 3.5.2 Biological bone deposition

Osteolysis in hip replacements is a common long-term complication. Osteolysis is a foreign body inflammatory response along the implant-bone interface and in the joint capsule and actually it can be seen as wear debris induced bone loss [198]. To a large extent, the body is capable of removing wear debris by the host defense mechanism, although the capacity is limited. The remaining wear particles are toxic to macrophages and they can secrete potent inflammatory mediators, which are indeed found in periprosthetic tissues, causing bone resorption, directly and indirectly by affecting osteoblasts, the bone building cells.

### 3.5.3 Stress shielding

Stress shielding is the result of bone remodelling, which can occur after a joint replacement using a stemmed component (see Appendix B). The relatively stiff stem, compared to bone, takes over most of the joint loading, for example at the proximal femur, resulting in a stress by-pass in this region. If the altered load distribution is changed more than a certain threshold level as compared to the natural condition, the bone will start adapting its morphology by a still very unknown remodelling process [118, 345]. In this region, the cortical bone gets thinner, whereas the density of trabecular bone around distal corners of the prosthesis increases. Especially non-cemented hip replacements show this phenomenon, as they have a larger stem diameter. The environment around the joint will weaken, resulting in an increased risk of bone fracture and stem loosening as well as unfavorable bone support in the case of a revision surgery [117, 345]. Prosthesis design must take into account this phenomenon, by stem geometry, proper material selection, proximal coating and fixation [118, 280]. However, this must be done, keeping in mind other design criteria such as component strength, interface stresses and micromotions, which may result in soft-tissue formation, migration and finally component loosening [77].

### 3.5.4 Loosening

Several acetabular components are used nowadays. Fixation can be either cemented (all PE or with a metal backing) or non-cemented (PE inlay with a metal backing). Revision rates of cemented, metal backed acetabular components are about 10% within 10 years (n=86) [50]. At a mean of 8.5 years a total of 4% (n=72) of the non-cemented metal backed acetabular components needed a revision [289]. Although the non-cemented acetabular component is the common used one [213], results depend on the design of the components and can be poor. In a study of 120 hip replacements, loosening was found in 17% and more than one third showed radiographical loosening [132]. Cemented metal-backed acetabular components are still frequently used nowadays [174], as they decrease stresses in the critical cement-bone interface. When selecting a metal backed component with a PE inlay, dissociation of the inlay from the metal backing can occur, although this happens very infrequently [33]. This depends on manufacturing tolerances, design (conformity of the metal shell and the UHMWPE inlay) as well as loading conditions of the hip joint. If the backside of the PE inlay is not conforming to the concave metal backing, peak stresses can result in wear and loosening [157].

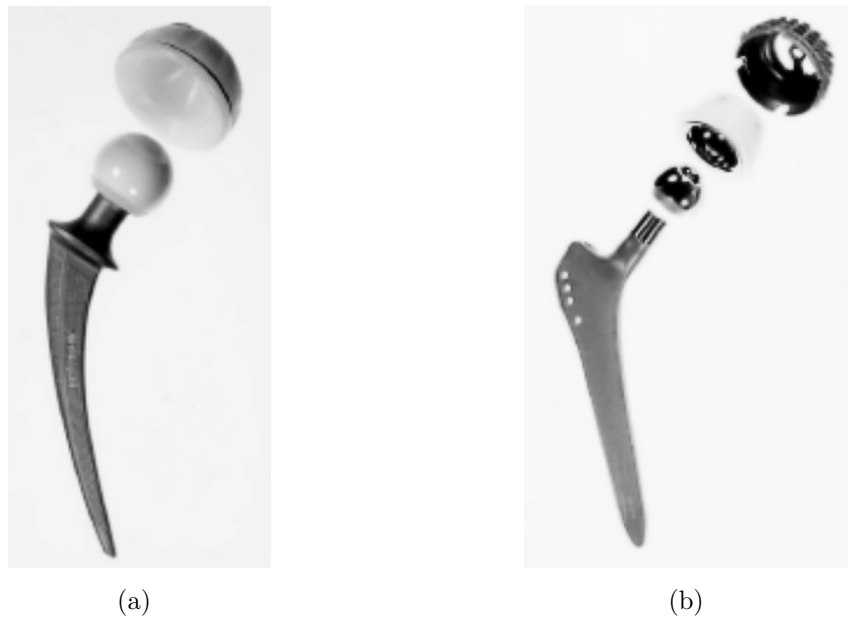


Figure 3.15: *Hip prostheses with different articular material combinations. (a) The Muller hip, with a ceramic head articulating against a UHMWPE acetabulum component. (b) The Zweimuller hip, with a metal against metal articular combination (with a PE inlay) [278]*

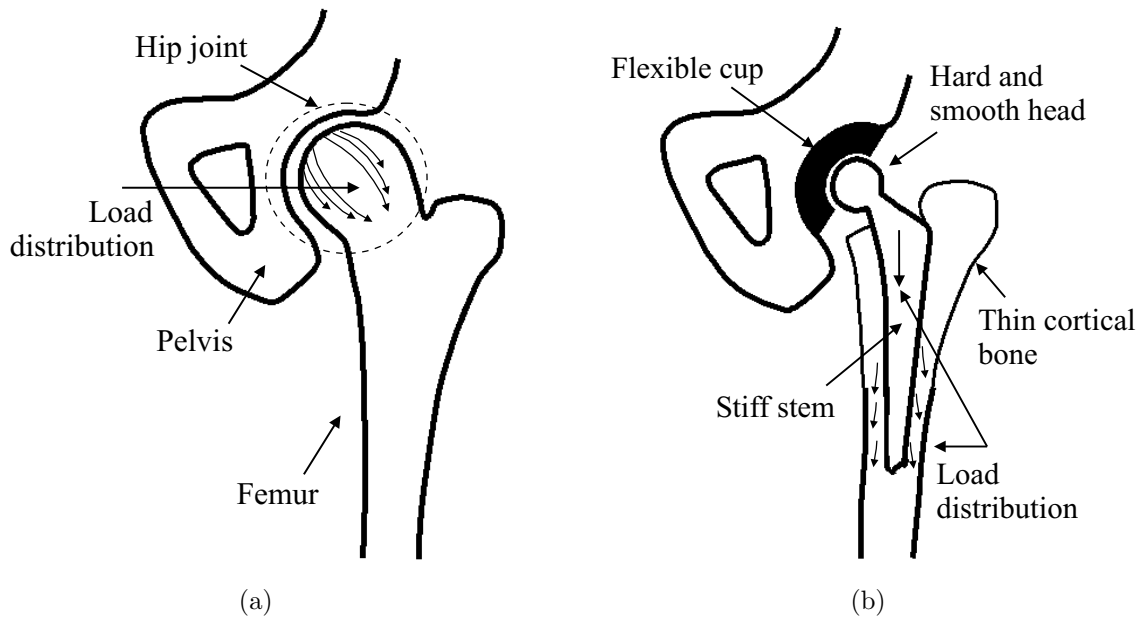


Figure 3.16: *Schematic representation of the load distribution in the hip joint. (a) In the anatomical hip joint the loading is distributed into the proximal cortical and trabecular bone. (b) In the replaced hip joint, the relative stiff stem will carry the proximal loading, leading to a more distal load distribution.*

### 3.6 Conclusions

Replacement of the hip and knee joint is a standard procedure in the case of excessive pain and limited joint functionality, with a survival rate of 85% after 15 years for hip replacements and slightly better in the case of knee replacements. Unfortunately, this doesn't hold for the ankle joint. Although direct functional improvement and pain relief are good, excessive complications occur within 3 to 7 years and it is frequently recommended not to use the ankle replacement. Instead, it is advised to switch to the ankle arthrodesis, in which the tibia and talus are fused. However, recent studies show more encouraging results of ankle replacements.

Due to the good results of the hip and knee replacement with respect to post-operative joint functionality and component fixation, their design issues are more related to long-term complications, such as stress shielding, component wear and component failure. Hip prosthesis design focuses on wear-through of the UHMWPE acetabulum component and design of the femoral stem, to improve stem fixation and to decrease stress shielding. The main design issue of the total knee prosthesis is the dilemma of component fixation versus knee stability, as knee flexion consists out of a combination of rolling, sliding and axial rotation. In the case of the ankle joint, designing a prosthesis which allows for anatomical articulation, joint stability

and long-term fixation seems to be a challenge and (conceptually) new designs must find an optimum or even cancel out this design dilemma.

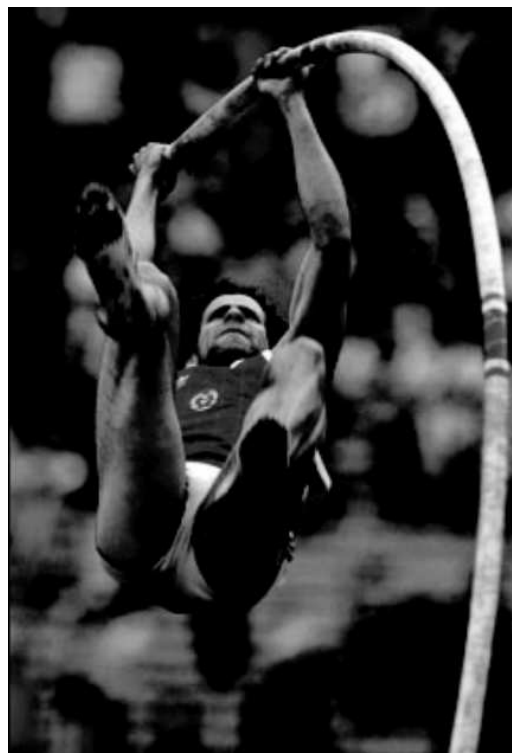
The hip and knee replacement perform much better in terms of long term patient satisfaction, compared to the shoulder and ankle replacement. Both hip and knee replacements show good long-term fixation and enough functional increase to easily perform activities of daily living. In the case of the ankle replacement, direct post-operative complications such as infection and bad wound healing still occur and mid-term follow-up studies showed a dramatic decline of the prosthesis survival. Although shoulder replacements show survival rates which are comparable to hip and knee replacements, post-operative functional increase is not sufficient to perform all ADL. This is also reflected in Table 3.1.

Table 3.1: Overview of the main characteristics of the shoulder, hip, knee and ankle joint

Topic	Shoulder	Hip	Knee	Ankle
Articulation	"ball in socket"	"ball in socket"	Roll - slide	Mainly single axis,
Ab. - Adduction	180 - 50	40 - 20	0 - 0	
Flexion - Extension	120 - 130	180 - 50	160 - 0	60 (plantar) - 30 (dorsal)
Exo.- Endorotation	75 - 75	13 - 36	60 - 0	
Max. joint forces	0.89 (abduction) (BW)	3.3 (walking)	6.0 (walking)	5.5 (walking)
Max. contact area	3 (abd. with weight) (BW)	8.7 (stumbling)	8.0 (downhill walking)	
# of replacements	507	-	1150	1408
Survival	11.000 (USA, 1997) 85% after 15 years	280.000 (USA, 1997) 85% after 15 years	338.000 (USA, 1997) 90% after 10 - 15 years	5000 (USA, 1995) 64% after 4.4 years
Main Complications	Component loosening, joint instability, bad functionality	Component wear, component loosening, component failure	Component wear, joint instability, component loosening, component failure	Component loosening, infection, bad wound healing

## Chapter 4

# Translational stiffness of the replaced shoulder joint



*An athlete testing the strength and stiffness of his vaulting pole*



## 4.1 Introduction

Total Shoulder Arthroplasty (TSR) is a common treatment for patients with a deteriorated glenohumeral joint, often a result of rheumatoid-arthritis or osteo-arthritis. However, especially patients suffering from rheumatoid-arthritis, often have a deteriorated Rotator Cuff, which is not able to provide the required joint compression force for proper joint stability. As a result, the glenoid component may experience high off-center loading, which may lead to tensile and compression stresses at the interface and even to a joint dislocation. The optimal geometry for the glenoid component to minimize off center loading, focused on joint conformity and constraint, keeping in mind other design criteria, still has to be investigated.

The shoulder endoprosthesis has conflicting design criteria, in that a sufficient Range of Motion (RoM), proper component fixation and prevention of humeral head dislocation cannot go together. For example, an increasing radius of curvature  $R_g$  of the glenoid component results in a decreasing constraint angle  $\theta_0$ , for a fixed glenoid superior-inferior chord length  $c_g$  (see Figure 4.1). The beneficial increased RoM will lead to increased eccentric glenoid component loading and possibility of humeral head dislocation. This off-center load, increased by pathology of the Rotator Cuff and other soft-tissues, may be the main contribution to glenoid component loosening [12, 167].

Several studies have analysed the behaviour of the shoulder joint loaded by a subluxation force. The studies can be divided in analyzing the mechanisms, which prevent subluxation and dislocation in healthy shoulder joints [31, 63, 350, 343], as well as in pathologic shoulder joints [245, 361] and in prosthesis design related studies [63, 135, 12]. The first group focused on the mechanisms and morphological structures, by means of anatomic cadaver studies with different dissection levels. The second group of examinations compared the biomechanical behaviour of shoulder joints with and without rotator cuff deficiencies. The third group examined the behaviour of the replaced shoulder, by means of clinical studies and experimental testing. Although these studies give insight in the stability of the shoulder joint, a thorough biomechanical analysis on the effect of design parameters on the stability is lacking and good criteria for shoulder component design are still not available.

Proper understanding of the effect of geometrical design parameters on the theoretical relationship between joint translations and joint forces may contribute to improved designs. This relationship can be described by the joint translational stiffness, this is the gradient of the subluxation force with respect to the corresponding humeral head displacement. The main objective of this study is to provide a theoretical approach to investigate the effect of geometrical design parameters on the joint translational stiffness, to be used in future prosthesis design and selection. Very often, the terms stability, subluxation, joint dislocation and stiffness are used in a misleading way. Therefore, first a standardization of definitions of these terms will be given.



at joint position 5 ( $\varphi_2 = \theta_0$ ,  $d_y = \frac{1}{2}c_g$ ) and to relocate the *HH* back inside the glenoid cavity, an external restoring force is needed. A joint dislocation is defined as articulation at joint position 5 or more downward ( $\varphi_2 > \theta_0$ ,  $d_y > 1/2c_g$ ). A similar description can be given for a superior directed subluxation force.

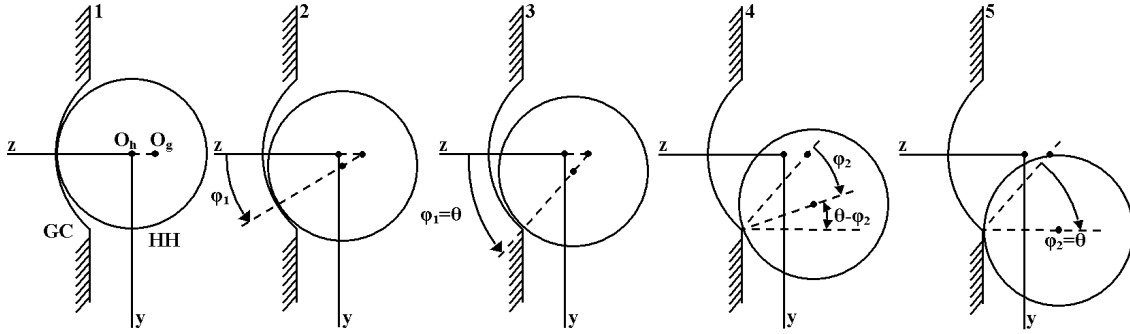


Figure 4.2: Overview of typical joint positions (1, 3, 5) and articular regions (2, 4). 1. Starting position with a centered *HH* ( $\varphi_1 = 0$ ) 2. *HH* articulation within glenoid cavity ( $0 < \varphi_1 < \theta_0$ ) 3. *HH* position with tangential surface contact at the glenoid rim ( $Gr_i$ ) ( $\varphi = \theta_0$ ) 4. Subluxation outside glenoid cavity ( $0 < \varphi_2 < \theta_0$ ). 5. *HH* position for maximal  $d_z$  ( $\varphi_2 = \theta_0$ )

## 4.2.2 Joint translational stiffness

In general, stiffness relates the magnitude of the deformation of a construction with the applied load. A well-known example is the spring stiffness  $K$ , which is influenced both by geometry and the spring material. This stiffness can be analysed by the elastic potential:

$$V = \frac{1}{2}Ku^2 \quad (4.1)$$

where  $V$  is the elastic potential,  $K$  the spring stiffness and  $u$  the displacement of the endpoint of the spring. The force  $F$  due to the displacement  $u$  is the derivative of the elastic potential  $V$  with respect to  $u$ :

$$F = \frac{\partial V}{\partial u} = Ku \quad (4.2)$$

The spring stiffness relates the variation of the spring force  $\Delta F$  due to a small variation of the displacement  $\Delta u$ :

$$K = \frac{\partial^2 V}{\partial^2 u} \quad (4.3)$$

Similarly, the joint translational stiffness relates variations of displacement of the humeral head component relative to the glenoid cavity with variations of the applied subluxation load in the same direction. In general, the joint translational stiffness is influenced by the materials and geometry of the glenoid and head components, the joint compression force and, due to the non-linear behaviour, also by the joint position. This quantity can be expressed as:

$$K_i = \frac{\partial F_i}{\partial d_i} \quad (4.4)$$

where  $K_i$  is the joint translational stiffness and  $d_i$  the displacement of the center of the humeral head in the direction of the force  $F_i$ . In general, the subscript  $i$  can be replaced by  $x$ ,  $y$  and  $z$ , resulting in the joint translational stiffness in the anterior-posterior, superior-inferior and medial-lateral direction, respectively. In the  $x$ - and  $y$ -direction this translational stiffness relates the joint subluxation forces ( $F_x$  and  $F_y$ ) and the displacement in the  $x$ - and  $y$ -direction ( $d_x$  and  $d_y$ ), respectively. In the  $z$ -direction this translational stiffness relates the joint traction force ( $F_z$ ) and the displacement in the negative  $z$ -direction ( $d_z$ ). In this study the joint translation stiffness in  $y$ -direction ( $K_y$ ) is analysed, as this is a common direction of humeral head instability.

### 4.2.3 Stability

In clinical studies, instability is often referred to as large translations of the humeral head in the glenoid cavity or even as a joint dislocation [31, 193, 350, 353]. In technical and biomechanical studies there is no absolute definition of stability, as it depends on the structure and force system of investigation as well as the perturbation. According to Leipholz (1987) stability can be explained as follows [168]:

*'If the magnitude of the perturbation of the perturbed system does not exceed a predetermined measure, the system is stable, else it is unstable.'*

In this static analysis, stability is defined as the reaction of the humeral head to a small displacement  $\delta d_y$  due to a subluxation force disturbance  $\delta F_y$  for a given joint

position. This stability depends on the sign of the joint translational stiffness  $K_y$  and can be expressed mathematically as:

- Stable:  $K_y = \frac{\partial F_y}{\partial d_y} > 0$ ,
- Neutral:  $K_y = \frac{\partial F_y}{\partial d_y} = 0$ ,
- Unstable:  $K_y = \frac{\partial F_y}{\partial d_y} < 0$ .

#### 4.2.4 Subluxation

Very often, the terms subluxation and dislocation are mixed up or used in a misleading way [135]. Subluxation in this study is defined as articulation about the glenoid rim, by which the  $HH$  can always be relocated by the RC. This is articulation in region 4 (see Figure 4.2). During articulation in region 2, at joint position 3 and during subluxation, the  $HH$  will return to joint position 1 when the applied  $F_y$  is removed.

#### 4.2.5 Dislocation

In this study,  $HH$  dislocation is defined as static equilibrium joint positions by which the RC is not able to relocate the  $HH$  and an external restoring force is needed. This is in the case of  $HH$  positions at  $\varphi_2 > \theta_0$  or  $d_y > \frac{1}{2}c_g$  (joint position 5 and more downward according to Figure 4.2). When increasing  $F_y$  for given  $F_z$  until the resultant force just directs outside the glenoid cavity ( $\varphi_1 > \theta_0$ ), uncontrolled joint translations outside the glenoid cavity will occur and no static force equilibrium will be obtained [10]. To relocate the  $HH$  in joint position 1, an external restoring force is needed.

### 4.3 Methods

#### 4.3.1 Assumptions

In this two-dimensional, static rigid-body analysis,  $F_z$  is the joint compression force, mainly resulting from muscle forces. This force is taken as 1000  $N$  and is assumed to be constant, which is justified by the fact that the influence of a displacement  $d_y$  of the humeral midpoint  $c_h$  on  $F_z$  is supposed to be small. In all analyses, the humeral component has a smaller radius of curvature than the glenoid component

(joint conformity  $\kappa < 1$ ). The components are assumed to be undeformable (rigid-body analysis) and the glenoid component is fixed with respect to the reference coordinate system. Friction is neglected in this analysis, leading to joint contact forces, which are perpendicular directed to the articular surfaces. Furthermore, the analysis is focused on head translations in the positive  $y$ -direction, although similar results can be obtained for humeral head translations in the negative  $y$ -direction, as well as in the positive and negative  $x$ -direction.

### 4.3.2 Calculation of joint displacements, subluxation force and joint translation stiffness

In this study, a potential field  $V$  is introduced to give the displaced rigid humeral head a potential energy, which can then be used to relate the subluxation force and joint translational stiffness  $K_y$  with the joint displacement  $d_y$  for all joint positions according to Figure 4.2. The subluxation force and joint translational stiffness are calculated by taking the first and second derivative of the potential energy with respect to  $d_y$ , respectively. The potential energy is zero at the origin of the coordinate system, with an increase of potential energy in the direction opposite to the force direction (see Figure 4.1). This is a two-dimensional analysis in the YOZ-plane, as  $F_x$  is not included. With  $y = d_y$  and  $z = -d_z$ , (see Figure 4.1), the potential energy can be expressed as:

$$V = -F_y d_y + F_z d_z \quad (4.5)$$

During articulation, the radius of curvature of both the glenoid and humeral component,  $R_g$  and  $R_h$ , as well as the glenoid superior-inferior chord length  $c_g$  determine the pattern of movement of the humeral head. As a result, also due to the rigid-body character,  $d_y$  and  $d_z$  are coupled. As the joint translational stiffness is related to the displacement  $d_y$ , this displacement is the chosen degree of freedom.

The analysis starts with the humeral head centered in the glenoid cavity (joint position 1 (see Figure 4.2)). The first part of the analysis is focused on articulation inside the glenoid cavity (articulation in region 2). Joint position 3 divides the first and second part of the analysis, which is articulation outside the glenoid cavity (articulation in region 4). The end point is where the instantaneous midpoint of the humeral head  $c_h$  has its most lateral position, in other words, when the humeral head starts to dislocate (joint position 5). For both articular regions 2 and 4 the

subluxation force  $F_y$  is a function of several parameters:

$$F_y = f(F_z, d_y, R_g, R_h, \theta_0) = \frac{\partial V}{\partial d_y} \quad (4.6)$$

and the joint translational stiffness  $K_y$  is the derivative of Equation 4.6 with respect to  $d_y$ :

$$K_y = \frac{\partial F_y}{\partial d_y} = \frac{\partial^2 V}{\partial^2 d_y} \quad (4.7)$$

**Articulation inside the glenoid cavity ( $0 < \varphi_1 < \theta_0$ , region 2 in Figure 4.2)**  
The results of the subluxation force  $F_y$  and translational stiffness  $K_y$  for articulation

in region 2 are derived in this section. Because rigid-bodies and constant radii of curvature are assumed, a relationship between  $d_y$  and  $d_z$  can be derived. The theorem of Pythagoras can be used to calculate  $\rho$  (see Figure 4.1a) and as a result also  $d_z$  as function of  $d_y$ :

$$\rho^2 = d_y^2 + (\rho - d_z)^2 \Rightarrow \rho^2 - d_y^2 = (\rho - d_z)^2 \Rightarrow d_z = \rho - \sqrt{\rho^2 - d_y^2} \quad (4.8)$$

The potential energy can be expressed in the coupled degrees of freedom ( $d_y$  and  $d_z$ ) (eq. 4.9) and setting the derivative of this potential function equal to zero, which is necessary for force equilibrium (eq. 4.10), leads to a relationship between  $F_y$ ,  $F_z$  and  $d_y$  (eq. 4.11). Consequently, the potential energy relative to the initial position ( $V = 0$ ) can be expressed as:

$$V = -F_y d_y + F_z d_z = -F_y d_y + F_z (\rho - \sqrt{\rho^2 - d_y^2}) \quad (4.9)$$

Static force equilibrium requires  $\frac{\partial V}{\partial d_y} = 0$ :

$$\frac{\partial V}{\partial d_y} = -F_y + F_z \frac{d_y}{\sqrt{\rho^2 - d_y^2}} = 0 \quad (4.10)$$

Consequently, this leads to the following expression for  $F_y$ :

$$F_y = F_z \frac{d_y}{\sqrt{\rho^2 - d_y^2}} \quad (4.11)$$

As no friction is assumed, this result can be checked geometrically, as  $\vec{F}_y + \vec{F}_z$  should be perpendicular to the glenoid surface, which only is true if  $F_y = F_z \tan \varphi_1$ . The proof for this:

$$\begin{aligned} \sqrt{\frac{d_y^2}{\rho^2 - d_y^2}} &= \sqrt{\frac{(\rho \sin \varphi_1)^2}{\rho^2(1 - \sin^2 \varphi_1)}} = \sqrt{\frac{\sin^2 \varphi_1}{1 - \sin^2 \varphi_1}} = \sqrt{\frac{\sin^2 \varphi_1}{\cos^2 \varphi_1}} = \tan \varphi_1 \\ &\Rightarrow F_y = F_z \tan \varphi_1 \end{aligned} \quad (4.12)$$

The subluxation force at joint position 3 is the maximal allowable subluxation force before a joint dislocation occurs  $F_{ymax}$ . From Equation 4.12 it follows that  $F_{ymax}$  depends on  $F_z$  and the constraint angle  $\theta_0$ .

The joint translational stiffness is obtained by the derivative of Equation 4.11 with respect to  $d_y$ :

$$K_y = \frac{\partial V^2}{\partial^2 d_y} = \frac{\partial F_y}{\partial d_y} = F_z \frac{\rho^2}{\sqrt{\rho^2 - d_y^2}(\rho^2 - d_y^2)} \quad (4.13)$$

#### Articulation about the glenoid rim ( $0 < \varphi_2 < \theta_0$ , region 4 in Figure 4.2)

The results for the subluxation force  $F_y$  and translational stiffness  $K_y$  for articulation

in region 4, are derived in this section. The relationship between  $d_y$  and  $d_z$  for unstable sliding is derived as follows (see Figure 4.1a):

$$\begin{aligned} d_y &= \rho \sin \theta_0 + R_h (\sin \theta_0 - \sin(\theta_0 - \varphi_2)) && \& \\ d_z &= \rho(1 - \cos \theta_0) + R_h (\cos(\theta_0 - \varphi_2) - \cos \theta_0) && \Rightarrow \\ d_z &= \rho(1 - \cos \theta_0) + \sqrt{R_h^2 - (R_h \sin \theta_0 - (d_y - \rho \sin \theta_0))^2} - R_h \cos \theta_0 \end{aligned} \quad (4.14)$$

Potential energy relative to the initial position ( $V = 0$ ) can be expressed as:

$$V = -F_y d_y + F_z d_z = -F_y d_y + F_z (\rho(1 - \cos \theta_0) + \sqrt{R_h^2 - T^2} - R_h \cos \theta_0) \quad (4.15)$$

where  $T = (R_h \sin \theta_0 - (d_y - \rho \sin \theta_0))$ . Static force equilibrium again requires  $\frac{\partial V}{\partial d_y} = 0$ :

$$\frac{\partial V}{\partial d_y} = -F_y + F_z \frac{T}{\sqrt{R_h^2 - T^2}} = 0 \quad (4.16)$$

Consequently, this leads to the following expression for  $F_y$ :

$$F_y = F_z \sqrt{\frac{T^2}{R_h^2 - T^2}} \quad (4.17)$$

For static force equilibrium and assuming no friction,  $F_y$  must be equal to  $F_z \tan(\theta_0 - \varphi_2)$ . The proof for this (using Equation 4.14):

$$\begin{aligned} \sqrt{\frac{T^2}{R_h^2 - T^2}} &= \sqrt{\frac{(R_h \sin \theta_0 - (d_y - \rho \sin \theta_0))^2}{R_h^2 - (R_h \sin \theta_0 - (d_y - \rho \sin \theta_0))^2}} = \\ &= \sqrt{\frac{(R_h \sin \theta_0 - (R_h (\sin \theta_0 - \sin(\theta_0 - \varphi_2))))^2}{R_h^2 - (R_h \sin \theta_0 - (R_h (\sin \theta_0 - \sin(\theta_0 - \varphi_2))))^2}} = \\ \sqrt{\frac{\sin^2(\theta_0 - \varphi_2)}{1 - \sin^2(\theta_0 - \varphi_2)}} &= \sqrt{\frac{\sin^2(\theta_0 - \varphi_2)}{\cos^2(\theta_0 - \varphi_2)}} = \tan(\theta_0 - \varphi_2) \Rightarrow F_y = F_z \tan(\theta_0 - \varphi_2) \end{aligned} \quad (4.18)$$

The joint translational stiffness is obtained by taking the derivative of Equation 4.17 with respect to  $d_y$ , resulting in:

$$K_y = -F_z \frac{(R_h^2 - T^2)T + T^3}{(R_h^2 - T^2)^2 \sqrt{\frac{T^2}{(R_h^2 - T^2)}}} \quad (4.19)$$

where  $T = (R_h \sin \theta_0 - (d_y - \rho \sin \theta_0))$ .

## 4.4 Results

In Figure 4.3 the equilibrium subluxation force  $F_y$  and  $K_y$  are plotted as function of the displacement  $d_y$  for given glenoid-humeral head component combination. If  $F_y = 0$ , the result is an equilibrium position with a centered head (joint position 1 in Figure 4.2 and Figure 4.3), while  $K_y \neq 0$  at this joint position. Increasing the subluxation force leads to displacements  $d_y$  and  $d_z$  in the case of non-conform articular

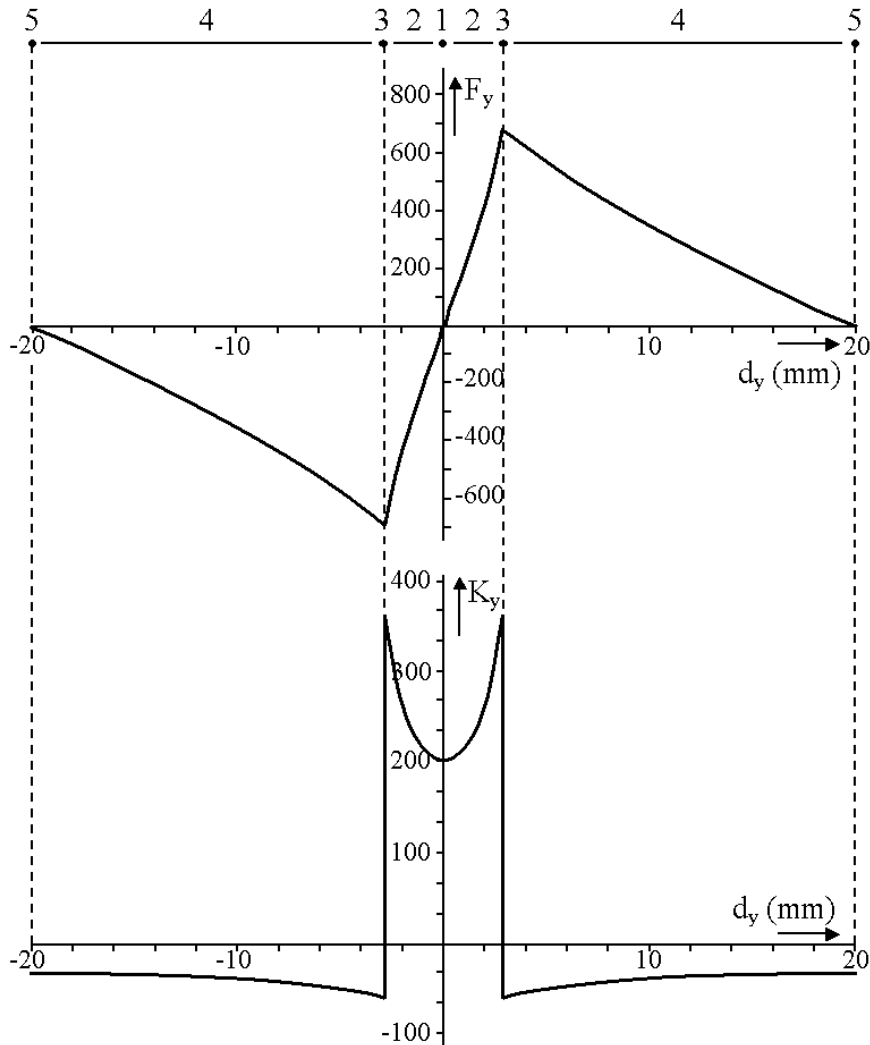


Figure 4.3: Joint subluxation ( $F_y$ ) and translational stiffness ( $K_y$ ) graphs for given glenoid and humerus component combination ( $R_g=35$  mm,  $c_g=40$  mm,  $\theta_0=34.85^\circ$ ,  $R_h=30$  mm) and compression force ( $F_z=1000$  N). Articulating positions 1, 3 and 5 and regions 2 and 4 are chosen as in Figure 4.2

surfaces (region 2). The increase of  $d_y$  gets smaller for  $0 < \varphi_1 < \theta_0$  with increasing  $F_y$ , because the tangential of the glenoid surface at the contact point directs more perpendicular to the line of action of  $F_y$ . This can be seen as a positive, increasing joint stiffness, which is also reflected in the stiffness graph.

At joint position 3, both the subluxation force and joint translational stiffness graphs of Figure 4.3 show a discontinuity.  $K_y$  changes from positive to negative, this is due to the fact that in region 4 ( $0 < \varphi_2 < \theta_0$ ), for increasing  $d_y$ , a decreasing  $F_y$  is required to obtain force equilibrium, in contrast to articulation in region 2. As the

humeral component is sliding or rotating about the glenoid rim, the negative sign of  $K_y$  can be explained due to the increasing and decreasing moment arm of  $F_y$  and  $F_z$ , respectively. At joint position 5, a zero subluxation force is required for force equilibrium, as the moment arm of  $F_z$  about the glenoid inferior rim ( $Gr_i$ ) is zero, while the moment arm of  $F_y$  is maximal. At this joint position,  $K_y$  has a negative value, whereas  $K_x$  is zero for further increasing  $d_y$ . This is due to the fact that an infinitesimal subluxation force  $F_y$  leads to large displacements  $d_y$ , according to Figure 4.2 in this rigid-body, frictionless analysis. However, articulation inferior to joint position 5 is outside the scope of this study. As the glenoid and humeral components are symmetrical in the YOZ-plane with respect to the  $z$ -axis, the same results can be obtained for subluxation in the superior direction.

Figure 4.4 shows shoulder joint subluxation force and joint translational stiffness graphs for glenoid-humeral head combinations with different glenoid radii of curvature  $R_g$ . The humeral head has a fixed radius of curvature  $R_h$  of 30 mm, while the glenoid has a fixed cord length  $c_g$  of 40 mm and radii of curvature  $R_g$  of 30, 35 and 40 mm, resulting in different constraint angles  $\theta_0$ . Due to different conformities  $\kappa$  and constraint angles  $\theta_0$ , the joint translational stiffness  $K_y$ , the maximal allowable subluxation force  $F_{ymax}$  and displacement  $d_y$  to joint position 3 are influenced. In the conform glenoid and humeral head ( $\kappa = 1$ ),  $K_y$  is positive infinite in region 2, as there is no displacement  $d_y$ . In this conform situation ( $\kappa = 1$ ) the glenoid radius of curvature is smallest ( $R_g = 30$  mm). This leads to the highest  $\theta_0$  and thus highest  $F_{ymax}$ , which decreases with increasing glenoid radius  $R_g$ . The displacement  $d_y$  to joint position 3 is  $\rho \sin \theta_0$  and is increasing with increasing non-conformity ( $\kappa < 1$ ), thereby decreasing  $K_y$ . In region 4, the relationship between  $F_y$  and  $d_y$  is geometrically influenced only by rotation or sliding of the humeral head about the glenoid rim  $Gr_i$ . As in this case the humeral radius  $R_h$  is kept constant, this relationship is identical for the different glenoid-humeral combinations, leading to a constant negative stiffness  $K_y$ . The displacement  $d_y$  to joint position 5 is constant for all component combinations, as  $c_g$  is fixed.

A similar analysis is done with a variable humeral head radius of curvature  $R_h$ . In Figure 4.5, the glenoid component has a fixed radius of curvature  $R_g$  of 35 mm, constraint  $\theta_0$  of  $40^\circ$  and  $c_g$  of 40 mm, leading to a constant  $F_{ymax}$ , while the humeral head has radii of curvature  $R_h$  of 35, 30 and 25 mm. A decreasing  $R_h$  results in increasing radial clearance  $\rho$  and as a result to an increased displacement  $d_y$  to joint position 3 and thus to a decreasing  $K_y$  in this region. The fixed  $c_g$ , and thus a constant displacement  $d_y$  to joint position 5 for all  $R_h$ , in combination with the constant  $F_{ymax}$ , leads to the fact that a lower positive stiffness in region 2 results in a higher negative stiffness in region 4. For example, the infinitely stiffness in region 2 for the conform combination, leads to the lowest stiffness in region 4.

In Figure 4.6, the glenoid superior-inferior chord length  $c_g$  is taken as 35, 40 and 45 mm, while radial clearance  $\rho$  is fixed at 5 mm ( $R_g=35$  and  $R_h=30$ ). This shows that there is no influence for both functions  $F_y(d_y)$  and  $K_y(d_y)$  in region 2, except

that region 2 is extended with increasing  $c_g$ . The increased constraint angle  $\theta_0$  leads to an increased  $F_{ymax}$ . Increasing  $c_g$  results in increased total displacements  $d_y$  up to joint position 5.

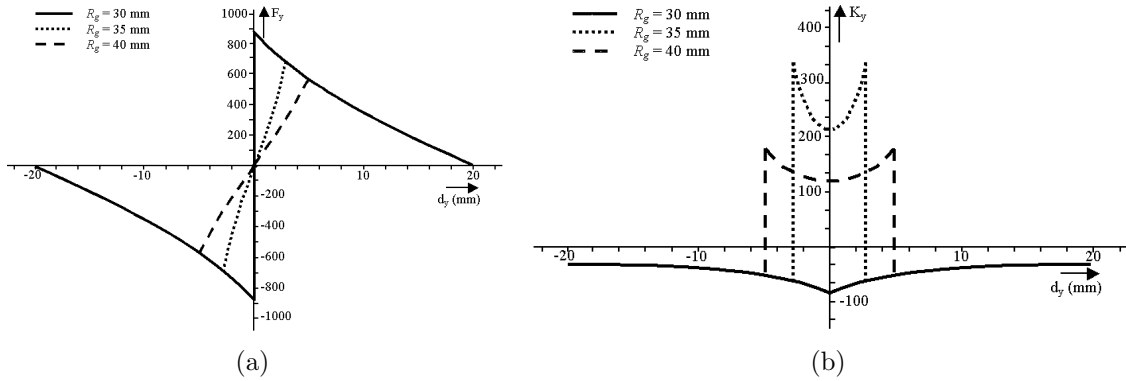


Figure 4.4: Joint subluxation ( $F_y$ ) and translational stiffness ( $K_y$ ) graphs with different glenoid radii of curvature  $R_g=30, 35, 40$  mm in combination with  $R_h=30$  mm and  $c_g=40$  mm (leading to  $\rho=0, 5$  and  $10$  mm and  $\theta_0=41.81^\circ, 34.85^\circ$ , and  $30^\circ$ , respectively)

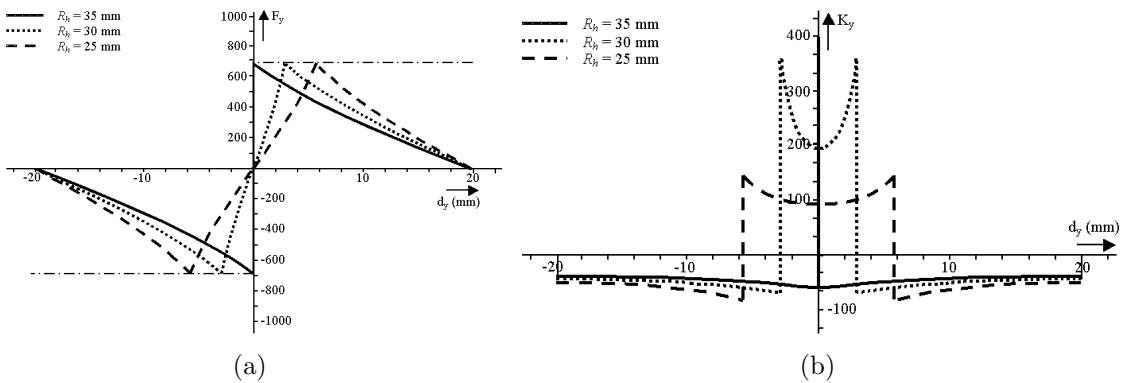


Figure 4.5: Joint subluxation ( $F_y$ ) and translational stiffness ( $K_y$ ) graphs with different humeral radii of curvature  $R_h=35, 30, 25$  mm in combination with  $R_g=35$  and  $c_g=40$  mm (leading to  $\theta_0=34.85^\circ$  and  $\rho=0, 5, 10$ , respectively)

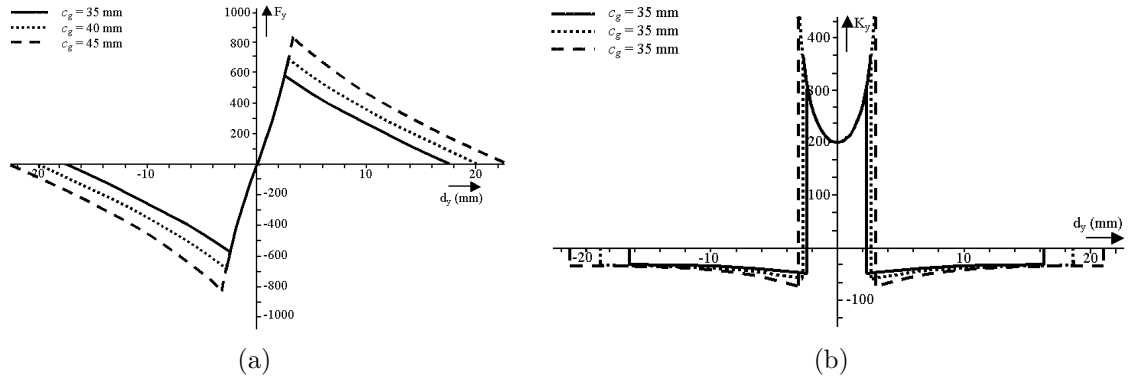


Figure 4.6: Joint subluxation ( $F_y$ ) and translational stiffness ( $F_y$ ) graphs with different glenoid superior-inferior chord lengths  $c_g$  of 35, 40, 45 mm in combination with  $R_g=35$  mm and  $R_h=30$  mm (leading to  $\rho=5$  mm and  $\theta_0=30^\circ, 34.85^\circ, 40^\circ$ )

## 4.5 Discussion

This study reconsidered some biomechanical definitions and introduced the shoulder translational stiffness  $K_y$ , which is the relation between humeral head translation  $d_y$  and subluxation force  $F_y$ . Joint stability is defined as the reaction to disturbances, which is stable for articulation inside the glenoid cavity and unstable during subluxation. The maximal allowable subluxation force  $F_{ymax}$  depends on the glenoid constraint angle  $\theta_0$  and compression force  $F_z$ . These are important design parameters, as a joint dislocation is a common complication after shoulder replacements [177, 352]. Material deformation has not been taken into account in this rigid-body analysis, although this will influence  $K_y$  as well as joint subluxation and dislocation behaviour. The relatively hard humeral head component will deform the glenoid component and underlying structures, which may result in a decreased joint translational stiffness and maximal allowable subluxation force before a joint dislocation occurs  $F_{ymax}$ . Also, the rigid-body character of this analysis explains the discontinuities in the subluxation force and translational stiffness graphs. However, as relatively stiff materials are used in the artificial shoulder, the effect of material deformation is assumed to be very small, although experimental methods must prove this.

This is a two-dimensional analysis of the joint translational stiffness, in the  $y$ -direction (superior-inferior), with coupled translations in the  $z$ -direction (medial-lateral). However, insight in the three-dimensional behaviour is actually shown in Figure 4.6. As both  $R_g$  and  $R_h$  are constant at the articular surface, only the  $c_g$  effects the 3D behaviour of the joint translational stiffness, as the  $c_g$  can be different in different subluxation directions. An example is an elliptical shaped glenoid component, with larger superior-inferior chord length than anterior-posterior. According to Figure 4.6, this results in smaller maximal allowable subluxation forces and joint translational stiffness in  $x$ -direction (anterior-posterior) than in  $y$ -direction

(superior-inferior). Humeral head and glenoid radius of curvature, as well as glenoid superior-inferior chord length are chosen according to [12]. Although the glenoid superior-inferior chord length  $c_g$  has patient specific dimensions [121] and should be fixed during prosthesis design investigation, this design parameter is examined to investigate its influence on  $K_y$ .

The joint compression force  $F_z$  is chosen as 1000  $N$ , which can be seen as an upper limit according to the literature [245, 122]. This force is taken constant during joint translations, as the influence of soft-tissue strain on compression force is assumed to be small, although with the same method a non-constant compression force can be included. Taking into account the influence of the joint position on the compression force, leads to adaptation of Equations 4.9 and 4.15, in that  $F_z$  becomes a function of  $d_y$ . In this study, insight is obtained in the influence of geometrical design parameters of the glenoid and humeral components as well as  $F_z$  on  $K_y$  and  $F_{y_{max}}$ . The constraint angle  $\theta_0$  influences  $F_{y_{max}}$  and joint translations  $d_y$  up to joint position 3. The glenoid superior-inferior chord length  $c_g$  relates the glenoid radius of curvature  $R_g$  and constraint angle  $\theta_0$  as follows:

$$c_g = 2R_g \sin\theta_0 \quad (4.20)$$

There is a large spread of  $c_g$  in anatomical shoulder joints [121], which should be taken into account during prosthesis selection, as it may influence the fixation strength of the glenoid component. For example, when selecting a glenoid component with larger  $c_g$  than the anatomical  $c_g$ , while fixing the constraint angle  $\theta_0$  by an increased  $R_g$  will lead to the same  $F_{y_{max}}$  with a shifted joint contact point. The increased moment arms about the joint contact point for joint position 1 of both  $F_z$  and  $F_{y_{max}}$  increase and as a result glenoid component tilting about the joint contact point for a centered  $HH$  due to off-center loading during articulation in region 2 will increase. This maximal tilting moment can be expressed as (in cw direction according to Figure 4.1):

$$M_c = R_g F_z \sin\theta_0 + R_g F_{y_{max}} (1 - \cos\theta_0) = R_g F_z \tan\theta_0 = R_g F_{y_{max}} \quad (4.21)$$

This increased maximal tilting moment due to the increased  $c_g$  leads to increased interface stresses, thereby reducing the chance on a successful long-term fixation. In this rigid-body analysis the radial clearance  $\rho = (R_g - R_h)$  only influences joint translations and joint translational stiffness during stable sliding. The advantage of these humeral head translations is that it can be used as a warning system to prevent a joint dislocation. When including material elasticity, radial clearance also influences contact stresses and material wear, which, from a design point of view, is the result of joint translations, compression force and material strength. During unstable subluxation, the humeral head radius of curvature  $R_h$  influences joint translations and the joint translational stiffness. One way to guarantee stable

articulation (articulation in region 2) is to assure that the compression force is sufficiently large, which can be done by means of involving the anatomical structures during surgery as well as integration of the joint contraction function of the soft-tissues in conceptually new prosthesis designs.

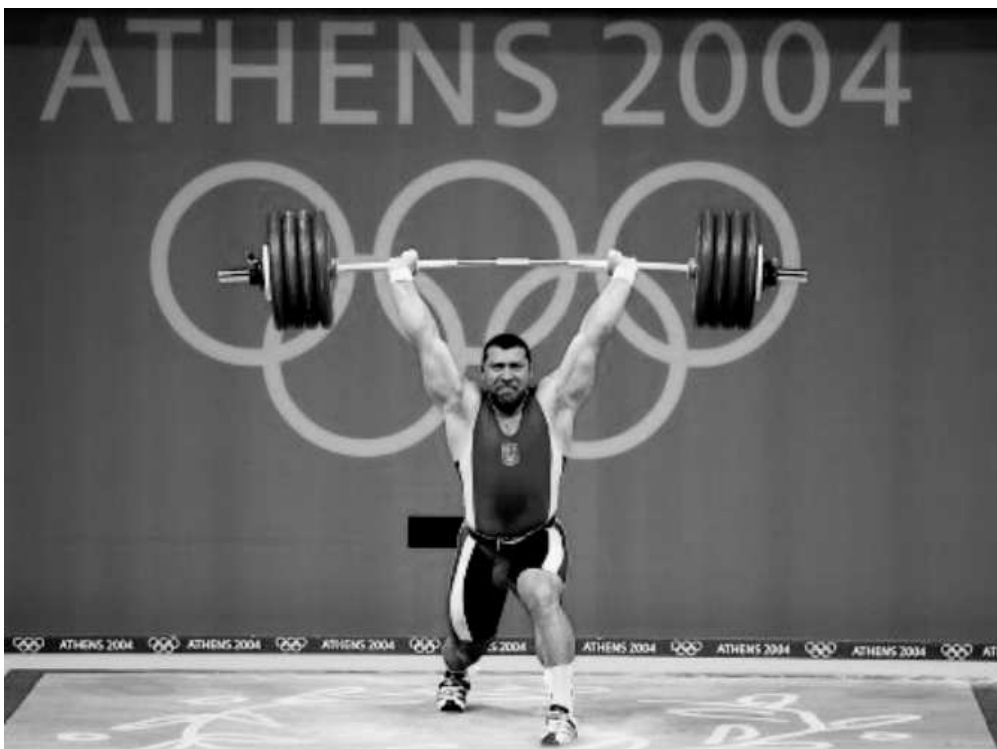
## 4.6 Conclusions

In this analytical study, joint translational stiffness  $K_y$  and maximal allowable subluxation force before a joint dislocation occurs  $F_{ymax}$  have been related to component design parameters and compression force  $F_z$ .  $K_y$  depends on the radius of curvature of both components, joint position and compression force  $F_z$ . The role of the stabilizing structures of the shoulder joint becomes clear by the influence of  $F_z$ . Additionally, it is found that humeral head translations can be divided in a stable and unstable region, depending on the sign of  $K_y$ .



## Chapter 5

# Force-controlled testing of shoulder prostheses



*Gennadiy Krasilnikov using his complete force capacity in the men's over 105 kg category weightlifting competition, Olympic Games, Athens, 2004*



## 5.1 Introduction

In Chapter 2 it is mentioned that the results of shoulder replacements must be improved in terms of long-term component fixation and post-operative shoulder joint functionality to increase patient satisfaction [105]. New prosthesis designs as well as improved surgical and fixation techniques must be developed and their performance must be validated using physiological loading and environmental conditions. Shoulder joint functionality causes repetitive eccentric loading of the glenoid component, leading to significant deformation of the implanted glenoid component structures. The flexural mismatch between component material, the bone cement and the surrounding bone tissue leads to high interface stresses. This may result in glenoid component loosening, as the materials react differently to the applied loading [255]. When evaluating glenoid component fixation, this failure mechanism must be considered for obtaining clinically relevant results.

Many experimental studies have investigated the effect of glenoid component design on its fixation by static loading [58, 87, 136] or cyclic loading [12, 14] of the glenoid component. In these experiments, glenoid components are fixated in bone substitutes and compressed against the humeral head. Cyclic loading of the glenoid components is the result of humeral head movements, which simulates shoulder joint subluxation. The repeatedly moving humeral head is fatiguing the implant-bone structure. In most of these studies, humeral head displacements are applied, e.g. the studies of Anglin et al. (2000) [12, 13], resulting in unknown and even unrealistic forces, depending on component geometry.

This can be explained using a rigid-body model (see Chapter 4), by investigating humeral head displacements in a conform and non-conform articulation. When applying a known increasing subluxation force and constant joint compression force, the humeral head will show zero and small displacements for the conform and non-conform articulation, respectively. Applying humeral head displacements in conform articulations must lead to structural deformation with accompanying high subluxation forces. Interface damage will occur immediately, always leading to the conclusion that non-conform articulations show better fixation performance. As a result, the conclusions of these studies might be doubtful with respect to the influence of certain design parameters, such as joint conformity, which is the subject of Chapter 6. The background of these displacement-controlled experiments, may be that a non-constant center of rotation (CoR) of the glenohumeral joint is assumed. However, as has been discussed in Section 2.3, the glenohumeral joint is commonly seen as a "ball-in-socket" joint, with a constant CoR.

In this study a new method of glenoid component testing is presented, with physiological glenoid component loading as a result of force-controlled humeral head movements. The force-controlled experimental set-up will be used for more realistic evaluation of component fixation of new glenoid component designs. The experimental set-up can be modified to be used to investigate prosthesis designs for similar

articular joints. The aim of the study is to demonstrate the new test set-up and to investigate the effect of bone substitute stiffness on glenoid component tilting.

## 5.2 Methods and Materials

### 5.2.1 Specimen structure

The glenoid components to be tested are machined out of medical grade Ultra-High-Molecular-Weight-Polyethylene (UHMWPE) (Chirulen 1020<sup>®</sup>, Poly-Hi Solidur GmbH, Vreden, Germany), with the geometry of a commercially available keeled design. Using self-manufactured glenoid components leads to better geometrical parameter control and more research flexibility compared to commercially available glenoid components. The components have a superior-inferior dimension  $c_g$  of 38.5 mm, corresponding to the measurements of Ianotti et al. [121] (see Table 2.1), a radial thickness of 7 mm and radius of curvature  $R_g$  of 29 mm, leading to a constraint angle  $\theta_0$  of 41.59° (see Figure 5.1). A self-manufactured CoCr humeral head with a radius of curvature  $R_h$  of 24 mm is used for articulating against the glenoid components, leading to a radial clearance  $\rho$  of 5 mm, a value which is often used in clinical practice. Although commercially available humeral heads have a decreasing radius of curvature towards the rim, to prevent soft-tissue damage, this will not influence the results of the proposed method of experimental investigation.

The glenoid components are fixed by Polymethyl-Methacrylate (PMMA) bone cement (Palamed G 20, Biomet Merck, Zwijndrecht, The Netherlands) into bone substitutes made of Polyurethane (Sawbones Europe AB, Malmö, Sweden). A homogenous cement thickness between implant and surrounding bone of 2 mm is used, to diminish the effect of thickness variations and to better investigate the effect of the geometrical parameters. To assure this homogenous cement thickness of 2 mm, a custom-made component alignment tool has been used, to insert the glenoid components into the bone substitutes (see Figure 5.2).

To demonstrate the functionality of the experimental set-up, a preliminary study to the effect of bone properties on glenoid tilting has been performed. Two types of bone substitutes have been used, namely a bone substitute with a solid, rigid morphology, having a stiffness and compressive strength of 260 MPa and 8.8 MPa, respectively, and one with an open cellular morphology, having stiffness and compressive strength of 47.5 MPa and 3.9 MPa, respectively. The stiffness of these two mechanically different bone substitutes are an upper and lower limit as found in literature (see Table B in Appendix B) and can also be seen as an indication for healthy and weakened trabecular bone. The glenoid-bone structures are fixed in a metal holder, which is connected to a guideway onto a horizontal sliding frame.

Complete clamping of glenoid bone specimens might not be realistic compared to the natural condition. The scapula is a triangular shaped bone, consisting of thin central parts (the scapular fossa) surrounded at the scapular edges by thicker margins [249], especially at the lateral edge. The most lateral and superior part of the glenoid bone structure is outside this triangular framework and has more freedom to deform (see Figure 5.1a). Therefore, only the medial half of the superior side of the bone substitute is clamped in the holder, to allow for a more natural deformation (see Figure 5.1b and c). All nuts of the clamp mechanism are tightened using a pre-set torque, to achieve good repeatability.

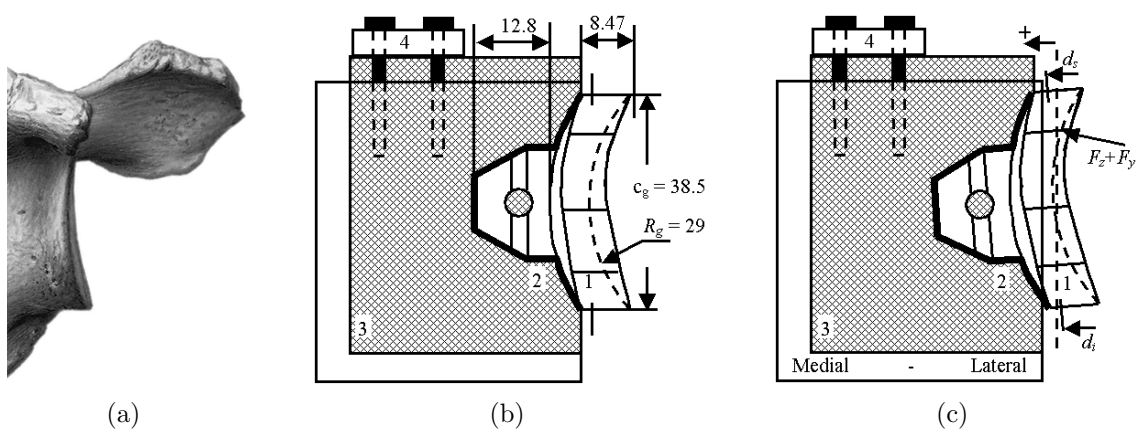


Figure 5.1: (a) Lateral scapula, demonstrating the lateral, superior edge of the glenoid cavity, which is free to deform in superior direction. (b,c) Glenoid component structure with dimensions (mm), (b) unloaded and (c) loaded. Where:  $d_i$  and  $d_s$  are the superior and inferior glenoid rim-displacements in medial-lateral direction, respectively,  $c_g$  is the SI glenoid chord length,  $F_y$  is the subluxation force acting at the center of the humeral head in the  $y$ -direction,  $F_z$  is the joint compression force acting at the center of the humeral head in the  $z$ -direction (see the List of Symbols). Displacements in medial direction are positive. 1. Glenoid component 2. Cement layer 3. Bone substitute 4. Clamp mechanism, to constrain the medial half of the superior surface of the glenoid specimen

## 5.2.2 Force-controlled fatigue testing

A force-controlled test set-up has been developed, which allows for humeral head translations as a result of known applied forces (see Figure 5.3). The humeral head (2 in Figure 5.3) is fixed to the shaft of a hydraulic actuator (12) of a materials tester (MTS, Eden Prairie, MN, USA) by vertical and horizontal force transducers (PW24C3, HBM, Darmstadt, Germany) (4 and 5, respectively), which measure the joint compression and subluxation force, respectively. Small displacements of the humeral head are applied by the hydraulic actuator and continually corrected if the

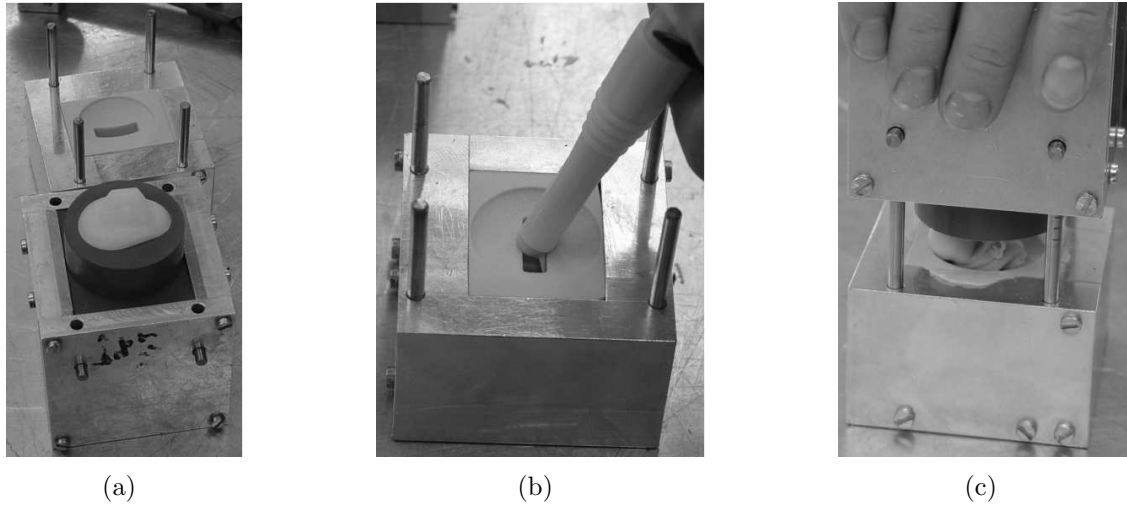


Figure 5.2: *Method of cementing glenoid components in the bone substitute using the alignment tool. (a) A rigid holder is used for the bone substitute and a negative mould is made of silicon rubber for the glenoid component. (b) Inserting bone cement using a special syringe. (c) The glenoid component is placed in position using the sliding frame with four pins, leading to a homogenous cement thickness of 2 mm*

measured peak subluxation force differs from the adjusted value, which is the so-called 'cascade' control mode.

By using a pneumatic cylinder, the glenoid components are compressed against the humeral head component, by a constant joint compression force of  $725 \pm 10 \text{ N}$ . The  $10 \text{ N}$  variation is due to the force-controlled humeral head displacements, which pushes the glenoid component structure into the pneumatic cylinder as a result of glenoid component concavity. Humeral head movement in superior direction is due to an applied hydraulic subluxation force  $F_y$ , cyclically varying between 0 and  $350 \pm 1 \text{ N}$  according to a sine function. These loading conditions correspond to arm abduction up to  $90^\circ$ , as analysed in a musculoskeletal model [108]. As a result, the humeral head moves from the zero position (center of the glenoid) to a superior position depending on glenoid component geometry. Load cycles start with a centered head ( $F_s = 0 \text{ N}$ ), and subsequently moves in superior direction due to the subluxation force with a maximum of  $350 \text{ N}$ , after which it returns to the centered position due to a decreasing subluxation force up to  $0 \text{ N}$  and a new cycle starts. A load cycle frequency of  $2 \text{ Hz}$  is chosen. Although shoulder movements are not performed with that high frequency, the separate movement may be rather fast. As a result, a compromise is used between reality and test efficiency.

Only the superior part of the glenoid component has been loaded, as this is the common direction of humeral head subluxation and to better investigate the effect of tensile and compression stresses on glenoid component fixation. In this study, for

each bone substitute three specimens have been loaded for 200.000 cycles, (corresponding to 44 load cycles per day for 12.5 years). Two glenoid components have undergone 1.000.000 cycles with given loading, to investigate if rim-displacements approximate a constant value after 200.000 load cycles.

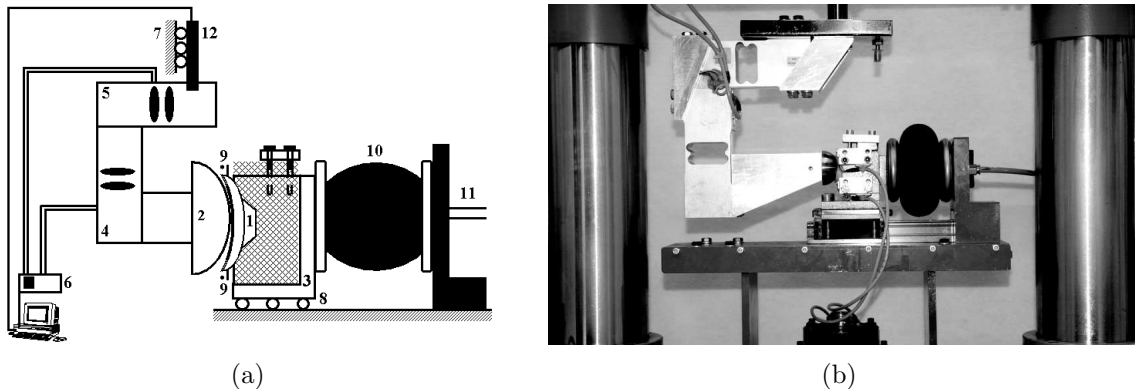


Figure 5.3: *The force-controlled test set-up. (a) Schematic overview of the test set-up. (b) The test set-up integrated in the MTS materials testing system. 1. Glenoid component 2. Humeral head 3. Glenoid bone substitute and metal holder 4. Vertical aligned load cell for measuring the joint compression force 5. Horizontal aligned load cell for measuring the joint subluxation force (PW24C3, HBM Darmstadt, Germany) 6. Signal amplifier (Peekel Instruments B.V., Rotterdam, The Netherlands) 7. Constraint only allowing vertical displacements 8. Constraint only allowing horizontal displacements 9. Superior and inferior rim-displacement sensors 10. Rodless pneumatic actuator (Festo B.V., Delft, The Netherlands) 11. Pressurized air input 12. Hydraulic actuator (MTS Systems Corporation, Eden Prairie, MN, U.S.A.). See Figure C.3a in Appendix C for a color representation*

### 5.2.3 Method of measurement and evaluation

#### Measuring structural deformation and humeral head displacement

Although debonding is the most clear definition for glenoid component loosening, in the literature no debonding was found during and after experimental fatigue testing and therefore other evaluation parameters have been looked for. Anglin et al. (2000) used glenoid rim-displacement as a measure for glenoid structure fixation performance, where larger glenoid rim-displacements indicate earlier complications at the interface of glenoid component fixation [12, 13]. In this study the same parameters, namely superior and inferior glenoid rim-displacements, were correlated to glenoid component fixation performance (see Figure 5.1). Glenoid component

loosening is thought to be due to glenoid component tilting, often referred to as glenoid component rocking, a result of eccentric loading [12, 58]. Eccentric loading, for example in the superior direction, will compress the superior side of the UHMWPE glenoid component ( $E=2.400 \text{ MPa}$ ) into the more flexible glenoid bone stock ( $E=47.5 \text{ MPa}$ ), leading to compressive stresses, whereas the inferior structure might undergo tensile stresses, due to structural deformation of the mechanically different materials. Structural deformation was determined during testing by measuring the superior and inferior rim-displacements in the medial-lateral direction,  $d_s$  and  $d_i$ , respectively, (see Figure 5.1), using custom-made displacement sensors (see Figure 5.4). The sensors are constructed out of a thin metal strip, clamped at one end and fixed to a small cylinder at the other end, which rests against a pin located at the glenoid component rims. Two strain gauges on both sides of the thin metal strip deform due to bending of the metal strip and are wired according to a Wheat-stone bridge. This is a chain of resistors, which measures the differential resistance by an applied constant voltage and the analog output is proportional to the deflection of the tip of the thin strip. The Wheat-stone bridge compensates for temperature difference and is used for zero-balancing.

After the 200.000 load cycles, 1,500 additional load cycles are applied and the maximal superior and minimal inferior rim-displacements, max.  $d_s$  and min.  $d_i$ , respectively, have been measured at load cycles 500, 1.000 and 1.500, whereafter the values are averaged. The measurements during these 1,500 additional load cycles have been repeated five times for each specimen, with the same loading conditions, so that each specimen finally undergoes a total of 7.500 additional load cycles. The maximal superior and minimal inferior rim-displacements are averaged for each specific bone substitute, which gives the final maximal superior and minimal inferior rim-displacements for each specific bone substitute. For each bone-substitute 3 specimens have been tested. Glenoid component tilting  $\lambda$ , a measure for upward and downward glenoid component rotation due to glenoid rim-displacements, is calculated as  $\lambda = \sin^{-1}((d_s - d_i)/c_g)^\circ$ , where  $c_g$  is 38.5 mm.

### Shear out testing for residual fixation strength evaluation

Although rim-displacements might be a good indication for the fixation performance of the glenoid structure, the real interface strength is a more realistic indicator. Therefore, after the fatigue tests have been completed and the rim-displacement measurements as well as visual inspection have been performed, the residual fixation strength is determined. In literature, many methods have been described, such as pull-out, push-in and shear-out [12] measurements. By 'push-in' testing, using an increasing compression force at the glenoid component, material failure will occur rather than the interface strength is being evaluated. Pull-out testing, using a laterally directed tensile force at the glenoid component, which will indeed lead to

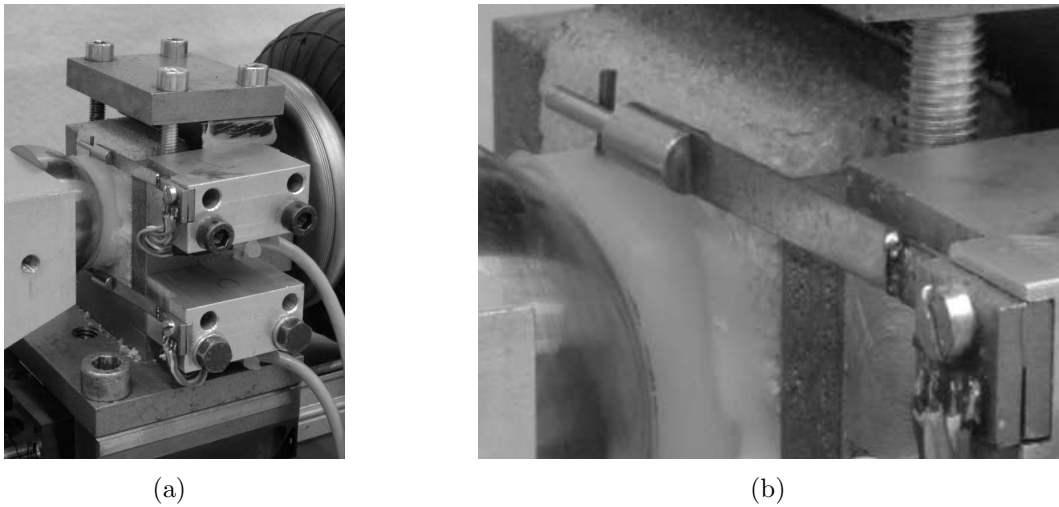


Figure 5.4: Close up of the rim-displacement sensors. (a) Humeral head (left) against the glenoid component, superiorly clamped at the medial half of the bone substitute. (b) Close up of the sensors for investigating glenoid component tilting, by measuring the medial-lateral displacements of the two pins in the superior and inferior glenoid rim. See Figure C.4 in Appendix C for color representations

interface failure, is a test with an un-physiological loading direction, thereby this method may give a not realistic interface strength.

In the present study, the interface strength has been determined by means of shear out testing according to ASTM F1829-98 [16]. A superior directed load is applied by a displacement-controlled metal plate at a speed  $0.1 \text{ mm/s}$  (see Figure 5.5). This speed was chosen to prevent the influence of time-dependent effects such as creep. As with the hydraulic actuator of the MTS materials tester it was easier to press downwards, the glenoid specimen is turned upside down in its holder, thereby mimicking a superior directed subluxation force  $F_y$ . A lateral shear force off-set  $d$  of  $4.5 \text{ mm}$  was chosen. The shear out force  $F_{shear}$  was monitored and the maximal value was taken as the shear out strength.

### Statistical evaluation

In this study, the effect of properties of the bone substitute on glenoid component tilting and residual fixation strength by shear out tests is evaluated by analyzing the obtained differences in superior and inferior glenoid rim-displacements and shear out strength, respectively, using the unpaired  $t$ -test with a confidential level of 95%.

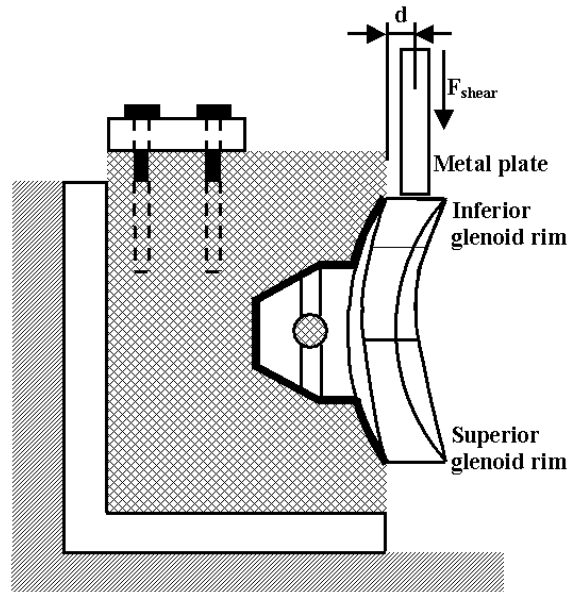


Figure 5.5: Method for evaluating the residual fixation strength by means of a shear out force after fatiguing the glenoid component. Where  $d$  is the lateral off-set of the shear force. As with the hydraulic actuator of the MTS materials tester it was easier to press downwards, the glenoid specimen is turned upside down, therefore the superior edge of the glenoid specimen is at the bottom.

### 5.3 Results

Within a few amount of load cycles the subluxation force reached the desired value and differences between the adjusted and measured values during testing were minimal. The custom-made rim-displacement sensors were calibrated and show a resolution of  $0.5 \mu\text{m}$  and are accurate up to displacements of  $5 \text{ mm}$ . A graphical representation of the joint subluxation force and superior rim-displacement versus cycle time is given in Figure 5.6. For the glenoid components cemented into the two different bone substitutes ( $n=3$ ) the rim-displacements were measured and the results are presented in Table 5.1. There was a significant difference of both rim-displacements and the shear out strength of the glenoid specimens cemented in the two different bone substitutes, using the unpaired  $t$ -test ( $p < 0.05$ ).

Complete loosening of the glenoid components, defined as glenoid component movement inside the bone when applying a very small loading, was not found. Not even for the two glenoid components which have been loaded for 1.000.000 cycles. However, for many glenoid components unbonding between glenoid component and bone cement was observed immediately after starting the experiments. This indicates that the UHMWPE glenoid components are fixed by mechanical interlocking rather than by adhesion.

After rim-displacement measurements, the residual fixation strength was determined by a shear out force, of which the results can be found in Table 5.1. From these results it is clear that higher structural deformations (as found with the open cellular bone) is related to a lower shear out strength.

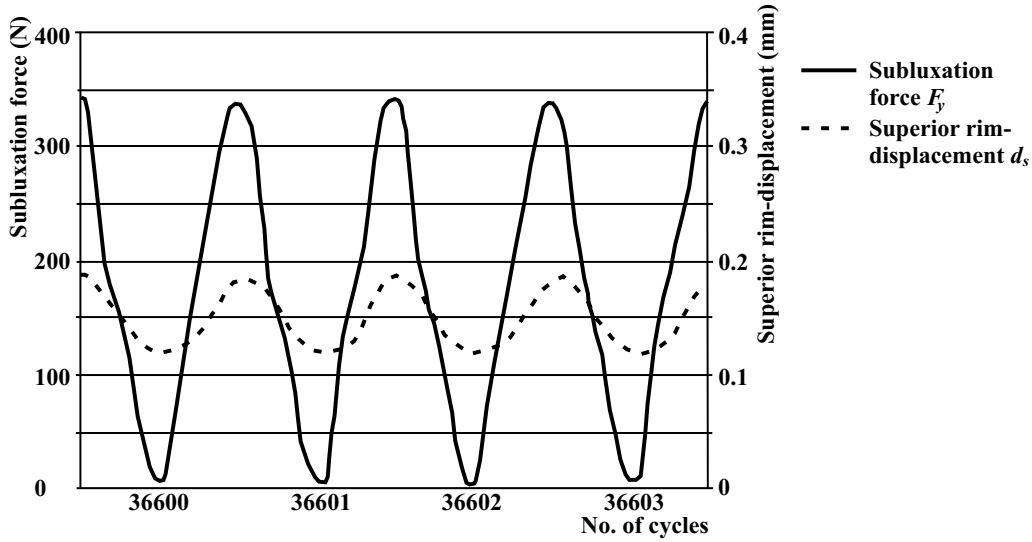


Figure 5.6: Graphical representation of the subluxation force and superior glenoid rim-displacement versus cycle time, during testing at four randomly chosen load cycles

Table 5.1: Results of the maximal superior and minimal inferior glenoid rim-displacement,  $\max. d_s$  and  $\min. d_i$ , respectively, in mm (mean (SD)) and shear out strength  $F_{shear}$  in N (mean (SD)) for the glenoid components with a radius of curvature of 29 mm and cemented into two different types of bone substitutes. Three glenoid specimens were tested for each bone substitute

Type of bone substitute	Stiffness ( $N/mm^2$ )	Max. $d_s$ (mm)	Min. $d_i$ (mm)	Tilting $\lambda$ ( $^\circ$ )	Max. $F_{shear}$ (N)
Solid bone	260	0.181 (0.02)	-0.00306 (0.007)	0.274	3185.3 (103)
Cellular bone	47.5	0.350 (0.02)	-0.0238 (0.01)	0.556	2631.1 (312)

## 5.4 Discussion

Anglin et al. (2000 and 2001) suggested combined force and displacement-controlled experimental testing in combination with rim-displacement measurements for design evaluation of glenoid components [12, 14]. By experimental testing, the maximal subluxation force with accompanying humeral head displacement was found and subsequently the glenoid components were loaded by 90% of the superior and inferior maximal humeral head displacement. This method assumes that glenohumeral

subluxation forces and humeral head displacements are the result of component geometry only, which might not be the most realistic assumption, especially for shallow components. As a result, largest rim-displacements were found for glenoid components with highest constraint angle  $\theta_0$ . However, this study shows similar rim-displacements as found in the study of Anglin et al. (2001) [14]. Bicknell et al. (2003) measured rim-displacements between the glenoid component and underlying bone, during joint loading of 250 N at different load angles [30]. They didn't apply a large amount of cycles before rim-displacement measurements, which might lead to unreliable results, as there is a run-in phase. In this phase, the absolute values of both rim-displacements increase and, providing that deformations are in the elastic region, their maximal and minimal reach a constant value. As a result of the different rim-displacement measurements and lower applied joint forces, the results are difficult to compare. However, they also found negative rim-displacements at the opposite side of glenoid component loading, similar to the results of the present study. Negative rim-displacements at the opposite side to glenoid component loading can occur in the case that the effect of glenoid component tilting exceeds that of joint compression, which causes both positive superior and inferior rim-displacements.

To my opinion, force-controlled humeral movement is the best option for experimental testing of glenoid components. However, it might be necessary to adjust the applied load spectrum for specific patient groups, as joint loading might be different due to the specific patient depended joint pathology. An example is RC arthropathy, which leads to decreased joint compression during joint movements.

In this study a homogenous cement thickness of 2 mm has been used, but such a constant cement thickness is impracticable in surgical practice. However, by using a constant cement thickness, the effect of, for example, joint conformity can be more accurately investigated, with higher significance, while the results still hold for the anatomic TSR.

Although differences in rim-displacement for different component designs might be a good indication to what extent the fixation of the glenoid component is damaged, this must be proven by residual fixation strength tests after fatigue testing. Such tests should always be made to better validate the effect of design parameters on component fixation.

As only the bone substitute has been changed, the different rim-displacements must be due the different material properties of the bone substitutes. This indicates that results for patients suffering from different diseases will have different loosening rates, as bone properties normally differ depending on the disease. As rim-displacements stabilize during the 200.000 cycles, it may well be that the deformations in the prosthetic structure are in the elastic region, as loading a structure in the plastic region will normally lead to increasing deformation.

It was found that many components did not adhere to the PMMA bone cement and are rather fixed by mechanical interlocking by holes and grooves at the medial surface of the glenoid component. As a result there will be micromotions between

the loaded UHMWPE component and the PMMA bone cement layer, resulting in abrasion of both UHMWPE and PMMA material. The relatively hard PMMA particles may find their way out of the UHMWPE-PMMA interface into the articular joint, where they cause third body wear [198, 358]. This wear mechanism increases the primary wear process between the articulating surfaces and therefore it may be a cause for component loosening.

Keels, with holes and grooves, or pegs are needed for good mechanical interlocking, which require much bone removal. It is unknown whether adhesion between the layers at this interface is beneficial for the presently used designs. However, adhesion of UHMWPE glenoid components may be used to develop a more superficial fixation in combination with design modifications. This method of component fixation will be investigated in Chapter 8.

The fact that no adhesion is present between the UHMWPE glenoid component and the PMMA bone cement also has consequences for the method of interface connections in Finite Element (FE) modelling. Commonly, this interface is supposed to be rigidly fixed and a full bonding is used, to connect the interface node-by-node. A more realistic method of interface modelling is to use contact elements and a coefficient of friction (CoF). The effect of the interface condition on the results of FE modelling is the subject of Chapter 9.

## 5.5 Conclusions

In this study, an experimental test set-up has been developed for evaluating the fixation strength of glenoid components to be used in a Total Shoulder Replacement. In the experimental set-up, humeral head motion is the result of applied forces. Using force-controlled humeral head motion will give better insight into the effect of geometrical design parameters of the glenoid component, compared to displacement-controlled humeral head motion. Custom-made displacement sensors are used to measure the structural deformation, indicating the future fixation performance of the glenoid component. Repeatable results are obtained and a significant difference in glenoid component tilting and shear out strength is found when using a more rigid or flexible bone substitute in this preliminary study.



## Chapter 6

# Effect of joint conformity on glenoid component fixation



*A lot of mimicking of the team of Spain during their session of  
the synchronized swimming competition, Olympic Games, Athens, 2004*



## 6.1 Introduction

The results of shoulder replacements in terms of post-operative functionality and long-term fixation must be improved to increase patient satisfaction [105, 353]. This study focuses on one geometrical design parameter, namely the joint conformity  $\kappa$ . Joint conformity  $\kappa$  is the ratio of the radius of curvature of the humeral head and the glenoid component and is calculated as  $\kappa = \frac{R_h}{R_g}$  (see Figure 6.1). Glenohumeral conformity in Total Shoulder Replacement (TSR) influences humeral head translations relative to the glenoid component, contact stresses on the glenoid component and accompanying component wear, which may finally lead to glenoid component radiolucency [135, 309, 336]. Humeral head translations in the superior ( $d_y$ ) and lateral ( $d_z$ ) direction increase with radial clearance  $\rho (= R_g - R_h)$ , and it can increase the glenoid component tilting moment  $M_c$  [129]. In a rigid-body model it can be demonstrated that this tilting moment  $M_c$  about the glenoid center at the articular surface  $c$ , a result of the eccentric joint contact forces acting on the glenoid component, is influenced by the radius of curvature of the glenoid component only, for given  $F_y$  and  $F_z$  (see Figure 6.1). The tilting moment  $M_c$  on the glenoid component deforms the Ultra-High-Molecular-Weight-Polyethylene (UHMWPE) glenoid component as well as the underlying cement layer and bone structure, which might lead to undesirable stresses at the interface and finally to component loosening. Clinically it is found that eccentric loading correlates with glenoid component loosening [291].

Two Finite Element (FE) studies have investigated the effect of joint conformity on stresses at the fixation. Lacroix and Prendergast (1997) analysed the cement stresses at the backside of low and high conform glenoid components and concluded that, with respect to cement stresses, more conform glenoid components should be used [161]. Couteau et al. (2001) also recommend a more conform glenoid component, as the decreased contact surface due to joint non-conformity leads to increased stresses at the glenoid component-cement interface [61]. High contact stresses, due to articular non-conformity, may exceed the yield strength of UHMWPE, resulting in higher risk of wear and subsurface cracks, leading to UHMWPE fatigue [309].

Only few clinical studies have investigated the influence of joint conformity on glenoid component fixation after TSR. Walch et al. (2002) evaluated 319 total shoulder arthroplasties with a range of radial clearances between 1.5 and 10 mm [336]. Although they found that more conform replacements show higher radiolucency scores, which is of great concern, this does not mean that more complications have to occur [34, 336]. In a retrieval study it was found that worn glenoid components better matched the humeral radius of curvature  $R_h$  than the original one, indicating the importance of articular conformity [110]. With respect to clinical results, it is unclear whether or not glenoid components must have high joint conformity with the humeral head [81].

Many experimental studies have investigated the effect of glenoid component design on its fixation by cyclic loading of the glenoid component. In general, glenoid

components are fixed in bone substitutes, compressed against the humeral head and humeral head movements repeatedly loaded the glenoid component structure, thereby fatiguing its interfaces. In these studies, humeral head displacements are applied, e.g. the studies of Anglin et al. (2000) [12, 13], resulting in unknown and even unrealistic forces. This can be explained using a rigid-body model (see Chapter 4), by investigating humeral head displacements in a conform and non-conform articulation, when applying a known increasing subluxation force and constant joint compression force. The humeral head will show zero and small displacements for the conform and non-conform articulation, respectively. Applying humeral head displacements in conform articulations must lead to structural deformation with accompanying high subluxation forces. Interface damage will occur immediately, always leading to the conclusion that non-conform articulations show better fixation performance. As a result, the conclusions of these studies might be doubtful with respect to the influence of glenohumeral conformity on glenoid component fixation. The aim of this study is to investigate the influence of glenohumeral conformity in TSR on glenoid component fixation, using the force-controlled experimental test set-up as described in Chapter 5.

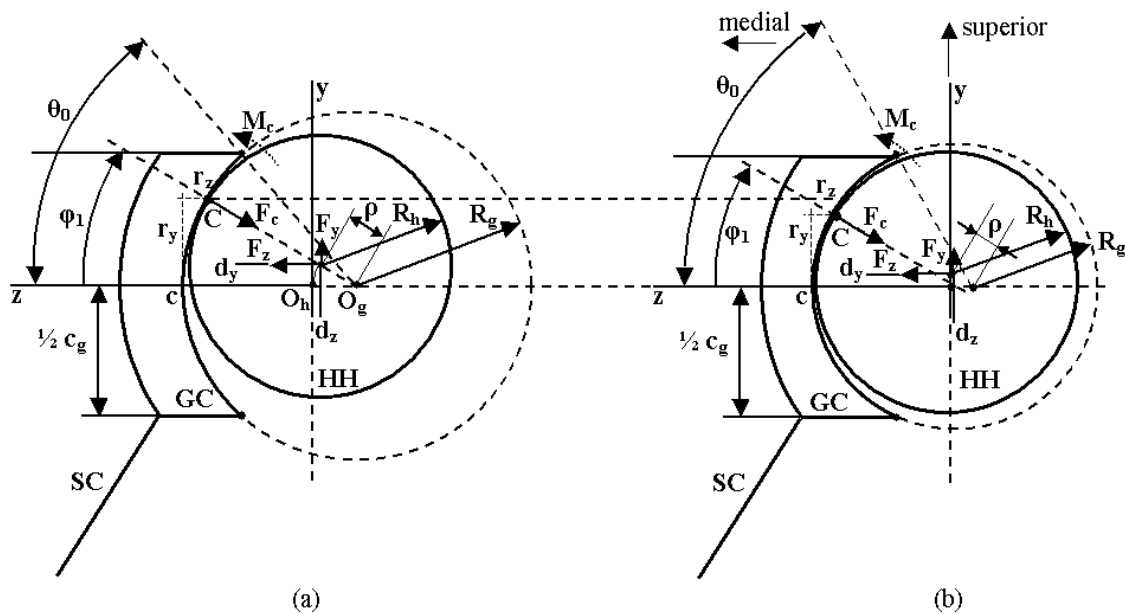


Figure 6.1: Schematic overview of the artificial shoulder joint (see also the List of Symbols). (a) A glenoid component with much larger radius of curvature than the humeral head (non-conform articulation). (b) An almost conform glenoid component

## 6.2 Materials and Methods

### 6.2.1 Specimen structure

Glenoid components were machined out of medical grade UHMWPE (Chirulen 1020<sup>®</sup>, Poly-Hi Solidur GmbH, Vreden, Germany), with the geometry of a commercially available keeled design. The components have a superior-inferior dimension  $c_g$  of 38.5 mm, corresponding to the measurements of Ianotti et al. [121] (see Table 2.1 in Chapter 2), a radial thickness of 7 mm and radii of curvature  $R_g$  of 29, 25 and 24 mm, leading to constraint angles  $\theta_0$  of 41.59°, 50,35° and 53.33°, respectively (see the List of Symbols and Figure 6.2). A CoCr humeral head with a radius of curvature  $R_h$  of 24 mm was used for articulating against the glenoid components. This leads to a radial clearance  $\rho$  of 5 mm (non conform), 1 mm (more conform) and 0 mm (exact conform) and conformity ratios  $\kappa$  of 0.83 (non conform), 0.96 (more conform) and 1 (exact conform). For each glenoid component radius of curvature, 5 glenoid specimens are investigated. The glenoid components were cemented into machined bone substitutes made of the cellular bone substitute as described in Chapter 5, with stiffness and compressive strength of 47.5 MPa and 3.9 MPa, respectively. The glenoid specimens fit into a metal holder and only the medial half of the superior side of the bone substitute is clamped, to allow for a more natural deformation (see Figure 6.2 and Section 5.2.1).

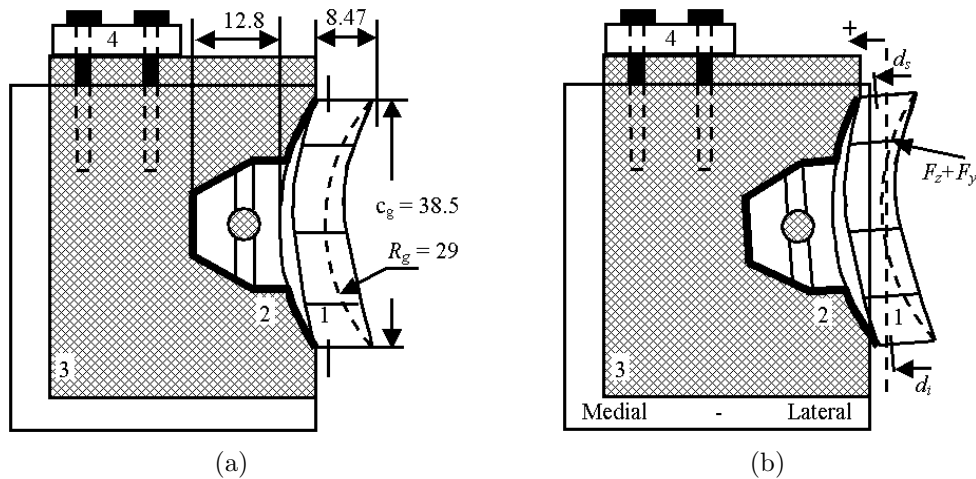


Figure 6.2: *Glenoid component structure with dimensions (mm), (a) unloaded and (b) loaded. Where:  $d_s$  and  $d_i$  are the superior and inferior glenoid rim-displacements in medial direction, respectively,  $F_y$  is the subluxation force acting at the center of the humeral head in the  $y$ -direction,  $F_z$  is the joint compression force acting at the center of the humeral head in the  $z$ -direction (see the List of Symbols). 1. Glenoid component 2. Cement layer 3. Bone substitute and metal holder 4. Clamping mechanism*

## 6.2.2 Force-controlled fatigue testing

The force-controlled shoulder simulator and test characteristics used for this study have been described in Chapter 5. For this study, similar loading conditions are used, namely a subluxation force  $F_y$ , cyclically varying between 0 and  $350 \pm 1$  N and a constant joint compression force of  $725 \pm 10$  N. For each radius of curvature, five specimens have been loaded for 200.000 cycles.

Additionally, two glenoid components with radii of curvature  $R_g$  of 25 and 29 mm have undergone 1.000.000 cycles with given loading. All components were visually inspected on loosening, defined as glenoid component movement inside the bone when applying only a very small force (e.g.  $< 5$  N).

## 6.2.3 Method of measurement and evaluation

### Measuring structural deformation and humeral head displacement

The rim-displacements have been measured, at intervals as described in Section 5.2.3. Humeral head displacements  $d_y$  are measured using the hydraulic actuator of the MTS materials tester. Additionally, humeral head displacements  $d_y$  at maximal subluxation force ( $F_y=350$  N) are compared to a frictionless rigid-body model (see Chapter 4).

### Shear out strength evaluation

All glenoid specimens were evaluated on their residual fixation strength by shear out experiments (see Section 5.2.3). According to ASTM standard ASTM F1829-98 [16], a displacement-controlled metal plate applied a superiorly-directed load at  $0.1$  mm/s. This speed was chosen to prevent the influence of time-dependent effects such as creep. A lateral shear force off-set  $d$  of 4.5 mm was chosen. The shear out force  $F_{shear}$  was monitored and the maximal value was taken as the shear out strength.

### Statistical evaluation

In this study, the effect of glenohumeral conformity on glenoid component tilting and residual fixation strength by shear out tests is evaluated by analyzing the obtained differences in superior and inferior glenoid rim-displacements and shear out strength, respectively, using the unpaired  $t$ -test with a confidential level of 95%.

### 6.3 Results

During cyclic loading, the superior  $d_s$  and inferior  $d_i$  rim-displacements increased and reached a constant value within 200.000 cycles (see Figure 6.3). The results of the rim-displacement measurements after the initial 200.000 cycles are given in Table 6.1 and in Figure 6.4. There was a significant difference between the maximal superior rim-displacement  $d_s$  of the conform ( $R_g=24$  mm), highly conform ( $R_g=25$  mm) and non-conform ( $R_g=29$  mm) articular combinations, using the unpaired  $t$ -test ( $p<0.05$ ). The minimal inferior rim-displacement  $d_i$  did not show this clear correlation with joint conformity, but for all specimens, negative inferior rim-displacements were found.

Maximal humeral head displacements  $d_y$  increased with decreasing joint conformity. Humeral head displacements were significantly different for the glenoid components with a radius of curvature  $R_g$  of 24 and 25 mm, compared to the 29 mm glenoid component ( $p<0.05$ ). Compared to the rigid-body model of Chapter 4, the maximal humeral head displacements  $d_y$  for articulating against glenoid components with a radius of curvature  $R_g$  of 24, 25 and 29 mm differed  $+\infty$ , -15.45 and -58.24 %.

None of the tested glenoid components, including the two glenoid components which have been loaded for 1.000.000 cycles, showed loosening after visual inspection. The shear out strength (max. value of  $F_{shear}$  during shear out tests) increased with increasing joint conformity, but this was not significant ( $p>0.05$ ). All tested glenoid specimens by the shear out force, showed a similar failure mode, namely an excessive plastic deformed glenoid component, rotated out of the cement layer about the keel with a loose superior cement part, cracked under  $45^\circ$  with the superior-inferior axis (see Figure 6.5).

Table 6.1: Maximal superior (Max.  $d_s$ ) and minimal inferior (Min.  $d_i$ ) glenoid rim-displacement (mm), glenoid component tilting  $\lambda = \sin^{-1}((d_s - d_i)/c_g)$  ( $^\circ$ ), where  $c_g$  is 38.5 mm), maximal humeral head displacement (Max.  $d_y$ ) (mm), of the experiments and the difference with the rigid-body model of Chapter 4 and shear out strength (Max.  $F_{shear}$ ) (N) (mean (SD)) for glenoid components with radii of curvature  $R_g$  of 24, 25 and 29 mm, articulating against a humeral head with radii of curvature  $R_h$  of 24 mm

Glenoid radius (mm)	Glenoid tilting by rim-displacement measurements					Shear out $F_{shear}$ (N)
	Max. $d_s$ (mm)	Min. $d_i$ (mm)	$\lambda$ ( $^\circ$ )	Max. $d_y$ (mm)	$\Delta$ to RB (%)	
24	0.163 (0.01)	-0.0257 (0.02)	0.28	0.607 (0.2)	$+\infty$	2707 (452)
25	0.299 (0.03)	-0.0362 (0.01)	0.49	0.651 (0.05)	-15.45	2648 (299)
29	0.350 (0.02)	-0.0238 (0.01)	0.56	1.386 (0.2)	-58.24	2631 (312)

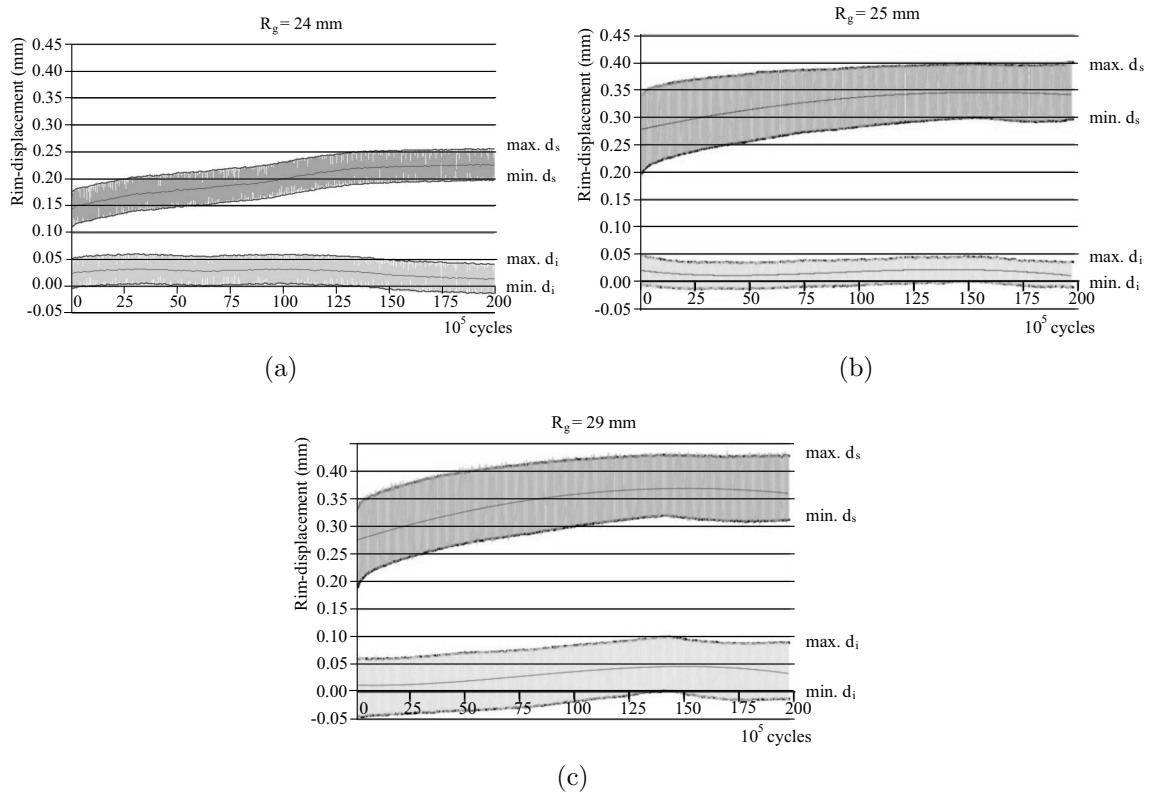


Figure 6.3: Typical glenoid rim-displacements during the 200,000 cycles of glenoid components with radii of curvature  $R_g$  of 24, 25 and 29 mm. Min. and max.  $d_s$  are the superior glenoid rim-displacements in medial direction at zero and maximal subluxation (350 N) force, respectively, and max. and min.  $d_i$  are the inferior glenoid rim-displacements in medial direction at zero and maximum subluxation force (350 N), respectively

## 6.4 Discussion

In this study, the effect of joint conformity on tilting and fixation strength of the cemented glenoid-bone structure has been investigated, by means of varying the radius of curvature of the glenoid component. A force-controlled test set-up has been developed, applying physiological joint subluxation and compression forces at the glenoid components. It was found that superior glenoid rim-displacements  $d_s$  decreased with increasing joint conformity. As the medial geometry of the glenoid components is kept constant, the differences in rim-displacements must be due to the different radius of curvature of the glenoid components. For given joint forces, the joint contact point is more centric for glenoid components with smaller radius of curvature, that is with higher joint conformity. The accompanying smaller structural deformation leads to lower strains and stresses at the interface, thereby it might postpone glenoid component loosening. Negative inferior rim-displacements

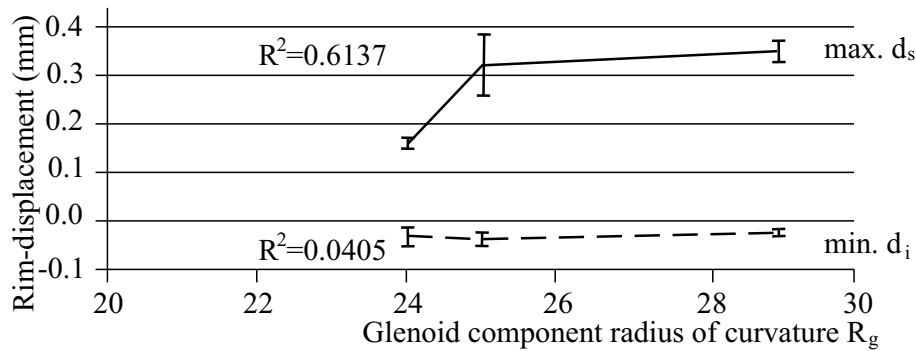


Figure 6.4: Results of the rim-displacement measurements for glenoid components with radii of curvature  $R_g$  of 24, 25 and 29 mm after 200.000 load cycles.  $R^2$  is the second order correlation coefficient

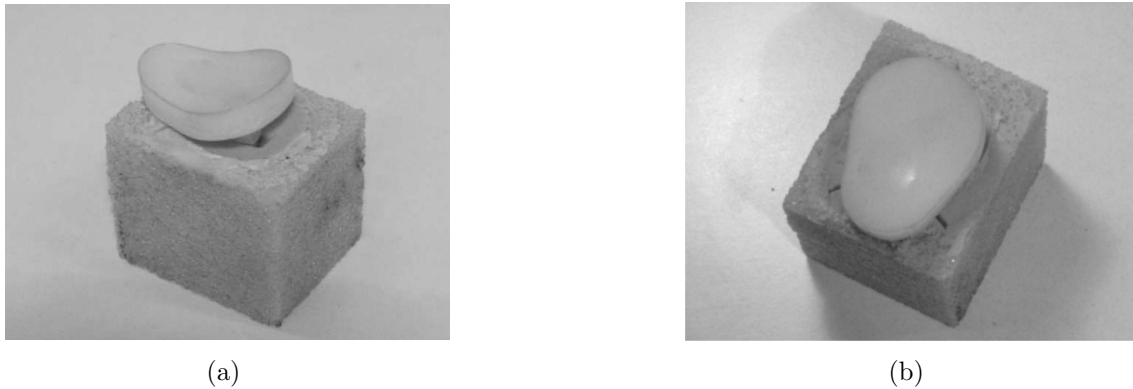


Figure 6.5: Glenoid component specimens after shear out tests. (a) Plastic deformation of the glenoid component around the keel structure. (b) The cement cracks are clearly visible

$d_i$  were found, indicating tensile stresses and strains at the bone-cement-component interfaces at the inferior side of the glenoid component. Indeed, the interfaces at the inferior glenoid are mentioned as critical zones for the presence of radiolucent lines, for example around the inferior keel [34].

In 'ball-in-socket' joints, such as the hip joint, the center of rotation (CoR) is fixed during articulation. Experimental testing of these joints should be done under force-controlled circumstances, using a physiological compression force (muscle forces) and subluxation force (external forces). The shoulder joint also can be seen as a 'ball-in-socket' joint, as stated by studies investigating the biomechanics of the shoulder joint [73, 139, 293, 244]. Many studies evaluating humeral head translations relative to the glenoid cavity in the healthy shoulder conclude that the CoR is fixed [73, 139, 293], others state that the humeral head shows only small translations [244], mainly as a result of cartilage deformation. The almost constant CoR in

natural glenohumeral joints during humeral movements implies that, if humeral head translations occur, these are the result of external subluxation forces, for example when carrying a bag. As a result, natural humeral head translations are the result of known applied external forces. When applying displacements in experimental testing, the resulting forces will depend on material properties and structural geometry and can be unrealistically high. Therefore, fatigue testing of the fixation of the glenoid component should be done by applying an external load spectrum on the humeral head according to typical 'activities of daily living' (ADL). Only this method of experimental testing provides proper insight into the effect of geometrical changes on the fixation of glenoid components. Anglin et al. (2000) suggested combined force and displacement-controlled experimental testing for the evaluation of glenoid components [12]. By experimental testing the maximal subluxation force with accompanying humeral head displacement was found and subsequently the glenoid components were loaded by 90% of the superior and inferior maximal humeral head displacement [12]. This method assumes that glenohumeral subluxation forces and humeral head displacements are the result of component geometry only, which might not be the most realistic assumption, especially for shallow components. Force-controlled humeral head movement seems to be a better option for experimental testing of glenoid components. Additionally, this method of testing allows for adjusting the applied forces to a pathologic specific load spectrum.

Maximal humeral head displacements  $d_y$  were compared to a rigid-body model and large differences were found. This is due to the fact that flexible materials are used in the experiments (see for example the difference in the case of a conform articulation in Table 6.1). However, in the case of articular non-conformity smaller displacements  $d_y$  are found as compared to the rigid-body model. This may be due to friction between the CoCr humeral head and the UHMWPE glenoid component, as this friction develops a force opposite to the subluxation force.

Most glenoid components showed immediate unbonding between glenoid component and bone cement after starting the experiments. This indicates that UHMWPE glenoid component fixation relies on mechanical locking rather than on adhesion. However, complete loosening of the glenoid components, as defined in Section 6.2, was not found after fatigue testing, not even for the two glenoid components which have been loaded for 1.000.000 cycles.

Although it was found in this study that higher joint conformity shows smaller structural deformation, with accompanying longer component fixation, in clinical practice other factors should be considered. In the case of a conform articulation, the accuracy of glenoid component positioning is of critical importance. A shifted glenoid component might lead to glenoid rim loading, leading to high local stresses, resulting in component deformation and wear. Proper alignment tools and modern (3D visualized) operation planning techniques are a requisite when using conform glenoid components.

## **6.5 Conclusions**

In this study the effect of joint conformity on component tilting and fixation strength of the cemented glenoid-bone structure has been investigated. It was found that higher articular conformity (smaller glenoid component radius of curvature) decreases glenoid component tilting, which might be advantageous for glenoid component fixation. If the orthopaedic surgeon is able to accurately position the glenoid component, the use of more conforming prostheses decreases the deformation of the replaced glenoid structure, which might be beneficial for long-term component fixation.



## Chapter 7

# Effect of glenoid component inclination on its fixation and humerus subluxation



*Hans Peter Steinacher and Roman Hagara searching for their optimal sailing angle during the open multihull tornado finals race, Olympic Games, Athens, 2004*



## 7.1 Introduction

Main complications after a TSR are shoulder subluxation, dislocation and component loosening [353]. The results of shoulder replacements must be improved to increase patient satisfaction and long-term component fixation [105, 353].

Correct component positioning by the surgeon is mentioned as a critical factor for functioning and survival of the TSR [286]. Glenoid component inclination angle, related to how much the glenoid component articular surface is facing upward or downward, is such a positioning factor. In a follow-up study, it was found that after an average of 92 months, 26% of the loosened glenoid components changed position and orientation and 3 out of 7 (43%) superior off-center loaded glenoid components showed radiographic loosening, which all were upward facing glenoid components [291]. Additionally, the inclination angle of the anatomical glenoid cavity is associated with Rotator-Cuff (RC) tears [116, 314], which may lead to decreased shoulder functionality. Wong et al. (2003) investigated the effect of glenoid inclination on superior humeral head migration in anatomical and prepared glenoid structures. Glenoid inclination angles of 5°, 10° and 15° were created using wedges and led to a decreased force to produce superior humeral head migration up to 37.5% [355].

Using a rigid-body model, it is calculated that increased glenoid component inclination locates the contact point more off-center and increases the accompanying tilting moment on this component. The increased component tilting, may lead to increased structural deformation, thereby affecting long-term glenoid component fixation. Glenoid component orientation may also change the constraint angle  $\theta_\gamma$  (see Figure 7.1). Thereby it influences humeral head migration, subluxation and it may increase the chance of a humerus dislocation, which are mentioned as main complications after a TSR. From a clinical and biomechanical perspective the importance of glenoid component inclination on shoulder joint functionality and survival of TSR has been indicated. However, the effect of glenoid component inclination on glenoid tilting and fixation as well as on humeral head subluxation in TSR is still unknown. In the present study, glenoid rim-displacements are related to glenoid fixation performance. Glenoid component loosening is thought to be due to glenoid component tilting, often referred to as glenoid component rocking, a result of off-center loading [12, 53]. Off-center loading, for example in the superior direction, will compress the superior side of the glenoid component into the glenoid bone stock, leading to compressive stresses, whereas the inferior structure might undergo tensile stresses, due to bone deformation and glenoid component tilting. This glenoid component tilting may lead to early glenoid component loosening after a TSR. However, it is still unknown how this is influenced by glenoid component inclination.

The aim of this study is to investigate the influence of glenoid component inclination in TSR on tilting of cemented glenoid-bone structures and humeral head subluxation, using a rigid-body model and a force-controlled testing apparatus.

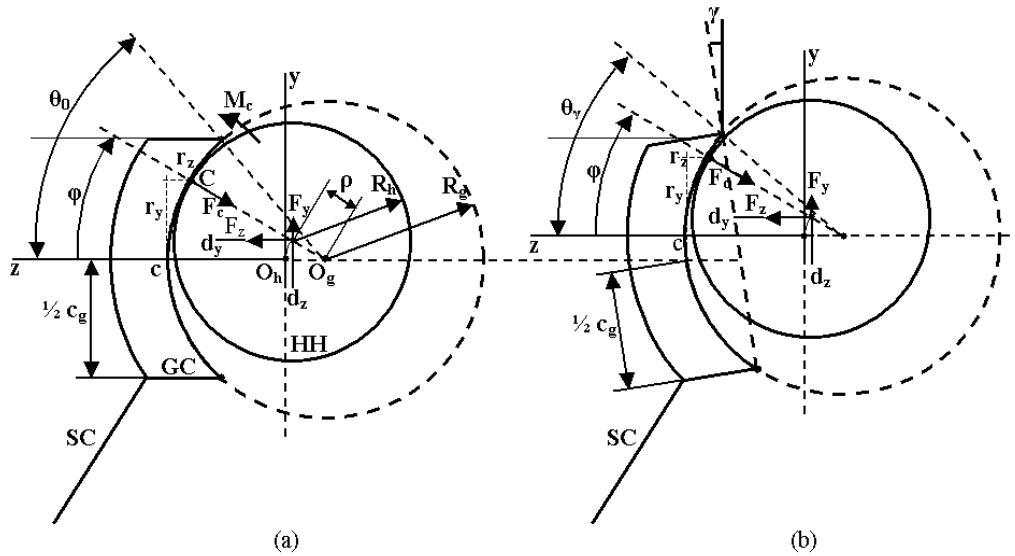


Figure 7.1: Schematic overview of the artificial shoulder joint (for description of the symbols see the List of Symbols). (a) Glenoid component, inserted with inclination angle  $\gamma=0$ . (b) Glenoid component, inserted with inclination angle  $\gamma>0$

## 7.2 Methods

### 7.2.1 Specimen structure

Glenoid components are machined out of medical grade Ultra-High-Molecular-Weight-Polyethylene (UHMWPE) (Chirulen 1020<sup>®</sup>, Poly-Hi Solidur GmbH, Vreden, Germany), with the geometry of a commercial available keeled design. The components have a superior-inferior dimension  $c_g$  of 38.5 mm, corresponding to the measurements of Ianotti et al. (1992) [121] (see Table 2.1), a radial thickness of 7 mm and a radius of curvature  $R_g$  of 29 mm, leading to a constraint angle  $\theta_0$  of 41.59° (see the List of Symbols and Figure 7.1). When increasing the inclination angle, leading to a more upward facing glenoid component, the constraint angle  $\theta_\gamma$  decreases equal to the increase of  $\gamma$ :  $\theta_\gamma = \theta_0 - \gamma$ . A CoCr humeral head with a radius of curvature  $R_h$  of 24 mm is used for articulating against the glenoid components, resulting in a radial clearance  $\rho$  of 5 mm. This value is chosen as it is presently a recommended value for commonly used glenohumeral replacements [336]. The glenoid components were cemented into machined bone substitutes made of the cellular bone substitute as described in Chapter 5, with stiffness and compressive strength of 47.5 MPa and 3.9 MPa, respectively. The glenoid specimens used in this study are similar to the glenoid specimens with a radius of curvature of 29 mm used in Chapter 6.

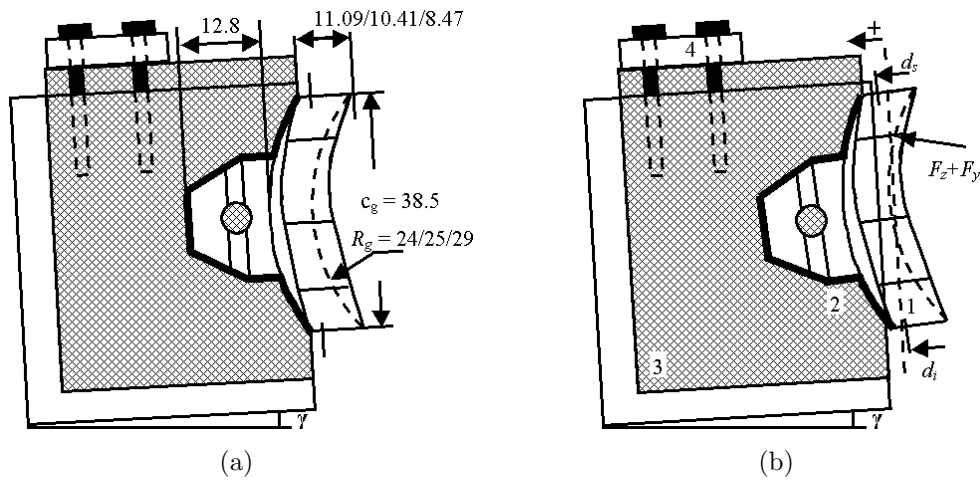


Figure 7.2: *Inclined glenoid component structure with dimensions (mm), (a) unloaded and (b) loaded. Where:  $\gamma$  is the inclination angle,  $d_i$  and  $d_s$  are the superior and inferior glenoid rim-displacements in medial direction, respectively,  $F_y$  is the subluxation force acting at the center of the humeral head in the  $y$ -direction,  $F_z$  is the joint compression force acting at the center of the humeral head in the  $z$ -direction (see the List of Symbols). 1. Glenoid component 2. Cement layer 3. Bone substitute and metal holder 4. Clamping mechanism*

## 7.2.2 Force-controlled fatigue testing

The basis of the force-controlled shoulder simulator and test characteristics used for this study have been described in Chapter 5. However, the set-up has been rotated using metal wedges, (see Figure 7.3), leading to a range of glenoid component inclination angles between  $-4.5^\circ$  up to  $4.5^\circ$  by steps of  $1.5^\circ$ . For this study, the loading conditions as described in Chapter 5 are used, namely a subluxation force  $F_y$ , cyclically varying between  $0$  and  $350 \pm 1$  N and a constant joint compression force  $F_z$  of  $725 \pm 10$  N. For each inclination angle, five specimens have been loaded for 200.000 cycles ( $n=5$ ).

## 7.2.3 Method of measurement and evaluation

### Measuring structural deformation and humeral head displacement

During the 200.000 load cycles, the superior and inferior rim-displacements  $d_s$  and  $d_i$  are monitored, using custom-made displacement sensors, which, together with the method of measuring glenoid rim-displacements, are described in Section 5.2.3. Humeral head displacement  $d_y$  is measured using the hydraulic actuator of the MTS materials tester and is compared to a rigid-body model (see Chapter 4). Using this

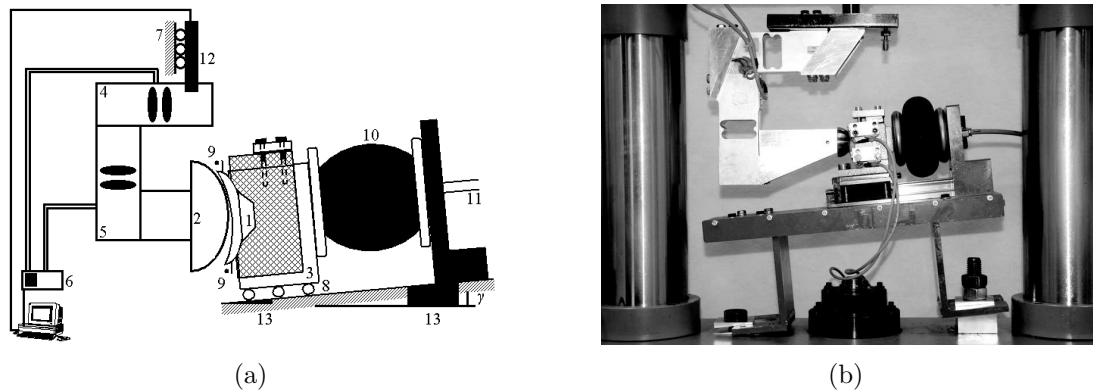


Figure 7.3: *The inclined force-controlled test set-up. (a) Schematic overview of the test set-up. (b) The set-up integrated in the materials testing system. 1. Glenoid component 2. Humeral head 3. Glenoid bone substitute and metal holder 4. Horizontal aligned load cell for measuring the subluxation force 5. Vertical aligned load cell for measuring the compression force (PW24C3, HBM Darmstadt, Germany) 6. Signal amplifier (Peekel Instruments B.V., Rotterdam, The Netherlands) 7. Linear bearing only allowing vertical displacements 8. Linear bearing only allowing horizontal displacements 9. Superior and inferior rim-displacement sensors 10. Rodless pneumatic actuator (Festo B.V., Delft, The Netherlands) 11. Pressurized air input 12. Hydraulic actuator (MTS Systems Corporation, Eden Prairie, MN, U.S.A.) 13. Metal wedges rotating the set-up, leading to the desired glenoid component inclination angle  $\gamma$ . See Figure C.3b in Appendix C for a color representation*

model, the humeral head displacement  $d_y$  can be calculated by  $d_y = \rho \sin \varphi$ , where  $\rho$  is the radial clearance between the glenoid and humeral component ( $R_g - R_h$ ) and  $\varphi = \tan^{-1}(F_y/F_z)$ . In this study  $\rho = 5 \text{ mm}$  and  $\varphi$  is  $25.77^\circ$  at the maximal subluxation force of  $350 \text{ N}$ , leading to a constant maximal humeral head displacement  $d_y$  of  $2.174 \text{ mm}$ .

### Humeral head subluxation

After fatigue testing and rim-displacement measurements, the effect of glenoid component inclination on superior humeral head subluxation has been evaluated. A range of inclination angles  $\gamma$  between  $-4.5^\circ$  and  $+3^\circ$  (downward and upward facing glenoid components, respectively) by steps of  $1.5^\circ$  is chosen, in a similar way as for the rim-displacement measurements. For each inclination angle, five specimens have been tested.

Humeral head subluxation is displacement-controlled, translating upward with a speed of  $0.17 \text{ mm/s}$ , starting from the center of the glenoid cavity up to almost half the glenoid component superior-inferior dimension  $c_g$  (see Figure 4.1), thereby al-

most causing humeral head dislocation. In this experiment humeral head movement is displacement-controlled, as this has been investigated for continuing humeral head translations after  $F_{y_{max}}$  has been reached. A force-controlled test is not possible in this unstable articular region (see Chapter 4). Small initial joint compression of about 30 N is applied, which increases during humeral head subluxation, due to glenoid component concavity and characteristics of the pneumatic system. During subluxation, both the subluxation force ( $F_y$ ) and compression force ( $F_z$ ) are monitored with a sampling rate of 400 Hz. Small joint compression is used, to minimize the effect of glenoid component deformation. The subluxation over joint compression force ratio  $\frac{F_y}{F_z}$  as a function of the humeral head displacement, as obtained in the experiment, is compared to the rigid-body model to create the possibility to easily interpolate or extrapolate the experimental results without extensive computational effort. This force ratio can be calculated for articulation inside the glenoid cavity (stable articulation, equation 7.1) and about the glenoid rim (unstable articulation, equation 7.2) (see Figures 1a and c in the List of Symbols):

$$\frac{F_y}{F_z} = \frac{d_y}{\sqrt{\rho^2 - d_y^2}} \quad (7.1)$$

$$\frac{F_y}{F_z} = \sqrt{\frac{(R_h \sin\theta_\gamma - (d_y - \rho \sin\theta_\gamma))^2}{R_h^2 - (R_h \sin\theta_\gamma - (d_y - \rho \sin\theta_\gamma))^2}} \quad (7.2)$$

where  $F_y$  and  $F_z$  are the joint subluxation and compression force, respectively,  $d_y$  the humeral head displacement in  $y$ -direction,  $\rho$  the radial clearance between the glenoid ( $R_g$ ) and humeral ( $R_h$ ) component and  $\theta_\gamma$  the glenoid component constraint angle for inclination angle  $\gamma$ . Using the rigid-body model, the changeover from stable to unstable articulation is at a humeral displacement  $d_y$  of  $d_y = \rho \sin\theta_\gamma$ , which simultaneously corresponds with the maximal subluxation over compression force ratio ( $= \frac{F_{y_{max}}}{F_z}$ ).

### **Statistical evaluation**

In this study, the effect of glenoid component inclination on glenoid component tilting and humeral head subluxation is evaluated by analyzing the obtained differences in superior and inferior glenoid rim-displacements and the subluxation over joint compression force ratio  $\frac{F_y}{F_z}$ , respectively, using the unpaired  $t$ -test with a confidential level of 95%.

## Component loosening

After fatigue testing, rim-displacement measurements and humeral head subluxation experiments, components were inspected visually on surface damage and component loosening. In this study, component loosening is defined if movement occurs between the glenoid component relative to the Polymethyl-Methacrylate (PMMA) bone cement - bone structure, when only applying a very small loading (e.g.  $<5 N$ ).

## 7.3 Results

The superior and inferior glenoid rim-displacements increase during the 200.000 load cycles, until they reach a constant value (see Figure 7.4). The absolute values of both the positive superior and negative inferior rim-displacement,  $d_s$  and  $d_i$  respectively, significantly increased for increasing inclination angles, using the unpaired  $t$ -test,  $p < 0.05$  (see Table 7.1 and Figure 7.5). Additionally, high correlation  $R^2$  with the inclination angle was found, with values of 0.8832 and 0.8318 for  $d_s$  and  $d_i$ , respectively. Positive and negative rim-displacements indicate compression into and translating of the glenoid component away from the bone substitute, respectively. Humeral head displacements  $d_y$  for maximal subluxation force  $F_y$  are given in Table 7.1, with an average of 1.986 (SD=0.3)  $mm$  and showed very small correlation with the inclination angle  $\gamma$  ( $R^2=0.208$ ), which is in agreement with the constant humeral head displacement as calculated using the rigid-body model. The difference between the experimental humeral head displacement and the rigid-body displacement ranged between -30.96% ( $\gamma=1.5^\circ$ ) and +7.08% ( $\gamma=4.5^\circ$ ). The variation in humeral head displacement might be due to different structural deformation depending on compression force and inclination angle  $\gamma$ .

After rim-displacement measurements, the effect of glenoid component inclination on superior humeral head subluxation has been investigated and compared to the rigid-body model (see Table 7.1 and Figure 7.6). As the humeral head moves in superior direction, an exponential increasing subluxation force is required during stable articulation (Figure 7.1), due to glenoid component geometry. The force ratio  $\frac{F_y}{F_z}$  increases up to a maximum, as the contact point between the glenoid and humeral component reaches the glenoid rim and thus depends on the constraint angle  $\theta_\gamma = \theta_0 - \gamma$ . Continuing superior humeral head translation goes together with a decreasing subluxation force, which is only influenced by the radius of curvature of the humeral head, articulating about the glenoid rim. For increasing glenoid component inclination angles, the maximal force ratio  $\frac{F_y}{F_z}$  as found in the experiments decreases from 1.13 ( $\gamma=-4.5^\circ$ ) to 0.61 ( $\gamma=3^\circ$ ). This difference is significant (unpaired  $t$ -test,  $p < 0.05$ ). In the rigid-body model, this force ratio decreased from 1.04 to 0.80 for the same inclination angles (see Table 7.1). Besides small scratches of the

UHMWPE component, no surface damage was found of the PMMA bone cement and bone substitute. Glenoid component loosening, as defined in this study, was not found for any of the components after experimental testing. However, not any component showed UHMWPE-PMMA bonding, as after glenoid specimen bisection, glenoid components were loose from the bone cement and could be easily removed.

Table 7.1: Results of the rim-displacement and subluxation experiments with a comparison to the rigid-body (RB) model (mean (SD)).  $\lambda$  is calculated as  $\sin^{-1}((d_s - d_i)/c_g)$  and  $\Delta RB$  is the differences of the experiments with respect to the rigid-body model

$\gamma$ ( $^\circ$ )	Glenoid tilting by rim-displacement measurements					Subluxation Exp.	
	Max. $d_s$ Exp. (mm)	Min. $d_i$ Exp. (mm)	$\lambda$ Exp. ( $^\circ$ )	$d_y$ at $F_y=350$ N Exp. (mm)	$\Delta RB$ (%)	Max. $F_y/F_z$ Exp. (-)	$\Delta RB$ (%)
-4.5	0.264 (0.02)	-0.00738 (0.01)	0.40	2.044 (0.1)	-5.97	1.13 (0.05)	+8.65
-3	0.330 (0.06)	-0.0414 (0.01)	0.55	1.973 (0.1)	-9.25	1.01 (0.04)	+2.02
-1.5	0.274 (0.02)	-0.04571 (0.02)	0.48	1.501 (0.2)	-30.96	0.87 (0.07)	-7.45
0	0.350 (0.02)	-0.0238 (0.01)	0.56	1.947 (0.3)	-10.44	-	-
1.5	0.397 (0.07)	-0.130 (0.04)	0.78	2.134 (0.5)	-1.84	0.68 (0.05)	-19.05
3	0.427 (0.08)	-0.132 (0.01)	0.83	1.973 (0.3)	-9.25	0.61 (0.04)	-23.75
4.5	0.484 (0.06)	-0.200 (0.03)	1.02	2.328 (0.2)	+7.08	-	-

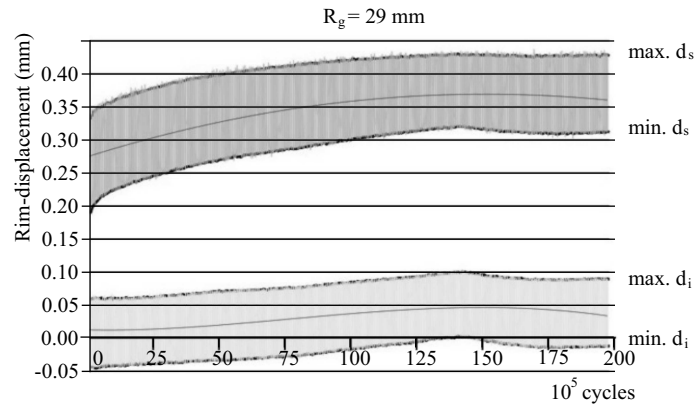


Figure 7.4: Development of glenoid rim-displacements during the 200,000 cycles of a glenoid component inserted with inclination  $\gamma=0^\circ$ , articulating against a humeral head with  $R_h=24$  mm. Max. and min.  $d_s$  are the superior glenoid rim-displacements in medial direction at zero and maximal (350 N) subluxation force, respectively, and max. and min.  $d_i$  are the inferior glenoid rim-displacements in medial direction at zero and maximal subluxation force (350 N), respectively

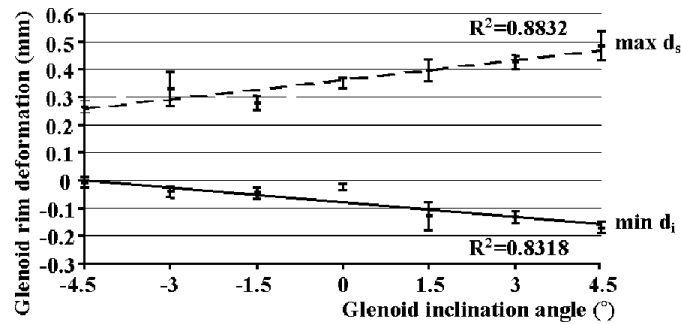


Figure 7.5: Results of the rim-displacement measurements for glenoid components inserted with inclination angles ranging between  $-4.5^\circ$  and  $+4.5^\circ$ . Max.  $d_s$  and min.  $d_i$  are the maximal superior and minimal inferior rim-displacement, respectively.  $R^2$  is the second order correlation coefficient

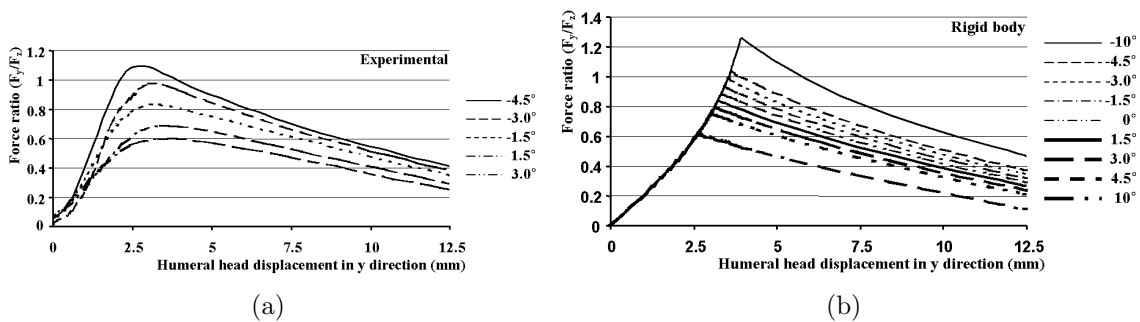


Figure 7.6: Results of the humeral head subluxation experiments for different glenoid inclination angles. (a) Results of the experiments for glenoid components inserted with inclination angles  $\gamma$  ranging between  $-4.5^\circ$  and  $3^\circ$ . (b) Results of the rigid-body model

## 7.4 Discussion

In this study, the influence of glenoid component inclination in TSR on tilting of cemented glenoid-bone structures and humeral head subluxation has been investigated, using a force-controlled test set-up with physiological loading conditions and a rigid-body model. It was found that increasing glenoid component inclination angles increased the absolute value of the positive superior ( $d_s$ ) and negative inferior rim-displacements ( $d_i$ ). As loading conditions and glenoid specimens are similar for different inclination angles, this difference in rim-displacements must be due to the glenoid component inclination angle only. The increasing rim-displacements also indicate increasing compression and tension in the superior and inferior structure,

respectively, of which especially tensile stresses can be harmful for glenoid component fixation. This has also been indicated in a study by Nagels et al. (2002), focusing on glenoid component loosening, in that study defined by the presence of radiolucent lines or a component shift. Glenoid component loosening was found to be present predominantly at the inferior side of the glenoid component [220]. Therefore, the results of the present study indicate decreased glenoid component loosening for decreasing glenoid inclination angles, as decreased component tilting and humeral head subluxation are found.

The absolute values of the inferior rim-displacements are smaller than the superior rim-displacements (see Figure 7.5), which is the result of three causes. First, only the superior glenoid surface has been loaded, leading to larger deformations of the superior glenoid and underlying structures. Second, the superior glenoid component contains less material volume, leading to larger deformations of this part of the glenoid component than the inferior part. Finally, although both the superior and inferior glenoid rim undergo equal joint compression at  $F_y=0$ , the component tilting should be added to the superior rim and subtracted from the inferior rim. Superior glenoid rim-displacements therefore increase, while inferior glenoid rim-displacements decrease and even get negative.

The difference of the smaller maximal force ratio  $\frac{F_{y,max}}{F_z}$  of the subluxation experiment compared to the rigid-body model is increasing for increasing inclination angles  $\gamma$ . This might be due to the influence of superior glenoid structure deformation, and friction between the CoCr humeral head and the UHMWPE glenoid component. Superior glenoid structure deformation decreases the constraint angle and thereby also the maximal force ratio and friction between the CoCr humeral head and the UHMWPE glenoid component increases the maximal force ratio [12].

Shoulder surgery is difficult, due to the bad exposure of the glenohumeral joint and joint pathology. However, the surgeon should keep in mind the importance of glenoid component inclination as found in this study. Additionally, the results of the present study indicate the need for accurate surgery, using improved alignment tools or computer assisted surgery. It is found that a more downward facing glenoid component shows smaller rim-displacements compared to an upward facing glenoid component, in the case of superior off-center loading.

Two well-known options exist to achieve a more downward facing glenoid component. If enough bone is present, bone reaming can be used, which is milling of the glenoid cavity to change its orientation. The other option is to use bone grafting, which is fixing small bone specimens to the glenoid cavity out of the removed humeral head to change glenoid cavity orientation. As it adds bone volume it doesn't weaken the glenoid structure and is a good method, although it might be difficult to perform [226, 306]. Another option is to insert glenoid components as shown in Figures 7.7b and c. The presented glenoid components consist of a metal backing, in which a glenoid inlay is positioned under an angle opposite to the inclination angle of the prepared glenoid bone. As a result, it neutralizes glenoid inclination,

leading to a smaller tilting moment and improved shoulder stability. This can be achieved by adapting either the UHMWPE inlay or the metal backing. The second option is better, as the chance of UHMWPE inlay dissociation and deformation are smaller for thinner UHMWPE components [339]. For given joint forces  $F_y$  (superior subluxation) and  $F_z$  (joint compression), glenoid component geometry and glenoid cavity inclination, the tilting moment about the inferior glenoid component rim at the bone-implant interface can be calculated using the rigid-body model. The moment arm of the joint contact force about the inferior rim decreases almost 14% using the design as presented in Figures 7.7b and c compared to an upward facing, standard glenoid component (Figure 7.7a), with dimensions and forces as used in this study and an inclination angle of  $+4.5^\circ$ . Future research must investigate the feasibility of this design option for resurfacing superior eroded glenoid bone stock. This design decreases the glenoid component inclination angle, which is found to be beneficial for shoulder functionality and long-term component fixation after a TSR.

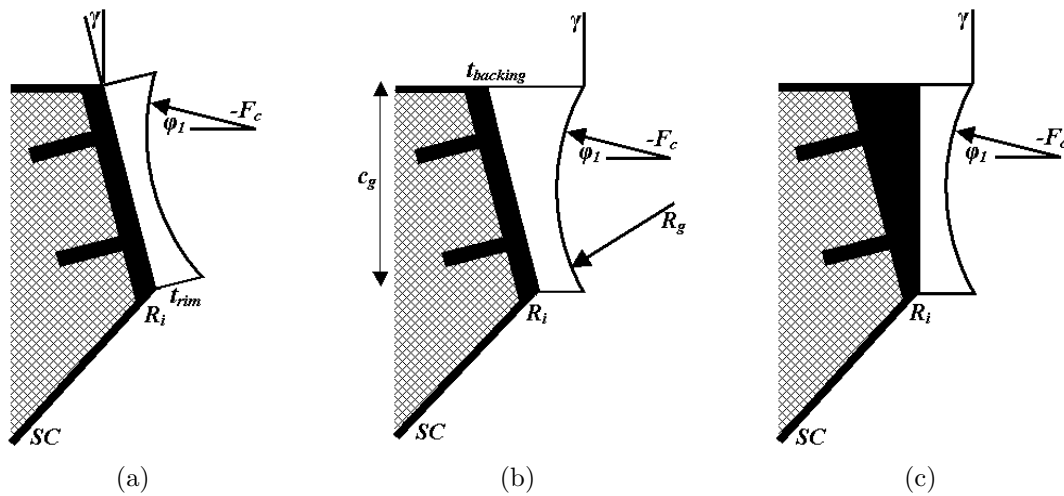


Figure 7.7: Design options for neutralizing glenoid inclination, for example due to superior glenoid erosion. a) Inserting a metal backed glenoid component positioned and orientated on the superior eroded glenoid cavity leads to an upward facing glenoid articular surface. b) and c) Metal backed glenoid components with a neutralized glenoid inclination angle with respect to the metal backing. This is done by adapting either the UHMWPE inlay (b) or the metal backing (c)

## **7.5 Conclusions**

In this study, the effect of glenoid component inclination on glenoid rim-displacements of the cemented glenoid-bone structure and on humeral head subluxation has been investigated. It was found that glenoid components inserted with an increased inclination angle, leading to more upward facing glenoid components, show increased values of the positive superior and negative inferior glenoid rim-displacements. This might influence glenoid component fixation, in that increasing glenoid structure deformation may increase the chance of early glenoid component loosening. Decreasing glenoid component inclination angles, leading to more downward facing glenoid components, allow for higher superior subluxation forces relative to the joint compression force, thereby increasing superior shoulder stability.

If the orthopedic surgeon has the possibility to accurately position the glenoid component with different inclination angles, a more downward facing glenoid component is preferable with respect to glenoid structural deformation and superior humeral head subluxation.



## Chapter 8

# Investigation of the adhesion performance of UHMWPE



*Surface treatment of the bottom of a sailing boat, to prevent the growth of osmosis*



## 8.1 Introduction

The conventional total shoulder replacement consists of a Cobalt Chromium (CoCr) convex component articulating against an Ultra-High-Molecular-Weight-Polyethylene (UHMWPE) concave component. Especially long-term fixation of the glenoid component is difficult to achieve, both due to the few amount of available bone material, necessary to achieve a rigid fixation, and the loading characteristics of the glenohumeral joint. Glenoid component fixation should be improved to improve the survival rates of shoulder replacements and thereby also patient satisfaction.

This study focuses on one design parameter, namely the fixation of UHMWPE glenoid components. Two methods of fixation are commonly used, namely cemented and bone ingrowth fixation, generally used for older and younger patients, respectively. In case of cemented fixation, the prepared bone stock is filled with unhardened Polymethyl-Methacrylate (PMMA) bone cement, the component is then positioned and held in place until the PMMA has hardened. However, UHMWPE, a non-polar material due to its symmetrical molecular structure, is hydrophobic by nature, as reflected by its wettability. As a result, adhesion of UHMWPE is difficult and in combination with using PMMA, which is more a filler than an adhesive, current cemented prosthetic components will mainly rely on mechanical interlocking. To improve the mechanical locking, the UHMWPE glenoid components have structures with grooves and holes at the backside surface of the component. The disadvantage of these structures is the large amount of bone to be removed. This weakens the surrounding structure and makes revision surgery, when needed, troublesome [15]. Another disadvantage of present used cemented components is fretting of the unbonded UHMWPE and PMMA surfaces, leading to third body wear of especially PMMA wear particles between the convex CoCr and concave UHMWPE articulating surfaces [253]. Improving the adhesion performance of UHMWPE may lead to improved long-term fixation of current components. Additionally, geometrically new designs may be developed, fixated partially or completely by adhesion, leading to easier surgery and less bone removal.

Current viable surface modification techniques for applications in the biomedical field are gas-phase based treatments as reviewed by Chu et al. (2002) [52]. Surface oxidation of polymers using gas-phase surface modification has been frequently investigated, such as Corona [95, 231, 308], radio frequency (RF) Glow-discharge [95, 231, 143] and UV/Ozone treatments [231, 183, 262]. Surface oxidation of polymers is the primary mechanism of these surface modification techniques and results in a higher wettability and improved adhesion properties compared to unmodified polymers [95, 308]. At present, there has not been a comprehensive comparison between the various gas-phase surface treatment methods available, encompassing both wettability and adhesive performance in determining the optimum method in improving the adhesive properties of these biomedical polymers.

The aim of the study is to investigate the adhesion of single lap-joints made out of medical grade UHMWPE after a UV/Ozone, Corona or RF Glow-discharge treatment. In addition, mechanical abrasion and a combination of methods are considered for comparison. A number of surface analyses were employed to better understand the changes at the surface.

## 8.2 Materials

Medical grade UHMWPE specimens (110x25x1.4 *mm*) (Chirulen 1020, Poly-Hi Solidur GmbH, Vreden, Germany) were cleaned using isopropanol and underwent different surface treatments (for material properties see Table B.1 in Appendix B). After undergoing one of the treatments, specimens were either evaluated by wettability and surface energy or bonded together by PMMA bone cement (Palamed G 20, Biomet Merck, Zwijndrecht, The Netherlands) or Methyl-Methacrylate MMA, which is a structural adhesive (MA300, ITW Plexus, Kettering, UK). Since untreated PMMA has no adhesive properties, MMA was used to gain better insight into the achievable adhesion performance and is chosen due to its similar chemical structure to PMMA.

## 8.3 Surface treatments

The applied surface modification techniques were UV/Ozone, Corona and the RF Glow-discharge treatment. The methods are all based on introducing oxygen-based functional groups onto the surface of the UHMWPE specimens. Thereby, the now asymmetric atomic structure becomes polar and electrically charged. Detailed workings of these surface treatments and their industrial applications have been described elsewhere [52, 308].

A fourth surface modification technique was added, namely surface roughening, to investigate the effect of increased surface area on adhesion. Additionally, a combination of surface roughening and the RF Glow-discharge treatment was investigated.

### UV/Ozone treatment

An in-house UV/Ozone apparatus was assembled using an 80 Watt mercury vapour Heraeus Noble light (NNIQ120), as shown in Figure 8.1a. Wavelengths were of the order of 184.9 and 253.7 *nm* and the samples were placed 20 *mm* away from this source. The tests were performed at atmospheric conditions and specimens were treated within a time range between 0 and 30 *min*. UV/Ozone requires long

treatment times and penetrates deepest into the bulk material [308, 235], which may affect the mechanical properties. Therefore, stiffness and strength of control and treated specimens were measured, but no differences in mechanical properties were found within the samples tested.

### Corona treatment

A TIGRES Corona gun CKG with a TIGRES power supply of 50  $Hz$  (Tigres GmbH, Rellingen, Germany) was used in this indirect Corona treatment. The gun consists of two metal electrode bars 15  $mm$  apart, between which a homogeneous Corona discharge of 50  $kHz$  is ignited. Compressed air flows at atmospheric conditions in-between the electrodes, forcing the discharge towards the substrate in the form of a cone with a parabolic base as shown in Figure 8.1b. Pre-tests had shown that the optimum operating distance between the source and the substrate was 10  $mm$ . Specimens were then treated within a time range between 0 to 120  $s$ . Manually moving the specimens underneath the Corona gun ensured that a wide enough surface area was treated.

### Radio frequency Glow-discharge treatment

The radio frequency (RF) Glow-discharge treatment was performed using a plasma apparatus (TNO laboratories Eindhoven, The Netherlands) and is shown in Figure 8.1c. The RF Glow-discharge was generated using a 13.56  $MHz$  ENI ACG-3 radio-frequency generator, coupled to an Astech ATH-50 matching impedance network, which minimizes the reflected power. A glass reaction chamber with diameter and length of 50 and 165  $mm$ , respectively, was used to contain the plasma. The chamber was fitted with an air inlet and surrounded by 10 turns of copper coil with a diameter of 1.8  $mm$ . The pressure needed to produce a stable uniform plasma at the specified frequency was 1  $mbar$ . A rotary pump with an inlet valve was used to pump the entire plasma system and to keep the pressure consistently at this low value. Cleaned specimens were positioned in the glass chamber, which was filled with atmospheric air. The reactor chamber was then evacuated for 1  $min$ , before initiating the plasma by increasing the input power to the coil and decreasing the glass chamber pressure. Two variables affected the level of activation of the surface; time of treatment and input power needed to initiate the plasma. The optimum input power of 200  $W$  was found through the results of single lap-joint shear strength pre-tests. Fixing this value, the treatment time was varied between 0-120  $s$ . Following treatment, the samples were kept in flowing gas for 5  $min$  before the reactor was evacuated. To allow for the decay of free radicals, air was allowed to enter the chamber to raise the pressure to atmospheric level.

### Mechanical abrasion

In order to test for the effect of surface area on the adhesive properties, samples were treated with a 80 FEPA *P* – grade sandpaper. The paper was mounted onto a sanding machine (Metabo, Nürtingen, Germany) to ensure that samples had the same abrasion motion and that time of treatment could be easily measured. Samples were exposed to treatments of 2, 5 and 10 s.

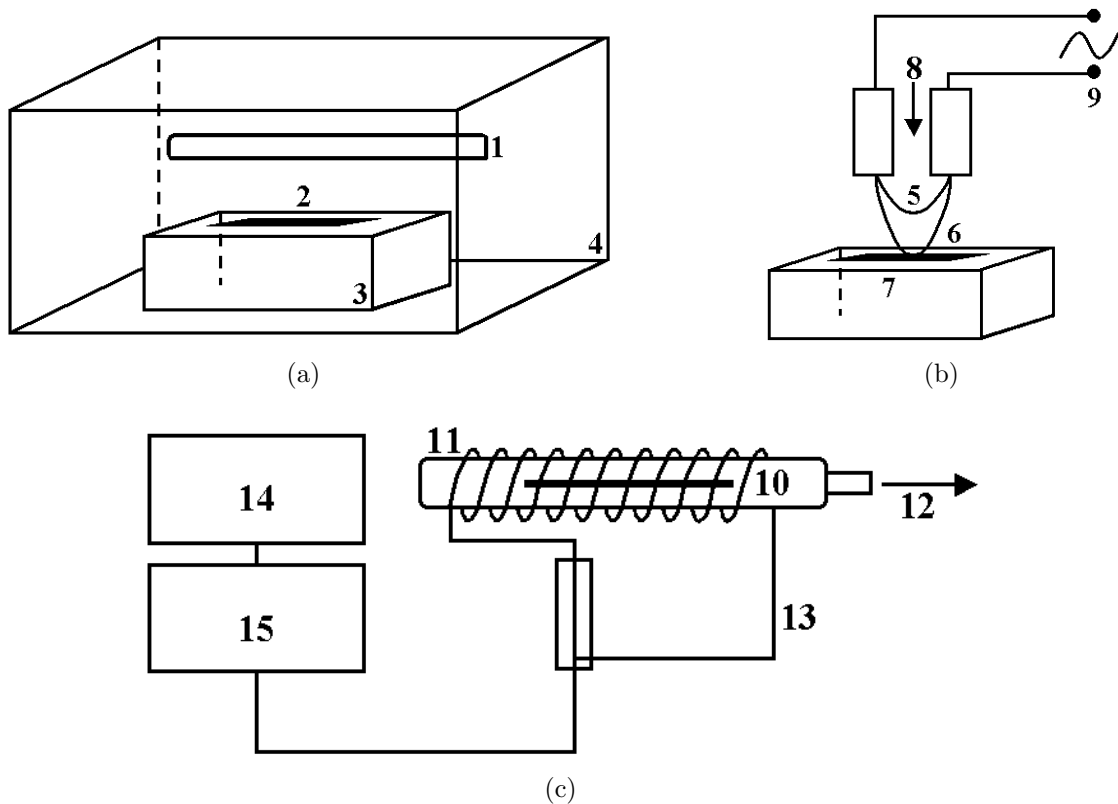


Figure 8.1: Schematic representations of the different surface treatments. (a) The UV/Ozone treatment. 1. UV-lamp 2. Sample 3. Sample holder 4. Chamber. (b) The Corona treatment. 5. Corona discharge 6. Parabolic base 7. Sample 8. Compressed air 9. High frequency source. (c) The radio frequency (RF) Glow-discharge treatment. 10. Sample 11. Vacuum chamber 12. To vacuum pomp 13. Copper wire 14. Radio frequency source 15. Matching impedance network

## 8.4 Analyses

Surface analysis techniques and single lap-joint shear tests were performed to investigate bonding characteristics and shear strength. For all surface analyses and shear strength experiments a number of three specimens ( $n=3$ ) were used, except for the shear strength experiments after ageing in a 0.9%  $\text{NaCl}$  solution, for which 2 lap-joints ( $n=2$ ) were used.

### Surface roughness

The effect of the different surface treatments on the surface roughness  $R_a$  of the UHMWPE specimens have been measured at the Tribology group of the Delft University of Technology (Surtronic 3P, Taylor-Hobson, Leicester, England).

### Wettability and surface energy

Wettability, indicating the spreading of a fluid drop over a surface, is a measure for adhesion performance. This can be quantified by the water contact angle, which is taken as the angle between the specimen surface inside the drop and the tangent of the drop at the sample surface as shown in Figure 8.2. A smaller angle indicates better wettability and adhesion. The wettability of every treatment parameter was measured using a ramé-Hart 100 contact goniometer (ramé-Hart, inc, Mountain Lakes, USA). A 3  $\mu\text{l}$  drop of water was placed manually onto the surface and the tangential cone method was used to model the shape of the drop and to measure the water contact angle. With the same equipment, measurements of the surface energy  $\sigma$  and their dispersive and polar contributions were taken using the Owens-Wendt-Rabel-Kaelble method [360]:  $\sigma = \sigma^d + \sigma^p$ , where  $\sigma^d$  and  $\sigma^p$  are the dispersive and polar parts of the surface energy respectively. Together with Young's equation ( $\gamma_{sv} = \gamma_{sl} + \gamma_{lv} \cos\alpha$ , where  $\gamma_{sv}$ ,  $\gamma_{sl}$ ,  $\gamma_{lv}$  are the surface energies between the solid-vapour, solid-liquid and liquid-vapour interfaces), it can be derived that the polar and dispersive part of the surface energy of the substrate can be found using 5 fluids with different polarity and known parameters. It is the polar part of the surface energy that is of particular importance, because it is this part that may be changed through surface modification. Five liquids of volume 3  $\mu\text{l}$  and varying surface tensions were used, namely purified water, glycerine, formaldehyde, aniline and tri-tolyl-phosphate.

### Interfacial shear strength

A common evaluation method of adhesive properties is by lap-joint testing. Although the applied interfacial shear load is a non-physiological load, shear stresses may occur in cemented prosthetic components, especially in the case of flat backside

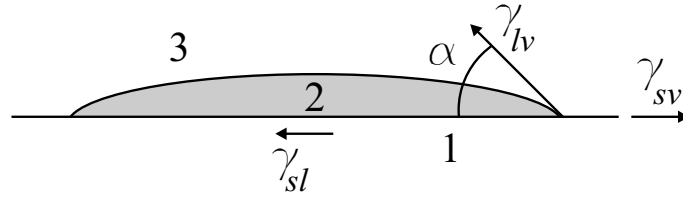


Figure 8.2: Definition of the water contact angle, as measured in this study. 1. Substrate 2. Liquid 3. Vapour.  $\gamma_{sv}$ ,  $\gamma_{sl}$ ,  $\gamma_{lv}$  are the surface energies between the solid-vapour, solid-liquid and liquid-vapour interfaces

surfaces [14] and around grooves and holes for mechanical locking. For the single lap-joints bonded by PMMA and MMA (see Figure 8.3a), a 20 mm overlap length was used. Before mixing, a small amount of glass beads of 0.8 and 0.2 mm diameter was added to the PMMA and MMA, respectively, to ensure a homogenous thickness of the adhesive layer (see Figure 8.3b). A relative thicker interface has been chosen for single lap-joints bonded by PMMA, as the bone cement interface for component fixation is normally thicker than the thickness for engineering adhesive layers. After bonding and curing for at least 24 hours, the single lap-joints were tested on a 20 kN Zwick testing apparatus (Zwick GmbH & Co. Ulm, Germany). Tests were performed at cross-head speeds of 3 and 6 mm/min for the specimens bonded with relatively stiff PMMA and more flexible MMA, respectively. The test speeds are chosen to minimize both the influence of viscoelasticity and material creep. To better simulate in-vivo conditions, the effect of ageing on the interfacial shear strength was investigated. After a 10 min UV/Ozone, 5 s abrasion or combined 5 s abrasion and 10 min UV/Ozone treatments, the specimens were bonded together by PMMA, stored in a 0.9% NaCl solution for 0, 2.7 and 7.3 weeks at 37° C, after which the interfacial strength was determined.

## 8.5 Results

### Surface roughness

The surface roughness of the UHMWPE specimens after the different treatments can be found in Table 8.1. No significant differences of the surface roughness were found between the treated and untreated specimens. Also not for the abrasion treatment, due to the large scatter in the data.

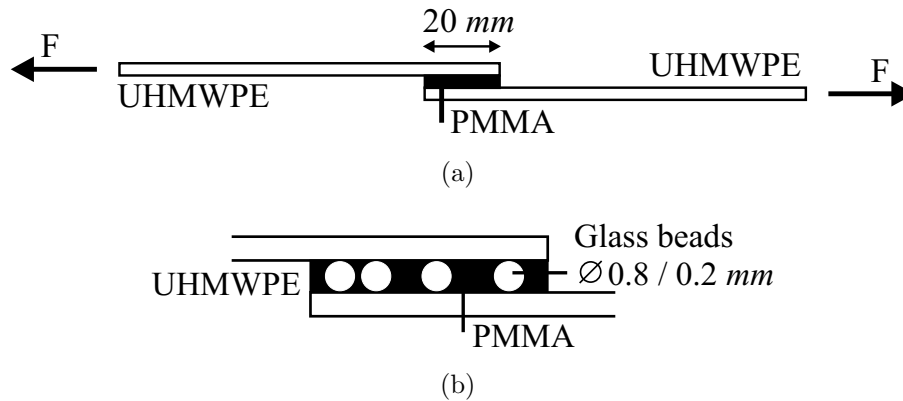


Figure 8.3: Schematic representation of the method of investigation of the interfacial shear strength. (a) A single lap joints by two UHMWPE sheet specimens, bonded together with constant adhesive thickness. (b) The constant adhesive thickness is achieved by the addition of glass beads with a diameter of 0.8 and 0.2 mm, for the PMMA bone cement and MMA adhesive, respectively

### Water contact angle

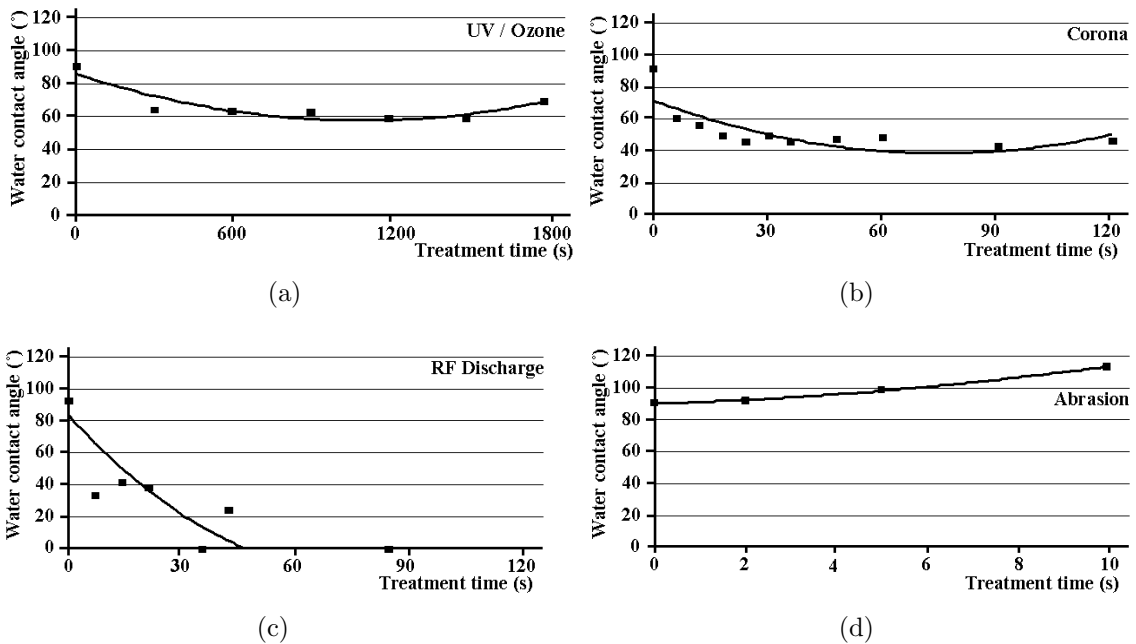
A summary of measured contact angles is graphically represented in Figure 8.4. The measurements were also taken after a time lap of ten minutes, as this was the maximum time that the samples were left before bonding, but no difference was found. A dramatic decrease in contact angles was seen after a treatment time of only a few seconds for both the Corona and RF Glow-discharge treatments, minutes for the UV/Ozone but not at all after the abrasion treatment. The tests performed gave the initial indication that the hydrophobicity of UHMWPE can be decreased markedly. Complete wetting resulted after a RF Glow-discharge of 25 s and this was not matched by any other treatment. Predictably, increasing the surface roughness increases the contact angle, which is the result of local peaks and valleys on the surface. Additionally, increasing the surface area of an already inert and hydrophobic substrate only provides more area that the water cannot spread over and hence the measured contact angle is larger.

### Surface Energy

The variation of surface energy with treatment time is presented in Figure 8.5. The increase in surface energy by the surface treatments is strongly related to the increase in the polar part of the surface energy. If any, there is a slight decrease in the dispersive component with the Corona treatment, most likely due to the introduction of oxygen-based functional groups and the disturbance of the former polymer surface. It appears that the RF Glow-discharge is the most efficient treat-

Table 8.1: Surface roughness of the UHMWPE specimens before and after surface treatments

Treatment	Roughness $R_a$ ( $\mu m$ )		Max. Error ( $\mu m$ )
	Parallel	Perpendicular	
None	0.37	0.92	0.12
Corona (60 s)	0.40	0.85	0.13
UV/Ozone (10 min)	0.42	0.81	0.20
RF Glow-discharge (30 s)	0.40	0.81	0.20
Abrasion (10 s, 80 FEPA P – grade)	4.89	5.69	3.43

Figure 8.4: Variation of the water contact angle with treatment time ( $t=0$  is control specimen), for different surface treatments. (a) UV/Ozone treatment. (b) Corona treatment. (c) Radio frequency Glow-discharge treatment. (d) Abrasion treatment (see Figure 8.2 for the definition of the water contact angle)

ment for the UHMWPE substrates, achieving in less than 20 s, a polar and overall surface energy that is reached after 60s of Corona treatment, and not at all by the UV/Ozone treatment. The surface energy has seemingly reached a maximum at 20 s and stays at this value for all times tested afterwards. This might indicate that the maximum surface energy of UHMWPE has been reached, although this could also mean that there was not enough reactive oxygen species present in the vacuum

to be implanted into the surface. Both the Corona and RF Glow-discharge treatments produce a polar part of the surface energy that becomes stronger than the dispersive part with time, whilst the same trend is not observed with the UV/Ozone treatment. The effect of this treatment on UHMWPE has to be questioned since the polar force gives an indication as to the extent of oxidation of the surface. It is apparent, with a maximum change of not more than  $10 \text{ mN/m}$  compared to  $35 \text{ mN/m}$  for the plasma treatments, that UV/Ozone has a minor effect on UHMWPE from this evidence only. In all cases there is a peak in the surface energies and it would be judicious to assume that the optimum treatment would be found in this time region, for afterwards, not only is there a fall in the polar component, but the efficiency of the treatment is also decreased.

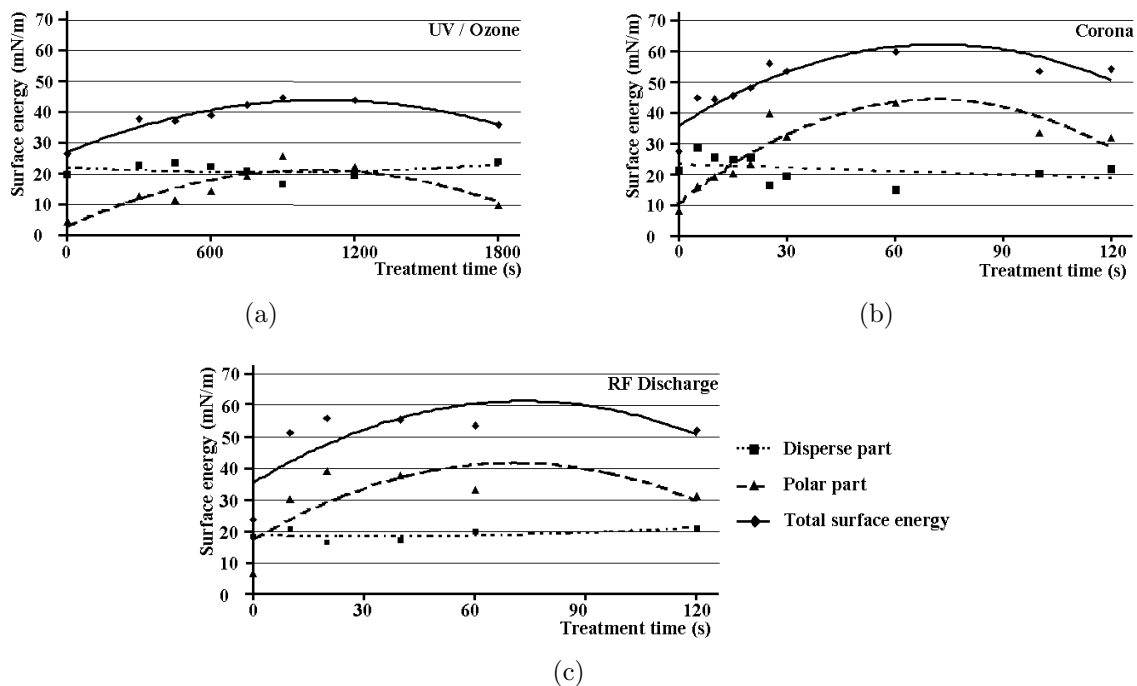


Figure 8.5: Variation of the surface energy with treatment time ( $t=0$  is control specimen), for different surface treatments. (a) UV/Ozone treatment. (b) Corona treatment. (c) Radio frequency discharge treatment

### Interfacial shear strength

Results of the interfacial shear strength experiments for UHMWPE specimens bonded by PMMA and MMA are given in Table 8.2 and in Figure 8.6. Although all treatments have improved the ultimate shear strength of the UHMWPE/PMMA single lap-joints, the extent of the improvement differed for individual treatments. Single

lap-joints of the treated UHMWPE specimens bonded by PMMA and MMA behaved similarly, both showing the same trends. The physical interaction that was able to be induced at the PMMA/UHMWPE interface was increased to the point where the PMMA was able to behave as an adhesive. Both abrasion and RF Glow-discharge had a greater effect on lap-joints bonded by PMMA than the UV/Ozone and Corona treatments and, after a combined abrasion RF Glow-discharge treatment, it was able to approach the shear strength of MMA-bonded samples. The extent of the increase in interfacial strength of the UHMWPE/MMA system was such that the failure mode had changed from cohesive failure to failure within the substrate with the onset of necking and plastic deformation of the UHMWPE specimens, displaying the potential of this treatment.

The general trends for the UV/Ozone and Corona treatments are similar to those as found by that of the surface energy, with the maximal shear stress values found at treatment times of maximum surface energy. This tendency is not followed with the RF Glow-discharge, which displays an increasing trend of shear strength increase to beyond the treatment time as expected by the wettability results.

Table 8.3 shows the effect of ageing in a 0.9% NaCl solution at 37°C. No significant change was found after 2.7 and 7.3 weeks, indicating the stable behavior of the applied treatments.

Table 8.2: *Shear strength (MPa) of UHMWPE single bonded lap-joints, bonded by MMA or PMMA, after different UHMWPE surface treatments. For the Abrasion treatment 80 FEPA P – grade sand paper has been used*

Surface treatment	Treatment time (s)		Shear strength (MPa)	
	MMA	PMMA	MMA	PMMA
None	-	-	0.31	0.13
Corona	300	900	0.48	0.30
UV/Ozone	20	40	1.1	0.35
RF Glow-discharge	60	90	0.93	0.72
Abrasion	2	10	0.4	0.53
Abrasion + RF Glow-discharge	10+40	10+25	UHMWPE failure	1.0

Table 8.3: *Shear strength (MPa) of UHMWPE single bonded lap-joints, bonded by MMA or PMMA after ageing in a 0.9% NaCl solution at 37° C. For the Abrasion treatment 80 FEPA P – grade sand paper has ben used*

Treatment	Surface treatment time (s)	Shear strength (MPa) after different ageing time (weeks)		
		0 (control)	2.7	7.3
UV/Ozone	600	0.18	0.14	0.18
Abrasion	~10	0.27	0.36	0.34
Abrasion + UV/Ozone	~10+600	0.74	0.55	0.76

## 8.6 Discussion

All three methods have improved the adhesion properties of UHMWPE to different extents. It is clear that with respect to efficiency, UV/Ozone is the poorest performer of all methods used and exposure time necessary is of the order of minutes compared to seconds for the others. The case may be that UHMWPE is transparent to the effects of this treatment and a similar result was found by Strobel et al. (1996) [308]. Numerous studies have stated that bulk damage and ageing transpires from the UV/Ozone treatment [85, 250], with no such observation from the other treatments and this is a serious factor when considering its use with biomaterials. Adsorption of atmospheric surface contaminants and reorganization of the surface molecules are two processes that occur [145, 243] and hydrophobic recovery is an unavoidable consequence of treated samples. Øiseth et al. (2002) had shown that RF Glow-discharge treatments took in the order of days for treated high-density-polyethylene to reach such a recovery and 24 hours for significant change [143]. Friedrich et al. (1998) found similar results with the indirect Corona treatment on polypropylene films [85]. From water contact angle measurements performed in this study, such ageing was not apparent in the short times tested. The time taken between treatment and application of the adhesive was kept as short as possible but with these results, such precautions were not necessary and this is particularly beneficial in the case of surgery where extra time pressure due to treating the prosthesis can be avoided.

There is a strong correlation between the variation of the polar force with time of treatment and the shear stress results for UV/Ozone and Corona treatments (see Figures 8.5a and b and Figures 8.6a and b). An increase of the polar force suggests an increase in the oxidation of the surface and from the results obtained, this could be directly correlated with an increase in lap-joint shear strength. This work therefore supports studies as performed by Owens (1975), who used low-density polyethylene with Corona treatment [233]. The interesting discovery in the present study using

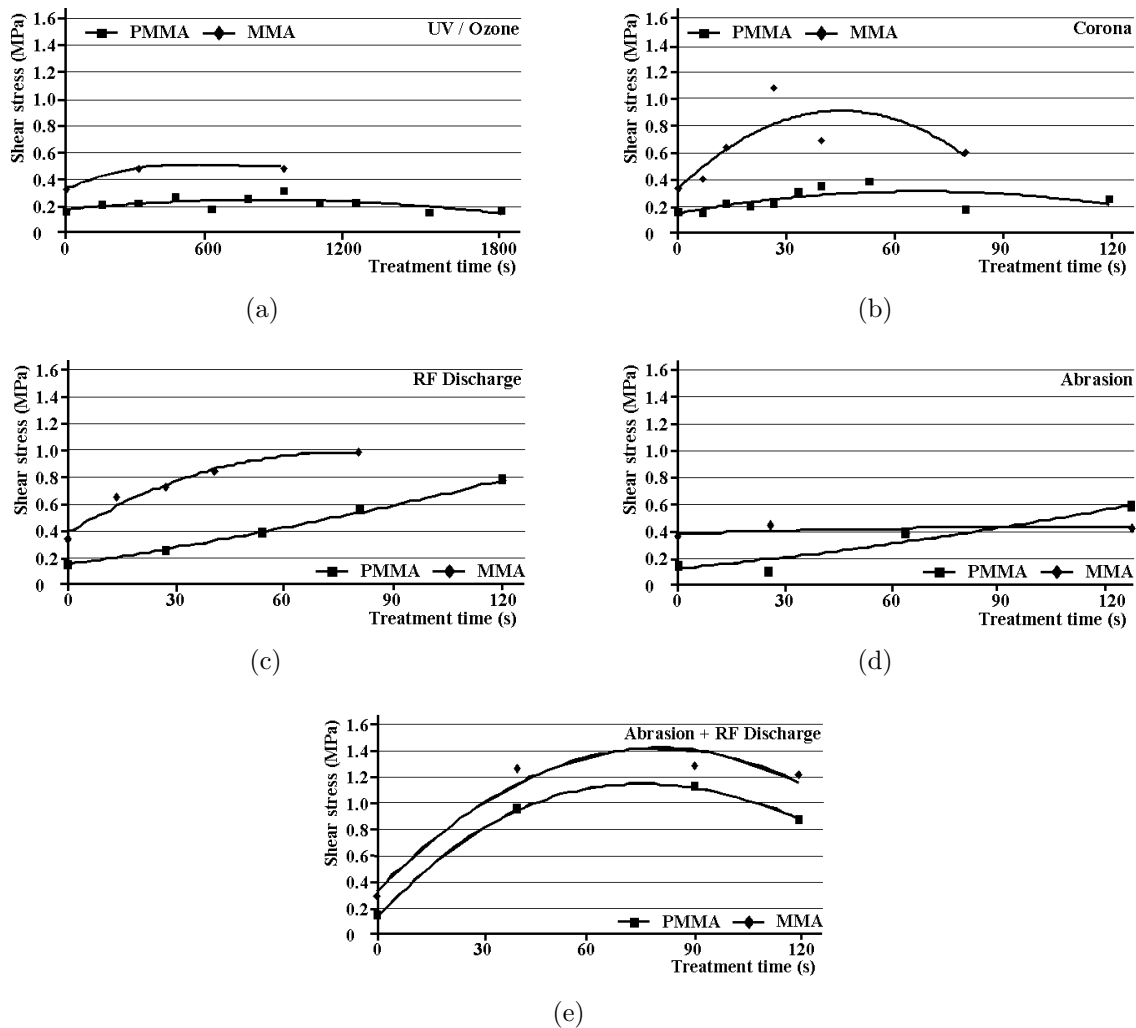


Figure 8.6: Variation of the interfacial shear stress with treatment time ( $t=0$  is control specimen), for different surface treatments. (a) UV/Ozone treatment. (b) Corona treatment. (c) Radio frequency discharge treatment (d) Abrasion treatment (e) Combined RF-discharge / abrasion treatment

UHMWPE is that surface energy, and particularly the polar force measurements, can be a very good qualitative predictor of the adhesive behaviour of UHMWPE. Hence, future work focused on improving the described surface treatments can be done using surface energy trends only. Although these similar trends with the water contact angle and shear stress results were found, wettability data can provide an over-optimistic prediction as to how the adhesion properties will improve. For example, RF Glow-discharge treated samples can have contact angle close to  $0^\circ$ , which is not reflected in the shear strength using either PMMA or MMA.

The extent as to how far these results should be taken into consideration with respect to the adhesive properties however, is debatable. Surface oxidation methods do result in varying amounts of chain scission of the polymer structure, lowering the molecular weight of the outermost surfaces [308, 145]. The lower molecular weight material is water-soluble, thereby clouding the interpretation of the treated samples giving false information as to the extent of wetting of the underlying surface, which is insoluble. In addition, there is also variation in measurements due to a number of contributing reasons. The substrate surface may not be perfectly uniform smooth due to machining lines and therefore the contact angles may show differences with specimen orientation. On sheet material, the liquid drops tended to elongate depending on the direction of the production process, resulting in the same effect of varying contact angles with specimen orientation. Nevertheless, this effect is assumed to be small and as a comparison, both the water contact angle and surface energy measurements are very useful tools.

Although all treatments have improved the ultimate shear strength of the single lap-joints bonded by PMMA, the extent of the improvement was not the same. A similar trend had occurred with the MMA adhesive with shear stress values that were generally twice as high, except for abrasion. However, to see if the effect of the best surface treatment as investigated could be further improved, a combination treatment of abrasion followed by RF Glow-discharge was examined. Recalling that PMMA has little to no adhesive properties, the combination treatment resulted in lap shear strength that completely outperformed all other UHMWPE/PMMA single lap-joints. In fact, the time of RF-discharge treatment was less in the case of the combination treatment, compared to the RF discharge treatment without mechanical abrasion. The combined treatment is not only more efficient, that is, less RF Glow-discharge treatment time needed for optimum shear strength results, but shear strength values were able to approach that of the MMA bonded samples. The same trend was found by Ogawa et al. (1999), in their study on interfacial shear strength of UHMWPE fibre/Polyethylene systems. Their results also indicate that there is an equal contribution to interfacial shear strength from surface roughness and surface modification [231].

It has been found that a combination of treatments was the best way to improve the adhesive properties of the UHMWPE/PMMA system in a simple shear load case. It is found that the effect of the combined treatment is more than simply summing the effect of the separate treatments, as abrasion increases the effective area for the surface treatments. Future studies are necessary to investigate the behaviour of these specimens under dynamic (fatigue) loading.

However, the results obtained in this study have shown that improved fixation can be acquired through surface modifications techniques. The potential to change current prosthetic designs in TSR that are based on fixation by adhesion might be realized. Additionally, research into a structural adhesive for in-vivo use may be very worthwhile.

## 8.7 Conclusions

The aim of this study was to investigate the effect of different surface modification techniques on the adhesion performance of UHMWPE, when bonded with PMMA bone cement or MMA adhesive. Adhesion properties improved to various degrees after all treatments in the following order of increasing effectiveness of the treatments: UV/Ozone, Corona, abrasion, RF Glow-discharge and a combined abrasion and RF Glow-discharge treatment and was not affected by ageing in a 0.9% NaCl at 37° C. Adhesive behaviour between the PMMA bone cement and UHMWPE showed similar trends with MMA and UHMWPE, which performed superiorly. Future research both into a new adhesive for in-vivo use and component design would be tremendously worthwhile, especially for this new concept of glenoid fixation.

## Chapter 9

# Effect of the cement-prosthesis interface on FE Modelling



*A curling team is busy creating a fluid film, which must maintain the sliding speed of their stone, thereby hopefully reaching the center of 'the house'*



## 9.1 Introduction

In Chapter 2, the need for design improvements of the shoulder replacement has been elaborated on. These design improvements must be validated, which can be done using experimental testing, including quasi-static and fatigue tests, as well as by numerical tools, e.g. the Finite Element (FE) method.

The FE method is very useful for investigating the performance of prosthetic designs, as this method allows for good parameter control, is fast and relatively cheap. However, accurate investigation of the artificial joints, results in very complex numerical models, consisting of the prosthetic components, the surrounding bone, several interfaces and multiple loading and constraint conditions. The model must be realistic, built up without errors and, if possible, it must be validated.

The complex FE models of artificial joints consist of many important details, which are not unambiguous and need discussion. One of these details for discussion is the cement-prosthesis interface, in the case Ultra-High-Molecular-Weight-Polyethylene (UHMWPE) components cemented by Polymethyl-Methacrylate (PMMA) are analysed. This interface may be physically unbonded, not only years after in-vivo use, but also direct post-operatively, as demonstrated by in-house experiments and from literature [133, 173]. Many FE models assume this interface to be rigidly bonded, which might be not correct, as also discussed by Stone et al. (1999) [307] and Couteau et al. (2001) [61]. A more realistic method is to use contact elements in combination with a coefficient of friction (CoF).

According to the authors of the present study, the effect of the modelling conditions of this interface on the results is still unknown. To investigate this effect, the CoF between PMMA and UHMWPE, which is never meant to be a bearing interface, should be investigated, as no values are found in literature.

The aim of this study, therefore, is twofold. First, the CoF between PMMA bone cement and UHMWPE will be determined experimentally, to be used for the second aim. This second aim is to investigate the effect of the interface condition between the PMMA bone cement layer and the UHMWPE glenoid component on cement stresses and glenoid component tilting by using FE modelling. Subsequently, these topics will be discussed in Section 9.2 and Section 9.3.

## 9.2 Experimental investigation of the coefficient of friction between PMMA and UHMWPE

### 9.2.1 Methods and materials

#### Materials

To measure the static and dynamic coefficient of friction (CoF) in a wet and dry environment, cylindrical PMMA bone cement specimens (Palamed G20, Biomet Merck, Zwijndrecht, The Netherlands) have been used. They are made by turning, during which they rotate about their longitudinal axis and the chisel is first positioned in front of the specimen at the preferred distance from the longitudinal axis and then pushed into the PMMA specimen, in longitudinal direction for  $\sim 2$  mm. As a result, the specimens with a height of 6 mm, are divided in a lower part with a diameter of 6.51 mm and an upper part with diameters of 6.51, 4.61, 3.76, 3.26 and 2.91 mm. In combination with a total load of 100 N, distributed over three identical PMMA specimens, this leads to contact pressures ranging between 1.0 and 5.0 MPa. This range corresponds to the maximal principal cement stresses, as found by Couteau et al. (2001) [61].

During measurements of the dynamic CoF, the surface of the brittle and more porous PMMA specimens becomes filled with the softer UHMWPE, resulting in a more smooth PMMA specimen surface. This is demonstrated using Scanning Electron Microscope (SEM) photo's (Scanning Microscope Jeol, JSM840A, Japan). As can be seen in Figures 9.1b and c, there is a clear difference in the surface porosity, also demonstrated by the difference in surface roughness of the PMMA specimens before and after measuring the dynamic CoF. Therefore, the static CoF has been measured of both new as well as UHMWPE-filled PMMA specimens, for good comparison with the dynamic CoF and to better simulate in-vivo conditions.

The upper part of the PMMA specimens contact a 1 mm thick UHMWPE disc (Chirulen 1020, Poly-Hi Solidur GmbH, Vreden, Germany). For material properties see Table B.1 in Appendix B.

#### Surface roughness

The surface roughness  $R_a$  of both the PMMA specimens and UHMWPE disc have been measured before testing and the PMMA specimens also after testing (Surtronic 3P, Taylor-Hobson, Leicester, England). The PMMA specimens have been measured and averaged for two perpendicular directions on the sliding surface and the UHMWPE disc has been measured and averaged on four locations of contact in sliding and perpendicular direction.

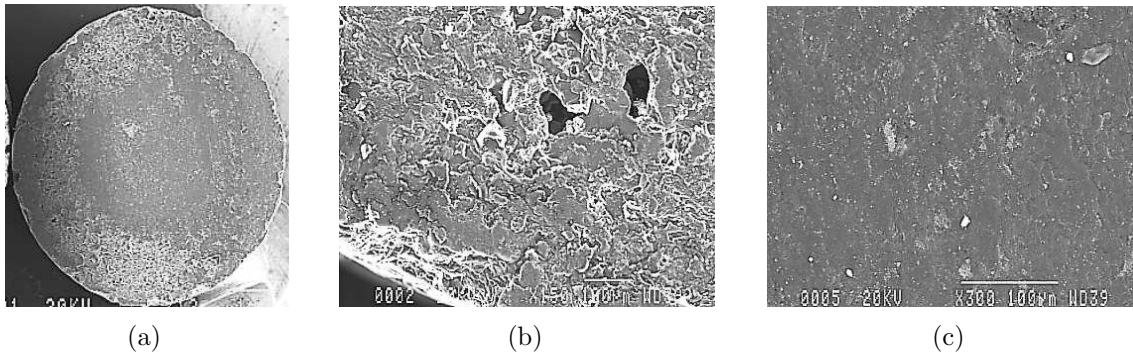


Figure 9.1: Scanning Electron Microscope (SEM) photo's of the contacting area of PMMA specimens. (a) Complete surface area, partially filled with UHMWPE (12x). (b) Detail of a porous location (150x). (c) Detail of a UHMWPE-filled location (300x)

### The static CoF

For measuring the static CoF, three PMMA specimens with similar diameter are placed into a triangular holder (see Figure 9.2). Before testing, the PMMA specimens were abraded against 1000 FEPA *P* – grade sandpaper. This was done to make sure that all three PMMA specimens had full surface contact with the UHMWPE disc and that all PMMA specimens had equal surface roughness. Although in-vivo surface roughness of the PMMA bone cement at the interface is unknown, the chosen FEPA *P* – grade value can be seen as an upper limit, leading to a relatively smooth PMMA specimen surface. The constant total weight placed on top is 100 *N*, leading to average contact pressures ranging between 1.0 and 5.0 *MPa*. Tests are performed in a dry and wet (water) environment at room temperature. A force sensor has been connected to the triangular holder, measuring the manually applied, increasing pulling force (see Figure 9.2). The force sensor is connected to a signal amplifier (Peekel Instruments B.V., Rotterdam, The Netherlands), which records the maximal applied force. This maximal applied force occurs just before the holder starts to move and is therefore used as a measure for the static CoF. The maximal applied pulling force ranged between 12.1 and 29.9 *N*, which was always reached within 10 *s*. This experiment has been repeated three times with different specimens for each contact pressure.

### The dynamic CoF

For measuring the dynamic CoF, three identical PMMA specimens are placed in the rotating holder of a standard pin-on-disc tester at the Tribology Research Group, Delft University of Technology, The Netherlands (see Figure 9.3). The PMMA specimens have similar dimensions as for the static CoF measurements. The specimens

slide against the UHMWPE disc with an applied contact force of 100  $N$ , thus also tested for a contact pressure ranging between 1.0 and 5.0  $MPa$ . Tests are performed in a dry and wet (water) environment at  $37^\circ$  with a sliding velocity of 50  $mm/s$ . This speed was chosen to prevent both influences of relaxation and visco-elasticity, although in a study by Zhang et al. (1998) it was found that the sliding velocity doesn't influence the CoF between UHMWPE and steel, in which serum was used as a lubricant [364]. After a run-in phase of at least 45 minutes, the dynamic CoF has been recorded and averaged over a period of approximately 2 hours. This experiment has been repeated three times with different specimens for each contact pressure.

### Statistical evaluation

In this study, the CoF for different conditions has been measured, namely dynamic and static, both in a wet and dry environment. Additionally, of the specimens for the measurement of the dynamic CoF, which become filled with UHMWPE, the static CoF has been measured in a dry and wet environment. All six different measurements have been performed for contact pressures ranging between 1 and 5  $MPa$ . To investigate the significance of the obtained results of the six different test conditions, the results are averaged with respect to the contact pressure and the unpaired  $t$ -test with a confidential level of 95% has been used. Additionally, the significance of the effect of contact pressure on the CoF has been investigated.

### 9.2.2 Results

Before each measurement, the surface roughness  $R_a$  at the sliding surface of the machined PMMA specimens and of the UHMWPE disc in sliding and perpendicular direction has been measured. Machined PMMA specimens have a roughness  $R_a$  of 1.695  $\mu m$  (SD=0.323) in both directions. After measuring the dynamic CoF, the surface roughness has been measured again for the PMMA specimens and a surface roughness of 0.464  $\mu m$  (SD=0.100) was found. The surface roughness of the UHMWPE disc in sliding and perpendicular direction was found to be 0.227  $\mu m$  (SD=0.0656) and 0.475  $\mu m$  (SD=0.0274), respectively.

The dynamic CoF in a dry and wet environment averaged 0.296 and 0.113, respectively, whereas the static CoF in a dry and wet environment averaged 0.297 and 0.252, respectively (see Table 9.1). The results are also presented graphically, to better demonstrate the influence of the contact pressure on the CoF (see Figure 9.4). The obtained differences in the CoF, averaged for the contact pressure for the dry and wet test conditions, are significant ( $p < 0.05$ ). The differences between the dynamic and static CoF for the dry test condition is not-significant ( $p > 0.05$ ) and for the wet condition significant ( $p < 0.05$ ), respectively. The static CoF of the

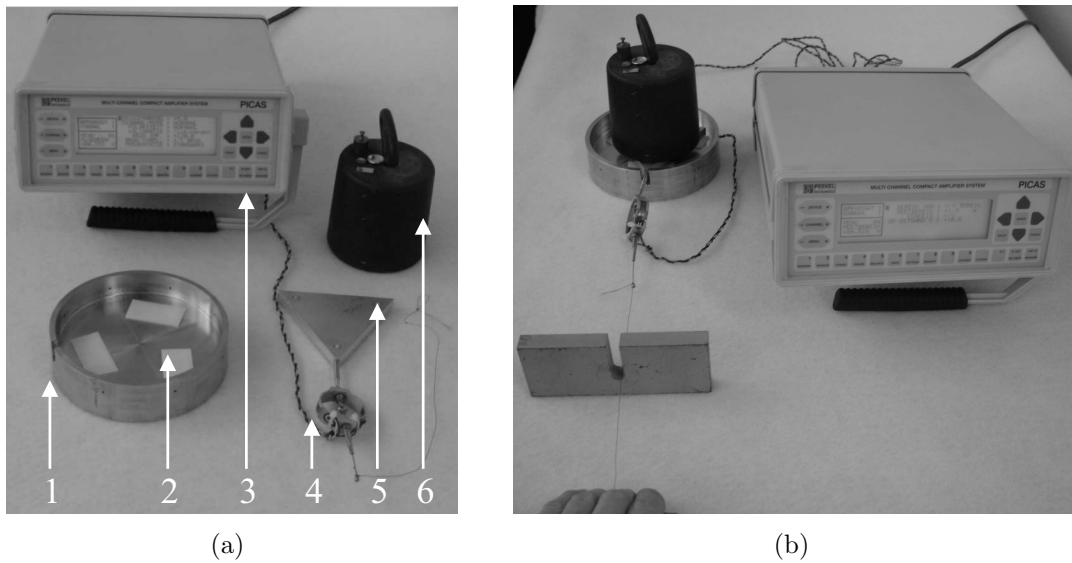


Figure 9.2: Overview of the experimental test set-up for measuring the static coefficient of friction. (a) Components for the measurements. 1. Metal holder for the UHMWPE sheet specimens. 2. UHMWPE specimens (3x). 3. Peekel signal amplifier. 4. Force transducer 5. PMMA specimen holder with PMMA specimens (3x). 6. Additional weight to obtain 100 N. (b) Assembled test set-up and method of force application

UHMWPE-filled specimens in a wet and dry environment averaged 0.153 and 0.142, respectively, which are both significantly different ( $p < 0.05$ ) compared to the static CoF of new specimens, in a dry and wet environment, respectively.

In Figure 9.4 it can be seen that the dynamic CoF is decreasing with increasing contact pressure, as is also found in literature for the CoF in sliding conditions [175]. The differences for the dynamic CoF with respect to contact pressure for dry test conditions is non-significant, whereas the dynamic CoF for wet test conditions with contact pressures of 4 and 5 MPa is significantly different compared to 1, 2, and 3 MPa ( $p < 0.05$ ).

### 9.2.3 Discussion

In this study the CoF between PMMA bone cement and UHMWPE has been investigated. The results are used to investigate the effect of interface conditions between the PMMA cement layer and the UHMWPE glenoid component on cement stresses and glenoid component tilting, using FE modelling.

The CoF for a given material combination is influenced by many parameters, such as surface roughness, method of manufacturing, load conditions etc. However, this study was not meant to investigate all influencing parameters on the CoF. The aim

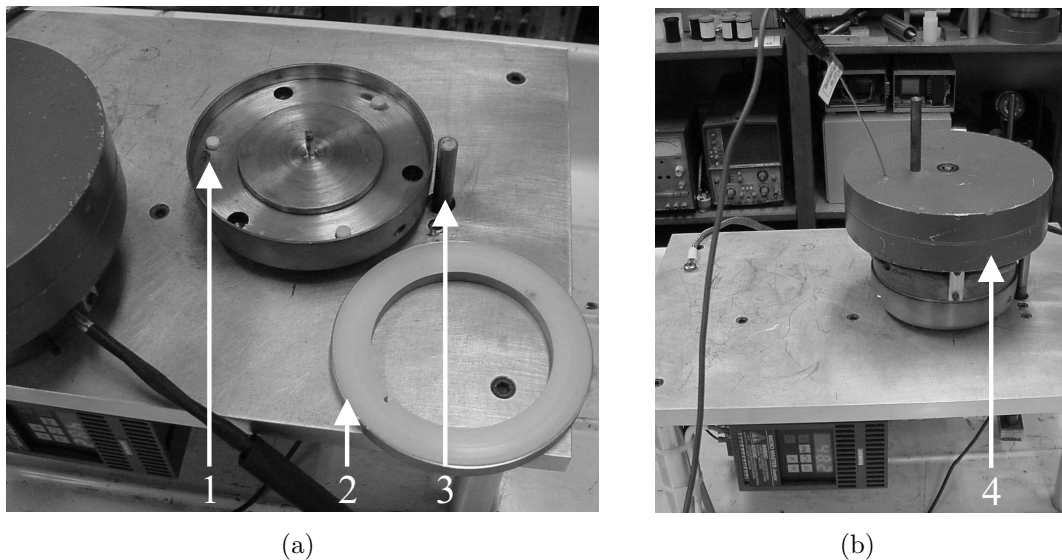


Figure 9.3: *Pin-on-disc tester (Tribology Research Group, Delft University of Technology, The Netherlands). 1. Three identical PMMA specimens are inserted in the brass rotating disc. 2. Metal ring with the UHMWPE disc, which is placed on top of the three PMMA specimens. 3. Vertical aligned pin with strain gauges to measure deflection. 4. 100 N weight with a horizontal aligned pin. The horizontal pin blocks against the vertical one with strain gauges and constraints the UHMWPE disc and the weight on top from rotating. The CoF is then measured by converting the deflection of this vertical beam*

of this study was to provide a CoF for a specific application, namely to be used in FE analyses of joint prosthesis design.

In a study of Lavielle (1991), a proportional relation was found between surface energy and friction behaviour of polymers [163]. This may also be of importance in the case of UHMWPE, as the surface energy may vary either by unwanted effects, for example due to sterilization methods, or be the desired result of surface modification techniques, such as described in Chapter 8.

Detailed contact properties of the PMMA - UHMWPE interface under in-vivo conditions are still unknown. As a result, different test-conditions are used to investigate if and to what extent interface conditions affect the CoF. As also the fluid properties at the PMMA - UHMWPE interface are unknown, water is used as a lubricant. From literature it is known that a somewhat higher CoF can be expected when serum is used instead of water [175].

It is found that a lower CoF is found in the case of a wet test condition. The fluid film separates the opposing surfaces and any load is carried by the pressure generated within the lubricant. As there is no direct contact between the surfaces, the CoF is lower. In the case of the dynamic test condition, this is intensified by 'Elasto-Hydrodynamic Lubrication' (EHL). EHL causes improved fluid film lubrication.

Table 9.1: *Dynamic and static coefficient of friction between UHMWPE and PMMA for different contact pressures and test conditions (mean (SD))*

Test condition	Pressure (MPa)					Mean
	1	2	3	4	5	
Dynamic / Dry	0.298 (0.018)	0.305 (0.021)	0.305 (0.031)	0.294 (0.012)	0.255 (0.048)	<b>0.291</b> <b>(0.038)</b>
Dynamic / Wet	0.127 (0.009)	0.124 (0.014)	0.121 (0.016)	0.09 (0.002)	0.102 (0.007)	<b>0.113</b> <b>(0.017)</b>
Static / Dry	0.299 (0.027)	0.295 (0.025)	0.285 (0.028)	0.31 (0.023)	0.296 (0.022)	<b>0.297</b> <b>(0.003)</b>
Static / Wet	0.261 (0.024)	0.247 (0.032)	0.23 (0.015)	0.241 (0.02)	0.28 (0.026)	<b>0.252</b> <b>(0.006)</b>
Static / UHMWPE - filled / Dry	0.152 (0.012)	-	0.178 (0.011)	-	0.129 (0.011)	<b>0.153</b> <b>(0.025)</b>
Static / UHMWPE - filled / wet	0.138 (0.006)	-	0.168 (0.008)	-	0.121 (0.007)	<b>0.142</b> <b>(0.024)</b>

tion, which is the result of a velocity difference between the two surfaces, creating a pressure difference at the tops of roughness peaks, thereby deforming these peaks and preventing direct contact [275].

In this study, a non-significant difference was found between the static and dynamic CoF in a dry environment. Even a larger dynamic than static CoF was found for contact pressures of 2 and 3 MPa. In literature this is found more often and may be the result of using different test methods and conditions for the static and dynamic CoF. Unfortunately, it was practically not possible in this study to use the same equipment to measure both the static and dynamic CoF. Also, environmental conditions were different when measuring the dynamic and static CoF, such as the temperature.

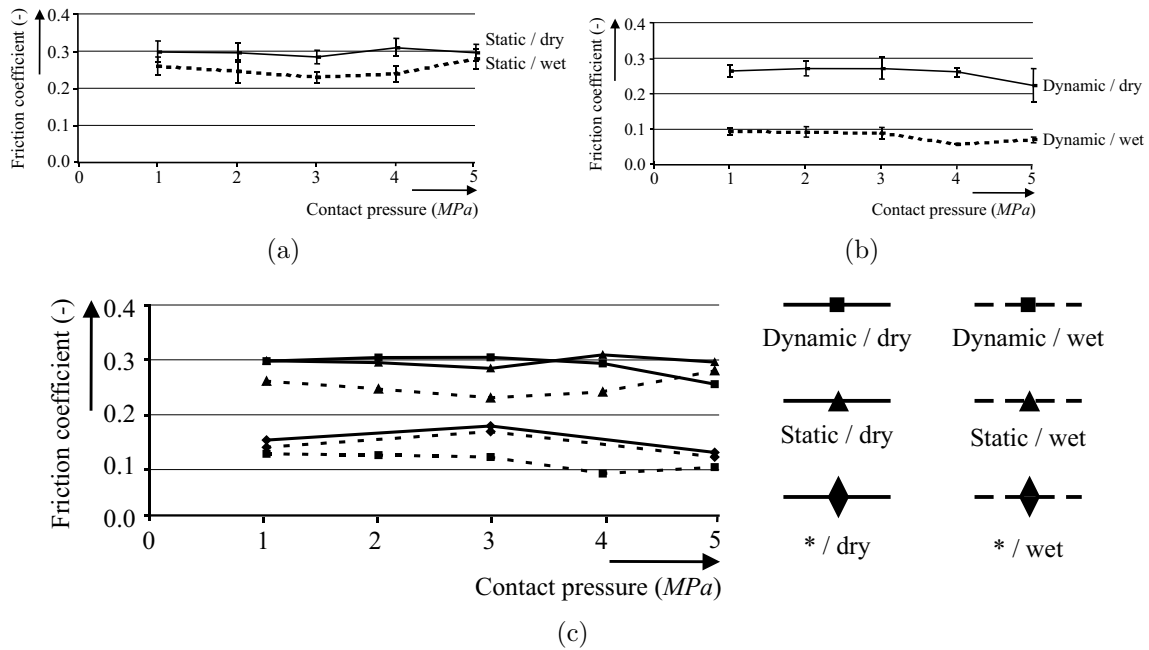


Figure 9.4: (a,b) Results of the static and dynamic coefficient of friction as function of the contact pressure in wet and dry test conditions, respectively. (c) Overview of the results of the six test conditions. \* PMMA specimens filled with UHMWPE

## 9.3 The effect of interface conditions on Finite Element Modelling of the artificial shoulder

### 9.3.1 Methods and materials

To investigate the effect of friction between the UHMWPE glenoid component and the PMMA bone cement on component stresses and glenoid tilting, a three dimensional FE model of the artificial glenoid structure has been developed (see Figure 9.5). The model consists of 42.417 C3D4 tetraeder elements and is analysed using ABAQUS, version 6.3-3 (ABAQUS Inc., Pawtucket, USA). The effect of the interface condition has been investigated for maximal principal stresses and the superior and inferior glenoid component rim-displacements,  $d_s$  and  $d_i$ , respectively (see the List of Symbols). Glenoid component tilting  $\lambda$ , which is a measure for upward and downward glenoid component rotation due to glenoid rim-displacements, may be the underlying cause of glenoid component loosening, especially if this tilting causes tensile stresses in the bone cement layer. This tilting can be calculated using the glenoid component rim-displacements by  $\lambda = \sin^{-1}((d_s - d_i)/c_g)$ , where  $c_g$  is the glenoid superior-inferior chord length (38.5 mm).

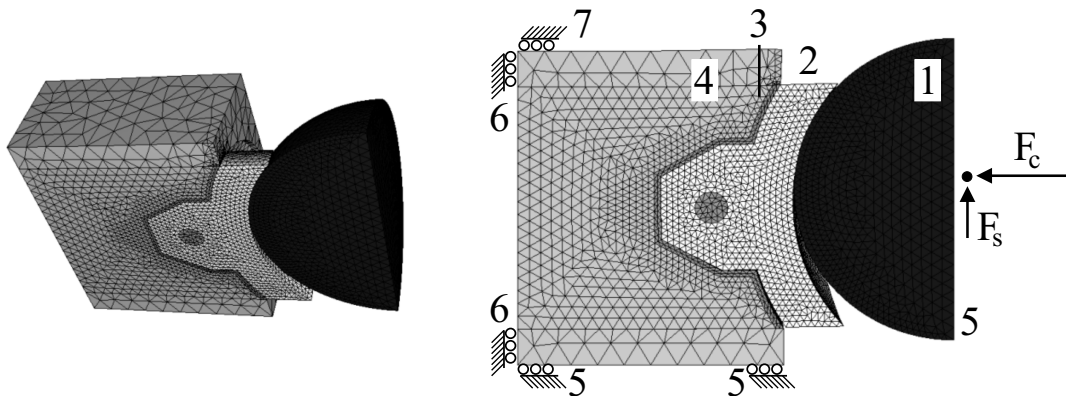


Figure 9.5: The glenoid structure as used for the symmetric three-dimensional Finite Element Model. 1. CoCr Humeral head 2. UHMWPE Glenoid component 3. PMMA cement layer 4. Bone structure 5, 6, 7. Wall constraints. Both the plane of symmetry and the parallel anterior wall are constrained in normal direction.  $F_s$  and  $F_c$  are the applied joint subluxation and compression forces, respectively

## Geometry

The geometry of the FE model is based on the experimental test set-up, described in Chapter 5. The half of the original symmetrical test specimen has been modelled, leading to a rectangular bone block, representing the glenoid part of the scapula, with outer dimensions of  $20 \times 50 \times 40$  mm ( $w \times h \times d$ ) (see Figure 9.5). Furthermore, the model consists of a 2 mm cement layer, the geometry of a commercially available keeled glenoid component with radius of curvature  $R_g$  of 29 mm, radial thickness of 7 mm and a height  $c_g$  of 38.5 mm. Finally, the load is applied using a humeral indenter with radius of curvature  $R_h$  of 24 mm.

## Material properties

Mechanical properties of the bone material are based on weak rheumatoid bone and, together with the properties of other materials used, can be found in Table 9.2. The distribution of the materials in the FE model is shown in Figure 9.5.

All materials used in the FE model are assumed linear elastic. The Young's modulus of 137.5 MPa of the bone structure is rather low, although within the range as found by Frich et al. (1997) [84].

## Interface conditions

Between the humeral indenter and the glenoid component a CoF of 0.1 is assumed, whereas for the CoF between the cement layer and glenoid component the six averaged results of the experiments have been used (see the final row in Table 9.1). Additionally, a CoF of 0, 0.01, 0.4, 0.6, 0.8 and 1 as well as a full bonding, which is

Table 9.2: *Material properties used in the Finite Element model*

Property	UHMWPE	PMMA	CoCr	Bone
Young's Modulus (GPa)	1.0	2.733	210	0.1375
Poisson's ratio $\nu$ (-)	0.4	0.3	0.3	0.3

a node-by node connection at the interface, have been applied to better investigate the effect of interface conditions on stresses in the cement and glenoid component tilting. As a result, a total of 13 analyses were carried out. The interface between the bone cement and the surrounding bone is modelled as a full bonding.

### Applied forces and boundary conditions

A joint compression force  $F_z$  of 725 N and a joint subluxation force  $F_s$  in superior direction of 350 N are applied at center of the humeral head indenter, similar to the experiments as described in Chapters 5 through 7.

All nodes on the inferior, medial, and anterior wall as well as those on the plane of symmetry of the bone structure are constrained in both normal directions of these planes. Of the superior wall of the bone structure, only the nodes on the medial half are constrained in both normal directions of this plane (see Figure 9.5). This is to allow for a more natural deformation pattern, conform to the experimental test set-up.

### Type of analysis

A geometrical non-linear analysis is carried out in two steps, in which in the first step the compression force is applied and in the second the analysis is continued with the application of the subluxation force.

## 9.3.2 Results

In this study, a FE analysis of a cemented keeled glenoid component has been carried out with different interface conditions between the PMMA bone cement and the UHMWPE glenoid component. An overview of the results of the maximal principal stresses and medial-lateral displacements of the three parts of the FE model for the 13 analyses can be found in Table 9.3. Figures 9.6 and 9.7 provide the distribution of the maximal principal stress and medial displacements for the glenoid component and bone cement layer. Additionally, Figures 9.8 and 9.9 give the maximal principal

stresses and the superior  $d_s$  and inferior  $d_i$  glenoid component rim-displacements as a function of the coefficient of friction at the interface as well as in the case of full bonding.

Clear differences were found in maximal principal stresses in the UHMWPE glenoid component, the PMMA bone cement and the bone structure for the different interface conditions. In the glenoid component, the difference of the maximal principal stresses due to different interface conditions, where a full bonding at the interface is taken as the reference (20.74 MPa), ranged between -15.8% (CoF=0) and -8.8% (CoF=1). In the bone cement, with a maximal principal stress of 21.3 MPa in the case of a full bonding, this difference ranged between +24.5% (CoF=0.113, which is the dynamic CoF in a wet environment) and +51.1% (CoF=0). Finally, the difference of the maximal principal stress in the bone structure ranged between +11.5% (CoF=1) and +18.8% (CoF=0), relating to an analysis with a full bonding at the interface (29.6 MPa).

Also, clear differences were found in tilting of the glenoid component, the PMMA bone cement and the bone structure for the different interface conditions. The difference in glenoid component tilting due to different interface conditions, where the very small tilting with a full bonding at the interface is taken as the reference (0.763°), ranged between +84.1% (CoF=0) and +37.0% (CoF=0.4). In the bone cement, with a tilting of 0.741° in the case of full bonding, this difference ranged between +15.8% (CoF=0.113, which is the dynamic CoF in a wet environment) and +9.9% (CoF=0.6). Finally, the difference of the maximal medial displacement in the bone structure ranged between +10.4% (CoF=0.8) and +15.4% (CoF=0), relating to an analysis with a full bonding at the interface (0.739°).

Good correlation was found between the maximal principal stress and the CoF at the UHMWPE and PMMA interface for the glenoid component and bone structure, with a correlation  $R^2$  of 0.9407 and 0.9914, respectively. A worse correlation of 0.6038 was found for the correlation between the maximal principal stress in the cement layer and the CoF. For the superior  $d_s$  and inferior  $d_i$  rim-displacements, a close to zero and high correlation of 0.0148 and 0.8964 were found, respectively. All applied interface conditions lead to negative inferior glenoid rim-displacements  $d_i$ , although in the case of full bonding this inferior rim-displacement is almost zero (-0.031 mm).

### 9.3.3 Discussion

In this study the effect of interface conditions between the UHMWPE glenoid component and the PMMA cement layer on cement stresses and glenoid component tilting has been investigated, using FE modelling. The background of this study is that no bonding was found between many glenoid components as found by in-house experiments. However, interface bonding between these two surfaces depends

on many factors, such as the type of UHMWPE and PMMA bone cement used, the method of sterilization and the method of storage. Additionally, surface modifications can be used to improve adhesion between UHMWPE and PMMA (see Chapter 8). In advance it is not known if the glenoid component will adhere to the bone cement.

Although the maximal stresses in the UHMWPE as obtained in the analysis (20.74 MPa with a full bonding at the interface) are somewhat lower than found in the study by Swieszkowski et al. (2003), who found 25 MPa [309], it is still close to the yield strength of UHMWPE. As a result, a similar conclusion can be drawn, that UHMWPE wear may indeed occur in joint replacements, as the UHMWPE yield strength may be exceeded.

The FE model as used in this study has not been validated. However, the aim of this study was not to develop a validated, detailed FE model of the scapula with a Total Shoulder Replacement. Our aim was to investigate the effect of interface conditions between PMMA bone cement and the UHMWPE component on cement stresses and glenoid component tilting in a FE model. However, some remarks can be made, when comparing the results of this study with the results of the experiments, on which the FE model is based on.

The superior and inferior rim-displacements of the glenoid component show a very similar qualitative behaviour compared to the experimental measurements. Both the experimental and computational results show glenoid component tilting out of the bone cement, opposite to the side of glenoid component loading. In the case of a full bonding at the interface this leads to tensile stresses in the bone cement and in all other cases to a gap between the glenoid component and the bone cement. Compared to the experimental results, the absolute values of the rim-displacements as calculated by the FE model are more than 1.5 times larger for the superior rim and almost 10 times larger for the inferior rim, for which the values were much smaller. The values in the case of a full bonding in the FE model are of the same order of magnitude to the results of the experimental measurements, although this interface condition was not found in most glenoid specimens during the experiments.

Very few similar studies focused on the investigation of the stresses in and around glenoid components using the FE technique. Couteau et al. (2001) investigated the effect of some surgical parameters on the stresses in the cement layer using a 3D FE model of the scapula [61]. Although they validated their FE model by experimental measurements and good agreement was found, nothing was mentioned about the interface conditions between glenoid component and cement. However, some of their results show stresses in the cement layer, which are of the same order of magnitude as found in our study.

In the present study, the superior  $d_s$  and inferior  $d_i$  rim-displacements show zero and high correlation with the CoF, respectively (see Figure 9.9). Therefore, it seems that compression of the superior glenoid structure is not influenced by the CoF, whereas the effect on deformation of the inferior glenoid structure is clearly present. It may

be that the increasing shear stiffness at the interface, due to the increased CoF, restrains gap-opening between the inferior glenoid component and the cement layer. In Section 5.4 it was questioned whether bonding between the glenoid component and the PMMA bone cement was beneficial for component fixation in the case of presently used glenoid component designs. In the present study, using a Finite Element model of the replaced shoulder, increased maximal principal stresses in the glenoid component was found, but also less glenoid component tilting, when applying a full bonding at this interface, compared to contact elements and a CoF. In the cement layer and bone substitute both lower maximal principal stresses and less medial-lateral displacements were found in the case of a full bonding at this interface. With respect to this, it can be concluded that physical adhesion between the UHMWPE glenoid component and the PMMA bone cement can be beneficial for the fixation of glenoid components. Although the presented FE model is different from the FE models with the geometry of a scapula, in which the glenoid components are inserted, the obtained differences of the results still demonstrate the importance of the interface conditions.

## 9.4 Conclusions

The aim of the study was to investigate the static and dynamic coefficient of friction (CoF) between PMMA and UHMWPE to be used to investigate the effect of friction on stresses in the bone cement and on glenoid component tilting using the FE technique.

Although test conditions have a great effect on the CoF, a non-significant difference was found between the static and dynamic CoF for a dry test condition. However, a dramatic decrease of the static CoF was found when using PMMA specimens, which were first used to measure the dynamic CoF. These porous PMMA specimens became filled with the softer UHMWPE during testing. This leads to decreased friction, which may also be the case for cemented glenoid components in-vivo.

A recommendation for future work is to measure both the static and dynamic CoF with the same equipment under similar circumstances. However, it wasn't our aim to perform an investigation of the CoF in great detail. Our aim was to indicate the CoF between PMMA bone cement and UHMWPE to be used in a FE model.

It is found that full bonding provides a small overestimation of the maximal principal stresses in the glenoid component, whereas in the bone cement and underlying bone it dramatically underestimates the maximal principal stresses, with respect to a CoF at the interface. Also, although full bonding only slightly underestimates the superior glenoid rim-displacements, it provides an unexpected behaviour of the inferior glenoid rim-displacements, as it prevents the glenoid component to tilt away from the cement, due to the node-by node connection at this interface. This indicates that, in the case bonding between UHMWPE and PMMA is present in-vivo, tensile stresses in the bone cement can occur, as there is a tendency for lateral

Table 9.3: Maximal principal stresses and medial displacements in the glenoid component, the PMMA bone cement and the bone structure for different interface conditions between the bone cement and glenoid component. \* Static / UHMWPE filled, sup. and inf. indicate superior and inferior, respectively. Glenoid component tilting  $\lambda$ , a measure for upward and downward glenoid component rotation due to glenoid rim-displacements, is calculated as  $\sin^{-1}((d_s - d_i)/c_g)$ , where  $c_g$  is 38.5 mm

Condition	CoF	UHMWPE glenoid			PMMA cement			Bone structure			
		Max. Pr. Stress (MPa)	Rim-displ. ( $d_s$ ) (mm)	Tilting ( $d_i$ ) ( $\lambda$ ) ( $^\circ$ )	Max. Pr. Stress (MPa)	Rim-displ. (mm)	sup. inf.	Max. Pr. Stress (MPa)	max. medial displ. (mm)	sup. inf.	
Dynamic/dry	0.291	17.61	0.565	-0.327	1.33	27.08	0.545	-0.0164	33.87	0.542	-0.0164
Dynamic/wet	0.113	17.63	0.560	-0.357	1.37	26.62	0.560	-0.0164	34.45	0.551	-0.0160
Static/dry	0.297	17.60	0.565	-0.326	1.33	27.04	0.544	-0.0164	33.85	0.542	-0.0164
Static/wet	0.252	17.62	0.564	-0.332	1.33	27.18	0.546	-0.164	33.98	0.544	-0.0164
* / dry	0.153	17.74	0.561	-0.349	1.36	26.85	0.550	-0.0163	34.30	0.548	-0.0163
* / wet	0.142	17.76	0.561	-0.351	1.36	28.75	0.550	-0.0163	34.34	0.549	-0.0164
-	0	17.47	0.568	-0.375	1.40	32.18	0.557	-0.0159	35.1	0.557	-0.0159
-	0.01	17.68	0.564	-0.376	1.40	31.66	0.557	-0.0160	35.08	0.555	-0.0160
-	0.4	17.64	0.568	-0.134	1.05	26.66	0.542	-0.0160	33.6	0.539	-0.0160
-	0.6	17.97	0.568	-0.298	1.29	26.7	0.537	-0.0170	33.25	0.534	-0.0170
-	0.8	18.63	0.565	-0.291	1.27	27.76	0.534	-0.0170	33.07	0.531	-0.0170
-	1	18.92	0.563	-0.286	1.26	28.88	0.532	-0.0178	32.95	0.532	-0.0171
Full bonding	-	20.74	0.482	-0.0303	0.76	21.30	0.467	-0.0307	29.55	0.467	-0.0296
Max.	-	20.74	0.568	-0.0303	1.40	32.18	0.557	-0.0159	35.08	0.557	-0.0159
Min.	-	17.47	0.482	-0.376	0.76	21.30	0.467	-0.0307	29.55	0.467	-0.0296

rim-displacements of the inferior glenoid component. A full bonding only slightly underestimates the medial displacements in the bone cement and underlying bone. A recommendation for future research is to perform a similar study in an existing, validated FE model, using the different CoF as found in this study and both keeled and pegged cemented components. As these FE models are frequently used for design validation, separate analyses with a full bonding and a CoF at the interface between glenoid component and bone cement should be performed, for a more realistic design validation.

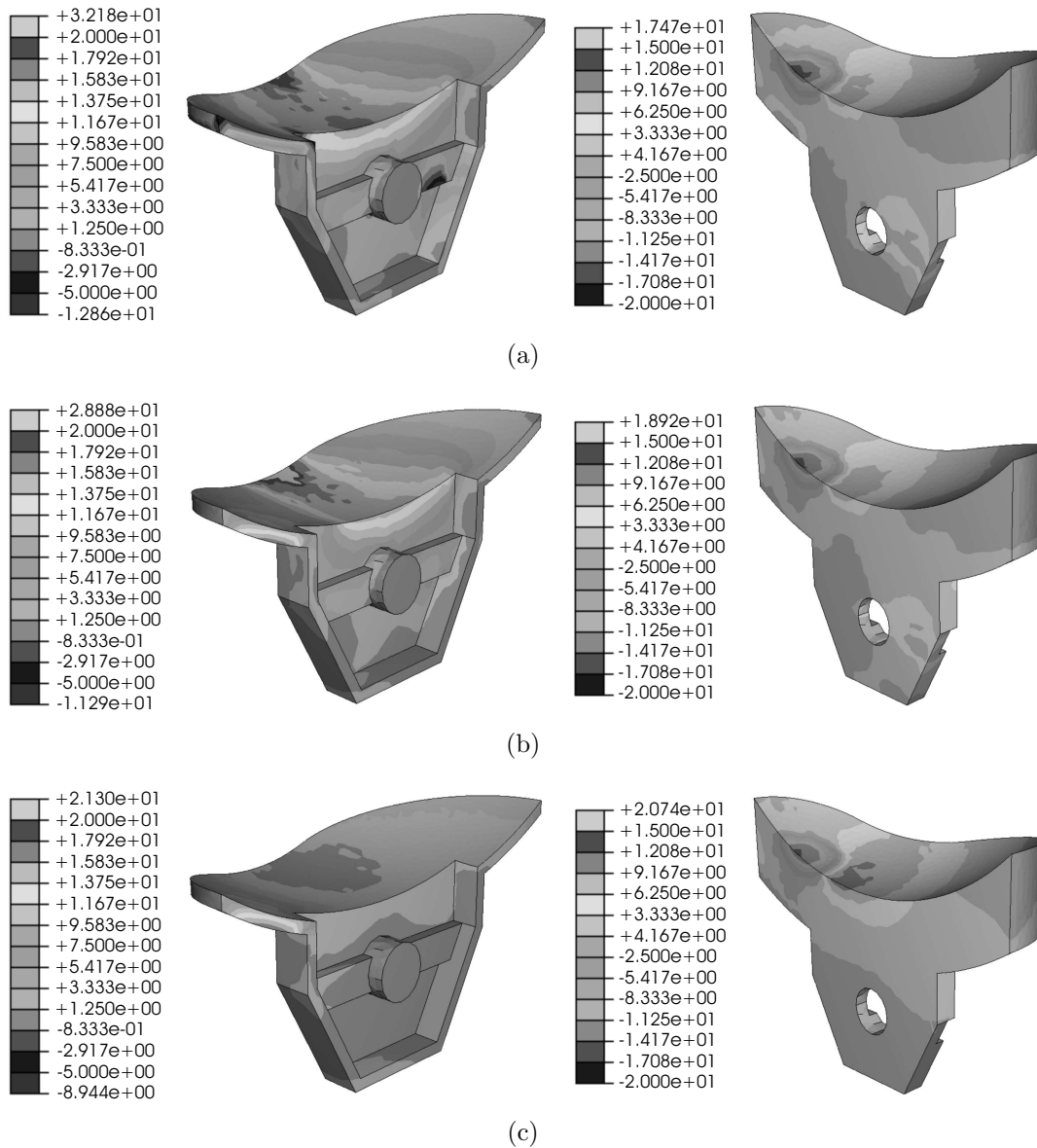


Figure 9.6: Maximal principal stresses (MPa) in the bone cement (left) and glenoid component as analysed using the FE model for different interface conditions, with a 725 N joint compression force and a 350 N superior directed joint subluxation force. (a) A CoF of 0 is applied at the UHMWPE - PMMA interface. (b) A CoF of 1 is applied at the UHMWPE - PMMA interface. (c) A full bonding is applied at the UHMWPE - PMMA interface. See Figure C.5 in Appendix C for color representations

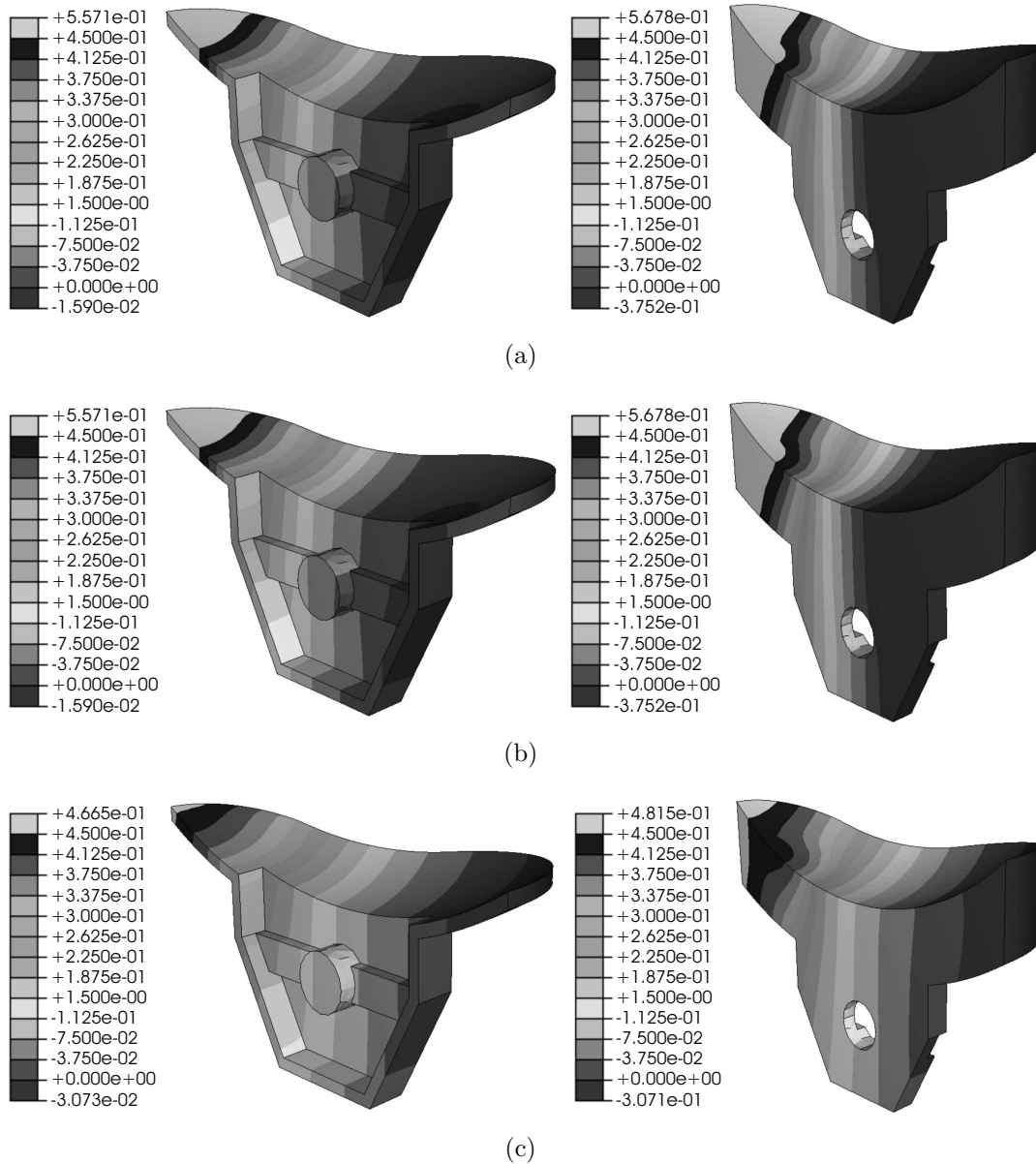


Figure 9.7: Maximal displacement (mm) in medial-lateral direction in the bone cement (left) and glenoid component as analysed in the FE model for different interface conditions, with a 725 N joint compression force and a 350 N superior directed joint subluxation force. (a) A CoF of 0 is applied at the UHMWPE - PMMA interface. (b) A CoF of 1 is applied at the UHMWPE - PMMA interface. (c) A full bonding is applied at the UHMWPE - PMMA interface. See Figure C.6 in Appendix C for color representations

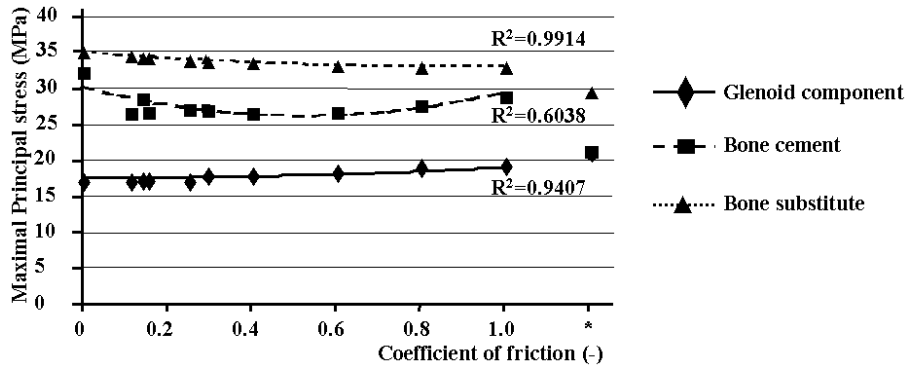


Figure 9.8: Effect of interface conditions on the maximal principal stresses in the glenoid component, bone cement and bone.  $R^2$  is the second order correlation coefficient

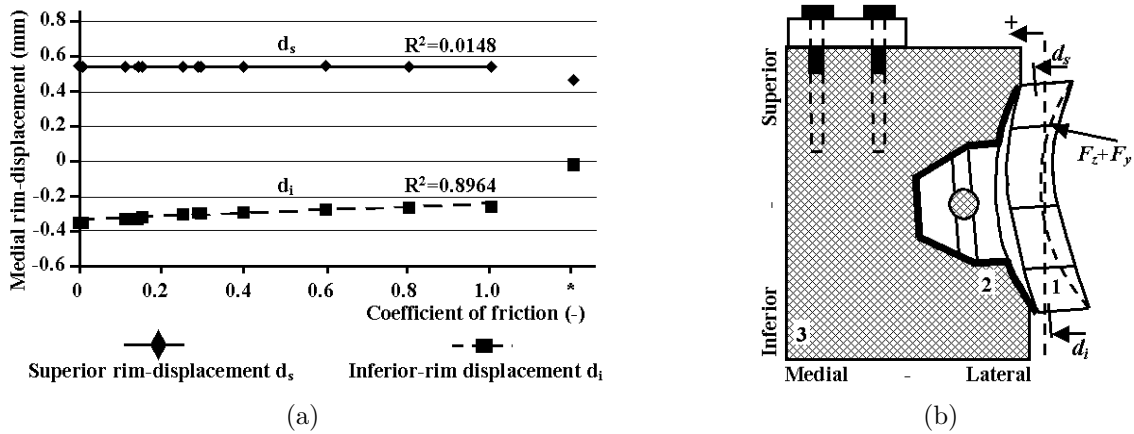
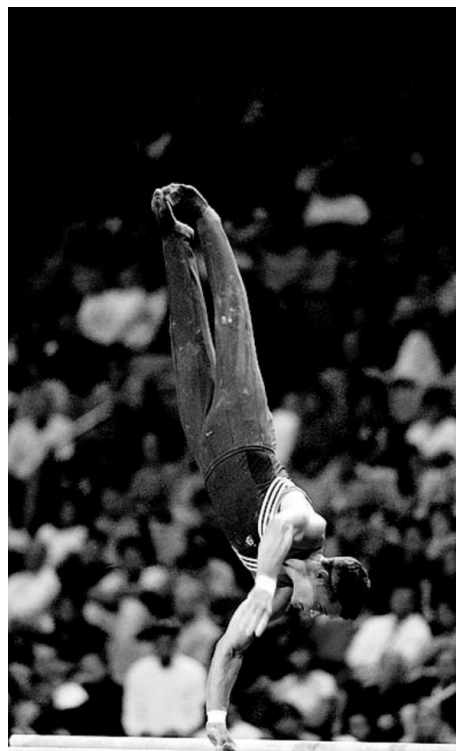


Figure 9.9: Effect of interface conditions on the superior and inferior rim-displacements,  $d_s$  and  $d_i$ , respectively. (a) Superior and inferior rim-displacements. (b) Definition of the superior and inferior rim-displacements. The positive (medial) direction is indicated.

\* Results of a full bonding at the interface.  $R^2$  is the second order correlation coefficient

## Chapter 10

# A self-stabilizing shoulder endo-prosthesis



*A gymnast during his horizontal bar session,  
demanding the impossible of shoulder stability*



## 10.1 Introduction

In Chapter 2, the pathological characteristics of glenohumeral joints with rheumatoid-arthritis and Rotator Cuff (RC)-arthropathy have been described. These joints have a deteriorated soft-tissue state, weakened bone properties and also excessive bone deformations can occur. There is a lack of joint compression due to a weakened or even torn Rotator Cuff (RC), leading to joint subluxation and instability, made worse by glenoid cavity erosion. It was mentioned that no reliable treatment is available at present, providing good joint stability and enough joint functionality to perform most activities of daily living for the mentioned patient group.

The overview of prosthesis concepts as used in the past and present in Chapter 2, demonstrates the design conflict between glenohumeral joint functionality and stability versus component fixation.

Joint stability in artificial joints with severe joint pathology is achieved by restraining the humeral head as it tends to subluxate. For example, standing up from a chair, with full assistance of the arm rests, leads to a subluxation force of at least 0.5 times body weight (BW) for each glenohumeral joint. In the case that no natural stability function is present, the components must pick up all subluxation forces, which are then distributed over their fixation. Two examples are the constrained glenoid component and the reversed prostheses, which both show complications with respect to long-term component fixation (see Chapter 2). The failure mechanism which causes the early component loosening, may be the excessive bending and shear stresses at the screw or bone ingrowth fixation. This is even more pronounced in the weakened rheumatoid bone.

On the other hand, using a conventional, unconstrained glenoid component may show better survival rates, but leads to shoulder subluxation or even a dislocation, as no natural stabilizers are present. Additionally, the decreased joint compression in combination with the common superior oriented glenoid cavity results in more eccentric glenoid component loading. This increases component wear and glenoid component tilting, thereby fatiguing its fixation. This implies that, after all, early component loosening can be expected (see Chapter 5).

A new prosthesis design must aim at proper joint stability and functionality, which may not be at the expense of component fixation. The glenohumeral joint anatomy and pathological state must form the basis for this new design. Furthermore, the new design must fulfill a set of requirements with respect to available space and biomechanics of the shoulder, joint range of motion, implantation, fixation strength, material biocompatibility and certification.

The aim of this study is to develop a glenohumeral joint prosthesis, which must regain joint functionality without the necessity of anatomical stabilizing structures. In addition, the survival rates must be better than presently used prostheses for patients with rheumatoid-arthritis and RC arthropathy. The design must be 'self-stabilizing', which implies that any destabilizing forces at the glenohumeral joint must be counteracted for by the prosthesis components and their fixation only.

The result of the study is a methodological description of principles of the new design. Although preliminary component fixation has been investigated, no prototype of the complete design has been manufactured and also no detailed design validation was performed.

Subsequently, the design requirements, biomechanical background, design description, component fixation and spin off will be presented in this chapter.

## 10.2 Design requirements

Next to the main goal of a joint replacement, which is pain relief, the new prosthesis design must fulfill a list of requirements before it can be regarded as a design concept, which can be innovative. The requirements are summarized in Table 10.2.

### 1. Joint stability

The design must be so-called 'self-stabilizing'. This implies that, next to guaranteeing force equilibrium, it must provide glenohumeral stability without using surrounding anatomical stabilizing soft-tissues, such as muscles and ligaments. Eccentric forces, such as external subluxation forces, must be counteracted by the prosthesis itself, to control the glenohumeral joint reaction force. Forces can only be distributed into the lateral scapula and proximal humerus.

### 2. Joint range of motion

The new design must allow for sufficient range of motion (RoM) to at least perform all ADL. An overview of the RoM requirements is given by Magermans et al. (2004) [186] (see Table 10.1). These data have been obtained by measuring 24 healthy subjects, who performed six activities of daily living. These six activities were selected based on their importance for independent living. The provided angles in Table 10.1 relate the orientation of the humerus to the fixed world. In other words, they include scapulo-thoracic motion, that is contribution of scapular rotation about the thorax (see Section 2.3). Unfortunately, unambiguous ratios of the scapulo-humeral rhythm for healthy shoulders are unknown, not to mention in the case of shoulder pathology. In pathologic shoulders, the scapulo-thoracic motion can be even more pronounced, as this is relatively unaffected, compared to glenohumeral articulation.

Assuming the most unfavorable ratio as found in literature of 1:2 (scapulo thoracic medial-lateral rotation : glenohumeral abduction) [251] in combination with a RoM of the artificial shoulder as described in Table 10.1, the new prosthesis design should allow the replaced shoulder to fulfill the abduction and adduction requirements.

In this study, only scapular medial-lateral rotation is taken into account, which influences glenohumeral abduction and adduction and is included when setting the

RoM requirements for the new prosthesis design. Scapular retraction and protraction, which is scapular rotation about a superior-inferior axis, thereby influencing glenohumeral flexion, is not taken into account in the requirements, as this contribution is much smaller [251].

As a result, the new prosthesis design must meet the requirements with respect to the three rotational degrees of freedom, divided in positive and negative directions, as given in column 5 of Table 10.1.

Table 10.1: *Range of motion requirements for a new shoulder prosthesis design. The three rotational degrees of freedom of the glenohumeral joint are measured during six activities of daily living of 24 healthy subjects [186]. \* Humerus angle between the longitudinal axis of the humerus and the thorax (the global coordinate system). \*\* Angle between the longitudinal axis of the humerus and the scapula in the artificial joint. \*\*\* Washing the opposite axilla*

ADL task	Main movement	Maximal angle* (°)	Mean angle* (SD) (°)	Design requirement** (°)
Reaching	Abduction	148.3	131.7 (10.4)	99
Washing***	Adduction	90.1	54.3 (18.7)	60
Combing hair	External rotation	71.2	55.4 (18.5)	71
Perineal care	Internal rotation	90.5	65.6 (14.8)	90
Lifting a bag	Forward flexion	148.0	131.3 (9.5)	148
Eat with spoon	Retro flexion	65.7	50.5 (8.1)	66

### 3. Joint biomechanics

Main biomechanical characteristics of the glenohumeral joint may not be altered. An example is the glenohumeral center of rotation (CoR), which, among others, determines the muscle moment arms. Muscle moment arms may not decrease, as it leads to increased muscle and joint reaction forces, which require increased effort of the patient and may lead to early component loosening. This must be taken into account in the design and during implantation of the components.

Additionally, it must be respected that there is still a discussion going on whether the CoR during glenohumeral motion is fixed or not (see Section 2.3). Rigid fixation of the CoR may lead to high interface stresses during articulation, due to the enforced, though little, humeral head translations. A certain flexibility of the CoR during articulation must be allowed for, although this is difficult to quantify.

### 4. Component fixation strength

The fixation of the new prosthesis design must fulfill fatigue and static strength requirements. Unfortunately, a detailed 24-hour shoulder load spectrum is not avail-

able, which makes it difficult to investigate the stresses in both biological and biomaterials and to validate component fixation [237]. However, the fixation of the new prosthesis design must allow for performing ADL for at least 10 to 15 years, to outperform presently used shoulder prostheses. Taking horizontal abduction as the basis shoulder movement, then the corresponding joint loading is 725  $N$  joint compression and 350  $N$  joint subluxation in a healthy shoulder, as calculated using a musculoskeletal model [108]. However, in the case of severe pathologic state of the joints of the target patient groups, especially of the RC muscles, the joint compression force is assumed to be absent.

Assuming multiple joint movements per day, the total number of joint loadings during the prosthesis life time may exceed 500.000 cycles (100 cycles/day x 365 days/year x 15 years). The fixation of the new prosthesis design must be able to pick up the given subluxation force to guarantee force equilibrium for at least 500.000 cycles. Therefore, fatigue tests of the prosthesis and its fixation should at least survive 500.000 load cycles with subluxation force of 350  $N$ .

The prosthesis design may also have to deal with peak forces, in the case of more demanding tasks but also due to a fall or bump. For setting the static strength requirements, the maximal occurring force in the prosthesis lifespan must be known. The prosthesis and its fixation must be able to deal with this force because permanent damage is not allowed. However, it is unfeasible to develop a prosthesis which must be able to undergo every possible occurring force.

In addition, the fixation strength should be just smaller than the strength of the underlying bone structure. If a fracture in the artificial joint may occur, then it is the fixation which is the weakest link and not the bone structure itself. A fracture of the already weakened bone structure may be impossible to repair, whereas it may be easier to replace a prosthetic component by surgical intervention.

In other areas of product design, where serious consequences may occur if product functions start to fail, a distribution of probability of occurring peak forces is used. The product must survive a peak force with a probability of an beforehand set percentage, often multiplied by a certain safety factor. A fall, which in the life of the prosthesis should never occur, but it could happen, may be used as a basis for static strength calculation. It is known that joints may undergo forces of several times body weight (BW) during falling, but accurate data for the shoulder are not available. As a result, this loading condition is difficult to use for strength requirements. To guarantee force equilibrium with the new glenohumeral prosthesis design, the major forces, which must be counteracted, are the subluxation forces. Using simple static equilibrium equations, the forces when pressing up from a chair can be calculated and will be used to set the static requirements for the new design. Slowly pressing up from a chair leads to a superior directed subluxation force  $F_s$  of at least 0.5 times BW on each shoulder joint, which has to be counteracted by the new prosthesis. This can be seen as a high demanding task for the target patient group, which will be done very infrequently, if at all.

A safety factor will be added for three reasons. First, because it will be difficult to evenly distribute the body weight over the two shoulders, leading to higher static subluxation forces in one of the shoulders, up to a maximum of 1 times BW, which implies a safety factor of 2. Second, because it is not a static but a dynamic movement, which leads to increased instantaneous subluxation forces, which must be taken into account. Finally, because material, surgical and other unforeseen shortcomings lead to uncertainty and may not be overlooked. If all three factors, i.e. the uncertainty of the force distribution over both shoulders, dynamic aspects and remaining factors, such as material, surgical and other factors, contribute to the uncertainty by a factor 1.25, the total safety factor is 4 ( $1.25^3 \cdot 2$ ). This safety factor is added to the subluxation force of 0.5 times BW, which requires the prosthesis and its fixation to at least pick up a subluxation force of 2 times BW.

## 5. Prosthesis implantation

The prosthetic components must allow for conventional surgery, without additional effort as compared to presently used prostheses. The surgical process as described in Section 2.4.3, should be respected. Further limitations are the difficult exposure of the glenoid bone stock, which is only visible and approachable from the lateral side, and the limited surgical working space.

## 6. Materials and components

All prosthetic components should be made out of certified biocompatible materials. Also, if possible, 'of-the-shelf' certified prosthetic components and parts, which are commercially available, should be used in the new design. Both requirements speed up the innovation process.

## 7. Dimensions and environment of the prosthetic system

The prosthesis is to be inserted into the anatomical glenohumeral joint, with limited space, specific geometry and dimensions. The surrounding soft-tissues, such as muscles and nerves, should be respected and their function must be preserved. The components must allow for easy insertion and during articulation, no joint impingement or blocking of nerves and muscles may occur.

# 10.3 The design

## 10.3.1 Restoring joint stability

The new prosthesis design is meant to improve glenohumeral joint stability for rheumatoid joints and in the case of Rotator Cuff (RC) pathology. In these joints, stability is decreased due to both decreased joint compression  $F_z$  and glenoid erosion, in the case the disease is present for a longer period. Glenoid cavity reaming

Table 10.2: Summary of the requirements for a self-stabilizing prosthesis

Design aspect	Requirement	Remark
<b>Joint stability</b>	The new prosthesis design must ensure joint stability without using stabilizing anatomical structures	Only the lateral scapula and proximal humerus can be used for force distribution
<b>Joint range of motion</b>	The new prosthesis design must allow for enough range of motion to perform ADL	Glenohumeral joint angles are listed in Table 10.1
<b>Joint biomechanics</b>	Joint biomechanics and kinematics may not be altered	Especially the center of rotation may not be changed
<b>Component fixation strength</b>	The prosthesis and its fixation must be able to pick up a subluxation force of at least 2 times BW	This is based on lifting from a chair, without help, and a safety factor of 4
<b>Prosthesis implantation</b>	Conventional surgery must be possible	Glenoid cavity is only approachable from the lateral side
<b>Materials and components</b>	Materials must be bio-compatible and certified.	If possible, commercially available components should be used
<b>Dimensions and environment</b>	Components must fit into the glenohumeral joint, without causing impingement at rest and during articulation	See Tables 2.1 and 2.2 for detailed dimensions of the glenohumeral joint

may improve glenohumeral stability by increasing the glenoid constraint angle  $\theta$ , although this may be difficult to realize in the case of excessive joint pathology. It is probably more interesting to focus on the initial anatomical defect, which caused the instability and to integrate the lost stability function in the new design. This was the basic idea for the development of the new self-stabilizing prosthesis.

Shear forces in the glenohumeral joint, such as subluxation forces  $F_s$ , are in healthy joints compensated for by a joint compression force  $F_z$  due to muscle activity and ligaments. Increased joint compression decreases the joint contact angle  $\varphi_1$  (see Figure 10.1b). This makes creating force equilibrium more easy and improves joint stability. Additionally, those ligaments, which become stressed due to the subluxation force, create an opposite directed, counteracting force, which leads to an additional decrease of the joint contact angle  $\varphi_1$  (see Figure 10.1c). As a result, this furthermore increases the improvement joint stability.

The lack of these joint stabilizing forces due to RC and ligament deficiencies, increase the off-center forces and, as a result, restoring these forces improves joint stability. Therefore, the biomechanical aim of the new design is to restore joint compression and to introduce a force opposite to the occurring subluxation force. This biomechanical design aim is presented in Figure 10.1c.



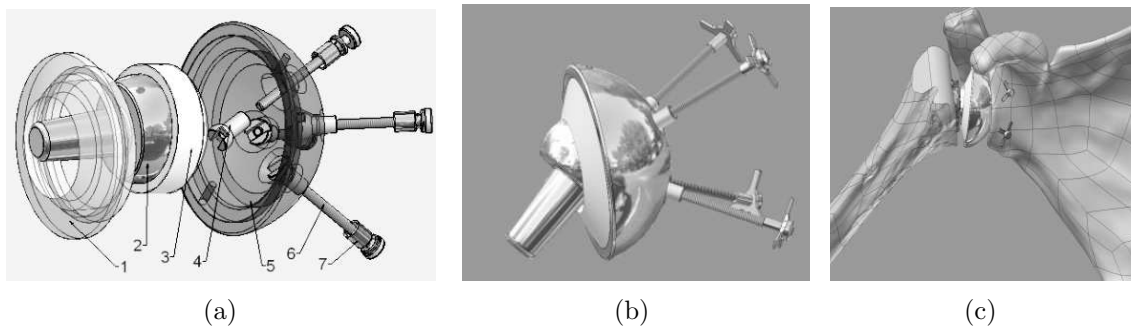


Figure 10.2: *Overview of the self-stabilizing glenohumeral prosthesis. (a) The bipolar prosthesis on component level. 1. Constraining disc 2. CoCr head for the inner bearing 3. UHMWPE disc for articulation 4. Nuts, for fixation of the artificial ligaments to the outer shell 5. Outer shell, fixed against the glenoid bone stock 6. Artificial ligaments 7. Bone anchors (b) The assembled prosthesis. (c) Artist impression of the replaced glenohumeral joint. See Figure C.7 in Appendix C for color representations*

of the anatomy of the individual patient, this method is difficult to use in practice. However, the conventional humeral head replacement, which is supposed to be directly connected to the scapula by artificial ligaments, can be replaced by a bipolar prosthesis. This is a commercially available prosthesis as described in Chapter 2, with a CoCr outer shell, a constrained Ultra-High-Molecular-Weight-Polyethylene (UHMWPE) inlay and a small CoCr ball component, fixed to the proximal humerus and articulating against the UHMWPE inlay. The idea is to fixate the outer shell to the glenoid cavity using artificial ligaments, which are fixed at the medial cortex of the glenoid bone stock. The new articulation is created by the small head inside this outer shell of the bipolar prosthesis.

### Method of principles of the new design

The presented design concept includes a bipolar humeral head replacement, of which the outer shell is semi-rigidly connected to the glenoid bone stock by 3 or 4 artificial ligaments (see Figure 10.2). From the outer shell, they diverge towards the glenoid bone stock. Guided by drilled openings, these ligaments go subsequently through the subchondral, trabecular and medial cortex of the glenoid bone, at which the ligaments will be fixed. In general, the medial cortex of the glenoid bone stock still has good mechanical bone properties, as this is away from the diseased joint. After the outer shell is positioned against the lateral glenoid cavity, the ligaments are fixed on the inner side of this shell, whereafter the prosthesis can be assembled.

Two methods of fixation of the artificial ligaments against the medial cortex of the glenoid bone are developed, keeping in mind the requirements of prosthesis implantation (see Table 10.2). The first method is to use bone anchors with a limited

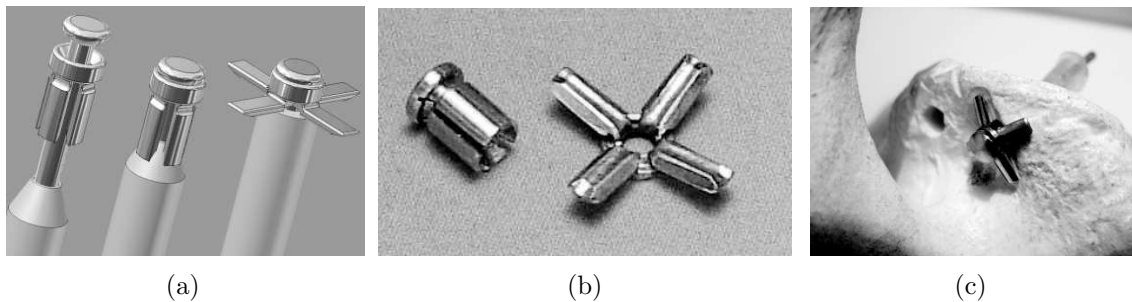


Figure 10.3: *The bone anchors and method of unfolding. (a) The bone anchor during its unfolding procedure. (b) Folded and unfolded bone anchors, with maximal diameters of 4.5 and 12 mm, respectively. (c) Unfolded bone anchor in position at the medial cortex of the glenoid bone stock*

initial diameter to be guided through the drilled bone hole. As the bone anchors come out of the medial cortex of the glenoid bone stock, they can be unfolded (see Figure 10.3b). If the ligaments become loaded, the unfolded bone anchors cannot be pulled back through the glenoid bone stock, as they are prevented by their increased diameter (see Figure 10.3c). The tensile forces in the ligaments are distributed by the bone anchors into the medial glenoid cortex of the glenoid bone stock.

A second method is to make use of ligaments with a clamped ball at their medial end. The ligaments are positioned in hollow screws, with the balls fitting in a concavity at the medial end of these hollow screws. The hollow screws are subsequently tightened through the subchondral, trabecular and medial cortex of the glenoid bone. These screws set themselves into the probably healthy medial trabecular and cortical bone of the medial glenoid bone stock. If the ligaments are loaded, the clamped balls are constrained by the hollow screws, preventing the ligaments to be pulled back through the glenoid bone stock. The tensile forces in the ligament are distributed by the hollow screws over all their screw thread into the cortical and trabecular bone (see Figures 10.4a and b). As the clamped balls at the ligaments can rotate in the medial concavity of the hollow screws, they minimize bending of the screw fixation in the case of humeral translations.

When all three or four ligaments are inserted, the outer shell of the bipolar head can be fixed at their other end. As the humeral head tends to sublunate in any direction, the ligaments become loaded. Then, either the bone anchors are pulled against the medial cortex of the glenoid bone, or the balls at the medial ligaments are pulled into the hollow screws, which distribute the forces into the medial cortex and trabecular bone of the glenoid bone stock. As a result, they prevent the humeral head from further translating out of the glenoid cavity. Both joint compression and the force opposite to the acting sublunate force will increase, due to ligament orientation and the coupled translations between humeral head translations in the lateral and

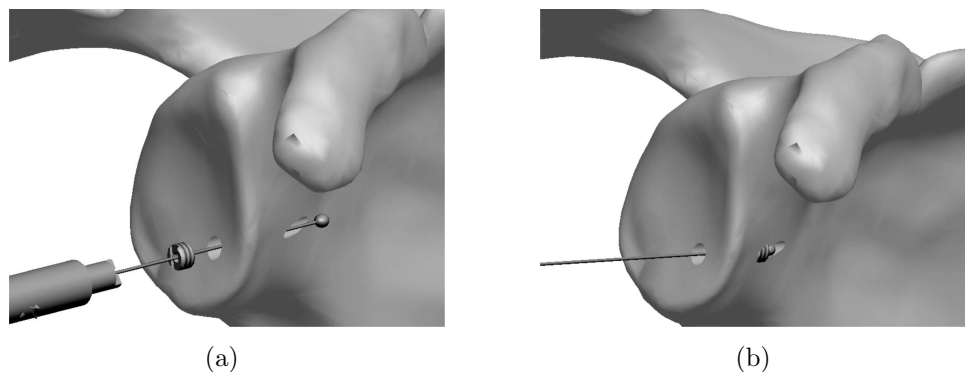


Figure 10.4: *Method of fixation by using a hollow screw and a ligament with an attached ball at the medial end. (a) The fixation system during insertion. (b) The assembled fixation system*

an arbitrary perpendicular direction (see equation 4.8 in Chapter 4). The ligaments are free to rotate about either the bone anchor or the hollow screw, thereby minimizing bending stresses around the fixation.

The outer shell of the bipolar prosthesis is fixed against the scapula and the inner bearing is supposed to form the new articulation and should allow for enough joint functionality to fulfill the RoM requirements. As this design allows for small translations of the humeral head relative to the glenoid cavity, it should not be mixed up with the 'constrained glenoid components', as used in the past.

The surgical procedure is presented in Figures 10.5a through f. After opening the joint to obtain a clear exposure of the glenoid cavity, the 3 or 4 holes can be drilled. In the case of using bone anchors, the diameter of the drilled holes is  $4.5\text{ mm}$ , for the hollow screw fixation this diameter can even be smaller. These drilled holes allow for guiding the ligaments and their fixation mechanism through the medial cortex of the glenoid bone stock. A spherical shaped drilling mould with equal radius of curvature as the final bipolar head can be positioned in the preferred orientation and allows for accurate and easy drilling (see Figure 10.5a). Then, the ligaments are placed through the drilled openings (Figures 10.5b). If using bone anchors for ligament fixation, they can now be unfolded using special equipment (see Figure 10.3a). If using ligament fixation with the clamped balls, the hollow screw can be inserted up to the medial cortex of the glenoid bone stock (see Figure 10.4b). Using either one of these fixation techniques, requires only a lateral approach and lateral exposure of the glenoid bone stock. After preparing the ligaments, the shell can be placed over the ligaments against the glenoid cavity (Figures 10.5c). The lateral end of the ligaments are fixed by nuts, which fit inside the lateral outer shell (Figure 10.5d). The ligaments are not pre-tensioned, as this may lead to problems associated with bone remodelling and material creep. A minimal pre-adjusted torque is applied on the nuts, which allows for a compromise between both proper orientation of the

bipolar prosthesis and small translations of the humerus. Then, the bipolar prosthesis can be assembled and connected to the humeral stem (Figure 10.5e). As soon as the ligaments become loaded, they prevent the replaced humerus from further translations, which leads to force equilibrium and joint stability (Figure 10.5f).

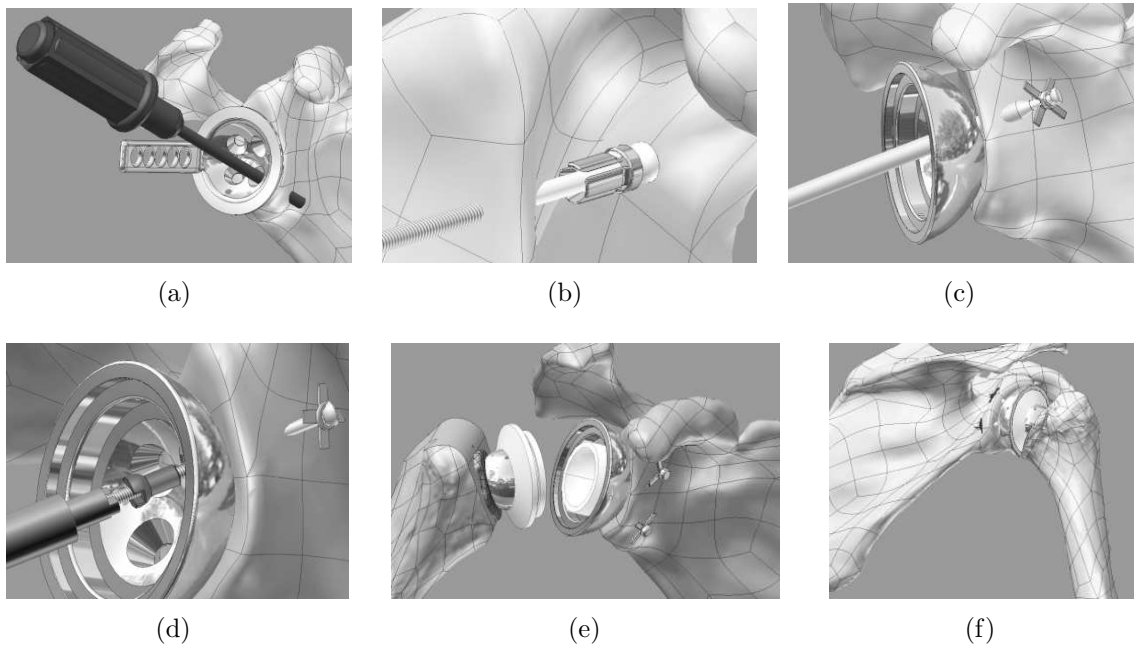


Figure 10.5: *Main steps of the surgical procedure. (a) Guided drilling, from lateral through the glenoid medial cortex. (b) Lateral insertion and unfolding of the bone anchors. (c) Positioning of the prosthetic outer shell over the ligaments. (d) Fixing the ligaments using nuts and special surgical instrumentation. (e) Assembling the bipolar prosthesis. (f) The self-stabilizing prosthesis at work as the replaced glenohumeral joint. See Figure C.8 in Appendix C for color representations*

## 10.4 The design in detail

### 10.4.1 Orientation of the ligaments

Ligament orientation influences ligament forces, stresses at the fixation and humeral head translations. Ligament orientation is limited by dimensions of the glenoid cavity and the prosthetic components. The dimensions of the glenoid cavity, such as the superior-inferior chord length ( $c_g$ ), determine the position and orientation of the drilled holes. Their virtual point of intersection with respect to the CoR influences the kinematic behaviour of the humeral head and the stresses of the ligaments (see Figure 10.6). Depending on the location of the virtual point of intersection with respect to the CoR, a superior directed subluxation force  $F_s$  will lead to:

- Upward rotation of the humeral head and an increase of (especially inferior) ligament stresses, if the virtual point of intersection is located medial to the CoR (see Figure 10.6d),
- No rotation of the humeral head and minimal ligament stresses, if the virtual point of intersection coincides with the CoR (see Figure 10.6e),
- Downward rotation of the humeral head and an increase of (especially superior) ligament stresses, if the virtual point of intersection is located lateral to the CoR (see Figure 10.6f).

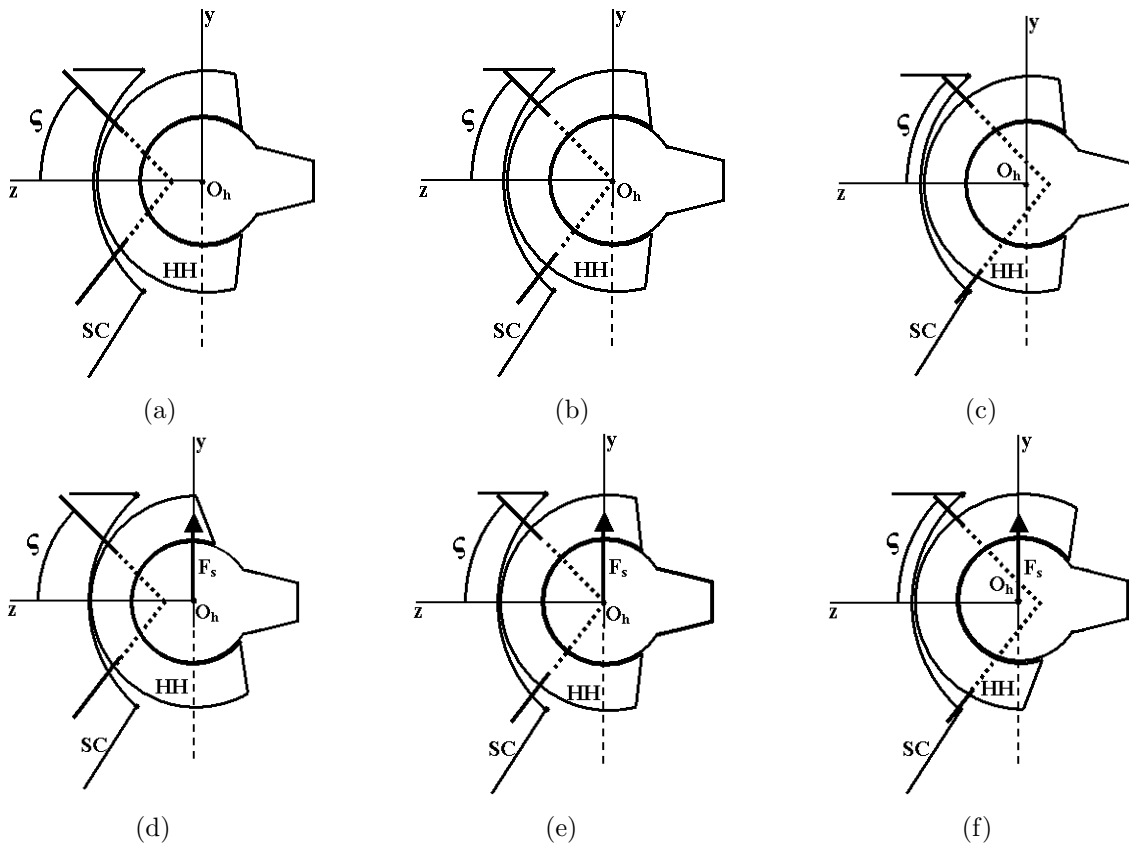


Figure 10.6: Schematic representation of the effect of location of the virtual point of intersection of the ligaments with respect to the CoR on the kinematic behaviour of the bipolar humeral head. The humerus is fixed at horizontal abduction and ligament angle  $\zeta$  is kept constant. (a), (b), (c) The virtual point of intersection is medial to the CoR, coincides with the CoR and is lateral to the CoR, respectively. (d), (e), (f) A superior directed subluxation force  $F_s$  will cause an upward rotation, no rotation and downward rotation of the bipolar prosthesis, respectively

### 10.4.2 Ligament forces

The ligaments must counteract the enforced subluxation forces, to guarantee force equilibrium. If a certain force eccentricity  $\varphi_1$  is allowed and ligament orientation  $\varsigma$  is known, the ligament force  $F_l$  and the joint contact force  $F_c$  can be calculated using static equilibrium in a two-dimensional rigid-body model (see Figure 10.7). Assuming that only the artificial ligaments opposite to the subluxation force are the counteracting forces and that two ligaments are counteracting, static force equilibrium in the  $y$ -direction requires:

$$\sum F \uparrow: 0 = F_s - F_c \cdot \sin\varphi_1 - 2 \cdot F_l \cdot \sin\varsigma \quad (10.1)$$

and in the  $z$ -direction:

$$\sum F \rightarrow: 0 = F_c \cdot \cos\varphi_1 - 2 \cdot F_l \cdot \cos\varsigma \quad (10.2)$$

Solving for the ligament forces  $F_l$  and joint contact force  $F_c$  gives:

$$F_l = \frac{F_s}{2(\cos\varsigma \cdot \tan\varphi_1 + \sin\varsigma)} \quad \text{and} \quad F_c = \frac{F_s \cdot \cos\varsigma}{(\cos\varsigma \cdot \sin\varphi_1 + \sin\varsigma \cdot \cos\varphi_1)} \quad (10.3)$$

With equation 10.3, the ligament forces  $F_l$  and joint contact force  $F_c$  can be calculated, for given ligament orientation  $\varsigma$ , the applied external subluxation force  $F_s$  and allowed force eccentricity  $\varphi_1$ . For example, assuming ligament angles  $\varsigma$  of  $15^\circ$ , a superior directed subluxation  $F_s$  of 1 times BW and a force eccentricity  $\varphi_1$  of  $20^\circ$ , gives a ligament force  $F_l$  of 0.82 times BW and a joint contact force  $F_c$  of 1.68 times BW. The result is a joint compression force  $F_z$  of  $2F_l \cos\varsigma = 1.58$  times BW and a superior directed subluxation force  $F_y$  of  $F_s - 2F_l \sin\varsigma = 0.58$  times BW, due to the downward orientation of the tensioned ligaments (see Figure 10.7).

### 10.4.3 Bone anchor and ligament stresses

To investigate the stresses in the bone anchors and underlying bone, two Finite Element (FE) analyses have been performed. The geometry of the models are based on a rectangular trabecular bone block with a layer of cortical bone on top, at which the bone anchors and ligaments are connected (see Figure 10.8). A first analysis includes a schematic bone anchor, with a simplified cross-shaped flat surface, and a ligament,

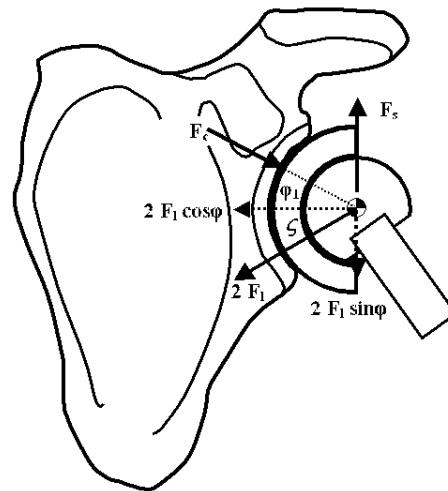


Figure 10.7: Schematic overview of the self-stabilizing artificial shoulder joint

at which a tensile force has been applied of  $240\text{ N}$  (in the double symmetric model  $60\text{ N}$ ). The model is built up with 6335 10-noded tetraeders, with an elastic modulus  $E$  of the trabecular bone, cortical bone and CoCr (bone anchor and ligament) of 0.5, 15 and  $210\text{ GPa}$  respectively, and all materials have a Poisson's ratio  $\nu$  of 0.3. The posterior and inferior sides are unconstrained, the planes of symmetry are constrained in both normal directions and the lateral side is clamped. The model is analysed by MSC/Marc (2003). As a result of the applied loading, the Von Mises stresses in the bone anchors are just below  $400\text{ MPa}$ , which is far below the yield strength of CoCr and the maximal principal stresses in the cortical and trabecular bone are in the order of  $-30$  and  $-5\text{ MPa}$ , respectively (see Figure 10.9a).

A second analysis investigated a schematic model of the self-stabilizing design, including the outer shell of the bipolar prosthesis. The outer shell is connected to the glenoid cavity by artificial ligaments, which are fixed to this outer shell by nuts and to the medial glenoid by a similar bone anchor as in the first analysis. A subluxation force  $F_y$  of  $350\text{ N}$  in superior direction has been applied at top of the outer shell (in the symmetric model  $175\text{ N}$ ). The model is built up with 28430 10-noded tetraeders, with similar material properties as in the first analysis. All translations are restricted at the medial surface and the planes of symmetry are constrained in both normal directions. As a result of the applied loading, again the Von Mises stresses just are below  $400\text{ MPa}$  and the maximal principal stresses in the cortical and trabecular bone are in the order of  $-30$  and  $-5\text{ MPa}$ , respectively (see Figure 10.9b).

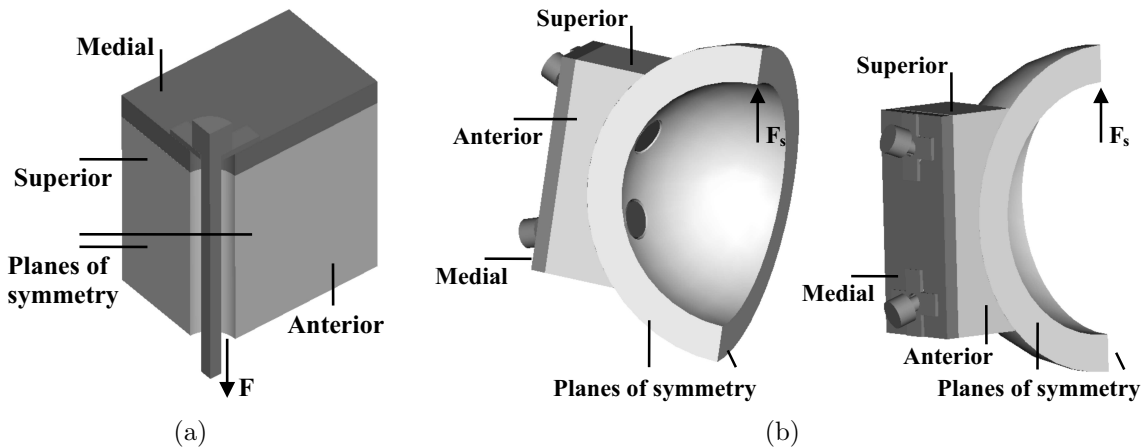


Figure 10.8: (a) Model for the FE analysis to investigate the stresses in the bone anchor, ligaments and underlying bone. (b) Model for the FE analysis including the bipolar head to investigate the stresses in the bone anchor, ligaments, underlying bone and outer shell. See Figure C.10 in Appendix C for color representations

## 10.5 Summary of the design description and reflection to the requirements

- The presented design creates glenohumeral stability, without making use of surrounding anatomical stabilizing structures. This is achieved by using a bipolar prosthesis, of which the outer shell is semi-rigidly connected to the medial cortex of the glenoid bone stock by artificial ligaments. As a subluxation force causes excessive humeral translations, the ligaments become loaded and prevent the bipolar humeral head from further translating out of the glenoid cavity (requirement 1).
- The bipolar prosthesis is dimensioned and oriented to allow for enough range of motion to perform all activities of daily living (requirement 2).
- Additionally, the positioning and dimensions of the bipolar prosthesis are chosen to not change the position of the center of rotation (CoR) of the natural glenohumeral joint (requirement 3).
- The artificial ligaments are constrained at the medial cortex of the glenoid, for which two methods are proposed. The first method is to unfold the flaps of bone anchors, which makes their diameter larger than the drilled holes, preventing the ligaments to be pulled back. The second method is to insert an artificial

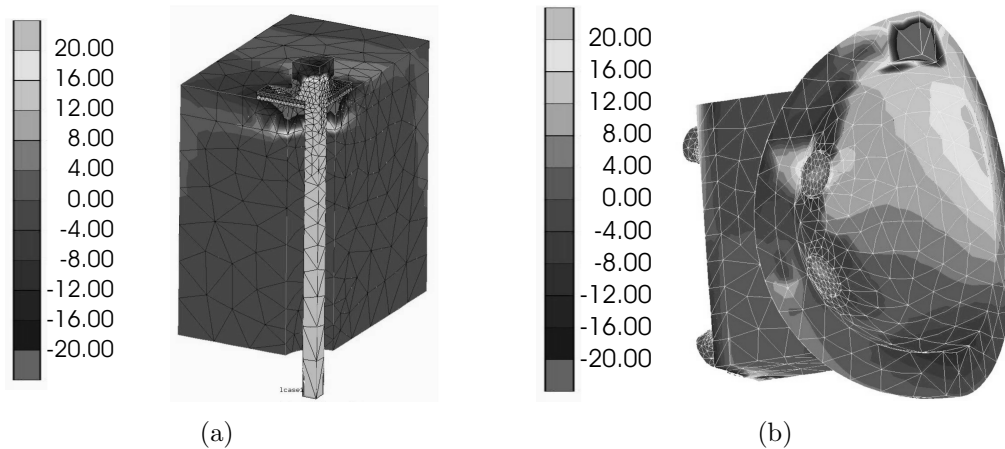


Figure 10.9: (a) Maximal principal stresses (MPa) in the bone structure, bone anchors and ligament of a simplified structure of the fixation system of the new prosthesis. The ligament is loaded by a 240 N tensile force. (b) Maximal principal stresses (MPa) in the bone structure, fixation system and outer shell of the new prosthesis, which is loaded by a 350 N subluxation in superior direction See Figure C.10 in Appendix C for color representations

ligament, with a clamped ball at the medial end, whereafter a hollow screw prevents the ligament with the clamped ball to be pulled back. No bending stresses will occur when using these methods of fixation. In addition, the semi-rigidly fixation with the artificial ligaments allow for a certain flexibility of the CoR during articulation, to minimize ligament stresses (requirement 4).

- By using a bipolar prosthesis and components made out of biocompatible materials, the process of clinical acceptance with respect to certification is made easier (requirement 5).
- Conventional surgical techniques should be sufficient for implantation of the prosthetic components. Next to joint preparation, only drilling using a drilling guide is needed for ligament insertion. Easy surgical instrumentation is needed for bone anchor unfolding or hollow screw insertion. The presented method of fixation of the artificial ligaments allows for an easy lateral approach of the glenoid cavity (requirement 6).
- As a commercially available bipolar prosthesis is used, prosthesis dimensions are guaranteed. Although bone anchor unfolding requires a height of 5 to 6 mm, the unfolded bone anchors are very superficial with a height of less than 4 mm. However, the method of fixation with the hollow screw does not require any space medial to the glenoid cortex (requirement 7).

## 10.6 Challenges

This study aimed at the development of a new prosthesis, which must function without the anatomical stabilizing structures and prosthesis survival rates must be better than presently used prosthesis systems for the target patient group. A conceptually new design has been developed, which seems promising with respect to the described requirements. However, much research remains to be done before the design can be regarded as an innovation.

First, some technical aspects need to be investigated and improved in more detail. Especially the method of ligament fixation using the bone anchors must be improved, as the fatigue properties are still unsatisfactory. Both the applied materials and design details must be improved and validated by FE and experimental techniques.

After it is demonstrated that the technical validation meets all requirements, the prototype should be used to demonstrate the feasibility of implantation of the design into a cadaveric shoulder by an experienced surgeon. If this is successful, the effectiveness of the design must be looked at, in other words, does the design really improve joint stability for the target patient group? A good method may be to subsequently investigate glenohumeral joint stability of a cadaveric, intact anatomical glenohumeral joint, then of the same joint without the RC muscles and ligaments and, finally, after inserting the new self-stabilizing design. If the results are still promising, animal test must demonstrate the functionality in an in-vivo and dynamic environment.

## 10.7 Spin-off applications

The presented conceptually new design has been developed specifically for the glenohumeral joint, but interesting spin-off applications are foreseen. An example where the presented fixation system can be an outcome, is in the case of fracture surgery. A proximal humerus fracture commonly consists of a fractured head and fractured greater tuberosities (see Figure 10.10a). The presently used treatment solution is to insert a hemi-arthroplasty and to fix the fractured tuberosities by suturing (see Figure 10.10b). Unfortunately, good primary fixation of the two tuberosities is difficult to achieve, leading to complications with good bone healing and long-term fixation of the bone pieces. An improved treatment solution must be found.

The described fixation method for the self-stabilizing prosthesis can be used for primary fixation of the bone pieces. After inserting the humeral stem, holes through the two fractured tuberosities can be drilled and the artificial ligaments can be inserted. The two described methods of ligament fixation can be used, which only require a single sided surgical approach. Additionally, by using accurate alignment tools, holes in the fins of presently used humeral stems can be used to better fix the

fractured bone pieces (see Figure 10.10c). Not only for the humerus fractures this may be an improvement, but also in the case of femoral fractures in the knee joint or ligament fixation at locations which are difficult to expose. Additionally, the two presented methods of ligament fixation can be applied when using minimal invasive surgical techniques.

These spin-off applications have not yet been investigated. In the case of primary fixation of bone pieces after humerus fractures, the design and surgical process as well as the static and fatigue strength must be validated. The possibility to make use of the fin of the humeral stem should be investigated, as this may result in improved fixation strength.

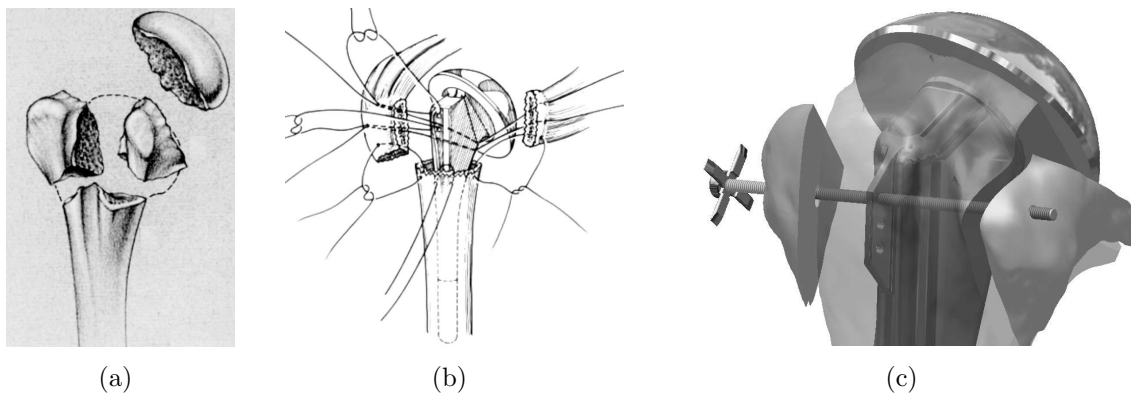


Figure 10.10: *The proximal humerus fracture and its treatment. (a) A proximal humerus fracture commonly consists of a fractured head, the two fractured tuberosities and the remaining humerus. (b) At present, the fractured bone pieces are sutured to create a primary fixation, which is not always successful and good bone ingrowth can not always be achieved. (c) The presented fixation system can be used for improved primary fixation after surgery*

## 10.8 Conclusions

The aim of the study was to develop a new glenohumeral prosthesis design, which must provide joint stability and proper joint functionality without the presence of anatomical stabilizing structures. It must show survival rates better than presently used systems for patients with glenohumeral joints, suffering from rheumatoid-arthritis or RC arthropathy.

A design is presented, existing of a bipolar humeral prosthesis, of which the outer shell is semi-rigidly positioned against the glenoid cavity. This is achieved by ligaments, which are fixed at the medial glenoid bone, by bone anchors or hollow screws. The fixation of the ligaments, for which only a lateral approach is sufficient, results

in pure compression and tensile forces. This improves long-term fixation of the prosthetic components. As the bipolar humeral head tends to translate out of the glenoid cavity, the ligaments undergo tensile forces, thereby preventing the humeral head from further translating out of the glenoid cavity. Implanting the presented design in rheumatoid glenohumeral joints or shoulders with RC arthropathy seems promising in terms of reconstruction of shoulder functionality and long-term component fixation.

Spin-off applications of the presented fixation technique are foreseen, especially around locations which are difficult to approach. Treatment of humeral fractures and ligament fixation are just two examples.



# Chapter 11

## Conclusions



*Paula Radcliff finishes after running  
the New York marathon 2004 in 2:23:09*



## 11.1 Accomplishments

The goal of the present work was to improve the design of the glenohumeral prosthesis, by investigating improvements of the presently used prosthesis designs and to explore conceptually new designs, especially for those patients, for whom a long-term reliable artificial joint, providing enough joint functionality, is not available at present.

After a thorough literature search and personal communications with several orthopedic surgeons, the main shortcomings of presently used glenohumeral prosthetic replacements became clear, as well as the unavailability of a reliable replacement for the rheumatoid shoulder and in the case of Rotator Cuff arthropathy. Long lasting component fixation seemed one of the main complications and should receive much attention in the case of conventional glenoid components. For rheumatoid shoulders and shoulders suffering from Rotator Cuff arthropathy, the very unfavorable combination of weakened bone materials and weakened or even severely damaged surrounding soft-tissues seems to be the reason for the bad performance of the presently used glenohumeral replacement systems.

The relationship between different geometrical design parameters, such as constraint angle and joint conformity, was investigated using an analytical approach in a rigid-body environment of the concave glenoid cavity and convex humeral head. A potential field was introduced and the translational stiffness was used to investigate the effect of the radius of curvature of both the glenoid and humeral head component on humeral head translations and joint stability. The interactions between the design parameters became clear and the translational stiffness seemed to be a good predictor for the joint stability, being positive and negative in the case of stable and unstable articulation, respectively. From this study, it was also concluded that parameters such as joint conformity and glenoid inclination affect glenoid component loading and thereby also glenoid component fixation. The obtained relations between the humeral head and glenoid cavity as well as the stability criteria can be used for future modelling and optimization of shoulder prosthesis components.

To investigate the effect of geometrical parameters in more detail, a new experimental method was developed, in which glenoid component loading and humeral head translations were the result of known applied forces. This method seemed an improvement over presently used methods, in which humeral head translations form the basis for glenoid component loading. In a ball-in-socket joint, such as the glenohumeral joint, this is incorrect, as during normal articulation no joint translations will occur.

Using this novel experimental method, the effect of joint conformity and glenoid inclination on glenoid component tilting was investigated. Glenoid component tilting is defined as the rotation of the glenoid component due to superior and inferior rim-displacements of the glenoid component under off-center forces and is directly related to fatigue stresses at the fixation interface. Glenohumeral conformity deter-

mines humeral head translations and also the point of contact at the glenoid articular surface, when adjusting the glenoid component radius of curvature. It was found that increased articular conformity is beneficial with respect to glenoid component tilting in the case of a tendency to superior glenohumeral subluxation. This was also reflected in the residual strength of the cemented components, as was found by shear out testing. If accurate surgery is possible, an almost conform articulation is preferable with respect to glenoid component tilting, humeral head translations and glenoid component wear.

Glenoid inclination, influenced by both patient and surgical factors, relates to how much the glenoid component articular surface is facing upward (positive inclination) or downward (negative inclination). It directly determines force eccentricity and thereby also glenoid component tilting. The effect of glenoid component inclination on glenoid component tilting and humeral head subluxation has been validated and it is found that, if possible, inserting a more downward facing glenoid is beneficial for joint stability in superior direction. Additionally, a novel design is proposed, in the case it is not possible to restore the glenoid inclination angle by surgical methods. Inserting a metal backed glenoid component with a linear increasing backing thickness from inferior to superior restores glenoid inclination.

During the investigation of the effect of joint conformity and glenoid inclination by experimental methods, it was found that no physical bonding was present between the Ultra-High-Molecular-Weight-Polyethylene (UHMWPE) glenoid component and the Polymethyl-Methacrylate (PMMA) bone cement. As a result, glenoid components are fixed by mechanical interlocking, rather than by adhesion. Keels, with holes and grooves, or pegs are needed to achieve this, which require much bone removal.

Two conclusions are drawn from these findings. First, adhered fixation of UHMWPE glenoid components could be investigated to decrease the amount of unwanted bone removal. Second, the method of connecting the UHMWPE glenoid component with the PMMA cement layer in Finite Element models should be reconsidered, as this is commonly done by a full-bonding of this interface.

To investigate the feasibility of adhered fixation of the UHMWPE glenoid components in combination with the PMMA bone cement, UHMWPE surface modification techniques were used. These surface modification techniques introduce oxide groups at the UHMWPE surface, changing it into a polar material, with better adhesion performance. It was found that after UV/Ozone, Corona or RF-Discharge treatments, the wettability, surface energy and static interface shear strength of UHMWPE single lap-joints increased significantly. A combined treatment of surface roughening and RF-Discharge showed the best results, even demonstrating necking of the UHMWPE single lap-joints. Subsequently, Methyl-Methacrylate (MMA) is used as an adhesive and better results were obtained by performing the similar study. It is demonstrated that the adhesion properties of UHMWPE can be improved considerably.

The second conclusion of the experiments regards the interface between the UHMWPE glenoid component and the PMMA bone cement layer in FE modelling. Full bonding of this interface might not always seem correct, as adhesion between UHMWPE and PMMA is not always found. The difference when applying a full bonding at this interface or using contact elements in combination with a coefficient of friction (CoF) on the results of FE modelling has been investigated.

First, the static and dynamic CoF between UHMWPE and PMMA have been measured, in a dry and wet environment. A significant difference between the dry and wet CoF was found and only a small difference between the static and dynamic CoF. Additionally, it was found that the PMMA specimen surfaces were filled with UHMWPE material after testing the dynamic CoF. These PMMA specimens were also used to measure the static CoF in a dry and wet environment and a significant difference was found with respect to the non-filled PMMA specimens.

Then, using the FE method, subsequently the six measured coefficients of friction, additional coefficients of friction of 0.01, 0.1 and 1 as well as a full bonding were applied at the interface between the UHMWPE component and the PMMA cement layer to investigate their effect on the results of FE modelling. The FE model in this study is derived from the structural geometry of the specimens as used in the experiments, with similar loading conditions and constraints. It was found that both maximal principal stresses and medial displacements of the bone substitute, cement layer and glenoid component dramatically increased when a CoF was applied, with respect to a full bonding at the interface. Although the results of the FE analyses are only very little influenced by the value of the CoF, using contact elements with a CoF at the UHMWPE-PMMA interface has a clear effect on the results in FE-modelling. Future validation of new cemented prosthesis components by the FE technique should be done both by a full-bonding as well as by using contact elements with a CoF at the UHMWPE-PMMA interface.

Next to investigating the anatomical prostheses, a second research strategy focused on the development of a conceptually new prosthesis design for rheumatoid patients and patients suffering from RC arthropathy. The design must provide enough stability and RoM for performing the activities of daily living and component fixation must outperform presently used systems for the target group.

The result is a design, which is based on the bipolar humeral head prosthesis. This bipolar prosthesis is semi-rigidly fixed to the lateral scapula by metal ligaments and allows for small humeral head translations. However, if humeral head translations increase, the ligaments become tensioned and restrict the humeral head from further translating out of the glenoid cavity. During the surgical procedure, the metal ligaments are guided through the glenoid bone structure and are fixed to the medial cortex of the glenoid. Two methods of ligament fixation are developed. The first method is to use bone anchors at the medial end of the ligaments, with a small initial diameter. After inserting them through the medial cortex, the bone anchors can be unfolded and their increased diameter prevents the ligament to be pulled

back through the glenoid bone stock. The second method is to use ligaments with a small clamped ball at their medial end. After guiding them through the drilled holes, a hollow screw placed over this ligament and is tightened through the glenoid trabecular and cortical bone and again prevents the ligaments to be pulled back. The implantation of the prosthesis including fixation of the ligaments to the medial cortex only requires a lateral approach. Using special surgical equipment, the bone anchors are unfolded and form a barb-structure. The final design allows for good and stable joint functionality, which is not at the expense of component fixation, as this is achieved outside the diseased joint and only undergoes pure tensile and compression forces.

The novel method of fixation of the ligaments leads to many spin-off applications. It can be used for primary fixation of the fractured humeral tuberosities during a shoulder replacement in the case of humerus fractures. Difficulties with good bone ingrowth of the fractured bone pieces is a significant problem after this treatment and good solutions are not available. However, much bone material is available for the proposed ligament fixation method with the additional benefit that it only requires a single sided approach.

A similar application is foreseen in the case of femoral fractures in the knee joint. By using the proposed fixation method, the fractured femoral condyles can be fixed by minimally invasive techniques, requiring only very little joint exposure. The proposed new prosthesis concept may also be used in the case of other joints, for which conventional methods are not successful.

## 11.2 Future research

To extend the research described in this thesis to a level that the design considerations can be used in clinical practice, more work has to be performed. Recommendations for this future research are described below.

Chapter 4 discusses the effect of component geometry on joint stability, limited by a two-dimensional rigid-body model. The glenohumeral joint, all biological and biomaterials as well as the loading conditions imply a three-dimensional character with elastic properties. To improve the presented analysis, it should be expanded to a three-dimensional model, including elasticity and dynamic behaviour. No direct attempts have been made to account for this, but a future coalescence with the Delft Shoulder Model [108] and the improved Finite Element Model of DIPEX 4 (see Chapter 1) may be the pointing basis for future fundamental research.

The experimental work of Chapters 5, 6 and 7 have demonstrated some future design adjustments to improve long-term glenoid component fixation and glenohumeral joint stability. An example of the results is the beneficial effect of increasing articular conformity and decreasing glenoid component inclination on joint translations

and glenoid component tilting. However, this is true only if the surgeon is able to accurately insert the glenoid component. To achieve this, improved surgical instrumentation is necessary in combination with three-dimensional visualized, computer assisted surgery, which are under investigation by DIPEX 1 and 2 (see Chapter 1). Research to the feasibility to implement these methods in the operation theater must be continued.

Additionally, the experiments have been done using synthetic bone substitutes, in-house manufactured glenoid components, which are then joined together by bone cement in an ex-vivo environment. This doesn't lead to the most realistic conditions. Although some natural bone properties are very well mirrored in the bone substitutes, most of their mechanical behaviour remains uncertain. Using cadaver material for future testing of prosthesis components, provides both more realistic material properties and geometry. Although only small adjustments are necessary to the experimental set-up to perform the tests in a fluid environment, at present, cadaver material is prohibited in non-biological laboratories. However, co-operation with a biological laboratory may lead to improved possibilities for experimental testing. In a biologic laboratory, with suitable equipment, the dislocation behaviour of the natural, pathologic and replaced glenohumeral joint can be examined in great detail. This leads to better mimicking of the human, biological reality.

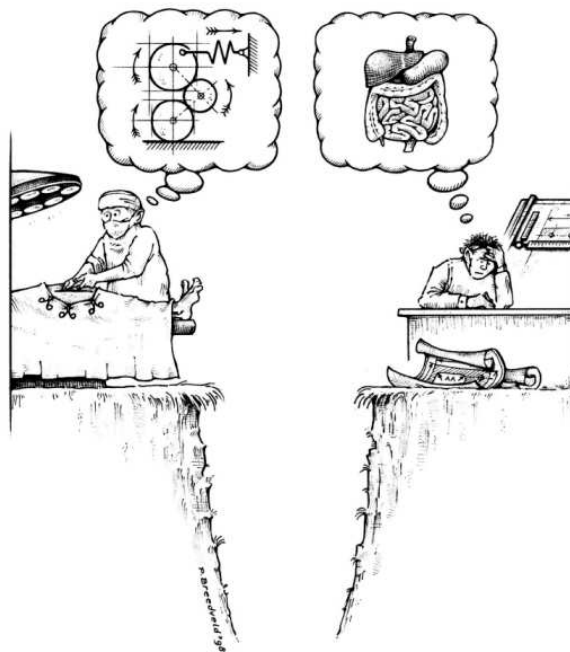
A glenohumeral replacement has been investigated, which must function without the rotator cuff, providing the patient enough strength and range of motion to perform activities of daily living. Although a pre-design has been worked out and range of motion and strength validation seems promising, many aspects are uncertain at the time of writing. Feasibility of implantation, effectiveness of the design concept and fixation strength in the natural joint have to be investigated in future.

Promising research on the presented design is not limited to the presented application. Spin-off applications exist, for example as primary fixation of fractured bone pieces during the first post-operative weeks using the proposed fixation technique as described in Chapter 10. Computational and experimental methods may be applied to validate these applications.



# Appendix A

## Medical terminology



*The communicative difficulties of multidisciplinary research, portrayed by Paul Breedveld, 1998*



## A.1 Terminology

Directions in the body and motion of limbs are described from the neutral position (see Figure A.1), which indicates the global coordinate system of the human body. The frontal plane divides the body in a frontal (anterior or ventral) and backside (posterior or dorsal) part. The sagittal plane divides the body in a left and right part and the ventral plane divides the body in an upper part (superior or cranial) and lower part (inferior or caudal). The mediosagittal plane divides the body in an equal left and right part.

Medial and lateral indicate a location or direction towards the mediosagittal plane and away from this plane, respectively. Anterior or ventral and posterior or dorsal indicate a location or direction towards the front and backside of the body, respectively. Superior or cranial and inferior or caudal indicate a location or direction towards the upper and lower part of the body. Proximal and distal indicate towards and away from the trunk, respectively.

Human motions are the result of rotations of one or multiple joints. In general, three rotations are possible. Abduction, which is the opposite of adduction, is motion away from the mediosagittal plane and increases the angle between the limb and the sagittal plane. Extension, the opposite of flexion, is motion back to the neutral position or tries to restore this position. The third rotation is axial-rotation and is the rotation about the long axis of a bone element. Internal rotation moves the anterior surface of the segment towards the midline of the body and is the opposite of external rotation [49].

## A.2 Ligaments, muscles and the glenoid labrum

The ligaments of the glenohumeral joint are given in Table A.1. The ligamentous structures are integrated in the joint capsule of the glenohumeral joint. The 17 muscles surrounding the shoulder are given in Table A.2, along with their function, origin and insertion. Four muscles form the so-called 'Rotator-Cuff', which are the subscapularis, supraspinatus, infraspinatus and teres minor muscles. The function of the Rotator Cuff (RC) muscles is to provide a torsional moment to allow for external and internal rotation as well as for providing joint compression for active, dynamic glenohumeral stability [236]. The glenohumeral capsule is positioned proximal from the RC, disappearing in the fascia of the M. Infraspinatus, Subscapularis, Coracobrachialis and the Biceps. The capsule is strengthened by the tendons of RC muscles. On the posterior side these are the Infraspinatus and Teres Minor, on the superior side this is the Supraspinatus and anterior it is the Subscapularis [210]. As like the hip joint, the shoulder joint has a labrum (see Figure 2.2), similar to the meniscus of the knee, but it has a different mechanical structure [111]. It deepens

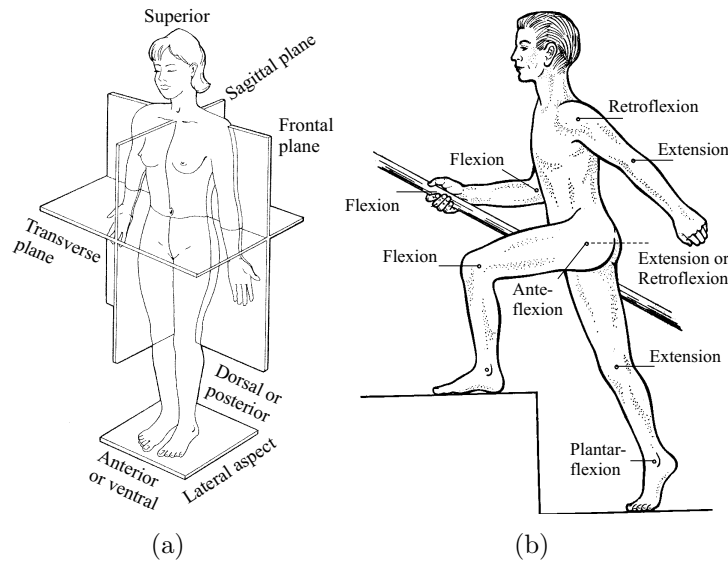


Figure A.1: *Anatomical base and definitions of human movements. (a) Neutral position of the human body and definition of the medical coordinate system and directions [106]. (b) Some movements of limbs of the human body*

Table A.1: *The ligaments of the shoulder girdle [209, 299]*

Ligament	Connection
Coracoacromial	Coracoid process and acromion
Superior transverse scapular	Superior rim of scapula and coracoid process
Costo-clavicular	First rib and clavicle
Conoideum	Clavicle and coracoid process
Trapezoid	Clavicle and coracoid process
Coraco-humeral	Coracoid process and humerus

the glenoid cavity, although it is doubtful whether this flexible rim provides additional stability. However, it is recognized that it provides neural proprioception, a sensory modality system that gives information about joint position and direction of glenohumeral movements. Special nerve endings, the proprioceptive mechanoreceptors, transduce mechanical signals into electrical signals to transmit information about the joint. A deficit of this system, for example after a joint replacement, can result in decreased joint stability [342].

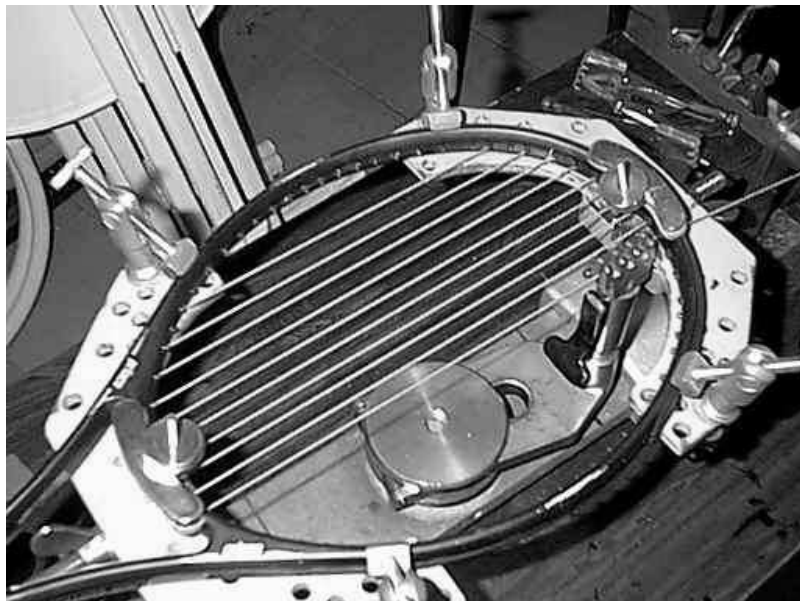
Table A.2: *The muscles of the shoulder girdle. The muscles are divided into three groups, according to their location of attachment to the bones. \* 'Rotator Cuff' muscles [106, 209]*

Group	Origins and insertions	Function
<b>Thoraco - Scapular</b>		
Serratus anterior	Anterior ribs - medial border Scapula	Abducts and Adducts Scapula
Trapezius	Thorax - clavícula (Acromion)	Abducts and rotates Scapula, elevates and depresses Scapula
Rhomboideus major	Thorax - medial border Scapula	Adducts and rotates Scapula
Rhomboideus minor	Thorax - medial border Scapula	Adducts Scapula
Pectoralis minor	Anterior ribs - coracoid process	Depresses Scapula
Subclavicularis	Thorax - Clavícula	Depresses clavícula - protraction
Levator scapulae	Thorax - angulus superior Scapula	Elevates Scapula
<b>Scapula - Humeral</b>		
Deltoid	Scapula and clavícula - Humerus	Abducts arm, flexes, extends and rotates
Supraspinatus*	Scapula - tuberculum majus humeri	Adducts Humerus
Infraspinatus*	Scapula - tuberculum majus humeri	Externally Rotates Humerus
Subscapularis*	Scapula - tuberculum minus humeri	Internally rotates Humerus
Teres minor*	Scapula - tuberculum minus humeri	Adducts and externally rotates Humerus
Teres major	Scapula - tuberculum minus humeri	Adducts, extends and externally rotates Humerus
Coracobrachialis	Coracoid process - Humerus	Flexes and adducts
Biceps brachii (long head)	Glenoid - Ulna	Flexes and supinates forearm
Triceps brachii (long head)	Glenoid - Humerus/Ulna	Extends forearm
<b>Thorax - Humeral</b>		
Pectoralis major	Thorax - tuberculum majus humeri	Flexes, extends, adducts and medially rotates Humerus
Latissimus dorsi	Thorax - tuberculum majus humeri	Adducts, extends and medially rotates Humerus



# Appendix B

## Biomaterials



*A tennis racket being strung using cat intestines*



## B.1 Introduction

Biological materials of the human body are different from other materials, due to their living character and thereby the possibility to react to changes in their environment. Biomaterials, which are materials to replace or assist tissues of the host body, are different in that they must fulfill biocompatibility requirements of different levels, depending on their future function and location inside the body. The load carrying biological materials in and around articular joints are cortical, trabecular and subchondral bone and the articular cartilage (see Figure B.1). Among others, conventional used biocompatible materials for joint replacements are Ultra-High-Molecular-Weight-Poly-Ethylene (UHMWPE), Cobalt-Chromium-Molybdene (CoCrMo) and Polymethyl-Methacrylate (PMMA). These and some other less used materials will be discussed in the next two sections and an overview of the material properties can be found in Table B.1.

## B.2 Bone and cartilage

Bone is a living, continually remodelling material, with specific micro and macro structural properties. It consists for 90% out of type 1 collagen fibrils, a visco-elastic material, which provides a certain ductility and fracture toughness. The other 10% consists out of non-collagenous components and mineral substances, such as Hydroxyapatite (HA) [37], a relatively stiff, elastic material, providing strength and stiffness to the bone. In other words, bone is a composite, that is a structure made of at least two mechanically differing materials, with superior properties as compared to the structure made out of the separate materials alone [285]. The stiffness of HA and Collagen is 70-114 *GPa* and 1 *GPa*, respectively [36]. As a result, bone can withstand high loads, without being too brittle.

Macroscopically, bone elements have of a more dense, stiff and strong outer skin and a lightweight kernel, formed by cortical bone and trabecular bone, respectively (see Figure B.1). The elastic modulus of cortical bone is 12-23 *GPa* [351]. The elastic modulus of trabecular bone depends both on location, e.g. proximal or distal, and direction, e.g. parallel or perpendicular to the joint loading. By using compression tests of cubic specimens, elastic moduli for the glenoid cavity of 410.8 (SD=114.2), 157.1 (SD=71.4) and 78.3 (SD=47.8) *MPa* are found perpendicular to the joint surface, in anterior-posterior (AP) direction and in superior-inferior (SI) direction, respectively [84]. Yield strength of trabecular bone ranges between 130 and 180 *MPa*, depending on direction and location, and for cortical bone it is approximately 180 *MPa* [351]. An analogy can be drawn between bone elements and the so called 'sandwich structures'. These are efficient structures where bending is dominant and where a high ratio of strength and stiffness over weight is required.

The skin mainly takes care of stresses due to bending and axial forces, whereas the kernel takes care of the shear forces and support of the skins. The sandwich structure is closed at the articular surfaces by subchondral bone and cartilage and they play an important role in lubrication, damping and load distribution [137, 215].

Both cartilage and subchondral bone layers have to fulfill two mechanical contradictory functions. On the one hand, these layers must have enough strength to handle high joint loads and on the other hand flexibility to provide joint conformity, which often does not go together in a monolithic material and as a result also these materials are built up as a composite.

Because of the complex composite character, articular cartilage exhibits anisotropic and nonlinear behaviour in compression, tension and shear. Moreover, the mechanical properties of cartilage depend on the depth from the articular surface. For instance, the deformation in axial direction decreases with depth. The highly hydrated (up to 80% of water content) composite structure, can be modelled as a poro-viscoelastic material with a relatively low compressive elastic modulus (100 - 200 MPa) [212]. The elastic modulus of cartilage increases with depth, especially in case of compressed cartilage [51]. Despite the low stiffness, articular cartilage is able to transmit high loads (up to 8 times body weight) due to the exudation of the fluid and the movement of fluid through the porous structure of cartilage. Together with synovial fluid, cartilage in articular joints provides a coefficient of friction between the articular surfaces ranging between 0.005 and 0.01 [212].

### **Bone Lives!!**

Bone is a living material, continually breaking down and building up bone cells, thereby renewing its structure. As a result of changed loading conditions, such as after a joint replacement, bone is adjusting its structure to a new equilibrium. The mechanism behind this is 'bone remodelling'.

### **Bone remodelling**

Bone remodelling is the phenomenon that bone is continually renewing and that it has the capability to adapt its morphology to amplitude and direction of loading patterns. This is according to Wolffs' Law [354]:

*'The form of bone being given, the bone elements place or displace themselves in the direction of the functional stress and increase or decrease their mass to reflect the amount of functional stress.'*

An example of bone remodelling is the increased bone density and morphological alignment in especially the proximal femur of runners and in the bone elements in the dominant upper extremities of tennis players. After a hip replacement, bone remodelling is the cause of stress shielding, a common failure mechanism for loosening of

stemmed components (see Section 3.5.3). In the case of humeral replacements, bone remodelling also can occur, as demonstrated in a study by Nagels et al. (2003) [221] (see Figure B.2).

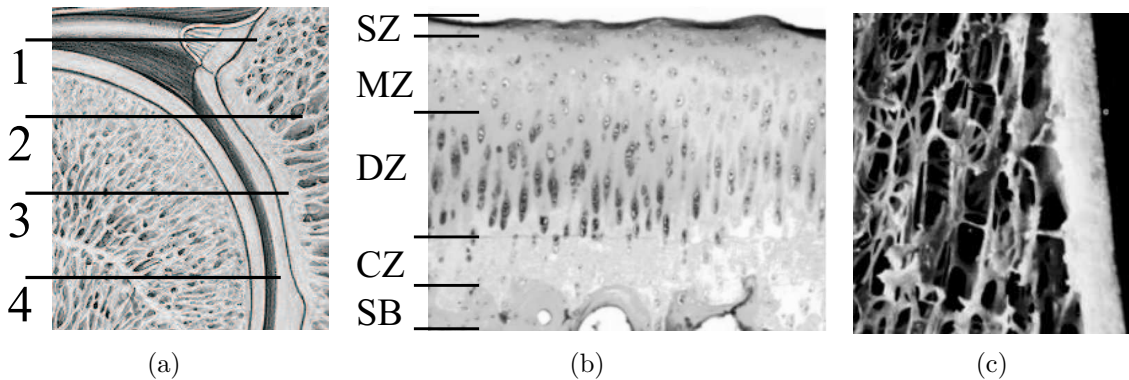


Figure B.1: *Biomaterials in articular joints.* (a) Part of a section of the glenohumeral joint. 1. Cortical bone 2. Trabecular bone 3. Subchondral bone 4. Cartilage. (b) Four layers (zones) of the articular cartilage: superficial (SZ), middle (MZ), deep (DZ) and calcified CZ) and the subchondral bone layer (SB). (c) Section of a human femur, with similarities to the sandwich structure. The kernel and facings exist out of the trabecular and cortical bone, respectively. Adapted from Spalteholz and Spanner [295]

### B.3 Materials for joint replacements

A definition of biocompatibility is given by Hill [112]:

*'Biocompatibility is the ability of a man made material to exist in an in-vivo environment for an acceptable period of time with no detrimental effect on the host.'*

Wintermantel and Ha (1996) add to this definition that the material is allowed to dissociate substances of the material in non-toxic concentrations [351]. It seems that biocompatibility determines more or less only the surface behaviour of the material and not the features of the bulk material. The result of the use of biocompatible materials for implants is the encase of the material to the interstitial tissue, with as little influence on the metabolism as possible. Although there are levels of biocompatibility [351], in case of endo-prostheses the highest level of biocompatibility is required [112].

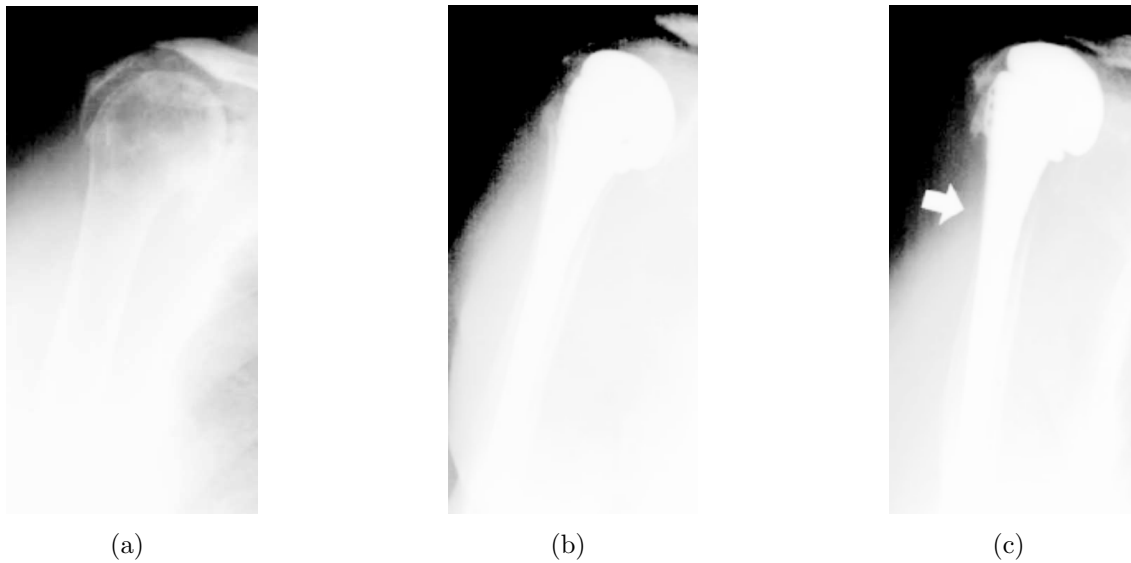


Figure B.2: *An example of stress shielding. (a) Pre-operative image. (b) Image obtained directly after surgery. (c) Image of the same patient after 7 years of follow-up. Arrow indicates region of cortical bone resorption. Adapted from [221]*

### CoCrMo

A very common used material for especially the convex components of joint replacements is Cobalt Chrome Molybdene (CoCrMo), casted as well as forged. Casted CoCrMo is a hard material, due to a high percentage of Carbon, resulting in little abrasion under sliding circumstances. Forged CoCrMo has good fatigue properties due to a small grain sizes. Despite the low vulnerability to corrosion of CoCrMo alloys, corrosion products have been found in blood and the tissue surrounding the prosthesis. CoCrMo particles with dimensions  $< 10 \mu m$  can be more toxic than the common used  $TiAl_6V_4$  alloy [351].

### Titanium

The titanium alloy  $TiAl_4V_6$  is used as prosthesis material, because of its high strength to weight ratio and good biocompatibility. This biocompatible capacity is due to a clean and stable oxide skin on the material, which also means that corrosion is not a big problem in case of Titanium alloys [351, 112]. Titanium alloys are highly receptive for bone ingrowth and can be used in combination with a smooth, textured and porous surface [62]. Titanium alloys generate more wear debris compared to Cobalt Chrome alloys, which might result in higher loosening rates of the counteracting softer UHMWPE components. Vanadium is used in small amounts, about 0.05%, for increasing toughness, fatigue properties and shock resistance. A

disadvantage of Vanadium is its toxicity to human cells, which is ten times worse as compared to CoCrMo [351]. As a result, the Vanadium free alloy TiAl6Nb7 has been developed, which is commercially available since 1990. Aluminum is added for its good fatigue properties and corrosion resistance, due to an oxide skin [351, 112]. The density of Titanium is about 55% of that of steel, but with the same tensile strength compared to casted CoCrMo, which reflects the main mechanical advantage of Titanium (see table B.1). Additionally, the Young's modulus is 50% as compared to CoCr-alloys, which decreases the effect of stress shielding and as a result less bone resorption occurs.

### **Ultra-High-Molecular-Weight-Poly-Ethylene (UHMWPE)**

Since the introduction of joint replacements, the common standard consists of a hard material (such as CoCr- or Ti-alloys) against a soft material (such as Ultra-High-Molecular-Weight-Poly-Ethylene (UHMWPE)). Many materials have been used as the soft articular surface, such as Polytetrafluoroethylene, Polyacetal, High Density Polyethylene (HDPE), polyesters and (UHMWPE). Polytetrafluoroethylene (Teflon, DuPont), has been used for its good chemical inertness and low coefficient of friction, but unfortunately it showed bad clinical results. The main problems of this material are the low resistance to creep and bad abrasive wear characteristics. Polyacetal has higher yield strength and crystallinity as compared to HDPE and is easier to manufacture (as parts made from Polyacetal can be injection molded). Short-term results were good, but results then dropped significantly as compared to the Charnley prosthesis (CoCr against HDPE) and after the mid 80' its use has been abandoned [173]. Charnley used HDPE in hip joint replacement, which became the relative standard for joint replacements. However, in the beginning of the 60's, Craven started testing with UHMWPE. This biocompatible material showed better results with respect to long-term survival, due to its good mechanical and chemical properties [26, 67]. Although UHMWPE has been used successfully for over 30 years [64], retrieved components showed fatigue cracks, excessive wear and component damage [67] and since the introduction there is still ongoing research to improve the material. Many material factors influence the results of the joint replacement with respect to component survival (including wear, fixation and component failure). These factors are the bulk material (structural) properties and the surface properties (smoothness, surface tension etc.). The bulk material properties are mainly influenced by the polymerization process (to control the molecular weight), cross-linking (see Figure B.3), reinforcing with PE fibers (to create a homocomposite) or Carbon fibres.

UHMWPE is built up from an even number of carbon atoms with a pair of hydrogen atoms, while the ends of the molecules are terminated by methylgroups (see Figure B.3). The monomers polymerise under high compression (103 - 155 MPa) and temperature (180 - 200° C, which is above the melting point) or at

medium temperature and pressure if the proper catalyst is selected. UHMWPE is a two-phase visco-plastic solid, with crystalline domains embedded in an amorphous matrix. Calcium stearate is added to remove residuals (such as catalysts), it acts as a lubricant and as a release agent. It may decrease ultimate tensile strength, elongation to break, fracture toughness and it affects the oxidation resistance after  $\gamma$ -radiation [158, 64]. The obtained product can be the final product (as the resin is polymerised by injection moulding in the final shape), small particles (140  $\mu m$  (GUR, Hoechst) - 300  $\mu m$  (1900, Montell)) or a semi-product, such as moulded plates and ram-extruded bar rods [158]. UHMWPE has a higher molecular weight as compared to HDPE, (and thus a higher viscosity and lower crystallinity), a higher melting point, lower density, lower elongation at break, a somewhat lower hardness, a higher impact strength and better resistance to wear [26]. Regarding van der Vegt (1982), UHMWPE is also tougher than HDPE [326].

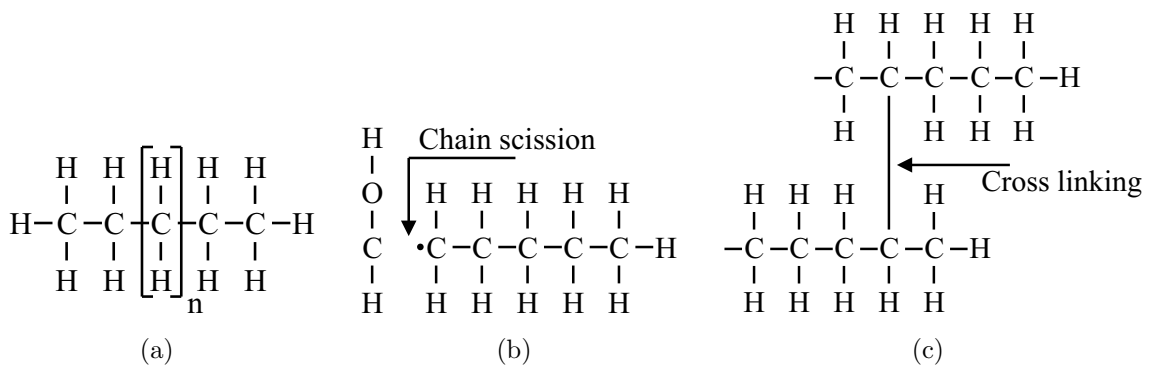


Figure B.3: *The chemical structure of UHMWPE (a) and its possibility for chain scission (b) to allow for crosslinking (c)*

### Polymethyl-Methacrylate (PMMA)

Polymethyl-Methacrylate (PMMA), used as bone cement, is an amorphous, hard polymer. Bone cement is made by a polymerization reaction of the small solid PMMA grains and the fluid monomer and a stabilizer is used to control the reaction. This polymerization reaction must be started using a polymerization catalyst, which can influence the final properties of PMMA. The fluid monomer is highly toxic to human tissue and it may not be brought into contact with bone before four to five minutes after adding the polymerization catalyst. The total time needed for complete polymerization is about ten to twelve minutes.

## Ceramics

Ceramics can offer some advantages in combination with the above mentioned materials, as it has superb biocompatibility due to its inertness, and it shows minimal wear rates as a result of its hardness and low surface roughness. Ceramics, such as aluminumoxide ( $\text{Al}_2\text{O}_3$ ) and Zirkonoxide ( $\text{ZrO}_2$ ), are used for convex head components and hydroxyapatite ( $\text{CA}_{10}(\text{PO}_4)_6(\text{OH})_2$ ) as surface coatings for stems or cup component, to allow for bone ingrowth fixation.

Young patients are indicated for bone ingrowth fixation, due to their good metabolism activities. The primary fixation in the first 6-8 weeks is determinative for the quality of the long-term fixation. This primary fixation is often achieved by screws (such as in the case of metal backed glenoid components), or press fit (such as in the case of femoral stem components). Old patients normally obtain a cemented prosthesis, to lighten the post-operative rehabilitation and because of their inferior bone ingrowth capacity. As mentioned, the most common used coating material is hydroxyapatite, with very similar chemical and mechanical properties to bone material. In fact, one of the constituents of bone is hydroxyapatite. Another advantage is the bioactive character, or osteoconductivity, of hydroxyapatite. It can stimulate bone to grow into the pores of the surface, resulting in a strong, self-regenerating bone-implant fixation. The present standard in hip replacements is a (partially) hydroxyapatite-coated stem. The goal of using hydroxyapatite is shortening of the rehabilitation time and a more proximal (anatomical) stress distribution. Hydroxyapatite is a calcium phosphate and exists both as an organic material and is available synthetically. Coating thickness is about  $25 \mu\text{m}$  and can debond as a result of a low Ph-value, cell-mediated resorption and mechanical causes, such as wear and fracture.

Aluminumoxid ( $\text{Al}_2\text{O}_3$ ) is used for its high resistance against abrasion and corrosion, its high strength and good biocompatibility. A smaller grain size results in better mechanical properties and better biocompatibility than Zirkonoxid ( $\text{ZrO}_2$ ). Elements from other materials are allowed in small concentrations, but it has to fulfill the requirements according to ISO 6474. Wear rates of artificial joints, with an articular combination made out of Aluminumoxid-UHMWPE can be two and a half times better as compared to a conventional metal-UHMWPE combination [126]. Potentials for the near future are the application of ceramic and metal parts, without polymer parts, to decrease wear rates [351].

Ceramics show good biocompatibility, but the mechanical properties make it difficult to use ceramics as a structural material. Although it has a high strength, its fracture toughness is nil, due to its extreme low elongation at fracture. In structures or assemblies with enforced displacements, ceramics should not be used, as they cannot perform in such conditions. In the past, head components made out of ceramics frequently showed head fracture [7], due to inferior ceramic quality and shortcomings in the fabrication process. At present, its main application is as a surface coating.

Table B.1: Mechanical properties of bone and common used biocompatible materials in orthopaedics [351, 285, 319, 195].  
\*Mechanical properties of bone depend on the location in the body and the direction of measurement

Materials	Density ( $g/cm^3$ )	Young's modulus (GPa)	Yield strength (MPa)	Compression strength (MPa)	Tensile strength (MPa)	Fatigue limit (MPa)
Trabecular bone*	~0.2-0.4	~0.04-0.3	-	130-180	60-160	-
Cortical bone*	~1.8	~12-23	-	~180	~160	-
CoCrMo	8.28	230	-	-	1175-1600	500-970
(forged)						
CoCrMo (casted)	8.28	230	-	-	650-1000	190-400
TiAl6V4	4.43	113.8	-	970	950	440-690
NiTi	6.45	28	-	-	850	-
LDPE	0.91-0.925	0.21	7.7-24.1	-	10	-
HDPE	0.941-0.965	1.4	2.4-31.7	4-25 (yield)	27	-
UHMWPE	0.94-0.99	0.8-2.7	21.5	-	41	-
PMMA	1.18	3.3	52 - 71	-	80	-
MMA	0.98	0.93-1.1	-	-	20-24	-
PEEK	1.28	3.6	90-110	29-150 (yield)	92	-
PSU	1.37	2.4	-	-	84	-
Al <sub>2</sub> O <sub>3</sub>	3.9	380-420	-	4000-5000	350	-
ZrO <sub>2</sub>	6.08	210	-	2000	650	-
Hydroxyapatite	3.05-3.15	80-120	-	300-900	40-200	-
Carbon fibers	1.75-1.9	190-490	-	-	3600-7060	-
Kevlar	1.44	83-186	-	-	3600-4100	-





# Appendix C

## Color Figures



*The colorful Gianni Romme during his 10 km race, world championship, Nagano, 1998*



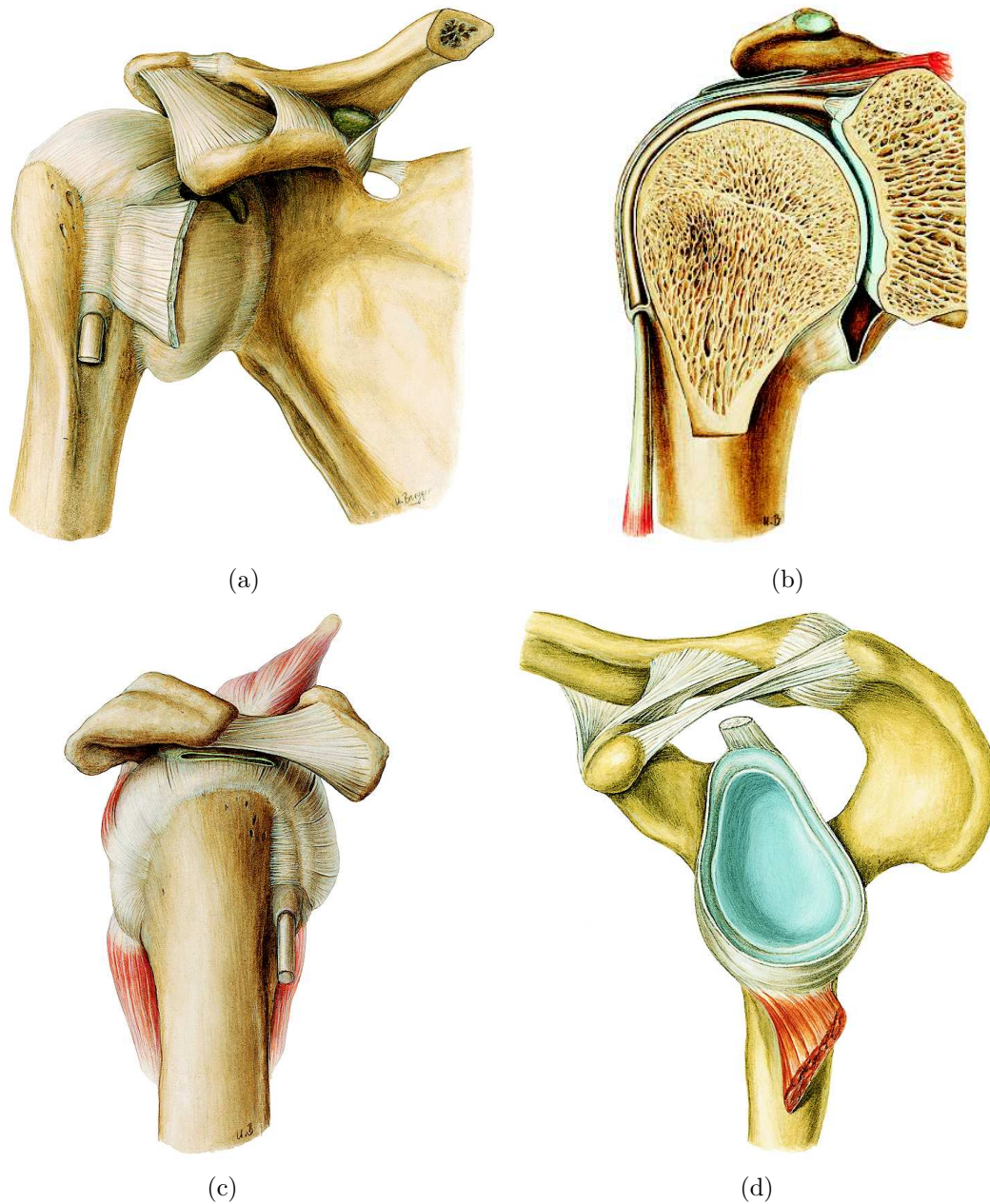


Figure C.1: *The glenohumeral joint. (a) Anterior view of the shoulder, including the humerus, scapula and lateral clavicle. (b) Frontal section of the right glenohumeral articulation. (c) Lateral view on the right glenohumeral articulation with the proximal humerus and Rotator Cuff (RC). (d) Lateral view on the left glenohumeral articulation. See also Figure 2.2. Adapted from Sobotta*

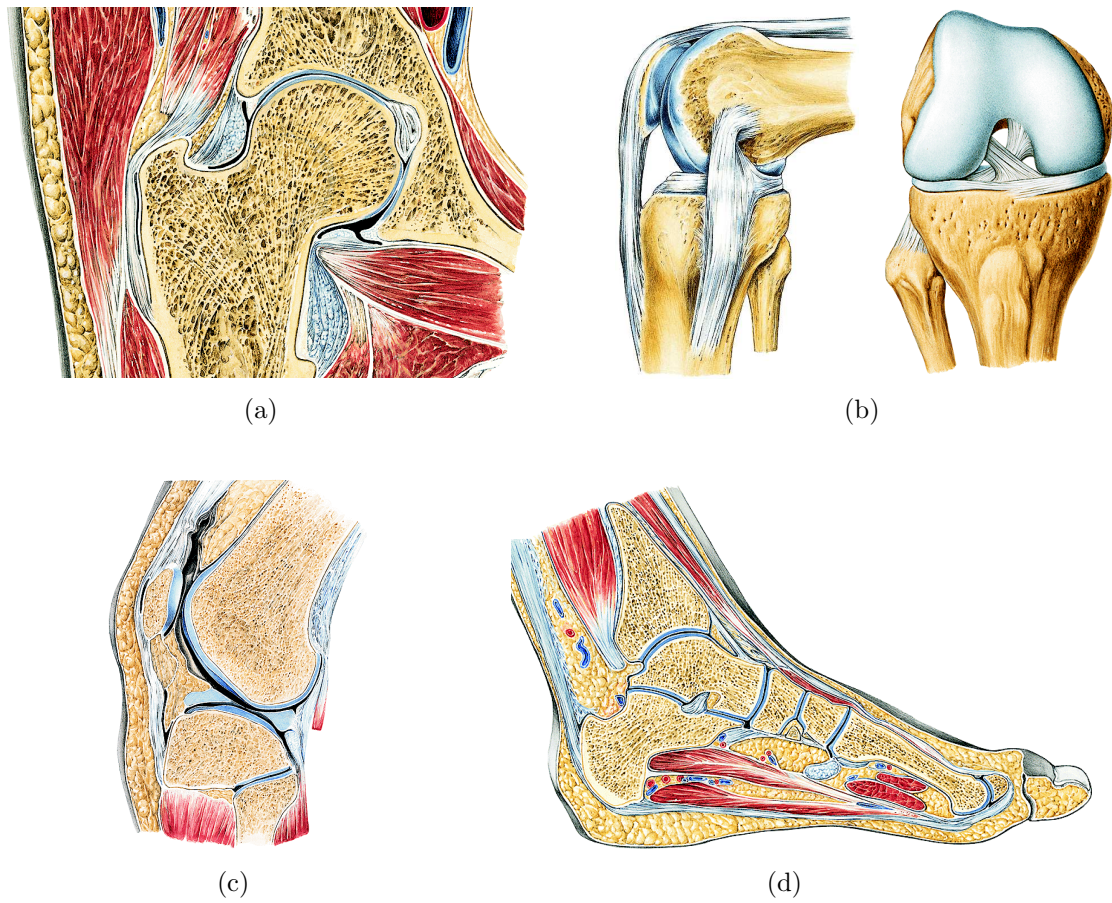
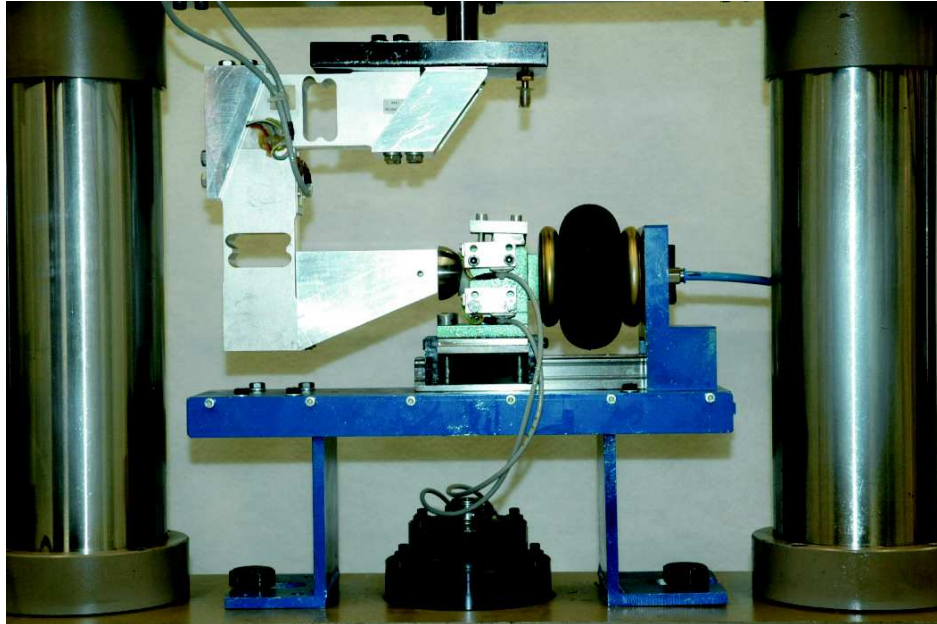
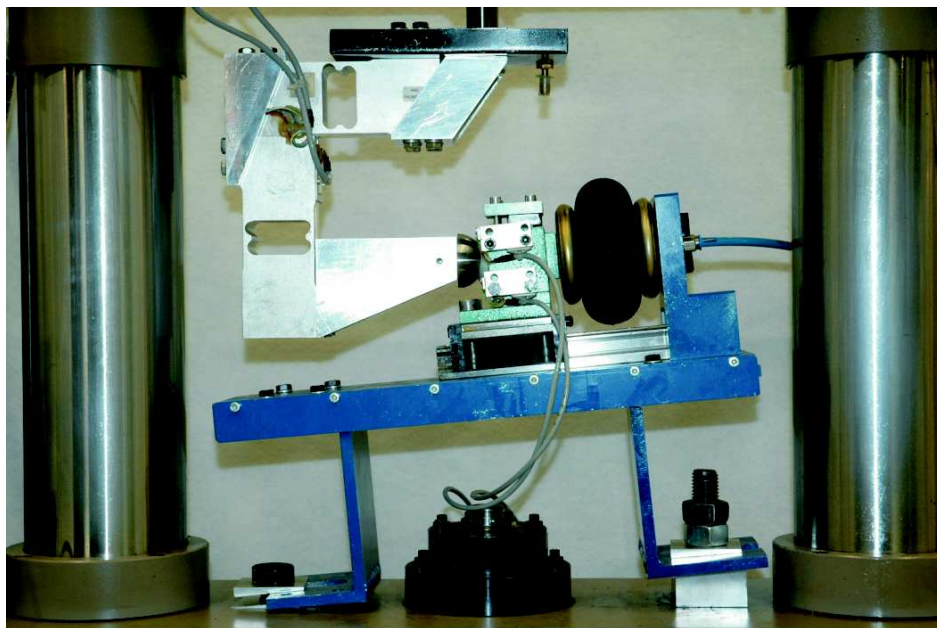


Figure C.2: *Some joints of the lower extremities. (a) Anterior section of the hip joint (articulatio coxae). (b) Medial (left) and anterior view on the knee joint (articulatio genus). (c) Medial-lateral section of the ankle joint (articulatio talocruralis). Adapted from Sobotta. See also Figures 3.1, 3.5 and 3.9*

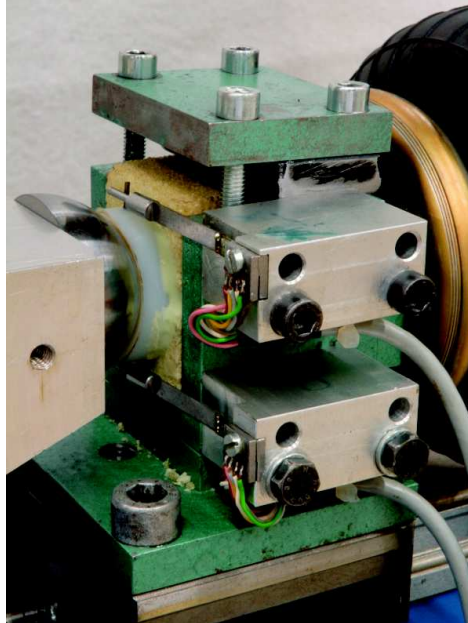


(a)

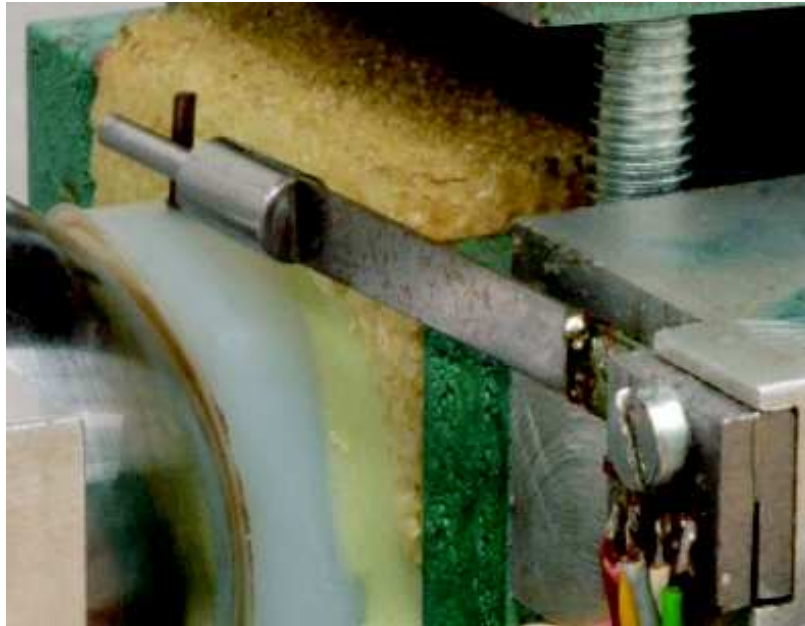


(b)

Figure C.3: (a) The test set-up integrated in the MTS materials testing system, with inclination angle  $\gamma = 0^\circ$ . (b) The test set-up integrated in the MTS materials testing system, with inclination angle  $\gamma < 0^\circ$ . See also Figures 5.3 and 7.3



(a)



(b)

Figure C.4: (a) Humeral head (left) against the glenoid component, superiorly clamped at the medial half of the bone substitute. (b) Close up of the sensors for investigating glenoid component tilting, by measuring the medial-lateral displacements of the two pins in the superior and inferior glenoid rim. See also Figure 5.4

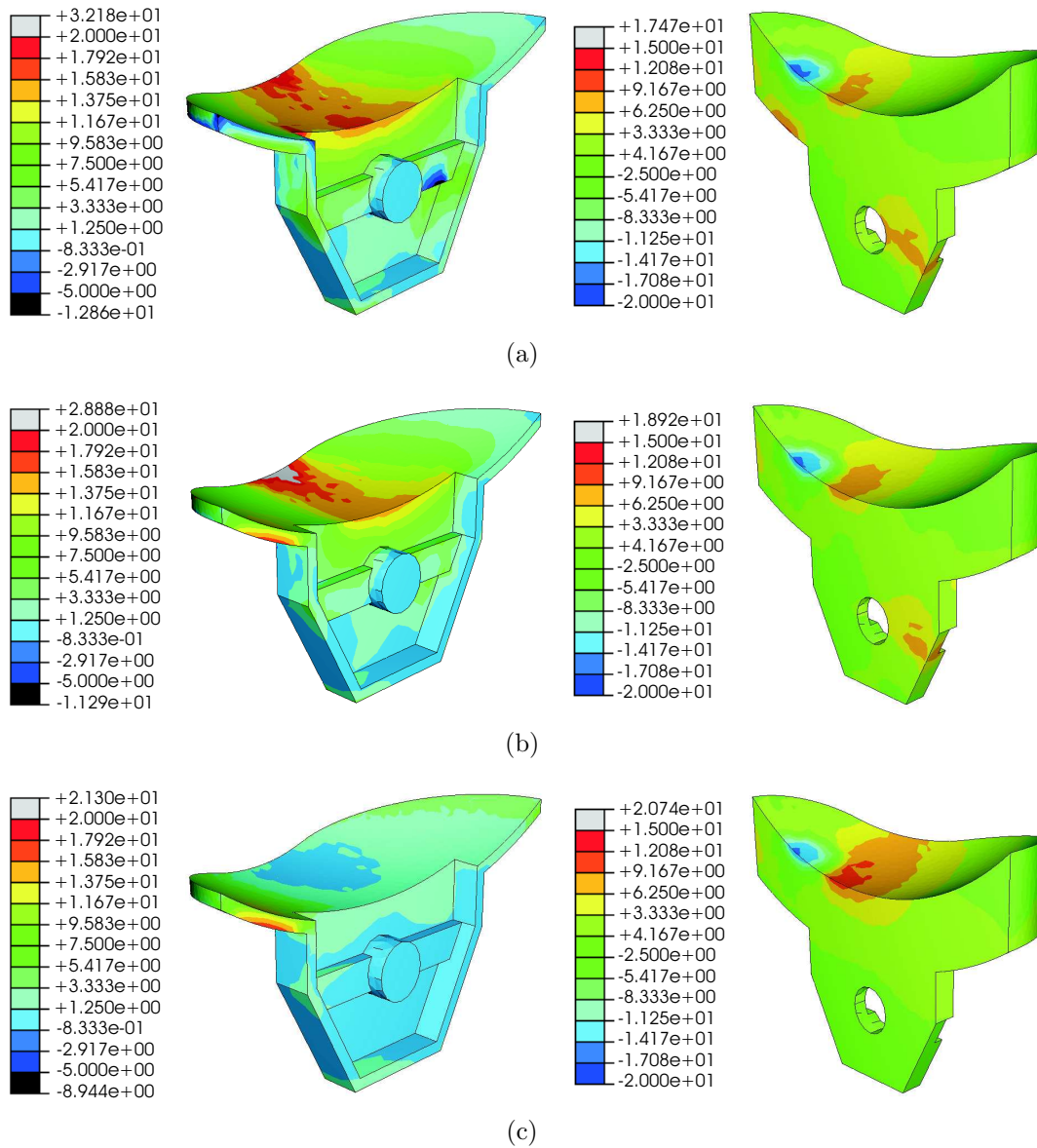


Figure C.5: Maximal principal stresses (MPa) in the bone cement (left) and glenoid component as analysed using the FE model for different interface conditions, with a 725 N joint compression force and a 350 N superior directed joint subluxation force. (a) A CoF of 0 is applied at the UHMWPE - PMMA interface. (b) A CoF of 1 is applied at the UHMWPE - PMMA interface. (c) A full bonding is applied at the UHMWPE - PMMA interface. See also Figure 9.6

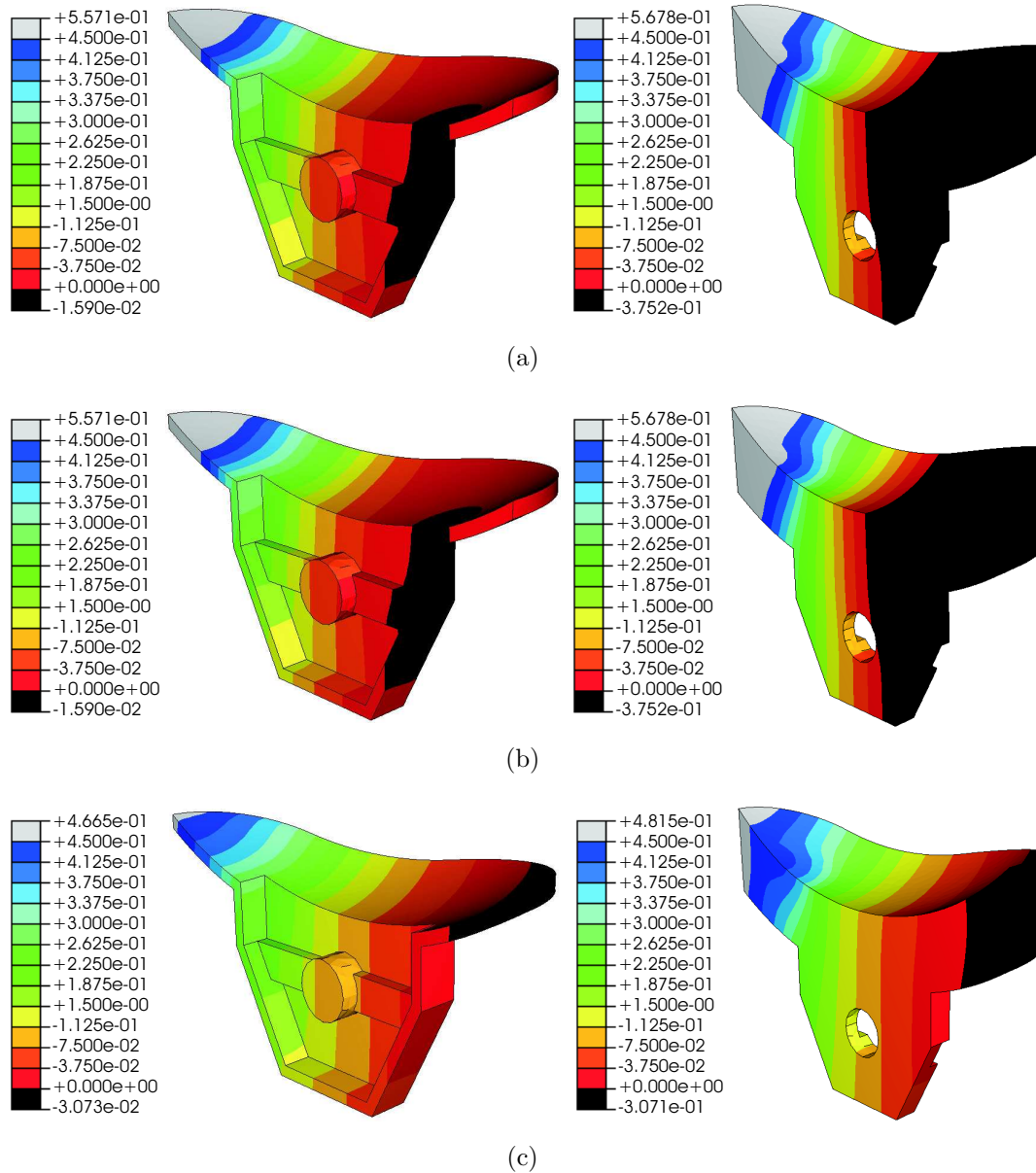
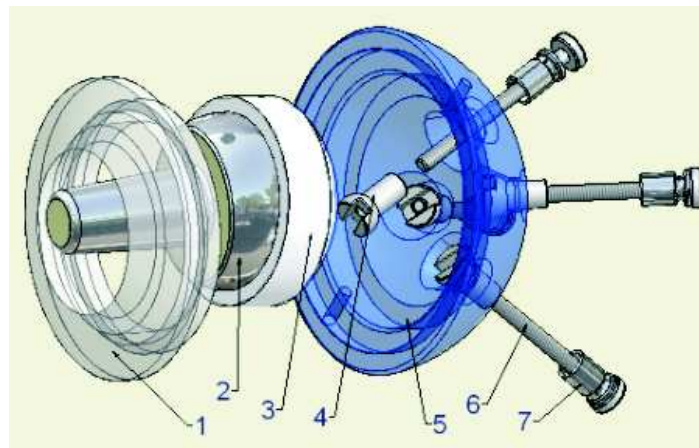


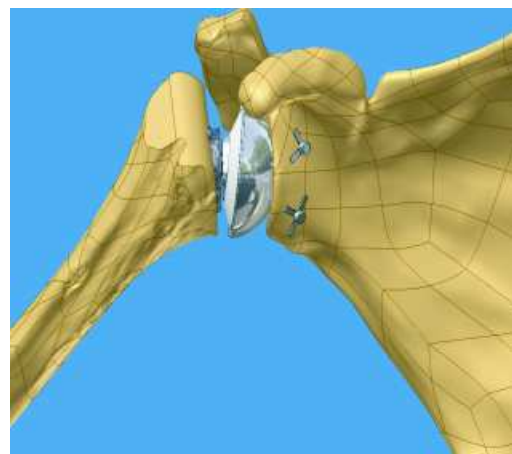
Figure C.6: Maximal medial-lateral displacement (mm) in the bone cement (left) and glenoid component as analysed in the FE model for different interface conditions, with a 725 N joint compression force and a 350 N superior directed joint subluxation force. (a) A CoF of 0 is applied at the UHMWPE - PMMA interface. (b) A CoF of 1 is applied at the UHMWPE - PMMA interface. (c) A full bonding is applied at the UHMWPE - PMMA interface. See also Figure 9.7



(a)



(b)



(c)

Figure C.7: *The self-stabilizing glenohumeral prosthesis. (a) The bipolar prosthesis on component level. 1. Constraining disc 2. CoCr head for the inner bearing 3. UHMWPE disc for articulation 4. Nuts, for fixation of the artificial ligaments to the outer shell 5. Outer shell, fixed against the glenoid bone stock 6. Artificial ligaments 7. Bone anchors (b) The assembled prosthesis. (c) Artist impression of the replaced glenohumeral joint. See also Figure 10.2*

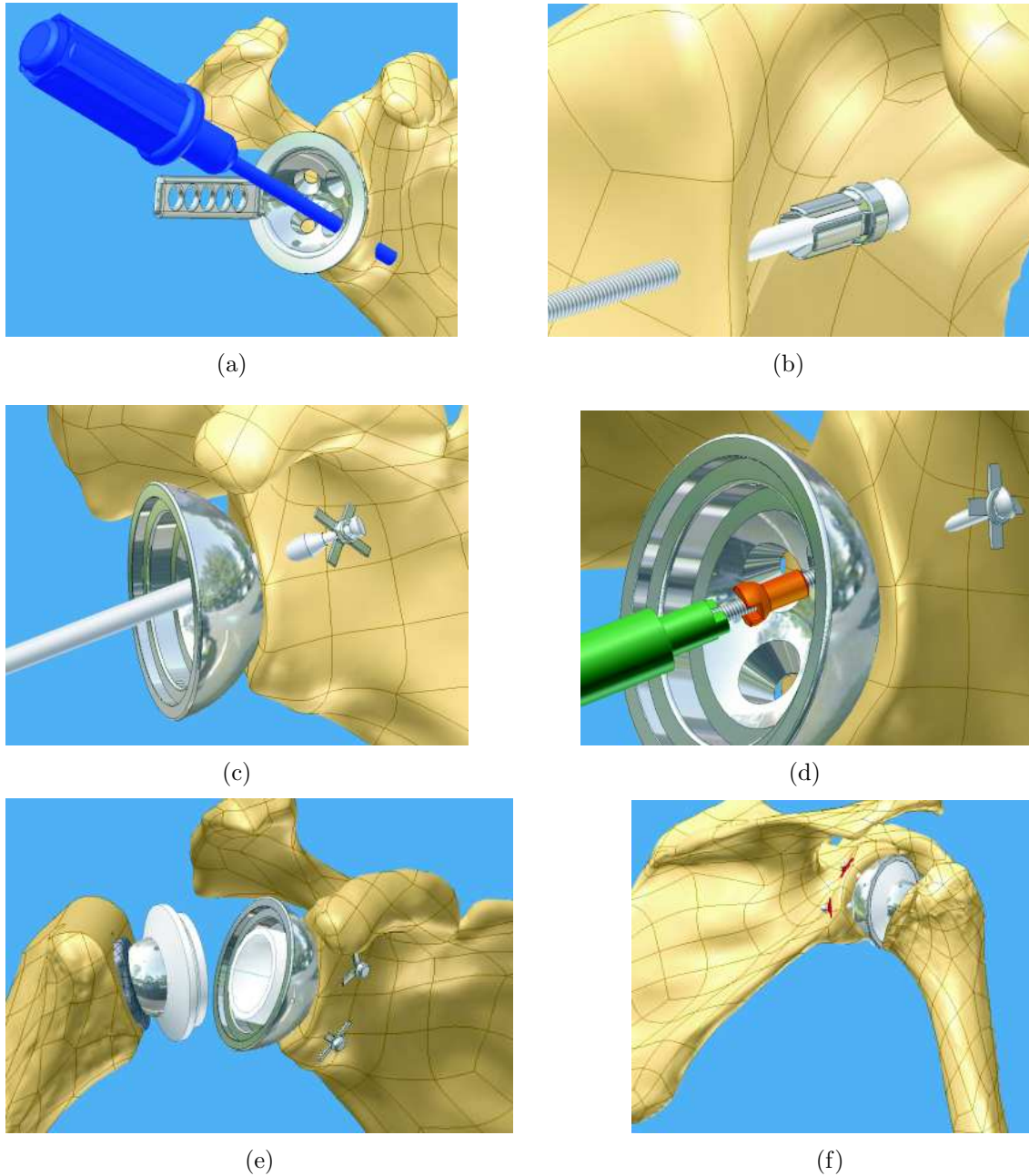


Figure C.8: Main steps of the surgical procedure. (a) Guided drilling, from lateral through the glenoid medial cortex. (b) Lateral insertion and unfolding of the bone anchors. (c) Positioning of the prosthetic outer shell over the ligaments. (d) Fixing the ligaments using nuts and special surgical instrumentation. (e) Assembling the bipolar prosthesis. (f) The self-stabilizing prosthesis at work as the replaced the glenohumeral joint. See also Figure 10.5

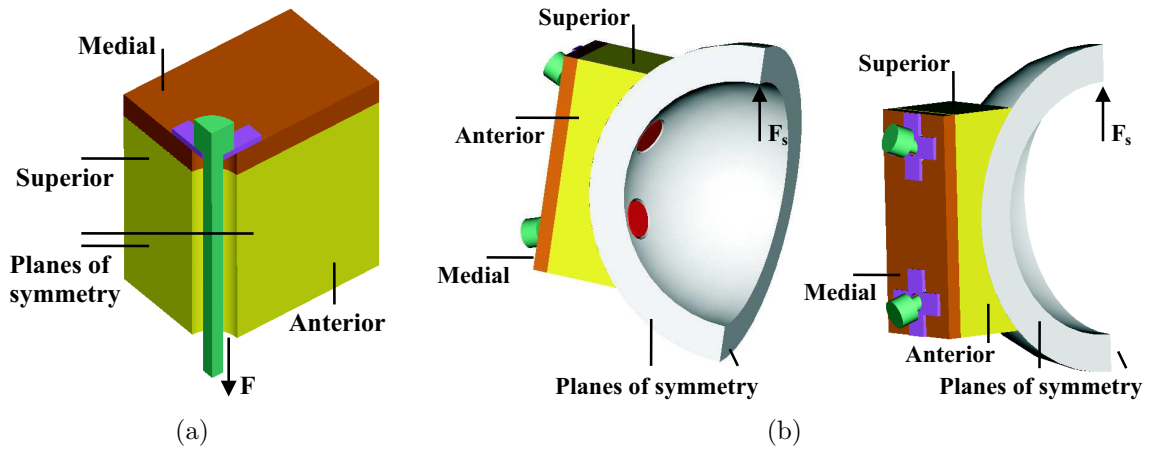


Figure C.9: (a) Model for the FE analysis to investigate the stresses in the bone anchor, ligaments and underlying bone. (b) Model for the FE analysis including the bipolar head to investigate the stresses in the bone anchor, ligaments and underlying bone. See also Figure 10.8

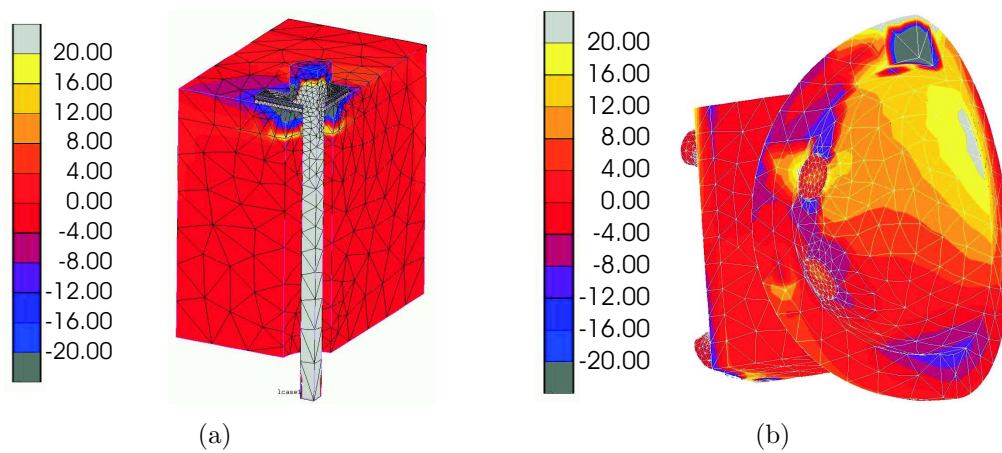


Figure C.10: (a) Maximal principal stresses (MPa) in the bone structure, bone anchors and ligament of a simplified structure of the fixation system of the new prosthesis. The ligament is loaded by a 240 N tensile force. (b) Maximal principal stresses (MPa) in the bone structure, fixation system and outer shell of the new prosthesis, which is loaded by a 350 N subluxation in superior direction. See also Figure 10.8



## References

- [1] American Academy of Orthopaedic Surgeons. URL: <http://www.aaos.org/>. Last visited: 24/05/2004.
- [2] Aagaard H, Verdonk R. *Function of the normal meniscus and consequences of meniscal resection*. Scand J Med Sci Sports. 9(3) (1999), 134 – 40.
- [3] Abernethy P, Aagaard H, *History of knee arthroplasty*, In Klenerman L. (ed.) The evolution of orthopaedic surgery. Lake, Royal Society of Medicine Press Ltd. (2000), 25 – 38.
- [4] Albee FH. *Original features in arthroplasty of the knee with improved prognosis*. Surg Gynecol ObstetScand. 47 (1928), 312.
- [5] Acevedo JI, Myerson MS. *Reconstructive alternatives for ankle arthritis*. Foot Ankle Clin. 4 (1999), 409 – 430.
- [6] Acklin YP, Berli BJ, Frick W, Elke R, Morscher EW. *Nine-year results of Muller cemented titanium Straight Stems in total hip replacement*. Arch Orthop Trauma Surg. 121(7) (2001), 391 – 398.
- [7] Allain J, Goutallier D, Voisin MC, Lemouel S. *Failure of a stainless-steel femoral head of a revision total hip arthroplasty performed after a fracture of a ceramic femoral head. A case report*. J Bone Joint Surg Am. 80(9) (1998), 1355 – 60.
- [8] Amstutz HC, Sew Hoy AL, Clarke IC. *UCLA anatomic total shoulder arthroplasty*. Clin Orthop. 155 (1981), 7 – 20.
- [9] Amstutz HC. *Innovations in design and technology. The story of hip arthroplasty*. Clin Orthop. 378 (2000), 23 – 30.
- [10] An K.N., Himeno S., Tsumura H., Kawai T., Chao E.Y. *Pressure distribution on articular surfaces: application to joint stability evaluation.*, J Biomech, 23(10) (1990), 1013 – 1020.
- [11] Anglin C, Wyss UP, Pichora DR. *Glenohumeral contact forces.*, Proc Inst Mech Eng [H], 214(6) (2000), 637 – 44.
- [12] Anglin C, Wyss UP, Pichora DR. *Shoulder prosthesis subluxation: theory and experiment*. J Shoulder Elbow Surg. 9 (2000), 104 – 114.

- [13] Anglin C, Wyss UP, Pichora DR. *Mechanical testing of shoulder prostheses and recommendations for glenoid design.*, J Shoulder Elbow Surg, 9(4). (2000), 323 – 31.
- [14] Anglin C, Wyss UP, Nyffeler RW, Gerber C. *Loosening performance of cemented glenoid prosthesis design pairs.* Clin Biomech. 16(2) (2001), 144 – 150.
- [15] Antuna S, Sperling JW, Cofield RH. *Reimplantation of a glenoid component after component removal and allograft bone grafting: a report of 3 cases.* J Shoulder Elbow Surg. 11(6) (2002), 637 – 41.
- [16] American Society for Testing and Materials (ASTM) F1829-98. Standard Test Method for Static Evaluation of the Glenoid Locking Mechanism in Shear (1998).
- [17] Aufranc OE. *Constructive hip surgery with a Vitallium mol. A report on 1000 cases of arthroplasty of the hip over a 15-year period.* J Bone Joint Surg. 39A (1957), 237 – 248.
- [18] Baer WS. *Arthroplasty with the aid of animal membrane.* Am J Orthop Surg. 16 (1918), 1 – 19, 94 – 115, 171 – 199.
- [19] Bagg SD, Forrest WJ. *A biomechanical analysis of scapular rotation during arm abduction in the scapular plane.* Am. J. Phys. med. Rehab. 67 (1988), 238 – 245.
- [20] Baltzopoulos V. *Muscular and tibiofemoral joint forces during iso-kinetic concentric knee extension.* Clin Biomech. 10(4) (1995), 208 – 214.
- [21] Bankston AB, Keating EM, Ranawat C, Faris PM, Ritter MA. *Comparison of polyethylene wear in machined versus molded polyethylene.* Clin Orthop. 317 (1995), 37 – 43.
- [22] Barnes CL, Collins DN, Nelson CL. *Cup arthroplasty, surface replacement arthroplasty, and femoral head resurfacing for osteonecrosis.* Semin Arthroplasty 2(3) (1991), 222 – 227.
- [23] Barrack RL. *Modularity of Prosthetic Implants.* Am J Orthop Surg. 2(1) (1994), 16 – 25.
- [24] Bauer G, Kinzl L. *Arthrodesis of the ankle joint.* Orthopade. 25(2) (1996), 158 – 165.
- [25] Beaulé PE, Schmalzried TP, Udomkiat P, Amstutz HC. *Jumbo femoral head for the treatment of recurrent dislocation following total hip replacement.* J Bone Joint Surg Am. 84A(2) (2002), 256 – 263.
- [26] Bellare A, Cohen RE. *Morphology of rod stock and compression-moulded sheets of ultra-high-molecular-weight polyethylene used in orthopaedic implants.* Biomaterials. 17(24) (1996), 2325 – 333.
- [27] Bergmann G, Graichen F, Rohlmann A. *Hip joint forces during walking and running, measured in two patients.* J Biomech. 8 (1993), 969 – 990.

- [28] Bergmann G, Deuretzbacher G, Heller M, Graichen F, Rohlmann A, Strauss J, Duda GN. *Hip contact forces and gait patterns from routine activities*. J Biomech. 34(7) (2001), 859–871.
- [29] Berry DJ, Harmsen WS, Cabanela ME, Morrey BF. *Twenty-five-year survivorship of two thousand consecutive primary Charnley total hip replacements: factors affecting survivorship of acetabular and femoral components* J Bone Joint Surg Am. 84A(2) (2002), 171–177.
- [30] Bicknell RT, Liew AS, Danter MR, Patterson SD, King GJ, Chess DG, Johnson JA. *Does keel size, the use of screws, and the use of bone cement affect fixation of a metal glenoid implant*. J Shoulder Elbow Surg. 12(3) (2003), 268–275.
- [31] Bigliani L, Kelkar R, Flatow E, Pollock R, van Mow, CM *Glenohumeral stability. Biomechanical properties of active and passive stabilizers.*, Clin Orthop, 330 (1996), 13–30.
- [32] Blaha JD. *The rationale for a total knee implant that confers anteroposterior stability throughout range of motion*, J Arthroplasty, 19(4) (2004), 22–26.
- [33] Blanco J, Tapia Casado L, Ramos Galea R, Leon Vasquez F. *Dissociation of a modular acetabular component in an uncemented total hip prosthesis. Effect of the modular design and anti-luxation rim. A case report*, Rev Chir Orthop Reparatrice Appar Mot, 85(3) (1999), 302–305.
- [34] Boileau P, Avidor C, Krishnan SG, Walch G, Kempf JF, Mole D. *Cemented polyethylene versus uncemented metal-backed glenoid components in total shoulder arthroplasty: a prospective, double-blind, randomized study.*, J Shoulder Elbow Surg, 2002, 11(4), 351-9.
- [35] Bolton-Maggs BG, Sudlow RA, Freeman MAR. *Total ankle arthroplasty: A long term review of the London Hospital experience*. J Bone Joint Surg. 67B (1985), 785–790.
- [36] Bonfield W. *Monitoring of Orthopedic Implants: A Biomaterials-Microelectronics Challenge (European Materials Research Society Monographs, Vol 7)*(Puers R. (Editor), Burny F.L.) ISBN 0444816208. North-Holland, Amsterdam, 1993.
- [37] Bonucci E. *Basic composition and structure of bone* In: Mechanical Testing of Bone and the Bone-Implant Interface, (Ed. An Y.H., Draughn R.H.) ISBN 0849302668. CRC Press, Boca Raton, USA, 1999.
- [38] Brown KD, Seligson D. *An optimal technique for ankle arthrodesis*. J Foot Ankle Surg. 43(1) (2004), 64–6.
- [39] Bryan RS, Peterson LF, Combs JJ Jr. *Polycentric knee arthroplasty. A review of 84 patients with more than one year follow-up*. Clin Orthop. 94 (1973), 136–139.

- [40] Buechel FF, Pappas MJ, DePalma AF. "Floating-socket" total shoulder replacement: anatomical, biomechanical, and surgical rationale., J Biomed Mater Res, 12(1). (1978), 89 – 114.
- [41] Buechel FF, Pappas MJ, Iorio LJ. New Jersey low contact stress total ankle replacement: biomechanical rationale and review of 23 cementless cases. Foot Ankle. 8(6) (1988), 279 – 290.
- [42] Buechel FF Sr, Buechel FF Jr, Pappas MJ, Dalessio J. Twenty-year evaluation of the New Jersey LCS Rotating Platform Knee Replacement. J Knee Surg. 15(2) (2002), 84 – 89.
- [43] Cameron B, Galatz L, Williams GR Jr. Factors affecting the outcome of total shoulder arthroplasty. Am J Orthop. 30(8) (2001), 613 – 623.
- [44] Campbell WC. Mobilization of joints with bony ankylosis. An analysis of 110 cases. J Am Med Assoc. 83 (1924), 976 – 981.
- [45] Campbell WC. Arthroplasty of the hip: An analysis of 48 cases. Surg Gynecol Obstet. 42 (1926), 9 – 17.
- [46] Campbell WC. Femoral mold arthroplasty Am J Surg. 29 (1940), 639 – 641.
- [47] Charnley J. Total hip replacement by low friction arthroplasty. Clin Orthop. 72 (1970), 7 – 21.
- [48] Charnley J. Low friction arthroplasty of the hip. Theory and Practice. Berlin, Springer (1979).
- [49] Chaffin DB, Andersson GB. Occupational Biomechanics, 2nd ed. ISBN 0471601349. New York, John Wiley & Sons, Inc. (1991).
- [50] Chen FS, Di Cesare PE, Kale AA, Lee JF, Frankel VH, Stuchin SA, Zuckerman JD. Results of cemented metal-backed acetabular components: a 10-year-average follow-up study. J Arthroplasty. 13(8) (1998), 867 – 873.
- [51] Chen AC, Bae WC, Schinagl RM, Sah RL. Depth- and strain-dependent mechanical and electromechanical properties of full-thickness bovine articular cartilage in confined compression. J Biomech. 34(1) (2001), 1 – 12.
- [52] Chu PK, Chen JY, Wang LP, Huang N. Plasma-surface modification of biomaterials. Mat. Sci. and Eng. R. 36 (2002), 143 – 206.
- [53] Churchill RS, Brems JJ, Kotschi H. Glenoid size, inclination, and version: an anatomic study. J Shoulder Elbow Surg. 10 (2001), 327 – 32.
- [54] Clarke HD, Trousdale RT. Component fracture in total knee arthroplasty. The Knee. 6 (1999), 261 – 267.
- [55] Close J. Some applications of functional anatomy of the ankle joint. J Bone Joint Surg. 38 (1956), 761 – 781.

- [56] Codman EA. *The shoulder*. G. Miller & Company, New York, 1934.
- [57] Collier JP, McNamara JL, Surprenant VA, Jensen RE, Surprenant HP. *All-polyethylene patellar components are not the answer*. Clin Orthop. 273 (1991), 198 – 203.
- [58] Collins D, Tencer A, Sidles J, Matsen F 3rd. *Edge displacement and deformation of glenoid components in response to eccentric loading. The effect of preparation of the glenoid bone*. J Bone Joint Surg Am. 74(4) (1992), 501 – 507.
- [59] Collins D, *Shoulder replacement: state of the art*. Sports medicine and Arthroscopy review. 7 (1999), 145 – 154.
- [60] Conti SF, Bisignan G, Martin R. *Update on total ankle replacement*. Semin Arthroplasty. 10 (1999), 62 – 71.
- [61] Couteau B, Mansat P, Estivaleres E, Darmana R, Mansat M, Egan J. *Finite element analysis of the mechanical behavior of a scapula implanted with a glenoid prosthesis.*, Clin Biomech, 16(7). (2001), 566 – 75.
- [62] Crowninshield R. *An overview of prosthetic materials for fixation.*, Clin Orthop, 235. (1988), 155 – 172.
- [63] Curl LA, Warren RF. *Glenohumeral joint stability. Selective cutting studies on the static capsular restraints.*, Clin Orthop, 330 (1996), 54 – 65.
- [64] Currier BH, Currier JH, Collier JP, Mayor MB. *Effect of fabrication method and resin type on performance of tibial bearings.*, J Biomed Mater Res, 53(2) (2000), 143 – 51.
- [65] Davey JR. *Choosing the socket in total hip arthroplasty* JCC. 38 (1995), S46 - S48.
- [66] Davy DT, Kotzar GM, Brown RH, Heiple KG, Goldberg VM, Heiple KG Jr, Berilla J, Burstein AH. *Telemetric force measurements across the hip after total arthroplasty* J Bone Joint Surg Am. 70(1) (1988), 45 – 50.
- [67] Deng M, Shalaby SW. *Properties of self-reinforced ultra-high-molecular-weight polyethylene composites*. Biomaterials. 18(9) (1997), 645 – 55.
- [68] Devane PA, Horne JG. *Assessment of polyethylene wear in total hip replacement*. Clin Orthop. 369 (1999), 59 – 72.
- [69] Diaz JA, Cohen SB, Warren RF, Craig EV, Allen AA. *Arthrodesis as a salvage procedure for recurrent instability of the shoulder*. J Shoulder Elbow Surg. 12(3) (2003), 237 – 41.
- [70] Digioia AM 3rd, Jaramaz B, Plakseychuk AY, Moody JE Jr, Nikou C, Labarca RS, Levison TJ, Picard F. *Comparison of a mechanical acetabular alignment guide with computer placement of the socket*. J Arthroplasty. 17(3) (2002), 359 – 364.

- [71] D'Lima DD, Oishi CS, Petersilge WJ, Colwell CW Jr, Walker RH. *100 cemented versus 100 noncemented stems with comparison of 25 matched pairs* Clin Orthop. 348 (1998), 140 – 148.
- [72] Doets HC, Brand R, Nelissen RGHH. *Totakl anke arthroplasty in inflammatory arthritis using a mobile-bearing design.*, Accepted for the American Academy Orthopedics Surgeons Meeting, San Fransisco (2001).
- [73] Doorenbosch, C.A., Mourits, A.J., Veeger, D.H., Harlaar, J., van der Helm, F.C.T. *Determination of functional rotation axes during elevation of the shoulder complex.*, J Orthop Sports Phys Ther, 31(3). (2001), 133 – 137.
- [74] Edwards TB, Kadakia NR, Boulahia A, Kempf JF, Boileau P, Nemoz C, Walch G. *A comparison of hemiarthroplasty and total shoulder arthroplasty in the treatment of primary glenohumeral osteoarthritis: results of a multicenter study.*, J Shoulder Elbow Surg. 12(3). (2003), 207 – 137.
- [75] Elfick AP, Hall RM, Pinder IM, Unsworth A. *The influence of femoral head surface roughness on the wear of ultrahigh molecular weight polyethylene sockets in cementless total hip replacement.* J Biomed Mater Res. 48(5) (1999), 712 – 718.
- [76] Engelbrecht, E., Stellbrink, G., *Total shoulder endoprosthesis design St. Georg.*, Chirurg, 47(10). (1976), 525 – 30.
- [77] Evans SL, Gregson PJ. *Composite technology in load-bearing orthopaedic implants.* Biomaterials. 19(15) (1998), 1329 – 1342.
- [78] Falez F, La Cava F, Panegrossi G. *Femoral prosthetic heads and their significance in polyethylene wear.* Int Orthop. 24(3) (2000), 126 – 129.
- [79] Ferguson SJ. *Excision of the knee joint: Recovery with a false joint and a useful limb.* Med Times Gaz. 1 (1861), 1.
- [80] Ferguson SJ, Bryant JT, Ganz R, Ito K. *The acetabular labrum seal: a poroelastic finite element model* Clin Biomech. 15(6) (2000), 463 – 468.
- [81] Flatow E.L. *Prosthetic design considerations in total shoulder arthroplasty.*, Semin Arthroplasty, 6 (1995), 233 – 244.
- [82] Frankle M.A., Kumar A.G. *Reverse Total Shoulder Replacement for Arthritis with an Irreparable Rotator cuff Tear.* Tech Shoulder elbow Surg. 4(2) (2003), 77 – 83.
- [83] Freeman MAR, Pinskerova V. *The movement of the normal tibio-femoral joint.* J Biomech. INPRESS XXX
- [84] Frich LH, Jensen NC, Odgaard A, Pedersen CM, Sojbjerg JO, Dalstra M. *Bone strength and material properties of the glenoid.* J Shoulder Elbow Surg. 6(2) (1997), 97 – 104.

- [85] Friedrich J, Wigant L, Unger W, Lippitz A, Wittrich H. *Corona, spark and combined UV and ozone modification of polymer films*. Surface and Coatings Technology. 98 (1998), 897 – 885
- [86] Fukubayashi T, Kurosawa H. *The contact area and pressure distribution pattern of the knee. A study of normal and osteoarthrotic knee joints*. Acta Orthop Scand. 51(6) (1980), 871 – 879.
- [87] Fukuda K, Chen CM, Cofield RH, Chao EY. *Biomechanical analysis of stability and fixation strength of total shoulder prostheses*. Orthopedics. 11(1) (1988), 141 – 149.
- [88] Gabriel SM, Dennis DA, Honey MJ, Scott RD. *Polyethylene wear on the distal tibial insert surface in total knee arthroplasty*. Knee. 5 (1997), 221 – 228.
- [89] Gidwani S, Langkamer VG. *Recurrent dislocation of a posterior-stabilized prosthesis: a series of three cases*. Knee. 8(4) (2001), 317 – 320.
- [90] Gill DR, Cofield RH, Morrey BF. *Ipsilateral total shoulder and elbow arthroplasties in patients who have rheumatoid arthritis*. J Bone Joint Surg Am. 81(8) (1999), 1128 – 37.
- [91] Glitsch U, Baumann W. *The three-dimensional determination of internal loads in the lower extremity*. J Biomech. 30(11) (1997), 1123 – 1131.
- [92] Gluck T. *Die invaginationsmethode der Osteo- und Arthroplastik*. Bel Klin Wochenscher. 28 (1890), 732 – 736, 752 – 757.
- [93] Gonzalez-Diaz R, Rodriguez-Merchan EC, Gilbert MS. *The role of shoulder fusion in the era of arthroplasty*. Int Orthop. 21(3) (1997), 204 – 9.
- [94] Grammont PM, Baulot E. *Delta shoulder prosthesis for rotator cuff rupture*. Orthopedics. 16(1) (1993), 65 – 8.
- [95] Green MD, Guild FJ, Adams RD. *Characterisation and comparison of industrially pre-treated homopolymer polypropylene, HF 135M*. J Adhesion & Adhesives. 22 (2002), 81 – 90.
- [96] Gunston FH. *Polycentric knee arthroplasty. Prosthetic simulation of normal knee movement*. J Bone Joint Surg Br. 53(2) (1971), 272 – 277.
- [97] Guyton JL. *Arthroplasty of ankle and knee* In: Canale St (S. T. Canale, S. Terry Canale, Willis C. Campbell ed.) Campbell's Operative Orthopaedics. Ed. 9. St. Louis, Mosby. (1998), 232 – 235.
- [98] Habermeyer, P., Ebert, T., *Current status and perspectives of shoulder replacement.*, Unfallchirurg, 101(9). (1999), 668 – 83.
- [99] Haboush EJ. *A new operation for arthroplasty of the hip based on biomechanics, photoelasticity, fast setting dental acrylic and other considerations* Bull Hosp Joint Dis. 13 (1953), 242 – 277.

- [100] Hagen RJ. *Ankle arthrodesis. Problems and pitfalls.* Clin Orthop. 202 (1986), 152 – 162.
- [101] Haggart GE. *Surgical treatment of degenerative arthritis of the knee joint* J Bone Joint Surg. 22 (1940), 717 – 729.
- [102] Hamadouche M, Kerboull L, Meunier A, Courpied JP, Kerboull M. *Total hip arthroplasty for the treatment of ankylosed hips: a five to twenty-one-year follow-up study.* J Bone Joint Surg Am. 83A(7) (2001), 992 – 998.
- [103] Haraguchi K, Sugano N, Nishii T, Sakai T, Yoshikawa H, Ohzono K. *Influence of polyethylene and femoral head surface quality on wear: a retrieval study.* Int Orthop. 25(1) (2001), 29 – 34.
- [104] Harryman, D., Sidles, J., Harris, S. and Matsen, F. *The role of the rotator interval capsule in passive motion and stability of the shoulder.* J Bone Joint Surg Am. 74(1) (1992), 53 – 66.
- [105] Hasan SS, Leith JM, Campbell B, Kapil R, Smith KL, Matsen FA 3rd. *Characteristics of unsatisfactory shoulder arthroplasties.* J Shoulder Elbow Surg. 11(5) (2002), 431 – 441.
- [106] Hay, J., Reid, J. *Anatomy, mechanics and human motion.*, ISBN 0130352136 Prentice Hall Inc., New York, 1988.
- [107] Heck DA, Partridge CM, Reuben JD, Lanzer WL, Lewis CG, Keating EM. *Prosthetic component failures in hip arthroplasty surgery* J Arthroplasty. 10(5) (1995), 575 – 580.
- [108] van der Helm FCT. *Analysis of the kinematic and dynamic behavior of the shoulder mechanism.* J Biomech. 27(5) (1994), 527 – 550.
- [109] Herder, JL. Energy free systems. Theory, conception and design of statically balanced spring mechanisms. PhD thesis, Delft University of Technology, Department of Design, Engineering and Production. (2001).
- [110] Hertel, R., Ballmer, F.T., *Observations on retrieved glenoid components.*, J Arthroplasty, 18(3). (2003), 361 – 6.
- [111] Hertz, H., *Significance of the limbus glenoidalis for the stability of the shoulder joint.*, Wien Klin Wochenschr Suppl, 152. (1984), 1 – 23.
- [112] Hill, D. *Design engineering of biomaterials for medical devices.* John Wiley & Sons, New York. (1998).
- [113] Hintermann B, Nigg BM, Sommer C. *Transfer of movement between calcaneus and tibia in vitro* Clin Biomech. 9 (1994), 349 – 355.
- [114] Hintermann B. *Short- and mid-term results with the STAR total ankle prosthesis.* Orthopade. 28(9) (1999), 792 – 803.

- [115] Hinterwimmer S, von Eisenhart-Rothe R, Siebert M, Welsch F. *Patella kinematics and patello-femoral contact areas in patients with genu varum and mild osteoarthritis*. Clin Biomech. 19(7) (2004), 704 – 10.
- [116] Hughes RE, Bryant CR, Hall JM, Wening J, Huston LJ, Kuhn JE, Carpenter JE, Blasier RB. *Glenoid inclination is associated with full-thickness rotator cuff tears*. Clin Orthop. 407 (2003), 86 – 91.
- [117] Huiskes R, Verdonschot N. *Biomechanics of the artificial joints: the hip* In: Basic Orthopaedic Biomechanics second edition (Ed. Mow C. Hayes W). Lippincott-Raven Publisher, Philadelphia. (1997), (11) 395 – 460.
- [118] Huiskes R. *The causes of failure for hip and knee arthroplasties*. Ned Tijdschr Geneesk. 142(37) (1998), 2035 – 2040.
- [119] Huiskes R, Verdonschot N, Nivbrant B. *Migration, stem shape, and surface finish in cemented total hip arthroplasty*. Clin Orthop. 355 (1998), 103 – 112.
- [120] Huiskes R. *If bone is the answer, then what is the question?* J Anat. 197 (2000), 145 – 56.
- [121] Iannotti J.P., Gabriel J.P., Schneck S.L., Evans B.G., Misra S. *The normal glenohumeral relationships. An anatomical study of one hundred and forty shoulders.*, J Bone Joint Surg Am, 74 (1992), 491 – 500.
- [122] Inman V.T., Saunders M., Abbott L.C. *Observations on the function of the shoulder joint.*, J Bone and Joint Surg, 26A (1944), 1 – 30.
- [123] Insall J, Scott WN, Ranawat CS. *The total condylar knee prosthesis. A report of two hundred and twenty cases*. J Bone Joint Surg Am. 61(2) (1979), 173 – 180.
- [124] Insall JN, Hood RW, Flawn LB, Sullivan DJ. *The total condylar knee prosthesis in gonarthrosis. A five to nine-year follow-up of the first one hundred consecutive replacements*. J Bone Joint Surg. 65(5) (1983), 619 – 628.
- [125] Morrey, B.F., Itoi, E., An, K.N., Lippitt, S.B. *Biomechanics of the shoulder* In: The Shoulder, Second edition (Ed. Matsen A.M. and Rockwood C.A.). ISBN 0721681344. W.B. Saunders Company, Philadelphia, 1998, 233 – 276.
- [126] Jazrawi LM, Bogner E, Della Valle CJ, Chen FS, Pak KI, Stuchin SA, Frankel VH, Di Cesare PE. *Wear rates of ceramic-on-ceramic bearing surfaces in total hip implants: a 12-year follow-up study*. J Arthroplasty. 14(7) (1999), 781 – 7.
- [127] Jenkins, DB. General survey of the lower limb. In: Jenkins DB., Hollinshead WH, Biblis M. (Eds). *Hollinshead's Functional Anatomy of the limbs and Back*. Philadelphia, Harcourt Brace & Company. 16 (1991), 233 – 238.
- [128] Jobe CM. *Biomechanics of the shoulder* In: The Shoulder, Second edition (Ed. Matsen A.M. and Rockwood C.A.). ISBN 0721681344. W.B. Saunders Company, Philadelphia, 1998, 34 – 98.

- [129] Johnson, R.L., *Total shoulder arthroplasty.*, Orthop Nurs, 12(1). (1993), 14 – 22.
- [130] Jones WN, Aufranc OE, Kermond EL. *Mold arthroplasty of the knee.* J Bone Joint Surg. 49 (1967), 1022.
- [131] Jonsson, B., Larsson, S.E., *Functional improvement and costs of hip and knee arthroplasty in destructive rheumatoid arthritis.*, Scand J Rheumatol, 20(5). (1991), 351 – 7.
- [132] Journeaux SF, Morgan DA, Donnelly WJ. *Poor results of the Freeman uncemented metal-backed acetabular component. Five-to-nine-year results.* J Bone Joint Surg Br. 82(2) (2000), 185 – 187.
- [133] Kang YH, Park JB. *Precoating of ultrahigh molecular weight polyethylene with polymethylmethacrylate: interfacial strength.* J Biomed Mater Res. 43(3) (1998), 261 – 269.
- [134] Karaismailoglu TN, Tomak Y, Gulman B. *Late detachment modular femoral component after primary total hip replacement.* Arch Orthop Trauma Surg. 121 (2001), 481 – 482.
- [135] Karduna AR, Williams GR, Williams JL, Iannotti JP, *Glenohumeral joint translations before and after total shoulder arthroplasty. A study in cadavera.*, J Bone Joint Surg Am, 79(8) (1997), 1166 – 1174.
- [136] Karduna AR, Williams GR, Iannotti JP, Williams JL. *Total shoulder arthroplasty biomechanics: a study of the forces and strains at the glenoid component.* J Biomech Eng. 120(1) (1998), 92 – 99.
- [137] Katayama T, Yamamoto H, Inoue N. *Optimum design of artificial joints considering initial fixation of prosthesis.* Composite structures. 32 (1995), 427– 33.
- [138] Kazar, B. and Relovszky, E. *Prognosis of primary dislocation of the shoulder.* Acta Orthop Scand. 40 (1969), 216.
- [139] Kelkar R, Wang VM, Flatow EL, Newton PM, Ateshian GA, Bigliani, LU, Pawluk RJ, Mow VC. *Glenohumeral mechanics: a study of articular geometry, contact, and kinematics.*, J Shoulder Elbow Surg, 10(1) (2001), 73 – 84.
- [140] Kellis E. *Tibiofemoral forces during maximal isokinetic eccentric and concentric efforts of the knee flexors.* Clin Biomech. 16(3) (2001), 229 – 236.
- [141] Kelly JD Jr, Norris TR. *Decision making in glenohumeral arthroplasty.* J Arthroplasty. 18(1) (2003), 75 – 82.
- [142] Kendrick JB 2nd, Noble PC, Tullos HS. *Distal stem design and the torsional stability of cementless femoral stems.* J Arthroplasty. 10(4) (1995), 463 – 469.
- [143] Kihlman Øiseth K, Krozer A, Kasemo BK, Lausmaa J. *Surface modification of spin-coated high-density polyethylene films by argon and oxygen glow discharge plasma treatments.* Appl. Surf. Science. 202 (2002), 92 – 103.

- [144] Kim YH, Kim VE. *Early migration of uncemented porous coated anatomic femoral component related to aseptic loosening* Clin Orthop. 295 (1993), 146 – 155.
- [145] Kinloch AJ. *Adhesion and Adhesives: Science & Technology*. London: Chapman and Hall; 1987.
- [146] Kitaoka HB. *Historical perspective of foot and ankle arthroplasty*. In Morrey BF (ed.) Joint replacement arthroplasty. New York, Churchill Livingstone. (1991), 1157 – 1172.
- [147] Kitaoka HB, Patzer GL. *Clinical results of the Mayo total ankle arthroplasty*. J Bone Joint Surg Am. 78(11) (1996), 1658 – 1664.
- [148] Klenerman L. *Arthroplasty of the hip*. In Klenerman L. (ed.) The evolution of orthopaedic surgery. Lake, Royal Society of Medicine Press Ltd. (2002), 13 – 23.
- [149] Klimkiewicz JJ, Iannotti JP, Rubash HE, Shanbhag AS *Aseptic loosening of the humeral component in total shoulder arthroplasty*. J Shoulder Elbow Surg. 7(4) (1998), 422 – 6.
- [150] Kofoed H. *Current status of ankle arthroplasty*. Berlin, Springer. (1998), 157 – 161.
- [151] Kofoed H. *The evolution of ankle arthroplasty*. Orthopade. 28(9) (1999), 804 – 811.
- [152] Komistek RD, Stiehl JB, Dennis DA, Paxson RD, Soutas-Little RW. *Mathematical model of the lower extremity joint reaction forces using Kane's method of dynamics*. J Biomech. 31(2) (1998), 185 – 189.
- [153] Kreder HJ, Deyo RA, Koepsell T, Swiontkowski MF, Kreuter W. *Relationship between the volume of total hip replacements performed by providers and the rates of postoperative complications in the state of Washington*. J Bone Joint Surg Am. 79(4) (1997), 485 – 94.
- [154] Kuhns JG. *Nylon membrane arthroplasty of the knee in chronic arthritis*. J Bone Joint Surg. 46A (1964), 448 – 449.
- [155] Kuiper JH, Huiskes R. *Mathematical optimization of elastic properties: application to cementless hip stem design*. J Biomech. 119(2) (1997), 166 – 174.
- [156] Kura H, Kitaoka HB, Luo ZP, An KN. *Measurement of surface contact area of the ankle joint*. Clin Biomech. 13(4-5) (1998), 365 – 370.
- [157] Kurtz SM, Ochoa JA, White CV, Srivastav S, Cournoyer J. *Backside non-conformity and locking restraints affect liner/shell load transfer mechanisms and relative motion in modular acetabular components for total hip replacement*. J Biomech. 31(5) (1998), 431 – 437.
- [158] Kurtz SM, Muratoglu OK, Evans M, Edidin AA. *Advances in the processing, sterilization, and crosslinking of ultra-high molecular weight polyethylene for total joint arthroplasty*. Biomaterials. 20(18) (1999), 1659 – 88.

- [159] Kuster MS, Wood GA, Sakurai S, Blatter G. *Stress in the patellarfemoral joint in downhill walking: a biomechanical study.* Z Unfallchir Versicherungsmed. 86 (1993), 178 – 183.
- [160] Kuster MS, Wood GA, Stachowiak GW, Gächter A. *Joint load considerations in total knee replacement* J Bone Joint Surg Br. 79(1) (1997), 109 – 113.
- [161] Lacroix D, Prendergast PJ *Stress analysis of glenoid component designs for shoulder arthroplasty.*, Proc. Instn. Mech. Engrs. Part H, Journal of engineering in Medicine, 211(6). (1997), 467 – 74.
- [162] Larsen A, Dale K, Eek M. *Radiographic evaluation of rheumatoid arthritis and related conditions by standard reference films.*, Acta Radiol Diagn (Stockh). 18(4). (1977), 481 – 91.
- [163] Lavielle L. *Polymer-polymer friction: Relation to adhesion.*, Wear. 151(1). (1991), 63 – 75.
- [164] Lazarus MD, Jensen KL, Southworth C, Matsen FA 3rd. *The radiographic evaluation of keeled and pegged glenoid component insertion.*, J Bone Joint Surg Am. 84-A(7). (2002), 1174 – 82.
- [165] Lee HL. *Total ankle arthroplasty. Indications, results, and biomechanical rationale.* Internet, URL: <http://www.orthofootankle.com/neufeldTAR.cfm>. (Last visited: 10-2004)
- [166] de Leest O, Rozing PM, Rozendaal LA, van der Helm FC, *Influence of glenohumeral prosthesis geometry and placement on shoulder muscle forces.* Clin Orthop. 330 (1996), 222 – 33.
- [167] Lehtinen JT, Belt EA, Kauppi MJ, Kaarela K, Kuusela PP, Kautiainen HJ, Lehto MU, *Bone destruction, upward migration, and medialisation of rheumatoid shoulder: a 15 year follow up study.*, Ann Rheum Dis, 60 (2001), 322 – 326.
- [168] Leipholz H. *Basic concepts and definitions.*, In: Leipholz, H., (Ed.), Stability theory, An introduction to the stability of dynamic systems and rigid bodies, second edition. Stuttgart: Teubner, (1987), 3 – 20.
- [169] Van Lenthe GH, de Waal Malefijt MC, Huiskes R. *Stress shielding after total knee replacement may cause bone resorption in the distal femur.* J Bone Joint Surg Br. 79(1) (1997), 117 – 122.
- [170] Levigne C, Franceschi JP. *Rheumatoid Arthritis of the shoulder: Radiological presentation and results of arthroplasty.* In: Shoulder Arthroplasty (Ed. Walch G. and Boileau P.). ISBN 3540633499. Springer-Verlag, Berlin, Heidelberg, 1999, 221 – 230.
- [171] Levy O, Funk L, Sforza G, Copeland SA. *Copeland surface replacement arthroplasty of the shoulder in rheumatoid arthritis.* J Bone Joint Surg Am. 86A(3) (2004), 512 – 8.

- [172] Lewis G. *The ankle joint prosthetic replacement: clinical performance and research challenges*. Foot Ankle Int. 15(9) (1994), 471 – 476.
- [173] Li S, Burstein AH. *Ultra-high molecular weight polyethylene. The material and its use in total joint implants*. J Bone Joint Surg Am. 76(7) (1994), 1080 – 90.
- [174] Lim LA, Carmichael SW, Cabanela ME. *Biomechanics of total hip arthroplasty*. Anat Rec. 257(3) (1999), 110 – 116.
- [175] Ling FF, and Peterson MB. *Simple model of metalworking friction under extreme pressures*. In: Ling F.F. and Pan C.H.T. (Eds.), Approaches to modelling of friction and wear. Springer-Verlag, New York, 1986, 83-85.
- [176] Lo IK, Parten PM, Burkhart SS., *The inverted pear glenoid: an indicator of significant glenoid bone loss.*, Arthroscopy, 20(2) (2004), 169 – 74.
- [177] Lohr J, Floren M, Schwyzer H, Simmen B, Gschwend N. *Shoulder joint instability after primary arthroplasty*. Orthopade, 27 (1998), 571 – 575.
- [178] Lonner JH, Lotke PA. *Aseptic complications after total knee arthroplasty*. J Am Acad Orthop Surg. 7(5) (1999), 311 – 324.
- [179] Lugli T. *Artificial shoulder joint by Pean (1893): the facts of an exceptional intervention and the prosthetic method*. Clin Orthop. 133 (1978), 215 – 8.
- [180] Luttgens, K. and Hamilton, N. Kinesiology: Scientific Basis. 9th Ed., Madison, WI: Brown & Benchmark, 1997.
- [181] MacAusland WR and MacAusland AR. *The mobilization of ankylosed joints by arthroplasty*. Philadelphia, Lea & Febiger. (1929).
- [182] MacIntosh DL. *Hemiarthroplasty of the knee using a space occupying prosthesis for painful varus and valgus deformities*. J Bone Joint Surg. 40A (1958), 1431.
- [183] MacManus LF, Walzar MJ, McIntyre NS. *Study of Ultraviolet Light and Ozone Surface Modification of Polypropylene*. J Polym Sci Pol Chem. 37 (1999), 2489 – 2501.
- [184] Magermans DJ, Nagels J, Chadwick EK, Veeger HEJ, Van der Helm FCT. *Motion patterns of the shoulder for patients with a shoulder endo-prosthesis during combing hair.*, Proceedings of the 4th meeting of the international shoudler group, Cleveland USA. (2002).
- [185] Magermans DJ, Smits NCMA, Chadwick EK, Veeger DH, van der Helm FCT, Rozing PM. *Discriminating factors for functional outcome after shoulder arthroplasty. A critical review of the literature.*, Acta Orthop Belg, 69(2). (2003), 127 – 36.
- [186] Magermans DJ *Biomechanical analysis of shoulder arthroplasty.*, PhD thesis, Delft University of Technology, Delft, The Netherlands. ISBN 9064644705 (2004).

- [187] Magnuson PB. *Joint debridement: Surgical treatment of degenerative arthritis*. Surg Gynecol Obstet. 73 (1941), 1.
- [188] Mahfouz MR, Traina SM, Komistek RD, Dennis DA. *In vivo determination of knee kinematics in patients with a hamstring or patellar tendon ACL graft*. J Knee Surg. 16(4) (2003), 197 – 202.
- [189] Maistrelli GL, Mahomed N, Garbuz D, Fornasier V, Harrington IJ, Binnington A. *Hydroxyapatite coating on carbon composite hip implants in dogs*. J Bone Joint Surg Br. 74(3) (1992), 452 – 56.
- [190] Manaster BJ. *Total hip arthroplasty: Imaging evaluation*. J South Orthop Assoc. 7(2) (1998), 95 – 108.
- [191] Mann RA. *Arthrodesis of the foot and ankle*. In: Mann RA, Coughlin MJ (eds.). *Surgery of the foot and ankle*. St. Louis, Mosby. (1993), 673 – 713.
- [192] Martin RB. *Towards a unifying theory of bone remodeling*. Bone. (1) (2000), 1 – 6.
- [193] Matsen FA III, Thomas SC, Rockwood CA, Wirth MA *Glenohumeral instability*. In: Matsen FA III, Rockwood CA. (Eds.), *The shoulder*, second edition. Philadelphia: W.B. Saunders Company Co., (1998), 611 – 754.
- [194] Matsuno H, Yudoh K, Kimura T. *Failure of the locking mechanisms in cementless acetabular components: a report of 3 cases*. Sicot Case-Reports: Jan 2002. URL: [www.sicot.org](http://www.sicot.org).
- [195] Matweb *The online materials information resource*. Last visited: May 2004. URL: [www.matweb.com](http://www.matweb.com).
- [196] Mazur JM, Schwartz E, Simon SR. *Ankle arthrodesis. Long-term follow-up with gait analysis*. J Bone Joint Surg Am. 61(7) (1979), 964 – 975.
- [197] McCarthy JC, Bono JV, O'Donnell PJ. *Custom and modular components in primary total hip replacement*. Clin Orthop. 344 (1997), 162 – 171.
- [198] McGee MA, Howie DW, Kostic K, Haynes DR, Wildenauer CI, Percy MJ, McLean JD. *Implant retrieval studies of the wear and loosening of prosthetic joints: a review*. Wear. 241 (2000), 158 – 165.
- [199] McGloughlin TM, Kavanagh AG. *Wear of ultra-high molecular weight polyethylene (UHMWPE) in total knee prostheses: a review of key influences*. Proc Inst Mech Eng [H]. 214(4) (2000), 349 – 59.
- [200] McKeever DC. *Tibial plateau prosthesis*. Clin Orthop. 18 (1960), 86 – 95.
- [201] McKellop H, Clarke I, Markolf K, Amstutz H. *Friction and wear properties of polymer, metal, and ceramic prosthetic joint materials evaluated on a multichannel screening device*. J Biomed Mater Res. 15(5) (1981), 619 – 53.

- [202] McKellop H, Shen FW, Lu B, Campbell P, Salovey R. *Effect of sterilization method and other modifications on the wear resistance of acetabular cups made of ultra-high molecular weight polyethylene. A hip-simulator study.* J Bone Joint Surg Am. 82-A(12) (2000), 1708 – 25.
- [203] McPherson EJ, Friedman RJ, An YH, Chokesi R, Dooley RL. *Anthropometric study of normal glenohumeral relationships.* J Shoulder Elbow Surg. 6(2) (1997), 105 – 12.
- [204] Michelson JD, Schmidt GR, Mizel MS. *Kinematics of a total arthroplasty of the ankle: comparison to normal ankle motion.* Foot Ankle Int. 21(4) (2000), 278 – 84.
- [205] Miller A, Friedman B. *Fascial arthroplasty of the knee.* J Bone Joint Surg. 34 (1952), 55 – 63.
- [206] Moore AT. *The self-locking metal hip prosthesis.* J Bone joint Surg. 39A (1947), 811 – 827.
- [207] Matsen AM, Rockwood CA, Wirth MA, Lippitt SB. *Glenohumeral arthritis and its management* In: The Shoulder, second edition (Ed. Matsen AM and Rockwood CA). ISBN 0721681344. W.B. Saunders Company, Philadelphia, 1998.
- [208] McCullagh PJJ. *Biomechanics and design of shoulder arthroplasty.* Proc Inst Mech Eng [H]. 209 (1995), 207 – 213.
- [209] Meskers C. *Quantitative assessment of shoulder function in a clinical setting. Methodological aspects and applications.*, PhD thesis, State University of Leiden. (1998).
- [210] Meijers KAE *A study of the articulation of the shoulder.*, PhD thesis, State University of Leiden. (1961).
- [211] Morrey BF. *Difficult complications after hip joint replacement. Dislocation.* Clin Orthop. 344 (1997), 179 – 187.
- [212] Mow C, Athesian GA *Lubrication and wear of diarthrodial joints.* In: Basic Orthopaedic Biomechanics. (Ed. Mow C, Hayes W). ISBN 0397516843. Lippincott-Raven Publishers, Philadelphia, 1997.
- [213] Morscher EW. *Current status of acetabular fixation in primary total hip arthroplasty.* Clin Orthop. 274 (1992), 172 – 193.
- [214] Morlock M, Schneider E, Bluhm A, Vollmer M, Bergmann G, Muller V, Honl M. *Duration and frequency of every day activities in total hip patients.* J Biomech. 34(7) (2001), 873 – 881.
- [215] Mow C, Ratcliffe A. *Structure and function of articular cartilage and meniscus.* In: Basic Orthopaedic Biomechanics. (Ed. Mow C, Hayes W). ISBN 0397516843. Lippincott-Raven Publishers, Philadelphia, 1997.

- [216] Müller HJ. *Form und Funktion der Scapula. Vergleichend-analytische Studien bei Carnivore un Ungulaten.* Z. f. Anat. u. Entwicklungsgeschichte. 126 (1967), 205 – 63.
- [217] Murphy JB. *Ankylosis: Clinical and experimental.* J Am Med Assoc. 44 (1905), 1573 – 1582, 1671 – 1678, 1749 – 1756.
- [218] Murphy JB. *Arthroplasty.* Ann Surg. 57 (1913), 593 – 647.
- [219] Nabeyama R, Matsuda S, Miura H, Kawano T, Nagamine R, Mawatari T, Tanaka K, Iwamoto Y. *Changes in anteroposterior stability following total knee arthroplasty.* J Orthop Sci. 8(4) (2003), 526 - 31.
- [220] Nagels J, Valstar ER, Stokdijk M, Rozing PM. *Patterns of loosening of the glenoid component.,* J Bone Joint Surg Br. 84(1) (2002), 83 – 7.
- [221] Nagels J, Stokdijk M, Rozing, PM. *Stress shielding and bone resorption in shoulder arthroplasty.,* J Shoulder Elbow Surg, 12(1) (2003), 35 – 9.
- [222] Neer CS, Brown TH Jr, McLaughlin HL. *Fracture of the neck of the humerus with dislocation of the head fragment.* Am J Surg, 85(3) (1953), 252 – 8.
- [223] Neer CS. *Articular replacement for the humeral head.* J Bone Joint Surg, 37(A) (1955), 215 – 228.
- [224] Neer C, Watson K, Stanton F. *Recent experience in total shoulder replacement.* J Bone Joint Surg, 64 (1982), 319 – 335.
- [225] Neer CS 2nd, Craig EV, Fukuda H. *Cuff-tear arthropathy.* J Bone Joint Surg Am., 65(9) (1983), 1232 – 44.
- [226] Neer CS 2nd, Morrison DS. *Glenoid bone-grafting in total shoulder arthroplasty.* J Bone Joint Surg Am., 70(8) (1988), 1154 – 62.
- [227] Nelissen RGHH, Doets HC, Meskers C. *The value of ankle prostheses: a gait analysis approach.* In: Kofoed H (ed.) Current status of ankle arthroplasty. Berlin, Springer. (1998), 72 – 77.
- [228] Neufeld SK, Lee TH. *Total ankle arthroplasty: indications, results, and biomechanical rationale.* Am J Orthop. 29(8) (2000), 593 – 602.
- [229] *NIH Consensus Statement Online. Total Hip Replacement* September 12-14 (1994), 1 – 13.
- [230] Nisell R. *Mechanics of the knee. A study of joint and muscle load with clinical applications.* Acta Orthop Scand Suppl. 216 (1985), 1 – 42.
- [231] Ogawa T, Mukai H, Osawa S. *Effects of functional groups and surface roughness on interfacial shear strength in ultrahigh molecular weight polyethylene fiber/polyethylene system.* J applied polymer science. 71(1999), 243 – 249.

- [232] Older J. *Low-friction arthroplasty of the hip. A 10-12-year follow-up study.* Clin Orthop. 211 (1986), 36 – 42.
- [233] Owens DK. *Mechanism of corona-induced self-adhesion of polyethylene film.* J. Appl. Polymer Sci. 19 (1975), 3315.
- [234] Pappas MJ, Buechel FF. *Biomechanics and design rationale: The Buechel-Pappas™ ankle replacement system.* Endotec Inc. Internet URL (01/08/2002): [http://www.endotec.com/pdf\\_files/ankle](http://www.endotec.com/pdf_files/ankle)
- [235] Park KD, Kim J, Yang SJ, Yao A, Park JB. *Preliminary study of interfacial shear strength between PMMA precoated UHMWPE acetabular cup and PMMA bone cement.* J Biomed Mater Res, 65B (2003), 272 – 9.
- [236] Parsons IM, Apreleva M, Fu FH, Woo SL. *The effect of rotator cuff tears on reaction forces at the glenohumeral joint.* J Orthop Res., 20(3) (2002), 439-46.
- [237] Paul JP. *Strength requirements for internal and external prostheses.* J Biomech. 32(4) (1999), 381 – 193.
- [238] Pearl M. and Kurutz S. *Geometric analysis of commonly used prosthetic systems for proximal humeral replacement.* J Bone Joint Surg Am. 81(5) (1999), 660 – 671.
- [239] Peltier LF. *A history of hip surgery.* In: Callaghan JJ, Rosenberg AG, Rubash HE (eds). The adult hip. Lippincott-Raven. (1998), 3 – 36.
- [240] Perez R, Rodriguez J, Deshmukh R, and Ranawat S. *Polyethylene wear and periprosthetic osteolysis in metal-backed acetabular components with cylindrical liners.* J Arthroplasty. 13 (1998), 1 – 7.
- [241] Petersen MM, Lauritzen JB, Pedersen JG, Lund B. *Decreased bone density of the distal femur after uncemented knee arthroplasty. A 1-year follow-up of 29 knees.* Acta Orthop Scand. 67(4) (1996), 339 – 344.
- [242] Poppen NK, Walker PS. *The StGeorg rotating total knee arthroplasty: A historical review.* The Knee. 6 (1999), 269 – 276.
- [243] Pijpers AP. and Meier RJ. *Adhesion behaviour of polypropylenes after flame treatment determined by XPS(ESCA) spectral analysis.* J Electron spectrosc. 121 (2001), 299 – 313.
- [244] Poppen NK, Walker PS. *Normal and abnormal motion of the shoulder.,* J bone Joint Surg Am., 58(2) (1976), 195 – 201.
- [245] Poppen NK, Walker PS. *Forces at the glenohumeral joint in abduction.,* Clin Orthop. 135 (1978), 165 – 170.
- [246] Post M, Jablon M. *Constrained total shoulder arthroplasty. Long-term follow-up observations.,* Clin Orthop. 173 (1983), 109 – 16.

- [247] Post M. *Constrained arthroplasty: its use and misuse.*, Semin Arthroplasty., 1(2) (1990), 151 – 9.
- [248] Potter TA, Weinfeld MS, Thomas WH. *Arthroplasty of the knee in rheumatoid arthritis and osteoarthritis. A follow-up study after implantation of the McKeever and MacIntosh prostheses.* J Bone Joint Surg Am. 54(1) (1972), 1 – 24.
- [249] Prescher A. *Anatomical basics, variations, and degenerative changes of the shoulder joint and shoulder girdle.* Eur J Radiol. 35(2) (2000), 88 – 102.
- [250] Premnath V, Harris WH, Jasty M, Merrill EW. *Gamma sterilization of UHMWPE articular implants: an analysis of the oxidation problem. Ultra High Molecular Weight Poly Ethylene.* Biomaterials. 17 (1996), 1741 – 53.
- [251] Pronk, G. The shoulder girdle. Analyzed and modelled kinematically. PhD thesis, Delft University of Technology, Department of Design, Engineering and Production. ISBN 90-37000533 (1991).
- [252] Putz R. and Pabst R. *Atlas of Human Anatomy.*, ISBN 0683300474. Lippincott, Williams and Wilkins (1996).
- [253] Que L, Topoleski LD. *Third-body wear of cobalt-chromium-molybdenum implant alloys initiated by bone and poly(methyl methacrylate) particles.* J Biomed Mater Res. 50(3) (2000), 322 – 330.
- [254] Quinet RJ, Winters EG. *Total joint replacement of the hip and knee.* Med Clin North Am. 76(5) (1992), 1235 – 1251.
- [255] Radler C, Wozasek GE, Seitz H, Vecsei V. *Distal femoral fracture through the screw hole of a ligament augmentation device fixation.* Arthroscopy. 16(7) (2000), 737 – 739.
- [256] Ramamohan N, Kelly IG. *Joint replacement in the rheumatoid shoulder.* Curr Orthop. 16(1) (2002), 1 – 14
- [257] Ranawat CS, Shine JJ. *Duo-condylar total knee arthroplasty.* Clin Orthop. 94 (1973), 185 – 195.
- [258] Ranawat CS, Peters LE, Umlas ME. *Fixation of the acetabular component. The case for cement* Clin Orthop. 344 (1997), 207 – 215.
- [259] Reinhardt A, Advani SG, Santare MH, Miller F. *Preliminary study on composite hip prostheses made by resin transfer molding.* J Comp Mat. 33(9) (1999), 852 – 870.
- [260] Revell PA, al-Saffar N, Kobayashi A. *Biological reaction to debris in relation to joint prostheses.* Proc Inst Mech Eng [H]. 211(2) (1997), 187 – 97.
- [261] Rinta-Kiikka I, Alberty A, Savilahti S, Pajamaki J, Tallroth K, Lindholm TS. *The clinical and radiological outcome of the rotating hinged knee prostheses in the long-term.* Ann Chir Gynaecol. 86(4) (1997), 349 – 359.

- [262] Romero-Snchez MD, Pastor-Blas MM, and Martn-Martnez JM. *UV treatment of synthetic styrene-butadiene-styrene*. Presented at the 3rd International Symposium on Polymer Surface Modification: Relevance to Adhesion, Newark, May 21-22, 2001.
- [263] Rorabeck CH. *The unstable total knee: causes and cures*. Knee. 8(3) (2001), 179 – 186.
- [264] Rozendaal LA. *Stability of the shoulder, intrinsic muscle proerties and reflexive control.*, PhD thesis, Delft University of Technology. ISBN 9090102310. Delft, 1998.
- [265] Rozendal R. *Inleiding in de Kinesiologie van de mens* Culemborg (The Netherlands): H. Stam Nederland B.V., (1969).
- [266] Rubash HE, Sinha RK, Shanbhag AS, Kim SY. *Pathogenesis of bone loss after total hip arthroplasty*. Orthop Clin North Am. 29(2) (1998), 173 – 186.
- [267] Rudigier J, Grundei H, Menzinger F. *Prosthetic Replacement of the Ankle in Posttraumatic Arthrosis. 10-Year Experience with the Cementless ESKA Ankle Prosthesis*. European Journal of Trauma. 2 (2001), 66 – 74.
- [268] Runciman, R.J. Biomechanical model of the shoulder joint. PhD thesis, University of Strathclyde, Bioengineering unit, Glasgow. (1993).
- [269] Rydell NW. *Forces acting on the femoral head-prosthesis. A study on strain gauge supplied prostheses in living persons*. Acta Orthop Scand. 37 (Supl. 88) (1966), 1 – 132.
- [270] Sait S, Scott WA. *Early results of isoelastic hemiarthroplasty in chronic shoulder arthritis*. Orthopedics. 23(5) (2000), 467 – 9.
- [271] Salter E, Nasca R, Shelly B. *Anatomical observations on the acromioclavicular joint and supporting ligaments*. Am J Sports Med. 15(3) (1987), 199 – 206.
- [272] Saltzman CL. *Total ankle arthroplasty: state of the art*. Instr Course Lect. 48 (1999), 263 – 268.
- [273] Sanchez-Sotelo J, Sperling JW, Rowland CM, Cofield RH. *Instability after shoulder arthroplasty: results of surgical treatment*. J Bone Joint Surg Am. 85-A(4) (2003), 622 – 31.
- [274] Santavirta SS, Lappalainen R, Pekko P, Anttila A, Konttinen YT. *The counterface, surface smoothness, tolerances, and coatings in total joint prostheses*. Clin Orthop. 369 (1999), 92 – 102.
- [275] Scholes SC, Smith SI, Ash HE, Unsworth A. *The lubrication and friction of conventional UHMWPE, novel compliant layer and hard bearing surfaces for use in total hip prostheses*. In: Hutchings IM (Ed.), Friction, lubrication and wear of artificial joints. London: Profesional Engineering publishing, (2003), 59 – 74.

- [276] Scifert CF, Brown TD, Lipman JD. *Finite element analysis of a novel design approach to resisting total hip dislocation*. Clin Biomech. 14(10) (1999), 697 – 703.
- [277] Sechrest RC. *A Patient's Guide to Knee Anatomy*. Internet, URL: [http://www.medicalmultimedialogroup.com/pated/knee\\_problemsanatomyknee\\_anatomy.html](http://www.medicalmultimedialogroup.com/pated/knee_problemsanatomyknee_anatomy.html). (2002).
- [278] Semlitsch M, Willert HG. *Clinical wear behaviour of ultra-high molecular weight polyethylene cups paired with metal and ceramic ball heads in comparison to metal-on-metal pairings of hip joint replacements*. Proc Inst Mech Eng [H]. 211(1) (1997), 73 – 88.
- [279] Severt R, Thomas BJ, Tsenter MJ, Amstutz HC, Kabo JM. *The influence of conformity and constraint on translational forces and frictional torque in total shoulder arthroplasty*. Clin Orthop. 292 (1993), 151 – 158.
- [280] Simes JA, Marques AT, Jeronimidis G. *Design of a controlled-stiffness composite proximal femoral prosthesis*. Compos Sci Technol. 60 (2000), 559 – 567.
- [281] Schmalzried TP, Suszczewicz ES, Northfield MR, Akizuki KH, Frankel RE, Belcher G, Amstutz HG. *Quantitative Assessment of Walking Activity after Total Hip or Knee Replacement*. J Bone Joint Surg Am. 80 (1998), 54 – 59.
- [282] Shands AR. *Fundamentals in hip surgery* In: Tronzo RG (ed). Surgery of the hip. Ed. 2. New York, Springer-Verlag. (1984), 1 – 26.
- [283] Shiers LG. *Arthroplasty of the knee: Interim report of a new method*. J Bone Joint Surg. 42B (1960), 31 – 39.
- [284] Simon WH, Friedenbergs S, Richardson S. *Joint congruence. A correlation of joint congruence and thickness of articular cartilage in dogs*. J Bone Joint Surg Am. 55(8) (1973), 1614 – 1620.
- [285] Skinner HB, *Composite technology for total hip arthroplasty*. Clin Orthop. 235 (1988), 224 – 36.
- [286] Skirving AP. *Total shoulder arthroplasty – current problems and possible solutions*. J Orthop Sci. 4 (1999), 42 – 53.
- [287] Smith-Petersen MN. *Treatment of malum coxae senilis, old slipped upper femoral epiphysis, intra pelvic protrusion of the acetabulum, and coxa plana by means of acetabuloplasty*. J Bone Joint Surg. 18 (1936), 869 – 880.
- [288] Smith-Petersen MN. *Evolution of mould arthroplasty of the hip joint*. J Bone Joint Surg. 30B (1948), 59 – 73.
- [289] Smith SE, Estok DM 2nd, Harris WH. *Average 12-year outcome of a chrome-cobalt, beaded, bony ingrowth acetabular component*. J Arthroplasty. 13(1) (1998), 50 – 60.

- [290] Smrke D, Beden R, Stankovski V. *Bipolar versus total hip endoprosthesis: functional results.* Arch Orthop Trauma Surg. 120(5-6) (2000), 259 – 61.
- [291] Sneppen O, Fruensgaard S, Johannsen HV, Olsen BS, Sojbjerg JO, Andersen NH. *Total shoulder replacement in rheumatoid arthritis: proximal migration and loosening.*, J Shoulder Elbow Surg. 1996, 5(1), 47-52.
- [292] Sodha S, Wei SY, Okereke E. *Evolution of Total Ankle Arthroplasty.* The University of Pennsylvania Orthopaedic Journal. 13 (2000), 18 – 21.
- [293] Soslowsky LJ, Flatow EL, Bigliani LU, Mow VC. *Articular geometry of the glenohumeral joint.*, Clin Orthop, 285 (1992), 181 – 190.
- [294] Soyer J, Avedikian J, Pries P, Clarac JP. *Long-term outcome of Charnley's femoral implant. A review of 309 cases with follow-up of minimum 20 years.* Rev Chir Orthop Reparatrice Appar Mot. 84(5) (1997), 416 – 422.
- [295] Spalteholz W, Spanner R. *Handatlas der Anatomie des Menschen.*, Scheltema & Holkema N.V., The Netherlands, 1996.
- [296] Speed JS, Trout PC. *Arthroplasty of the knee. A follow-up study.* J Bone Joint Surg. 31B (1949), 53 – 60.
- [297] Sperling JW, Cofield RH, Rowland CM. *Neer hemiarthroplasty and Neer total shoulder arthroplasty in patients fifty years old or less. Long-term results.*, J Bone Joint Surg Am, 80(4). (1998), 464 – 73.
- [298] Stansfield BW, Nicol AC. *Hip joint contact forces in normal subjects and subjects with total hip prostheses: walking and stair and ramp negotiation.* Clin Biomech. 17(2) (2002), 130 – 139.
- [299] Staubesand, J. *Atlas of Human Anatomy, 3rd edition.* Vienna: Urban & Schwarzenberg. (1986).
- [300] Stauffer RN, Chao EY, Brewster RC. *Force and motion analysis of the normal, diseased, and prosthetic ankle joint.* Clin Orthop. 127 (1977), 189 – 196.
- [301] Stauffer RN. *Total joint arthroplasty. The ankle.* Mayo Clin Proc. 54(9) (1979), 570 – 575.
- [302] Steinberg ME. *Evolution and development of surface replacement arthroplasty.* Orthop Clin North Am. 13 (1982), 661 – 662.
- [303] Steinberg ME. *Summary and conclusions.* Orthop Clin North Am. 13 (1982), 895 – 902.
- [304] Steinberg ME. *Reconstructive surgery of the adult hip: An overview.* In Steinberg ME (ed.) The hip and its disorders. Philadelphia, WB Saunders Company. (1991), 705 – 725.
- [305] Steinberg DR, Steinberg ME. *The early history of arthroplasty in the United States.* Clin Orthop. 374 (2000), 55 – 89.

- [306] Steinmann SP, Cofield RH. *Bone grafting for glenoid deficiency in total shoulder replacement.* J Shoulder Elbow Surg. 9 (2000), 361 – 7.
- [307] Stone KD, Grabowski JJ, Cofield RH, Morrey BF, An KN, *Stress analyses of glenoid components in total shoulder arthroplasty.*, J Shoulder Elbow Surg, 8(2) (1999), 151 – 8.
- [308] Strobel M, Walzak WJ, Hill JM, Lin A, Karbasheski E, Lyons CS. *A comparison of gas-phase methods of modifying polymer surfaces.*, In: Mittal KL, Lyons CS, Strobel M. (Eds.) Polymer Surface Modification: Relevance to Adhesion. Coronet books; 1994: 233-251.
- [309] Swieszkowski W, Bednarz P, Prendergast PJ. *Contact stresses in the glenoid component in total shoulder arthroplasty.*, Proc Inst Mech Eng [H], 217(1) (2003), 49 – 57.
- [310] Swieszkowski W, van der Pijl AJ, Bersee HEN. *Wear simulator for in vitro shoulder prostheses testing.*, Acta of Bioengineering and Biomechanics, 5(1). (2003), 489 – 494.
- [311] Swanson AB, de Groot Swanson G, Maupin BK, Wei JN, Khalil MA., *Bipolar implant shoulder arthroplasty.*, Orthopedics, 9(3). (1986), 343 – 51.
- [312] Swarts E, Miller SJ, Keogh CV, Lim G, Beaver RJ. *Fractured Whiteside Ortholoc II knee components* J Arthroplasty. 16(7) (2001), 927 – 934.
- [313] Tan V, Seldes RM, Katz MA, Freedhand AM, Klimkiewicz JJ, Fitzgerald RH Jr. *Contribution of acetabular labrum to articulating surface area and femoral head coverage in adult hip joints: an anatomic study in cadavera.* Am J Orthop. 30(11) (2001), 809 – 812.
- [314] Tétreault P, Krueger A, Zurakowski D, Gerber C. *Glenoid version and rotator cuff tears.* J Orthop Res. 22(1) (2004), 202 – 207.
- [315] Thoma W, Schreiber S, Hovy L. *Computer-assisted implant positioning in knee endoprosthesis. Kinematic analysis for optimization of surgical technique.* Orthopade. 29(7) (2000), 614 – 626.
- [316] Thomas BJ, Cracchiolo A 3rd, Lee YF, Chow GH, Navarro R, Dorey F. *Total knee arthroplasty in rheumatoid arthritis. A comparison of the polycentric and total condylar prostheses.* Clin Orthop. 265 (1991), 129 – 136.
- [317] Thompson FR. *An essay on the development of arthroplasty of the hip.* Clin Orthop. 44 (1966), 73 – 82.
- [318] Thompson WO, Debski RE, Boardman ND 3rd, Taskiran E, Warner JJ, Fu FH, Woo SL. *A biomechanical analysis of rotator cuff deficiency in a cadaveric model.*, Am J Sports Med, 24 (1996), 286 – 292.
- [319] van Tooren MJL, Sinke J, Bersee, HEN. *Composites: Materials, Structures & Manufacturing Processes.* TU Delft (1993).

- [320] Torchia ME, Cofield RH, Settegren CR. *Total shoulder arthroplasty with the Neer prosthesis: long-term results*. J Shoulder Elbow Surg. 6(6) (1997), 495 – 505.
- [321] Townley CO. *Articular plate replacement arthroplasty for the knee joint*. Clin Orthop. 36 (1964), 77 – 85.
- [322] Trick LW. *The total guide to total primary hips*. Orthopedic special edition. 7(2) (2001), 49 – 68.
- [323] Turner RH, Aufranc OE. *Femoral stem replacement arthroplasty of the knee*. Surg Clin North Am. 49(4) (1969), 917 – 927.
- [324] Turner CH. *Three rules for bone adaptation to mechanical stimuli*. Bone. 23(5) (1998), 399 – 407.
- [325] Unger AS, Inglis AE, Mow CS, Figgie HE 3rd. *Total ankle arthroplasty in rheumatoid arthritis: a long-term follow-up study*. Foot Ankle. 8(4) (1988), 173 – 179.
- [326] van der Vegt AK. *Kunststoffen, Technische Hogeschool Delft*. (1982).
- [327] Venable CS, Stuck WG, Beach A. *The effects of bone on the presence of metals; Based upon electrolyses; An experimental study*. Ann Surg. 105 (1937), 917 – 938.
- [328] Verdonschot N, Huiskes R. *Subsidence of THA stems due to acrylic cement creep is extremely sensitive to interface friction*. J Biomech. 29(12) (1996), 1569 – 1575.
- [329] Verdonschot N, Huiskes R. *The effects of cement-stem debonding in THA on the long-term failure probability of cement*. J Biomech. 30(8) (1997), 792 – 802.
- [330] Verdonschot N, Huiskes R. *Surface roughness of debonded straight-tapered stems in cemented THA reduces subsidence but not cement damage*. Biomaterials. 19(19) (1998), 1773 – 1779.
- [331] Verneuil AS. *De la creation d'une fausse articulation par section ou resection partielle de l'os l'ankylose vraie ou fausse de la machoire inferieure*. Arch Gen Med. 15 (1860), 174 – 195.
- [332] Villa T, Migliavacca F, Gastaldi D, Colombo M, Pietrabissa R. *Contact stresses and fatigue life in a knee prosthesis: comparison between in vitro measurements and computational simulations*. J Biomech. 37(1) (2004), 45 – 53.
- [333] Vincke KG. *Evaluation of knee arthroplasty*. In: Scot WN (ed.) The Knee. St Louis, Mosby. (1994), 1045 – 1078.
- [334] Walch G. and Boileau P. *Prosthetic adaptability: a new concept for shoulder arthroplasty*. J Shoulder Elbow Surg. 8(5) (1999), 443 – 5.

- [335] Walch A, Boulahia A, Badet R, Riand N, Kempf JF. *Primary Gleno-humeral Osteoarthritis: Clinical and Radiographic Classification*. In: Shoulder Arthropalsty (Ed. Walch G. and Boileau P.). ISBN 3540633499. Springer-Verlag, Berlin, Heidelberg, 1999, 195 – 201.
- [336] Walch G, Edwards TB, Boulahia A, Boileau P, Mole D, Adeleine P. *The influence of glenohumeral prosthetic mismatch on glenoid radiolucent lines: results of a multicenter study.*, J Bone Joint Surg Am, 2002, 84(A12), 2186 – 91.
- [337] Wallace WA *The dynamic study of shoulder movement.*, In: Bailey I., Kessel L. (Eds.), Shoulder surgery. Springer-Verlag, berlin, (1982), 179 – 143.
- [338] Wallace AL, Phillips RL, MacDougal GA, Walsh WR, Sonnabend DH. *Resurfacing of the glenoid in total shoulder arthroplasty. A comparison, at a mean of five years, of prostheses inserted with and without cement.*, J Bone Joint Surg Am, 1999, 81(4), 510 – 8.
- [339] Wallace AL, Walsh WR, Sonnabend DH. *Dissociation of the glenoid component in cementless total shoulder arthroplasty.*, J Shoulder Elbow Surg, 1999, 8(1), 81 – 4.
- [340] Walldius B. *Arthroplasty of the knee using an endoprosthesis*. Acta Orthop Scand. 30 (1960), 137.
- [341] Waugh TR, Evanski PM, McMaster WC. *Irvine ankle arthroplasty. Prosthetic design and surgical technique*. Clin Orthop. 114 (1976), 180 – 184.
- [342] Warner J, Lephart S, Fu F. *Role of proprioception in pathoetiology of shoulder instability.*, Clin Orthop, 330 (1996), 35 – 39.
- [343] Warner JJ, Bowen MK, Deng X, Torzilli PA, Warren RF. *Effect of joint compression on inferior stability of the glenohumeral joint.*, J Shoulder Elbow Surg, 8(1) (1999), 31 – 36.
- [344] Weinans H. *Mechanically induced bone adaptations around orthopaedic implants*. PhD thesis, Nijmegen Catholic University, Nijmegen, The Netherlands. (1991).
- [345] Weinans H, Huiskes R, van Rietbergen B, Sumner DR, Turner TM, Galante JO. *Adaptive bone remodeling around bonded noncemented total hip arthroplasty: a comparison between animal experiments and computer simulation*. J Orthop Res. 11(4) (1993), 500 – 513.
- [346] Wheeler JP, Miles AW, Clift SE. *The influence of the stem-cement interface in total hip replacement—a comparison of experimental and finite element approaches*. Proc Inst Mech Eng [H]. 211(2) (1997), 181 – 186.
- [347] Wheeler's Textbook of Orthopaedics.
- [348] Wiklund I, Romanus BA. *Comparison of quality of life before and after arthroplasty in patients who had arthrosis of the hip joint*. J Bone Joint Surg Am. 73(5) (1991), 765 – 769.

- [349] Wiles P. *The surgery of the osteoarthritic hip*. Br J Surg. 45 (1958), 488 – 497.
- [350] Wilk KE, Arrigo CA, Andrews JR. *Current concepts: the stabilizing structures of the glenohumeral joint.*, J Orthop Sports Phys Ther, 25 (1997), 364 – 379.
- [351] Wintermantel E, and Ha S. *Biocompatibele Werkstoffe und Bauweisen. Implantaten fur Medizin und Umwelt*. (1996) Springer Verlag, Berlin.
- [352] Wirth M, Rockwood C. *Complications of shoulder arthroplasty.*, Clin Orthop, 307 (1994), 47 – 69.
- [353] Wirth M, Rockwood C. *Complications of shoulder arthroplasty*. J Bone Joint Surg Am, 8(4) (1996), 603 – 616.
- [354] Wolff J. *Das Gesetz der Tranzformation der Knochen. Translated as: The law of Bone Remodeling*. Springer Verlag, Berlin. (1892).
- [355] Wong AS, Gallo L, Kuhn JE, Carpenter JE, Hughes RE. *The effect of glenoid inclination on superior humeral head migration*. J Shoulder Elbow Surg. 12(4) (1996), 360 – 4.
- [356] Woodruff MJ, Cohen AP, Bradley JG. *Arthroplasty of the shoulder in rheumatoid arthritis with rotator cuff dysfunction*. Int Orthop. 27(1) (2003), 7 – 10.
- [357] Worland RL, Jessup DE, Arredondo J, Warburton KJ. *Bipolar shoulder arthroplasty for rotator cuff arthropathy*. J Shoulder Elbow Surg. 6(6) (1997), 512 – 5.
- [358] Wright TM (Editor), Goodman SB (Editor), Amstutz HC. *Implant Wear: The Future of Total Joint Replacement*. American Academy of Orthopaedic Surgeons. (1996).
- [359] Wynn AH, Wilde AH. *Long-term follow-up of the Conaxial (Beck-Steffee) total ankle arthroplasty*. Foot Ankle. 13(6) (1992), 303 – 306.
- [360] Wu S. *Polymer interface and adhesion.*, New York: Marcel Dekker Inc., (1982).
- [361] Yamaguchi K, Sher JS, Andersen WK, Garretson R, Uribe JW, Hechtman K, Neviasser RJ. *Glenohumeral motion in patients with rotator cuff tears: a comparison of asymptomatic and symptomatic shoulders.*, J Shoulder Elbow Surg, 9. (2000),6 – 11.
- [362] Yildiz H, Chang FK, Goodman SJ. *Composite hip prosthesis design. II. Simulation*. Biomed Mater Res. 39(1) (1998), 102 – 119.
- [363] Young HH. *Use of a hinged Vitallium prosthesis for arthroplasty of the knee: A preliminary report*. J Bone Joint Surg. 45A (1963), 1627 – 1642.
- [364] Zhang SW. *State-of-the-art of polymer tribology*. Tribol. Int. 31 (1998), 49 – 60.

- [365] Ziegler BS, Lachiewicz PF. *Survivorship analysis of cemented total hip arthroplasty acetabular components implanted with second-generation techniques*. J Arthroplasty. 11(6) (1996), 750 – 756.

# List of Publications

This thesis is based on the following publications:

Oosterom R, van Keulen F, Rozing PM. Introduction to Shoulder Endo-Prosthesis Design - A Review. In: Proceedings of the third conference of the international shoulder group, 2000, Newcastle upon Tyne, UK, 2000, 72 – 75.

Swieszkowski W, Oosterom R, Bersee HEN, Beukers A. Cartilage and subchondral bone as a composite structure. Proceed. 13th International Conference on Composite Materials, Beijing, China, 2001, ID 1491.

Oosterom R, Bersee HEN. Composites for Human Joint Replacements. Proceed. 13th International Conference on Composite Materials, Beijing, China, 2001, ID 1492.

Oosterom R, Swieszkowski W, Bersee HEN, van der Helm FCT. Patient factors in shoulder arthroplasty. Acta of Bioengineering and Biomechanics, 3, Supl.2, 2001, 393 – 399.

Oosterom R, Herder JL, van der Helm, FCT, Swieszkowski W, Bersee HEN. Translational stiffness of the replaced shoulder joint. J Biomech. 36(12), 2003, 1897 – 1907.

Oosterom R, Rozing PM, Verdonshot NJJ, Bersee HEN. Fixation of the cup component in total shoulder arthroplasty: Evaluation of the effect of joint conformity. Proceed. 14th International Conference on Composite Materials, San Diego, U.S.A, 2003, ID 1553.

Oosterom R, van Ostayen RAJ, Swieszkowski W, Hoevenaar AH, Bersee HEN. The dynamic coefficient of friction between UHMWPE and PMMA. Proceedings of the international conference biomechanics 2003. Acta of bioengineering and biomechanics, 5, Suppl. 1, 2003, 353 – 357.

Oosterom R, Bersee, HEN. Force controlled fatigue testing of shoulder prostheses. *Exp. Tech.* 28(5), 2004, 33 – 37.

Oosterom R, Rozing PM, Verdonschot NJJ, Bersee HEN. Effect of joint conformity on glenoid component fixation in Total Shoulder Arthroplasty. *Proc Inst Mech Eng [H]*, 218(5), 2004, 339 – 347.

Oosterom R, Rozing PM, Bersee HEN. Effect of glenoid component inclination on its fixation and humeral head subluxation in total shoulder arthroplasty. *Clin Biomech*, 19(10), 1000 – 1008

Oosterom R, Ahmed T, Poulis JA, Bersee HEN. Improvement of adhesion properties of UHMWPE by different surface modification techniques for component fixation in total joint arthroplasty. Submitted to: *Proceed. 15th International Conference on Composite Materials*, Durban, South Africa, 2005.

Oosterom R, van Ostayen RAJ, Antonelli V, Bersee HEN. The effect of interface conditions on Finite Element Modelling of the artificial shoulder. Submitted to *Proc Inst Mech Eng [H]*.

Oosterom R, van der Pijl AJ, van der Helm FCT, Herder JL, Bersee HEN. Een zelfstabiliserende schouderprothese. Patent pending, no. NL 46.338

# List of Figures

1.1	The research strategy . . . . .	6
2.1	The Body and the Shoulder . . . . .	12
2.2	The glenohumeral joint . . . . .	13
2.3	The humerus and scapula . . . . .	14
2.4	Geometrical parameters of the humerus, glenoid and their relation . .	16
2.5	Shoulder pathology . . . . .	17
2.6	Overview of historical shoulder replacements . . . . .	22
2.7	Overview of conceptually different glenoid components . . . . .	22
2.8	Conceptually different shoulder replacement systems . . . . .	24
2.9	Common complications after a shoulder replacement . . . . .	30
2.10	Two geometrically different glenoid components . . . . .	33
3.1	The hip . . . . .	37
3.2	Overview of historical hip replacements . . . . .	40
3.3	Presently used hip prostheses . . . . .	41
3.4	Common complications after hip replacements . . . . .	44
3.5	The knee . . . . .	45
3.6	Overview of historical knee replacements . . . . .	48
3.7	Presently used knee prostheses . . . . .	49
3.8	Common complications after knee replacements . . . . .	51
3.9	The ankle . . . . .	52
3.10	X-ray of the ankle . . . . .	52
3.11	Ankle arthrodesis . . . . .	55
3.12	presently used ankle prostheses . . . . .	56
3.13	Complications after ankle replacements . . . . .	57
3.14	Surface skewness . . . . .	62
3.15	Different materials in hip replacements . . . . .	63
3.16	Load distribution in hip replacements . . . . .	64
4.1	Schematic representation of the artificial glenohumeral joint . . . . .	70
4.2	definition of joint positions and articulations . . . . .	71
4.3	Example of a joint translational stiffness graph . . . . .	78

4.4	Effect of glenoid radius of curvature on humeral head subluxation . . .	80
4.5	Effect of humeral head radius of curvature on humeral head subluxation	80
4.6	Effect of glenoid component chord length on humeral head subluxation	81
5.1	Glenoid specimen structure . . . . .	89
5.2	Method of cementing of glenoid components . . . . .	90
5.3	The force-controlled test set-up . . . . .	91
5.4	The displacement sensors . . . . .	93
5.5	Shear-out strength . . . . .	94
5.6	Subluxation force and superior glenoid rim-displacement v. cycle time	95
6.1	Schematic overview of the artificial shoulder joint . . . . .	102
6.2	Glenoid specimen structure . . . . .	103
6.3	Glenoid rim-displacements during fatigue testing . . . . .	106
6.4	Results of the experiments on glenoid conformity . . . . .	107
6.5	Failure modes of the tested glenoid specimens after shear-out testing	107
7.1	Schematic overview of the artificial shoulder joint . . . . .	114
7.2	Glenoid specimen structure . . . . .	115
7.3	The force-controlled test set-up . . . . .	116
7.4	Development of glenoid rim-displacements during the 200.000 cycles .	119
7.5	Rim-displacements versus glenoid component inclination angle . . . .	120
7.6	Results of the humeral head subluxation measurements . . . . .	120
7.7	Design options for more downward facing glenoid components . . . .	122
8.1	Schematic representations of the different surface treatments . . . . .	130
8.2	The water contact angle . . . . .	132
8.3	Method of investigation of the interfacial shear strength . . . . .	133
8.4	Variation of the water contact angle for different surface treatments .	134
8.5	Variation of the surface energy for different surface treatments . . . .	135
8.6	Variation of the interfacial shear stress for different surface treatments	138
9.1	SEM photo's of the contacting area of PMMA specimens . . . . .	145
9.2	Method of investigating the static coefficient of friction . . . . .	147
9.3	Method of investigating the dynamic coefficient of friction . . . . .	148
9.4	The static and dynamic c.o.f between UHMWPE and PMMA . . . . .	150
9.5	Finite Element model to investigate the effect of interface conditions .	151
9.6	Max. principal stresses in the bone cement and glenoid component . .	158
9.7	Max. ML displacement in the bone cement and glenoid component .	159
9.8	Max. principal stress in the glenoid component, bone cement and bone	160
9.9	Rim-displacements of the glenoid component . . . . .	160
10.1	Biomechanical design background of the self-stabilizing prosthesis . .	169

---

10.2	The self-stabilizing glenohumeral prosthesis . . . . .	170
10.3	The bone anchors and method of unfolding . . . . .	171
10.4	The cable fixation with hollow screw . . . . .	172
10.5	Surgical procedure of the self-stabilizing glenohumeral prosthesis . . .	173
10.6	Effect of the location of the CoR of the self-stabilizing prosthesis . . .	174
10.7	Schematic overview of the self-stabilizing artificial shoulder joint . . .	176
10.8	Simple Finite Element model of the self-stabilizing prosthesis . . . . .	177
10.9	Finite Element model of the self-stabilizing prosthesis . . . . .	178
10.10	Humeral fracture treatment as a spin-off example . . . . .	180
A.1	Anatomical planes and definitions of human movements . . . . .	194
B.1	Biomaterials in articular joints . . . . .	201
B.2	An example of stress shielding . . . . .	202
B.3	The chemical structure of UHMWPE . . . . .	204
C.1	Color representations of the glenohumeral joint . . . . .	211
C.2	Color representations of the joints of the lower extremities . . . . .	212
C.3	Color representations of the experimental test set-ups . . . . .	213
C.4	Color representations of the displacement sensors . . . . .	214
C.5	Color representations of the maximal principal stress in the glenoid component, bone cement and bone . . . . .	215
C.6	Color representations of the maximal medial-lateral displacement in the bone cement and glenoid component . . . . .	216
C.7	Color representations of the self-stabilizing glenohumeral prosthesis .	217
C.8	Color representations of the surgical procedure of the self-stabilizing glenohumeral prosthesis . . . . .	218
C.9	Color representation of the FE model of the self-stabilizing gleno- humeral prosthesis . . . . .	219
C.10	Color representations of the results of the FE analysis of the self- stabilizing glenohumeral prosthesis . . . . .	219



## List of Tables

2.1	Dimensions of the glenoid cavity and humeral head . . . . .	15
2.2	Radius of curvature of the glenoid cavity and humeral head . . . . .	15
2.3	Max. bone element angles of the shoulder during common tasks of daily living . . . . .	20
2.4	Shoulder stability . . . . .	21
3.1	Characteristics of the shoulder, hip, knee and ankle joint . . . . .	66
5.1	Effect of bone properties on glenoid component rim-displacements . .	95
6.1	Effect of joint conformity on glenoid component rim-displacements . .	105
7.1	Effect of glenoid inclination on glenoid component rim-displacements	119
8.1	Surface roughness of the UHMWPE specimens . . . . .	134
8.2	Effect of surface treatment on shear strength of UHMWPE lap-joints	136
8.3	Effect of ageing on shear strength of UHMWPE lap-joints . . . . .	137
9.1	The static and dynamic c.o.f between UHMWPE and PMMA . . . . .	149
9.2	Material properties used in the Finite Element model . . . . .	152
9.3	Maximal principal stress in the glenoid component, bone cement and bone . . . . .	156
10.1	Range of motion requirements of the shoulder to perform ADL . . . . .	165
10.2	Requirements for a self-stabilizing prosthesis . . . . .	168
A.1	The ligaments of the shoulder girdle . . . . .	194
A.2	The muscles of the shoulder girdle . . . . .	195
B.1	Mechanical properties of common used biocompatible materials . . .	206



# Summary

## Design Considerations for the Glenohumeral Endoprosthesis

Shoulder replacements can show good results in terms of survival rates, for certain patient groups even similar to hip and knee replacements. Unfortunately, results in terms of post-operative joint functionality are inferior with additionally more complications and these results must be improved to increase patient satisfaction.

The results in terms of component fixation and post-operative functionality are determined by patient characteristics, the design of the prosthesis, the surgeon and post-operative rehabilitation. In general, two patient groups can be distinguished, namely patients with glenohumeral joints suffering from osteo-arthritis or rheumatoid-arthritis. The difference is that in osteoarthritic joints the surrounding soft-tissues are unaffected, whereas these tissues may be excessively deteriorated or even torn in the case of rheumatoid-arthritic joints. Whereas mimicking the natural anatomy is the primary goal in osteoarthritic joints, in the case of rheumatoid-arthritic joints, a well fixed replacement with good stability is to be created, which asks for different approaches.

Using a rigid-body model of the artificial glenohumeral joint, including a potential field, the effect of, among others, the radius of curvature of both the glenoid and humeral head component on humeral head translations and joint stability is investigated. Clear relations between applied forces, geometrical parameters and humeral head translations for different articular positions are given. The joint translational stiffness, which is the derivative of the applied subluxation force with respect to the humeral head displacement in corresponding direction, seems to be a good predictor for joint stability, being positive and negative in the case of a stable and unstable joint, respectively.

Parallel to the Finite Element (FE) method, experimental testing is frequently used, as it may demonstrate unexpected effects, which were not implemented in the FE model. However, both methods should be made as realistic as possible. An experimental test set-up is developed, in which humeral head displacements are the result of known applied forces. This provides a more realistic method to investigate the effect of joint conformity and glenoid inclination on glenoid component tilting, as

compared to conventional methods, in which humeral head translations are applied. Using this new test equipment, it is found that in the case of a tendency to superior subluxation, increased articular conformity and decreased glenoid component inclination are beneficial with respect to glenoid component tilting. Additionally, it is found that, in this case, a decreased glenoid inclination increases joint stability.

The experiments also demonstrated that in most cases no physical bonding is present between the Ultra-High-Molecular-Weight-Polyethylene (UHMWPE) glenoid component and the Polymethyl-Methacrylate (PMMA) bone cement. This indicates that glenoid components are fixed by mechanical interlocking, rather than by adhesion. Keels, with holes and grooves, or pegs are needed to achieve this, which require much bone removal. It is unknown whether adhesion in this interface is beneficial for the presently used designs. However, adhered fixation of UHMWPE glenoid components, in combination with design modifications, can be interesting to develop a more superficial fixation. Therefore, methods to improve adhesion properties of UHMWPE have been investigated. Different surface modification techniques are used to oxidize thin UHMWPE specimens, which are then bonded into single lap-joints with PMMA bone cement or MMA adhesive and subsequently tested on shear strength. A combined surface roughening and Radio Frequency-Discharge treatment showed the highest interface shear strength, even resulting in UHMWPE necking of the single lap-joints.

The absence of physical bonding between most UHMWPE glenoid components and the PMMA bone cement also implies that the common used full bonding at this interface in Finite Element (FE) models may be incorrect and contact elements in combination with a coefficient of friction (CoF) at this interface may result in a better approximation of the reality. A FE analysis of the glenohumeral joint replacement demonstrated that full bonding provides a small overestimation of the maximal principal stresses in the glenoid component, whereas it dramatically underestimates the maximal principal stresses in the bone cement and underlying bone, with respect to a CoF at the interface. Also, although full bonding only slightly underestimates the superior glenoid rim-displacements, it provides a complete wrong behaviour of the inferior glenoid rim-displacements, as it doesn't allow the glenoid component to tilt away from the cement. A full bonding only slightly underestimates the medial displacements in the bone cement and underlying bone.

At present, no reliable solution is available for shoulders, which are severely affected by rheumatoid-arthritis or Rotator Cuff arthropathy. This is mainly because of the very unfavorable combination of weakened or even severely damaged surrounding soft-tissues, such as muscles and ligaments, and deteriorated bone materials in an already bad approachable and small bone volume for component fixation. A conceptually new design has been developed, in which a bipolar humeral head is semi-rigidly connected to the lateral scapula using artificial ligaments. The 3 or 4 ligaments diverge from the outer shell towards the glenoid bone stock. Guided by drilled openings, these ligaments go subsequently through the subchondral bone,

trabecular bone and medial cortex of the glenoid bone at which they are fixed. The ligaments are fixed at the medial cortex of the glenoid bone stock, either by using bone anchors or by inserting ligaments with a clamped ball at their medial end in combination with hollow screws, tightened in the healthy trabecular and cortical bone. Both methods only require a lateral approach and lead to pure compressive and tensile forces at the fixation. As the humeral head tends to subluxate in any arbitrary direction, the ligaments become tensioned, thereby preventing the humeral head from further translating out of the glenoid cavity. Meanwhile, the bipolar head provides enough range of motion to perform the activities of daily living. The presented fixation techniques of the ligaments have some interesting spin-off applications, especially in the case of bone fractures and minimal invasive surgery.

Keywords: shoulder prosthesis, glenoid component fixation, shoulder stability, rigid-body model, force-controlled testing, joint conformity, glenoid component inclination, UHMWPE adhesion, Finite Element Model, coefficient of friction, self-stabilizing prosthesis

Rogier Oosterom, 2004



# Samenvatting

## Ontwerp consideraties voor de Glenohumerale Endoprothese

Vervanging van het schoudergewricht laat goede resultaten zien als het gaat om de levensduur, voor bepaalde patiëntgroepen zelfs gelijk aan die van heup- en kniegewrichten. Echter, de resultaten in termen van post-operatieve functionaliteit van de schouder zijn een stuk slechter met tevens meer complicaties en deze resultaten moeten worden verbeterd voor een toename van de tevredenheid van de patiënt.

Het resultaat in termen van component fixatie en post-operatieve functionaliteit worden bepaald door de patiënt, het ontwerp van de prothese, de chirurg en de post-operatieve zorg. In het algemeen kunnen twee patiëntgroepen worden onderscheiden, te weten patiënten met glenohumerale gewrichten aangetast door osteoarthrose of door reumatoïde artritis. Deze twee groepen onderscheiden zich met name, doordat osteoarthrose alleen het bot aantast, terwijl in het geval van reumatoïde artritis ook de omringende zachte weefsels, zoals de ligamenten en spieren van het gewricht, in ernstige mate aangetast kunnen zijn of zelfs gescheurd. Het doel van de vervanging van arthrose gewrichten is het reconstrueren van de originele anatomie, terwijl dit voor reumatoïde gewrichten het creëren van stabiliteit van het gewricht en goede component fixatie is. Dit vraagt om verschillende benaderingen.

Met behulp van een schematisch 'rigid-body model' van de vervangen schouder, waarbij de geometrie vastligt door gebruik te maken van oneindig stijve materialen, is het effect van onder andere de kromtestraal van zowel de glenoid als humerale component op humeruskop translaties en stabiliteit van het gewricht bekeken. Duidelijke verbanden zijn gegeven tussen de aangebrachte krachten, geometrische parameters en humeruskop translaties voor verschillende articulatie gebieden. De 'gewrichtstranslatiestijfheid', gedefinieerd als de afgeleide van de aangebrachte subluxatiekracht naar humeruskop translaties in dezelfde richting, blijkt goed de gewrichtsstabiliteit te kunnen voorspellen en is respectievelijk positief en negatief in het geval van een stabiel en onstabiel gewricht.

Naast de Eindige Elementen (EE) methode, worden experimentele technieken veelvuldig gebruikt om ontwerpen te valideren, aangezien deze onverwachte effecten kunnen laten zien, die niet in de EE modellen konden worden meegenomen. Echter,

beide methoden moeten zo goed mogelijk de realiteit benaderen. Een testopstelling is ontwikkeld, waarbij de humeruskop translaties het gevolg zijn van bekende krachten. Zo kan op een realistischer manier het effect van gewrichtsconformiteit en glenoid inclinatie bekeken worden, ten opzichte van een nu vaak gebruikte andere methode, waarbij humeruskop translaties worden aangebracht. In deze nieuwe testopstelling wordt het kantelen van het glenoid component gemeten als gevolg van de aangebrachte wisselende belasting. Dit herhaald kantelen wordt gezien als een belangrijk faalmechanisme van de totale schoudervervanging. Met behulp van deze opstelling kan worden aangetoond dat, in het geval van subluxatie in superieure richting, een toename van gewrichtsconformiteit en een afname van glenoid inclinatie het kantelen van de glenoid component doet afnemen. Tevens kon worden laten zien dat in dit geval een afname van de glenoid component inclinatie een toename van gewrichtsstabiliteit oplevert.

De experimenten hebben ook laten zien dat er in veel gevallen geen hechting aanwezig is tussen het Ultra-High-Molecular-Weight-Poly-Ethylene (UHMWPE) glenoid component en het Polymethyl-Methacrylate (PMMA) botcement. Dit betekent dat de glenoid componenten met name vastzitten door middel van mechanische interlocking, in plaats van door fysische hechting. Zogenaamde keels, met gaten en groeven, en pegs aan de achterzijde van de glenoid componenten, zijn hiervoor nodig, die een hoop botverwijdering vereisen. Het is onbekend of deze hechting wel of niet gunstig is in combinatie met de huidig gebruikte ontwerpen. Echter, hechting van glenoid componenten zou gebruikt kunnen worden voor het ontwikkelen van een minder diepe methode van fixeren in combinatie met ontwerp modificaties. Daarom zijn de methoden ter verbetering van de hechtingseigenschappen van UHMWPE onderzocht. Verschillende oppervlakte behandelingstechnieken zijn gebruikt om het oppervlak van dunne UHMWPE schijfjes te oxideren, die dan met een enkelvoudige overlap aan elkaar gelijmd zijn met PMMA botcement of Methyl-Methacrylate lijm en vervolgens op afschuifsterkte getest. Een gecombineerde behandeling van opruwen en een radio-frequentie plasma ontladingsbehandeling bleek te resulteren in de hoogste afschuifsterkte, wat zelfs insnoering van het UHMWPE vlak bij de overlap tot gevolg had.

Dat er geen fysische hechting aanwezig is tussen de UHMWPE glenoid component en het PMMA botcement, houdt ook in dat de vaak gebruikte volledige verbinding van deze interface in EE modellen, waarbij de knooppunten van de elementen 1 op 1 verbonden worden, een onjuist methode is. Het gebruik van contact elementen in combinatie met een wrijvingscoëfficiënt zou een betere benadering van de werkelijkheid kunnen opleveren. Met behulp van een EE analyse is gevonden dat bij een volledige verbinding van de interface, de 'principal stresses' in de glenoid component enigszins overschat worden, terwijl juist in het botcement en onderliggende bot deze 'principal stresses' duidelijk onderschat zijn, ten opzichte van een analyse met een wrijvingscoëfficiënt en contact elementen. Hoewel een volledige verbinding slechts een kleine onderschatting geeft van de rand-verplaatsing van de superieure glenoid com-

ponent, laat het een geheel verkeerd beeld zien van de rand-verplaatsingen aan de inferieure zijde van de glenoid component. Dit laatste komt, doordat een volledige verbinding een kanteling uit het bot van de inferieure rand van het glenoid component niet toelaat. Tenslotte laat een volledige verbinding slechts een kleine onderschatting zien van de mediale verplaatsingen van het botcement en onderliggend bot.

Voor patiënten met een ernstig pathologisch glenohumeraal gewricht als gevolg van reumatoïde arthritis en Rotator Cuff arthropathy is er momenteel geen succesvolle oplossing beschikbaar. Dit komt met name door de zeer ongunstige combinatie van verzwakte of zelfs gescheurde omringende zachte weefsels, zoals spieren en ligamenten, en verslechterd botmateriaal in een moeilijk toegankelijk en klein bot volume voor component fixatie. Een conceptueel nieuw ontwerp is ontwikkeld, waarbij een zogenaamde bi-polair humerale prothese semi-rigide gefixeerd is met de laterale scapula, gebruik makende van artificiële ligamenten. De 3 of 4 ligamenten divergeren vanuit de buitenschaal van het bi-polaire gewricht richting het glenoid botgedeelte van de scapula. Geleid door geboorde gaten, gaan deze ligamenten dan respectievelijk door het subchondrale, trabeculaire en uiteindelijke ook door het mediale cortex van het glenoid gedeelte van de scapula, alwaar ze worden gefixeerd. Fixatie van de ligamenten wordt tot stand gebracht door het uitklappen van botankers of door het inbrengen van ligamenten met een gefixeerd balletje aan hun mediale uiteinde in combinatie met holle schroeven, die in het gezonde trabeculaire en corticale bot van het glenoid geschroefd worden. Voor beide methoden van fixeren is een lateraal chirurgische ingreep voldoende en geldt dat alleen trek- en drukkrachten optreden rond de fixatie van de ligamenten. Als nu de humerale kop dreigt te subluxeren in elke willekeurige richting, komen de ligamenten onder spanning te staan en verhinderen verdere translatie van de humerale kop uit de glenoid holte. , garandeert de bi-polaire prothese voldoende bewegingsvrijheid om de activiteiten van het dagelijks leven uit te kunnen voeren. De gepresenteerde methode van fixeren van de ligamenten hebben een aantal interessante spin-off toepassingen, met name in het geval van bot fracturen en minimaal invasieve chirurgie.

Trefwoorden: schouder prothese, glenoid component fixatie, schouder stabiliteit, rigid-body model, krachtgestuurd testen, gewrichtsconformiteit, glenoid component inclinatie, UHMWPE hechting, Eindig Elementen Model, wrijvingscoëfficiënt, zelfstabiliserende prothese

Rogier Oosterom, 2004



# Acknowledgements

Although already mentioned in the preface, I would like to thank Henk Stassen for initiating the DIPEX project. His probably never-ending enthusiasm and extensive network were very helpful for completing my PhD study.

Not only for my work but also for me as a person, I have been very lucky that Wojciech Swieszkowski (Wojtek) was my direct colleague during my PhD study. Especially in the beginning, we learned much from our different working methods, which grew into a very professional co-operation. Although now there is a geographical distance, I hope that we can still continue our discussions.

Beng! After just starting up my PhD study, there he was: Harald Bersee! Next to his supervision, which especially focused on the broad perspective of our research, he was also a personal coach for me. Although we had some tough discussions, as the project progressed this coaching became more intense and useful.

My promotor, Prof. Ir. Adriaan Beukers, is a very nonconform, astonishing person. His capacity to make at first sight unclear connections between different subjects and ideas, never led to direct answers to questions. However, on the long run this way of thinking learned me to widen the perspective on design solutions, which especially had big influence on the conceptual design.

The broad perspective, this time on the clinical practice, was furthermore increased by my second promotor, Prof. dr. P.M. Rozing. His indescribable experience and knowledge on the shoulder and orthopedic surgery were very helpful for the research directions and contents of the present work.

For me, Fred van Keulen and Frans van der Helm are more than just supervisors as part of the DIPEX management team. Already during my graduation project Fred learned me to criticize the work done by others and myself. Hopefully, this has a clear influence on the quality of my research. Next to the discussions about everything, but especially on the GH<sup>+</sup>, the cycling weekends, better known as the Cyclo sportive d'Epaule, with Frans and many others, are yearly weekends to look forward to.

I would like to thank Just Herder, who was, next to Frans, Wojtek and Albert van der Pijl, part of the GH<sup>+</sup> design team. Only entering Just's room of creativity gave a mysterious feeling about the upcoming ideas. His ideas and knowledge about design simplicity were of great benefit for the GH<sup>+</sup>.

Halfway through the project, Albert strengthened our team at the Faculty of Aerospace Engineering. Among others, I thank him for working out the GH<sup>+</sup> using CAD, developing design details, especially the fixation techniques, as well as his helpful critics on the PhD thesis.

The work done by several (former) students proved to be of significant importance as a source of ideas and a compensation medium for the lack of time. Gary, Duncan, Tahira and Talmai: thanks for the great dedication from you all!

During my PhD work, many design ideas came up which I often wanted to demonstrate and needed to be manufactured next to much test-equipment and many test-specimens. Things that I wanted from our workshop usually were difficult to make, if at all, which was also the result of my limited drawing capabilities. Therefore, I would like to thank Bertus, Herman, Ed and Kees for decoding my drawings and everything they made for me, but also for broadening my mind with their email-attachments.

I also thank Hans and Hans. Hans for our discussions to improve my test-methods and for his capacity to make the most tiny electrical gadgets perfectly fitting in my experimental set-ups. Hans for his knowledge on adhesion and surface modifications and his assistance, together with Tahira, for our experiments. But also for our conversations, such as about research, house renovations and travelling.

Sometimes, days at work can be hard and then it is nice to have people around, who recognize my mood at the first glimp. I would like to thank Gemma for doing so and for listening to the stories behind the sometimes terrible moods, but also for all other stories we had to tell each other. Next to this, I thank her for being the L<sup>A</sup>T<sub>E</sub>X queen, making the layout of my thesis as it is.

I would like to thank all other colleagues of PT, VM and the DIPEX project for their assistance as well as for the fun we had at work, conferences and parties! Without you all, work would have been much more boring. Thanks guys and girls!!

Although not always noticed by myself, there is life next to a PhD study! I thank all my friends for waking me up so once and awhile and taking me far away from work. Especially I thank Joost for all our holidays, weekends, evenings and uncountable sport hours and also Michel, for our journeys, sporting activities and conversations! Last but not least, I thank my parents and sister for everything they did and still do. Without their help, life would sometimes have been much more difficult to handle! Thanks Mir, Betto, Leonietje, Mum and Dad.

# Curriculum Vitae

## About the author

The author of this thesis was born on the 18<sup>th</sup> of April 1976 in Alkmaar, The Netherlands. After finishing his secondary education at Huygenwaard in Heerhugowaard, he studied Aerospace Engineering at the Delft University of Technology, The Netherlands. After his practical work at BMW in Germany, he finished his study on a graduation project focusing on the improvement of the glenohumeral endo-prosthesis at the Structural Optimization and Computational Mechanics Group of Mechanical Engineering, Delft University of Technology, under the supervision of Fred van Keulen.

During his graduation it didn't take much time to consider a PhD position within the extensive DIPEX research project. Keeping in mind his desire for design and applied research, it was a logical step to go back to the Faculty of Aerospace Engineering to start his PhD study on the improvement of the glenohumeral endo-prosthesis, as part of DIPEX.